The American Mineralogist

Journal of the Mineralogical Society of America

VOL. 45 — NOVEMBER-DECEMBER, 1960 — Nos. 11 and 12

Contents

(*Continued on Cover 2*)

Published bi-monthly by the Society

(*Contents continued*)

Mineralogical Society of America

The enlarged issues of this journal for 1960 are made possible by a grant from the Penrose Fund of the Geological Society of America.

The American Mineralogist—Journal of the Mineralogical Society of America

The journal, containing articles on mineralogy, crystallography, and allied sciences, is issued every two months. Contributions are invited.

The general conduct of the journal is in the hands of the editor, Lewis S. Ramsdell, Department of Mineralogy, University of Michigan, to whom all manuscripts should be submitted.

Second class postage paid at Menasha, Wisconsin. Acceptance for mailing at the special rate of postage provided for in section 1103, Act of Oct. 3, 1917, paragraph 4 section 429 P. L. & R. authorized March 13, 1922.

Notice of change of address, orders, and remittances should be sent to Marjorie Hooker, c/o U. S. Geological Survey, Washington 25, D. C.

Printed by the George Banta Company, Inc., Menasha, Wisconsin
Printed in the United States of America

THE AMERICAN MINERALOGIST

JOURNAL OF THE MINERALOGICAL SOCIETY OF AMERICA

Vol. 45 NOVEMBER-DECEMBER, 1960 Nos. 11 and 12

ETTRINGITE FROM FRANKLIN, NEW JERSEY*

CORNELIUS S. HURLBUT, JR., *Harvard University*, AND JOHN L. BAUM, *The New Jersey Zinc Co., Franklin, New Jersey.*

ABSTRACT

Ettringite at Franklin, New Jersey occurs as white to colorless crystals 2–3 millimeters across with the only crystal form $\{10\bar{1}2\}$. The axial ratio determined from their measurement is $a:c=1:0.9554$. Specific gravity is 1.77 (meas); 1.79 (cal). Perfect $\{1010\}$ cleavage. Optically (−), $\omega=1.491$, $\epsilon=1.470\pm0.001$. After heating to 110° C, optically (+), $\omega=1.538$ $\epsilon=1.541$. Chemical analysis: CaO 27.3, Al_2O_3 5.1, SiO_2 3.1, SO_3 12.8, B_2O_3 3.2, H_2O 48.6, Total 100.1. A general formula can be written: $Ca_6(Si, Al, B)_3(SO_4)_2(O, OH)_{12}(OH)_4\cdot 26H_2O$ of which there are 8 formula weights per unit cell. The unit cell dimensions are $a_0=22.28$ Å, $c_0=21.29$ Å giving a ratio $a_0:c_0=1:0.9556$.

INTRODUCTION AND OCCURRENCE

During the latter part of 1945 an occurrence of unusual minerals was encountered in the Franklin mine of The New Jersey Zinc Company at Franklin in Sussex County, New Jersey. Immediately above the 800 ft. level, about 15 feet in the ore from the hanging wall, and close to the north side of the Palmer shaft pillar, the occurrence was noticed by the miners and called to the attention of the geologist. Specimens were collected for eventual study from the vein system which was arranged in an H pattern and connected with a potash feldspar zone above. The veins, a foot or so wide, consisted largely of andradite garnet and manganophyllite but there were local concentrations of hancockite near the floor and of other silicates and native copper closer to the feldspar above. The silicates such as roeblingite, hancockite, clinohedrite, xonotlite, rhodonite, thompsonite and datolite post date emplacement of the feldspar and represent a reworking of the adjacent veins by solutions which have corroded cavities and formed spongy zones in the garnet-mica vein system. Fig. 1.

Conspicuous among the crystallized minerals in the cavities were white

* Contribution no. 398 from the Department of Mineralogy and Petrography, Harvard University.

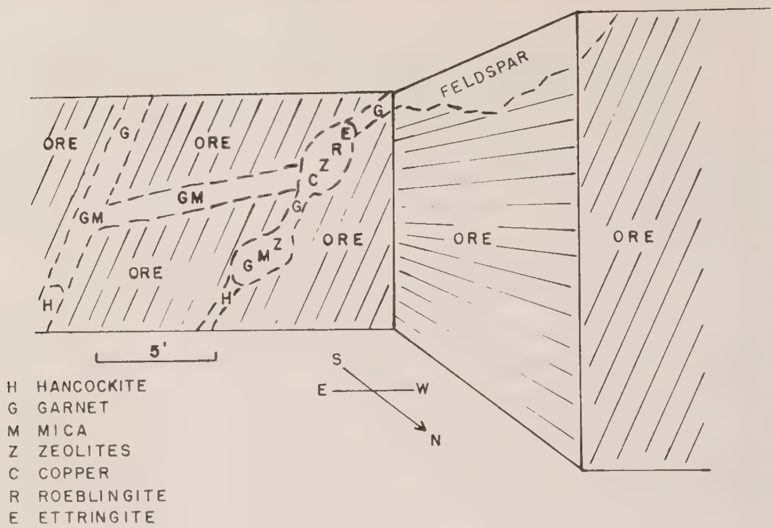

FIG. 1. Vein system of banded ore.

to partially clear crystals of ettringite with the only form a low hexagonal dipyramid. Since these crystals were quite unlike any other mineral described from Franklin, they were not immediately identified. The most spectacular specimens show a surface of minute light brown muscovite crystals coating the cavities in garnet-manganophyllite vein rock. On this surface clinohedrite crystals nearly a half inch in diameter are accompanied by white tufts of thompsonite and crystals of ettringite attached by an edge. Subsequently additional material came to light elsewhere in the mine and was collected for its fluorescence due to admixed clinohedrite. Crystals of ettringite in the second occurrence completely coated the 2 inch by 4 inch surface preserved, but they are etched and unsuited for measurement.

PHYSICAL PROPERTIES

The Franklin ettringite has as the only crystal form the flattened hexagonal dipyramid, $\{10\bar{1}2\}$, (Fig. 2). This is a habit heretofore not described for ettringite, although the form was observed by Lehmann (1874) and noted in the original description of the mineral. The largest crystals are 4 millimeters across whereas the average size is between 2 and 3 millimeters. A few are colorless and transparent and give excellent signals on the reflecting goniometer but most are milky white with etched and pitted faces. The measured ρ angle of $\{1012\}$ is 28°53′ giving an axial ratio of $a:c=1:0.9554$. This compares well with an axial ratio of $a_0:c_0=1:0.9556$ derived from x-ray measurements.

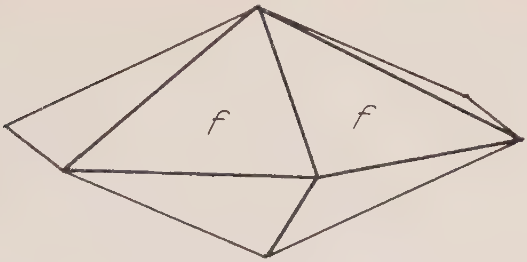

FIG. 2. Ettringite crystal.

The specific gravity of the Franklin ettringite is 1.77 as measured by the suspension method in a mixture of bromoform and acetone. (Calculated specific gravity, 1.79.) There is perfect {1010} cleavage. The optical properties are at greater variance from published data than the other physical properties and are shown in Table 1 compared with those of ettringite from Scawt Hill and Ettringen. The indices of refraction of the Franklin mineral were obtained on colorless crystals; those of white crystals are slightly higher.

Both the refractive indices and birefringence of the Franklin ettringite are considerably greater than ettringite from Scawt Hill and Ettringen. Larsen and Berman (1934) give the indices of refraction as $\omega=1.488$, $\epsilon=1.474$ which Bannister (1936) suggests were probably obtained on partially dehydrated material. This seems unlikely for as the mineral dehydrates ϵ increases more rapidly than ω and the birefringence becomes less. Although the source of the Larsen and Berman material is unknown,

TABLE 1. OPTICAL PROPERTIES OF ETTRINGITE

Locality	1 Franklin	2 Scawt Hill	3 Ettringen	4 Synthetic
ω	1.491 } ±0.001	1.4655	1.4661	1.464
ϵ	1.470 }	1.4618	1.4612	1.458
	uniaxial	uniaxial	uniaxial	uniaxial
	(−)	(−)	(−)	(−)
	After heating to 110° C.			
ω	1.538	1.50 mean index	1.513	
ϵ	1.541		1.522	
	uniaxial	uniaxial	uniaxial	
	(+)	(+)	(+)	

1. Determined during present study.
2. Bannister (1936) by minimum deviation.
3. Brauns (1922). Indices after heating determined during present study.
4. Lerch, Ashton and Bogue (1929).

it is probable that the indices reported by them were obtained on a mineral approaching the Franklin ettringite in composition.

Chemical Composition

A chemical analysis of the Franklin ettringite was made by Mr. Jun Ito on 800 milligrams of carefully selected material, mostly colorless crystals. The analysis is compared in Table 2 with earlier analyses.

Table 2. Chemical Analysis of Ettringite

	1. Franklin	2. Scawt Hill	3. Ettringen
CaO	27.3	26.6	27.27
Al_2O_3	5.1	7.0	7.76
SiO_2	3.1		
SO_3	12.8	18.8	16.64
B_2O_3	3.2		
H_2O-	39.4		
H_2O+	9.2	46.3	45.82
CO_2	Trace	0.8	
Total	100.1	99.5	97.49
Sp.G.	1.770	1.772	1.750

1. Franklin, N. J. Jun Ito *analyst.*
2. Scawt Hill, Antrim County, Ireland, M. H. Hey analyst in Bannister (1936).
3. Ettringen, Germany, Lehmann (1874).

The presence in the Franklin ettringite of B_2O_3 and SiO_2 and lesser amounts of Al_2O_3 and SO_3 than in other ettringite argue that this mineral might be regarded as a new species. However, since in all its crystallographic and physical properties it corresponds to those of ettringite, it seems wise to consider it a variety rather than a new mineral.

The formula for the Franklin ettringite, adhering closely to the chemical analysis can be written expressing the content of the unit cell as follows:

$$Ca_{48}[SiO_3(OH)]_5[Al(OH)_4]_{10}[B(OH)_4]_9[SO_4]_{16}[(OH)_4]_8\cdot 208H_2O$$

The following general formula for the Franklin mineral (1) for which there are 8 formula weights per unit cell compares with the accepted formula of ettringite (2) as:

$$1.\ Ca_6(Si, Al, B)_3(SO_4)_2(O, OH)_{12}(OH)_4\cdot 26H_2O$$

$$2.\ Ca_6\quad Al_2\quad (SO_4)_3\qquad (OH)_{12}\cdot 26H_2O$$

X-ray Study

Both rotation and Weissenberg x-ray photographs were taken with the crystal rotating about the c axis and a horizontal axis normal to the $\{10\bar{1}0\}$ cleavage. The rotation photograph about c corresponded spot for spot with the classic rotation photograph of ettringite from Scawt Hill, County Antrim, Ireland first published by Bragg and Bragg (1933), and later by Bannister (1936) and by Bragg (1937). The spots of this photograph (Scawt Hill) are elongated parallel to the rotation axis, whereas the spots on the photograph of the Franklin mineral are sharp. The rotation photograph of a Franklin crystal rotating about the [1010] axis gave well defined layer lines, measurement of which yielded an identity period along the axis of 19.27 Å; ($d_{10\bar{1}0}$). Using this value the length of the a axis was determined as 22.25 Å; roughly twice the length reported by Bannister.

Table 3. Unit Cell Dimensions of Ettringite

	1 Franklin	2 Scawt Hill[1]	3 Ettringen	4 Synthetic[2]
a_0	22.28 Å	22.47 Å	22.46 Å	22.46 Å
c_0	21.29	21.46	21.42	21.44
c_0/a_0	0.9556	0.9551	0.9537	0.9546

[1] The unit cell dimensions for ettringite given by Bannister (1936) were $a_0=11.26$ Å, $c_0=21.48$ Å (kX converted to angstrom units) determined by the rotation method.

[2] The unit cell dimensions for synthetic ettringite were determined by the powder method, Bureau of Standards (1958), as $a_0=11.23$ Å $c_0=21.44$ Å.

Because of the identity of the c axis rotation photographs of the Franklin and Scawt Hill material, it seemed reasonable to assume that the unit cell dimensions would be similar. Professor C. E. Tilley kindly furnished a cleavage fragment of Scawt Hill ettringite for examination. A rotation photograph about $[10\bar{1}0]$ yielded d_{1010} slightly greater than that given by the Franklin mineral.

A specimen of ettringite from Ettringen, the original locality, was kindly loaned the authors by Professor Joseph Murdoch. Professor Murdoch obtained this specimen from Dr. Hanswilhelm Beil of Göttingen for the purpose of comparing it with a mineral from Crestmore, California suspected of being ettringite. X-ray photographs of the Ettringen mineral also yielded an a_0 similar to that of the Franklin ettringite. From this evidence one must conclude that the a axis of ettringite is approxi-

mately twice that given by Bannister (1936) resulting in a unit cell of four times the volume. It is interesting to note that Lehmann (1874) and Brauns (1922) gave indices for the crystal forms observed by them that are compatible with the doubling of the *a* axis.

In Table 3 the unit cell dimensions of ettringite from Franklin, Scawt Hill, and Ettringen are given determined from 0-layer line Weissenberg photographs made during the present study.

TABLE 4. *d* SPACINGS OF ETTRINGITE

Copper radiation, nickel filter

hkil	Franklin			Synthetic Nat. Bu. Standards	
	Measured d, Å	Measured I	Calculated d, Å	Measured d, Å	Measured I
$20\bar{2}0$	9.65	10	9.648	9.73	10
$22\bar{4}0$	5.58	8	5.570	5.61	8
$22\bar{4}2$	4.93	2	4.935	4.98	2
$20\bar{2}4$	4.65	3	4.660	4.69	4
$22\bar{4}4$	3.84	5	3.848	3.88	5
$42\bar{6}2$	3.44	4	3.449	3.48	3
$60\bar{6}0$	3.21	6	3.216	3.24	2
$60\bar{6}4$	2.75	1	2.756	2.77	4
$62\bar{8}2$	2.59	3	2.595	2.62	2
$42\bar{6}6$	2.54	4	2.543	2.56	5
$44\bar{8}6$	2.19	2	2.190	2.21	4

The unit cell dimensions of the Franklin ettringite are smaller than those of the mineral from other localities. These undoubtedly reflect the substitution of boron and silicon for sulfur and aluminum. The smaller dimensions are also shown in the *d* spacings of Table 4. This table lists only the stronger lines. A complete list of *d* spacings is given by the National Bureau of Standards (1959). In Table 4 the indices of the National Bureau of Standards data are changed to conform with a doubling of the *a* axis.

The space group of ettringite was determined as $P6_3/mmc$, the same as given by Bannister (1936). The calculated specific gravity of the Franklin ettringite is 1.79. The specific gravity of 8 $[Ca_6Al_2(SO_4)_3(OH)_{12} \cdot 26H_2O]$ calculated by the NBS (1959) using their lattice constants is 1.754 at 25° C.

REFERENCES

BANNISTER, F. A. (1936), Ettringite from Scawt Hill, Co. Antrim, *Min. Mag.*, **24**, 324–329.
BRAGG, W. H., AND BRAGG, W. L. (1933), The Crystalline State, London.

Bragg, W. L. (1937), Atomic Structure of Minerals, Cornell University Press.

Brauns, R. (1922), Die Mineralien der Niederrheinischen Vulkangebiete. Stuttgart.

Larsen, E. S., and Berman, H. (1934), The Microscopic Determination of the Nonopaque Minerals, U.S.G.S. Bull 848, 2nd edition.

Lehman, J. (1874), Über den Ettringit, ein neues Mineral, in Kalkeinschüssen der Lova von Ettringen (Laacher Gebiet). *Neues Jahrb, Min.*, 273.

Lerch, W., Ashton, F. W., and Bogue, R. H. (1939), *Bur. Standards Jour. Research*, **2**, 715.

National Bureau of Standards Circular 539 (1959), Standard *X*-Ray Diffraction Powder Patterns, 3–4.

Manuscript received February 15, 1960.

A CRYSTAL CHEMICAL STUDY OF THE VANADIUM OXIDE MINERALS, HÄGGITE AND DOLORESITE*

HOWARD T. EVANS, JR. AND MARY E. MROSE,
U. S. Geological Survey, Washington, D. C.

ABSTRACT

Small, black vanadium oxide crystals obtained from a sandstone drill core taken near Carlile, Wyoming, were found by single-crystal x-ray diffraction techniques to consist of two monoclinic phases. Crystal structure analysis showed one phase to be a new mineral, häggite, having the following crystallographic properties: space group $C2/m$; cell dimensions, $a=12.17$ Å, $b=2.99$, $c=4.83$, $\beta=98°15'$; cell contents, $H_6V_4O_{12}$. The second phase ("phase B") was found to have crystallographic properties identical with those of the previously described doloresite: space group, $C2/m$; cell dimensions, $a=19.64$ Å, $b=2.99$, $c=4.83$, $\beta=103°55'$; cell contents, $H_8V_6O_{16}$ or $H_{10}V_6O_{16}$. The presence of the hydrogen atoms was established by recognizing hydrogen bonds from oxygen oxygen distances and vanadium-oxygen bond distributions. To obtain the best interatomic distance data, the structures of both phases were refined by least squares analysis.

Häggite, phase B, and duttonite (H_2VO_3) are considered to be members of a homologous series of general composition $H_{2n-2}V_nO_{3n-2}$, with $n=4$, 6 and ∞, respectively.

The problem of the chemical nature of doloresite was solved with information obtained from a study of the Carlile crystals. Doloresite is invariably twinned on (100) on a submicroscopic scale, producing pseudo-orthorhombic x-ray patterns. The x-ray intensities of the twin composite reflections are well accounted for in terms of the crystal structure found for phase B. Phase B is not twinned, but is intergrown with häggite in parallel orientation (b and c axes coincident) on a submicroscopic scale. The structural relationships and modes of occurrence of these minerals lead to the hypothetical conclusion that doloresite ($H_8V_6O_{16}$) is metastable and is formed by solid state oxidation of phase B ($H_{10}V_6O_{16}$), which is formed by metasomatic replacement of montroseite. The häggite and phase B from Carlile appear to have been directly crystallized from the primary mineralizing solutions. The mechanisms whereby these processes may have taken place are described.

INTRODUCTION

After montroseite and paramontroseite, the most frequently encountered vanadium oxide mineral in the Colorado Plateau ore deposits is doloresite. This new mineral, easily recognized and characterized petrographically, for a long time resisted definitive study because of its variable chemical composition, anomalous crystallography and intimate association with other vanadium oxide minerals. It is fibrous in character, and it was readily established that the structural spacing along the fibre direction is 3.0 Å, thus suggesting a relationship to montroseite. We made extensive efforts without success in the earlier stages to determine the essential nature of the mineral through crystal structure analysis based on single-crystal intensity data of limited range and quality. Failure was certain because the crystals are twinned and the analysis was

* Publication authorized by the Director, U. S. Geological Survey.

made in terms of an incorrect orthorhombic cell, as described in a later section.

After nearly a year of diligent effort, the doloresite problem was set aside for awhile and attention turned to another vanadium oxide mineral which came from Carlile, Wyoming. Of this material we had available a number of small crystals extracted from a sandstone matrix. *X*-ray patterns of these crystals revealed the presence of two separate phases, both monoclinic, intergrown in parallel orientation on a microscopic scale. One of these, it was discovered, by applying a simple twin law, could be made to account for both the geometry and intensities of the diffraction patterns of doloresite. The crystal structures of both phases in the Wyoming crystals were readily solved from Patterson projections, and this result led directly to the solution of the doloresite problem. Following these developments, the description of the mineral doloresite was completed and published by Stern, Stieff, Evans and Sherwood (1957). A preliminary description of the structures of häggite (one of the Wyoming phases) and doloresite has been given previously (Evans and Mrose, 1958). A detailed description of the analysis and interpretation of the crystal structures of these minerals is the objective of this paper.

The Carlile, Wyoming Crystals

In 1956 we received a sample of a black vanadium oxide in the form of several small crystals (maximum size, 0.1 mm.) which had been worked out of a sandstone matrix by M. E. Thompson of the Geological Survey. The sample was taken from a drill core at a depth of 180–181 feet in drill hole TR-713, which is in the NE$\frac{1}{4}$SE$\frac{1}{4}$ sec. 27, T. 52 N., R. 66 W., Crook County, Wyoming. This horizon is in a highly mineralized, unnamed siltstone member of the Lakota formation (Lower Cretaceous age), about 13 feet below the base of the Fuson member.* Spectrographic tests showed the presence only of vanadium and a minor amount of iron, and an *x*-ray powder diagram revealed a pattern hitherto unknown for a natural mineral. There was no possibility of making a chemical analysis of the mineral, and the only hope of discovering its constitution was through *x*-ray single-crystal studies. Fortunately, the crystals gave excellent Buerger precession patterns, at least in comparison with those usually given by vanadium oxide minerals. The outstanding feature of these patterns was the presence of a short crystallographic axis of 3.0 Å, as in montroseite and doloresite. The diffraction net normal to this axis gave a clearly resolved pattern of sharp spots as shown in Fig. 1*a*. This pattern consists of perfectly straight rows of spots, with an inter-row spacing

* The information concerning this core was kindly supplied by Miss Darlene N. Peacock of the Atomic Energy Commission.

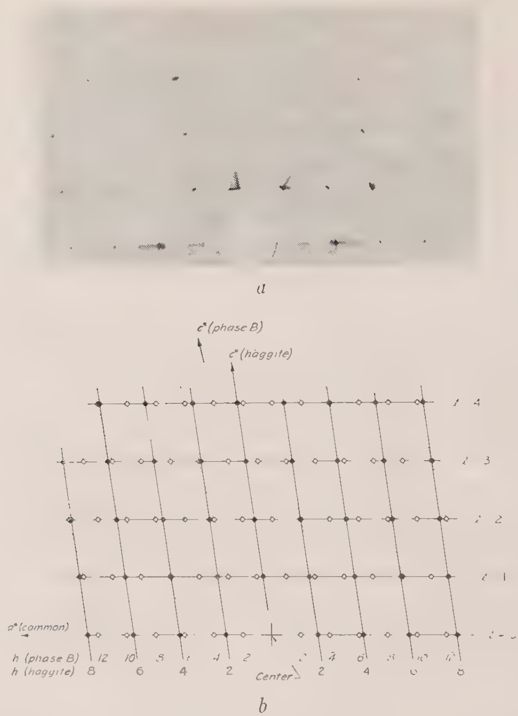

FIG. 1. *a*. Buerger precession photograph of $(h0l)$ net of a crystal from Carlile, Wyoming (MoKα radiation). *b*. Interpretation of *a*: full circles, full lines, häggite reciprocal lattice; open circles, dotted lines, phase B lattice.

corresponding to 4.83 Å; but the spots within the rows appeared to be irregularly arranged. It was found that the pattern could be accounted for in all detail in terms of two superimposed monoclinic lattices with equal and common b and c axes, but different a axes and β angles. Measurement of Buerger precession photographs of the $(hk0)$, and $(h0l)$ and $(h1l)$ nets gave the following dimensions for the two lattices, designated as shown:

	Phase A	Phase B
Space group	both $C2/m$, Cm or $C2$	
a	12.17 ± 0.05 Å	19.64 ± 0.06 Å
b	2.99 ± 0.01	2.99 ± 0.01
c	4.83 ± 0.02	4.83 ± 0.02
β	$98°15' \pm 5'$	$103°55' \pm 5'$
Vol.	173.9 Å^3	275.3 Å^3

The explanation of the $(h0l)$ net shown in Fig. 1*a* is shown graphically in Fig. 1*b*. The powder pattern of these crystals gave the data listed in

Table 1 wherein the identity of each line in terms of the lattice of phase A or B is indicated.

For the purpose of structure analysis, the intensities of the ($h0l$) reflections were measured on Weissenberg patterns by means of visual comparison with a calibrated strip made with one of the x-ray reflections. For phase A, 58 independent data were collected, and for phase B, 63 data. In only nine cases did reflections from the two lattices overlap seriously enough to prevent individual measurement. The pattern of phase A was always considerably stronger than that of phase B, presumably owing to its predominance in the crystal, so that it was expected that the data of phase A were the more reliable. These data were suitably corrected for the Lorentz and polarization factors, but not for absorption.

Crystal Structure Analysis of Häggite (Phase A)

Unit cell contents and structure

The geometry of the unit cells of phases A and B places severe limits on the contents of the unit cells. Of the chemistry, it was known only that the major constituents were limited to vanadium, oxygen and hydrogen. By analogy to montroseite and similar oxides (Evans and Mrose, 1955), it seemed proper to associate with the 3.0 Å spacing a structure consisting of chains of octahedra stretched along the b axis by sharing edges. In such a structure all atoms readily lie on mirror planes normal to the chain axis, so, partly for this reason, the space group was assumed to be $C2/m$. The volume of the cell will accommodate exactly 12 oxygen atoms of specific volume 17.4 Å^3. (In montroseite, the specific volume is 17.2 Å^3; Evans and Block, 1953.) In the space group $C2/m$, there must be an even number of atoms in the unit cell. In addition, the average valence of vanadium was assumed to be between three and four. With these restrictions, the following formulations of the unit cell contents are allowed:

I. $H_{14}V_2O_{10}$	V. $H_4V_4O_{10}$
II. $H_{12}V_2O_{10}$	VI. $H_2V_6O_{10}$
III. $H_8V_4O_{10}$	VII. V_6O_{10}
IV. $H_6V_4O_{10}$	

The structure of phase A was readily determined from the Patterson map, which is shown in Fig. 2a. In this map all the vectors characteristic of the double zig-zag octahedral chain (Fig. 2b) are easily recognized. With the knowledge of the presence of this structural feature and its orientation in the structure, it was soon determined, mainly from geometrical considerations, that the zig-zag chains are joined through the apices of the octahedrons into sheets extending parallel to the (001) plane. Structure factors for such an arrangement gave good agreement

TABLE 1. POWDER X-RAY DIFFRACTION DATA FOR BLACK VANADIUM OXIDE CRYSTALS FROM CARLILE, WYOMING

CuKα radiation; camera diameter 114.6 mm.; min. obs. d=12 Å.
d(calc.) given for häggite to 1.500 Å; for phase B to 2.50 Å

Phase B		Häggite (phase A)		Carlile crystals	
hkl	d(calc.)	*hkl*	d(calc.)	d(obs.)	I
200	9.52				
		200	6.02	6.04	4
		001	4.78	4.80	100
400	4.70				
001	4.69			4.73	3
$\bar{2}01$	4.68				
		$\bar{2}01$	4.04	4.05	50
201	3.85			3.87	3 (brd)
$\bar{4}01$	3.83				
		201	3.51	3.51	12
600	3.17			3.18	2
		400	3.01	3.02	25
401	3.00				
110	2.95				
601	2.95				
		110	2.90	2.91	3
		$\bar{4}01$	2.73	2.74	6
$\bar{1}11$	2.54				
021	2.52	$\bar{1}11$	2.52		
		111	2.443	2.44	25
		401	2.398		
		310	2.398		
		002	2.390	2.39	3
		$\bar{2}02$	2.340		
		$\bar{3}11$	2.221	2.22	3
		202	2.120	2.12	4
		311	2.073	2.071	3
		$\bar{4}02$	2.018		
		600	2.007	2.010	3
		$\bar{6}01$	1.954	1.959	18
		$\bar{1}12$	1.877	1.878	4
		510	1.875		
		511	1.817		
		112	1.814	1.815	12
		$\bar{3}12$	1.770	1.788	4
		601	1.763		
		402	1.754		
		$\bar{5}11$	1.684	1.686	6
		$\bar{6}02$	1.659	1.662	4
		312	1.625		
		$\bar{2}03$	1.598	1.600	3
		003	1.593		
		$\bar{5}12$	1.563	1.567	4
		800	1.505		
		$\bar{4}03$	1.500		
				1.492	12
				1.419	2
				1.400	3
				1.378	6
				1.347	3
				1.291	6
				1.199	3
				1.172	4

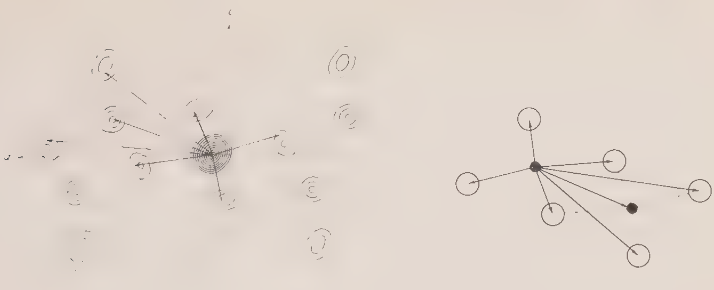

a *b*

FIG. 2. *a*. Patterson projection on (010) of häggite. *b*. Vectors of the double octahedral chain of montroseite.

with the observed amplitudes, and with three repeated calculations, the final electron density shown in Fig. 3 was obtained.

Hydrogen atoms

This result restricts the formulation to III, IV and V, leaving only the question of the number of hydrogen atoms present. This must, of course, be found by an indirect approach. The first indication comes from the presence of six short oxygen-oxygen distances of about 2.7 Å across the interlayer region of the structure. Crystal chemical principles require that such distances as these be associated with hydrogen bonds, so that we may thus account for six hydrogen atoms. To decide whether there are other hydrogen atoms present not involved in hydrogen bonding, we must attempt to estimate the distribution of electrons among the several vanadium-oxygen bonds. For this purpose, we may begin by dividing the three or four electron pairs associated with vanadium equally among the six oxygen ligands. This approach would lead us to suspect that O_1 is a hydroxyl group. Before accepting this conclusion, we must examine the vanadium-oxygen bond lengths to determine whether or not the bonding in the octahedron is actually uniform.

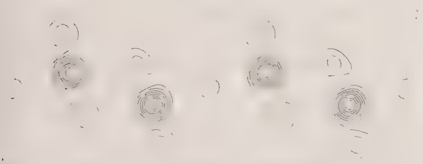

FIG. 3. Electron density projection on (010) of häggite. Dotted contour, zero electrons/A^2; contour interval, 5 electrons/A^2.

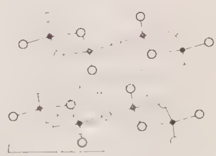

FIG. 4. Interatomic distances in häggite.

TABLE 2. STRUCTURE PARAMETERS FOR HÄGGITE (PHASE A)

Space group: $C2/m$, Int. Tab. No. 12

Atoms	x	y (cycles)	z	B (Å²)
4 V in (i)	0.1378 ± 0.0005	0	0.3967 ± 0.0012	4.16 ± 0.13
2 O_1 in (c)	0	0	$\frac{1}{2}$	5.87 ± 0.98
4 O_2 in (i)	0.6094 ± 0.0018	0	0.133 ± 0.004	4.90 ± 0.59
4 O_3 in (i)	0.3026 ± 0.0019	0	0.346 ± 0.004	5.14 ± 0.59

Crystal structure refinement

To obtain the best measurement of the bond lengths in phase A, the structure was refined by the method of least squares analysis. This calculation was carried out by hand methods in the early stages, and completed with a program written for the Burroughs 205 digital computer. The approximation was used in which the nondiagonal terms of the normal equations are neglected, as described in the case of montroseite (Evans and Mrose, 1955). The weighting factor was chosen according to the absolute value of F, as follows:

$$\text{for} \quad |F(\text{obs})| > 4|F(\text{min})|, \qquad \sqrt{w} = 4|F(\text{min})|/|F(\text{obs})|;$$
$$\text{for} \quad |F(\text{obs})| < 4|F(\text{min})|, \qquad \sqrt{w} = |F(\text{obs})|/4|F(\text{min})|.$$

Each atom was assigned an individual isotropic temperature factor. By this route, the reliability factor was reduced to $R = 0.143$. The observed and calculated structure amplitudes, F(obs) and F(calc), show good agreement.*

The final coordinates, temperature factors and corresponding standard deviations are given in Table 2. The interatomic distances, illustrated in Fig. 4, are listed in Table 3.

Vanadium-oxygen bonds

The six vanadium-oxygen bonds in the octahedron, as shown by Table 3, vary in length from 1.82 to 2.06 Å. This range must correspond to a considerable variation in bond number. In a discussion of the structure of vanadium pentoxide, Byström and Wilhelmi (1951) have shown that an approximation of the bond number of a vanadium-oxygen bond may be obtained from the empirical relation of Pauling (1947):

$$D_n - D_1 = -2k \log n$$

in which the constants $D_1 = 1.77$ Å and $k = 0.39$. (For metals Pauling uses $k = 0.300$.)

* A copy of the F(obs) and F(calc) values may be obtained from the authors.

TABLE 3. INTERATOMIC DISTANCES IN HÄGGITE (PHASE A)
(SEE FIG. 4)

Atoms	Vector	Distance Å	Atoms	Vector	Distance Å
V-O_1	A	1.82 ± 0.02	O_1-O_2	E	2.80 ± 0.03
V-O_2	B	1.97	O_1-O_3	F	2.84
V-O_3	C	2.01	O_2-O_3	G	2.59
V-O_3	D	2.06	O_2-O_3	H	2.85
			O_3-O_3	J	2.58
			O_2-O_3	K	2.69
V-V	P	3.15 ± 0.01	O_2-O_2	L	2.79
			O_1-O_2	M	3.49
			O_3-O_3	N	3.72

Evans (unpublished work) has found that for certain metavanadates whose structures are well refined, better consistency is obtained with $D_1 = 1.81$ Å. Applying this law to the vanadium-oxygen octahedron in phase A, the following distribution is obtained:

	D_n	n
V-O_1	1.82 Å	0.98
V-O_2(2)	1.97	0.63
V-O_3(2)	2.01	0.55
V-O_3	2.06	0.48
	Total n	3.82

From this result it is unsafe to deduce directly the valence of vanadium because of the large accumulative errors in n. The indication is clear, on the other hand, that the V-O_1 bond is close to a full single bond. Since O_1 receives two of these bonds, we may conclude that it cannot carry a hydrogen atom, and therefore does not represent a hydroxyl group.

Constitution of häggite

The distribution of bonds over the oxygen atoms is consistent with the hydrogen bonds located earlier, but does not admit the presence of any other hydrogen atoms in the unit cell. We are thus led to the unique formulation for phase A of IV above:

$$H_6V_4O_{10} \quad \text{or} \quad V_2O_3 \cdot V_2O_4 \cdot 3H_2O.$$

Further arguments in support of this composition are given in a later section. Phase A is thus established as a new mineral species. In honor of Professor Gunnar Hägg of the University of Stockholm and his inestimable contributions to our knowledge of crystal chemistry, we propose the name häggite for this mineral. It will be referred to by this name in the remainder of this paper.

Crystal Structure Analysis of Phase B

Unit cell contents and structure

The crystal structure of phase B was worked out in the same way as that of häggite. The unit cell volume will just accommodate 16 oxygen atoms of specific volume 17.2 Å³. Again assuming the space group to be $C2/m$ and the same restrictions to apply as for häggite, the possible formulations for phase B are the following:

VIII.	$H_{20}V_4O_{16}$	XIV.	$H_8V_6O_{16}$
IX.	$H_{18}V_4O_{16}$	XV.	$H_8V_8O_{16}$
X.	$H_{16}V_4O_{16}$	XVI.	$H_6V_8O_{16}$
XI.	$H_{14}V_6O_{16}$	XVII.	$H_4V_8O_{16}$
XII.	$H_{12}V_6O_{16}$	XVIII.	$H_2V_8O_{16}$
XIII.	$H_{10}V_6O_{16}$	XIX.	V_8O_{16}

The Patterson map for phase B, shown in Fig. 5, again shows the vectors of the double octahedral chain. Geometrical considerations based on this chain oriented as shown by the Patterson function quickly lead to the conclusion that there are also present single octahedron chains, with which the double chains are linked alternately by sharing octahedral apices as in häggite, to form sheets extending parallel to the (001) plane. Structure factor calculations indicated that such a model is a valid one, and finally led to the electron density map shown in Fig. 6. In this way the formulation of phase B was restricted to XI, XII, XIII or XIV. The electron density map shows the presence of 10 short interlayer oxygen-oxygen distances or hydrogen bonds. This evidence leads to formula XIII for phase B, unless evidence for the presence of additional hydrogen atoms not involved in hydrogen bonds is found.

Crystal structure refinement

The 63 ($h0l$) data for phase B were refined by the method of least squares analysis, just as for häggite. The final reliability factor was $R=0.164$. The structure parameters are given in Table 4. The interatomic distances, as shown in Fig. 7, are listed in Table 5. As expected the errors

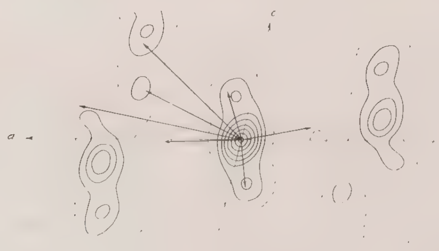

Fig. 5. Patterson projection of (010) of phase B.

TABLE 4. STRUCTURE PARAMETERS FOR PHASE B AND DOLORESITE

Space group: $C2/m$, Int. Tab. No. 12

Atoms	x	y (cycles)	z	B (Å²)
2 V_1 in (c)	0	0	$\frac{1}{2}$	2.26
4 V_2 in (i)	0.1766 ± 0.0007	0	0.3680 ± 0.0028	2.43
4 O_1 in (i)	0.470 ± 0.003	0	0.248 ± 0.012	5.47
4 O_2 in (i)	0.095 ± 0.004	0	0.427 ± 0.015	10.17
4 O_3 in (i)	0.665 ± 0.003	0	0.095 ± 0.012	5.17
4 O_4 in (i)	0.286 ± 0.003	0	0.362 ± 0.011	4.31

in these distances are larger than those obtained for häggite, because of the poorer quality of the measured data, but they are sufficiently small to permit some useful estimates of bond number to be made.

Vanadium-oxygen bonds

Applying Pauling's relation to this structure, the following bond distributions are found:

	D_n	n
V_1–O_1(4)	1.93 Å	.70
V_1–O_2(2)	1.98	.60
	Total n	4.00
V_2–O_2	1.70 Å	1.39
V_2–O_3(2)	1.97	.62
V_2–O_4(2)	2.01	.56
V_2–O_4	2.13	.39
	Total n	4.14

As in häggite, the oxygen atom which links the chains in the a-axis direction is joined to two vanadium atoms which supply it with a total valency of 1.99. It seems most probable that O_2 is not a hydroxyl group.

Constitution of phase B

By arguments simular to those used for häggite, it is concluded that the number of hydrogen atoms in the unit cell is 10, as a maximum. Thus, formulation XIII is the most probable composition of phase B:

$$H_{10}V_6O_{16} \quad \text{or} \quad V_2O_3 \cdot 2V_2O_4 \cdot 5H_2O$$

In this case, we must recognize the possibility that the number of hydrogen atoms is less, or 8 as a minimum. Phase B would then be identical with doloresite which corresponds to formula XIV, as described in the

FIG. 6. Electron density projection on (010) of phase B. Contours as in Fig. 3.

next section. The relationship between phase B and doloresite is discussed in a succeeding section.

Possible ordering of hydrogen bonds

In both häggite and phase B, it will be noted that one of the hydrogen bonds is bisected by a symmetry center. This bond cannot in fact be centrosymmetric, so that the formal definition of the structure must be qualified to account for this anomaly. It is certain that any one chain of hydrogen bonds, 3 in the chain in häggite, and 5 in phase B, must be polarized with all the hydrogen bonds oriented in one direction or the other along this chain. Following this postulate, two further relations among the hydrogen bonds may occur: (1) the polarizations of the separate hydrogen bond chains are oriented at random throughout the structure; and (2) the polarizations are oriented in a parallel or some antiparallel array. In the first case, the structure symmetry will be truly $C2/m$, and the structure parameters will be an average of the local positions assumed according to the orientation (instantaneous or permanent)

TABLE 5. INTERATOMIC DISTANCES IN PHASE B AND DOLORESITE (SEE FIG. 7)

Atoms	Vector	Distance Å	Atoms	Vector	Distance Å
V_1-O_1	A	1.93±0.07	O_2-O_1	G	2.72±0.10
V_1-O_2	B	1.98	O_2-O_1	H	2.81
V_2-O_2	C	1.70	O_1-O_1	J	2.44
V_2-O_4	D	2.01	O_4-O_4	K	2.60
V_2-O_3	E	1.97	O_4-O_2	L	2.77
V_2-O_4	F	2.13	O_2-O_3	M	2.79
			O_3-O_4	N	2.82
			O_4-O_3	P	2.57
V_2-V_2	W	3.23±0.02	O_4-O_3	Q	2.62
			O_3-O_1	R	2.79
			O_1-O_1	S	2.88
			O_2-O_3	T	3.52
			O_2-O_1	U	3.53
			O_1-O_1	V	3.75

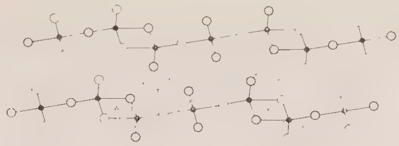

FIG. 7. Interatomic distances in phase B.

of the adjacent hydrogen bonds. The variations found in the temperature factors of the various oxygen atoms may be a result of this averaging process. In the second case, the space group symmetry of the structure would be lowered to *Cm*. Again, the observed temperature factors would be influenced by our procedure of refining the structure in terms of the more symmetrical space group. No attempt has been made to carry the refinement of the structures of häggite and phase B further in the space group *Cm*. Therefore, we cannot draw any conclusion as to which of the hydrogen bond arrangements, ordered or disordered, is actually present in these structures.

STRUCTURE OF DOLORESITE

Crystallography of doloresite

In the description of the brown, fibrous mineral doloresite by Stern, Stieff, Evans and Sherwood (1957), a brief account of the approach to the problem of chemical constitution and structure of this mineral has already been given. The crystal flakes give generally very poor diffraction patterns, partly because of their fibrous character, and partly because of the admixture of oriented paramontroseite. A specimen was finally obtained from the Monument No. 2 mine in Monument Valley, Arizona, which was relatively free of paramontroseite. A Buerger precession photograph of a net plane normal to the fibre axis (3.0 Å spacing), made with a crystal fragment from this specimen, is shown in Fig. 8*a*. Although the reflections are still somewhat diffuse, an orthorhombic lattice is clearly indicated. Measurement of this and other patterns leads to the following data:

Space group: *Im2m*

$a = 19.11$ Å

$b = 2.98$

$c = 4.86$

Vol. $= 277$ Å^3.

This unit cell proved to be false at a later stage when it was discovered that the lattice could be exactly accounted for in terms of the monoclinic

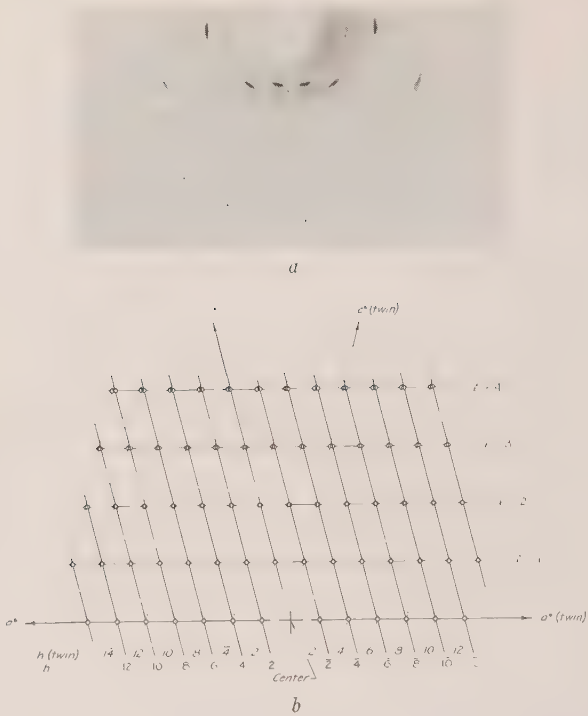

FIG. 8. *a*. Buerger precession photograph of $(h0l)$ net of doloresite, normal to fiber axis. *b*. Interpretation of *a*: full lines, primary reciprocal lattice; dotted lines, twin lattice. Note the orthorhombic symmetry of the photograph.

unit cell of phase B. If the phase B unit cell is transformed according to the matrix 101/010/001, its dimensions* are:

Space group: $I2/m$

$$a = 19.07 \text{ Å}$$
$$b = 2.99$$
$$c = 4.83$$
$$\beta = 90°18'$$

By twinning on (100), the apparently orthorhombic lattice is produced, as shown in Fig. 8*b*.

Early attempts to interpret the "orthorhombic" structure

Until work was begun on the crystals from Carlile, Wyoming, the presence of twinning in doloresite was not suspected. As explained in the

* This setting of the unit cell is, in fact, the conventional setting of Donnay and Nowacki (1957). The unit cell used in this paper is retained in order to simplify the description of the structures and their interrelationships.

Introduction, a concerted effort was made to solve the structure in terms of the false orthorhombic unit cell. It may be of interest to describe this work briefly, in order to illustrate the extent to which a completely blind lead can be followed, especially in the use of the Fourier method of structure analysis.

Intensities were measured for the $(h0l)$ and $(h1l)$ reflections on Weissenberg films by visual estimate and corrected for Lorentz and polarization factors. These data were used to prepare the Patterson section $P(u0w)$ (spurious, because the intensities measured were all twinned composites). It was known from the unit cell volume that the cell contained 16 oxygen atoms, but the number of vanadium atoms was taken as 4, 6 or 8 in various trials. It was quickly found that no arrangement of octahedra was possible in the space group *Immm*, so the symmetry was assumed to be *Im2m*. Several trial arrangements of the vanadium atoms were evolved compatible with the "Patterson" function. Each led to a recog-

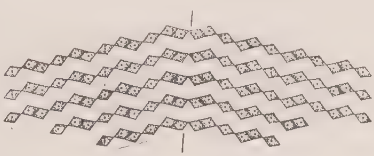

FIG. 9. Possible mechanism of twinning of doloresite, by a mirror operation.

nizable electron density projection. Only one showed any indication of oxygen atoms. This structure, the best of those tried, could not be refined to give a reliability factor lower than 0.35. The failure to find any structure that would refine beyond this point led us to abandon further work in this direction. Our experience with this problem provides a good example of the obliging nature of the Fourier method in crystal structure analysis, even when based on a completely erroneous crystallographic interpretation.

Verification of the true structure of doloresite

It has been noted that the geometry of the doloresite lattice corresponds to a phase B lattice twinned on (100). It was further found that the intensities of the $(h0l)$ reflections of doloresite, measured as indicated above, could be fully accounted for if it was assumed that each was the sum of the intensities of two reflections of the phase B lattice superimposed by the twin operation. After the refinement of phase B was completed, a set of structure factors was calculated using the final structure parameters obtained for phase B, but with an overall temperature factor of $B=4.0$ Å^2 instead of the individual temperature factors shown in Table 4. By combining these calculated F^2 values appropriately for the

twin composites and taking square root for comparison with the measured doloresite "F" values, a reliability factor of 0.098 was obtained. An attempt to refine the structure further in terms of the doloresite data did not lead to any significant change in the phase B structural parameters. The calculated and observed structure factors are in good agreement.

Crystal Chemical Relationship Between Montroseite and Doloresite

Twinning in doloresite

A universal property of the mineral doloresite is its submicroscopic lamellar twinning on (100). No crystals have ever been found which do not give perfect pseudo-orthorhombic diffraction patterns. It is of considerable interest to examine this twinning in terms of the crystal structure of doloresite, and its mode of origin. The usual mechanism of twinning makes use of some element in the structure which can play a common role in the original crystal and in the twinned counterpart which is related to it by some symmetry operation. In this case, as shown in Fig. 9, we may use the O_2 atoms as a twin "bridge" by passing a mirror plane through them parallel to the c axis. Such a mechanism is feasible, especially if a hydrogen bond is invoked to join oxygen atoms O_3 (distance 2.57 Å) across the twin plane. Such a fusion may actually be accomplished in several ways, to join two single octahedron chains, two double chains, or a single and a double chain, at the composition plane (which may or may not be a mirror plane).

Another mechanism is equally feasible, and is actually more plausible in light of the relationship of doloresite to its parent, montroseite. In Fig. 10 is shown an arrangement in which the double chain of one sheet in one crystal is joined to double chains in two sheets in the twin component.

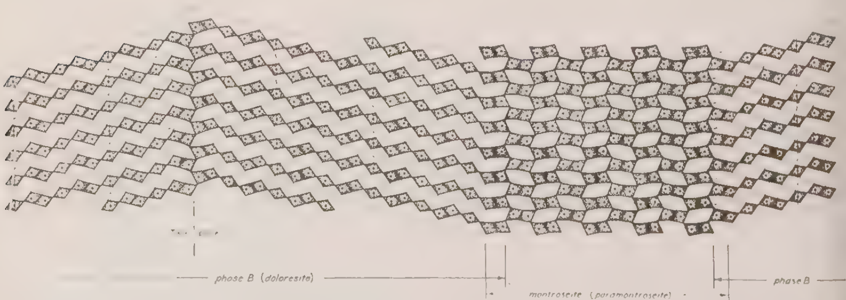

FIG. 10. Probable mechanism of twinning of doloresite, by a diagonal glide operation, shown at the left. Coalescence of the montroseite structure with the doloresite structure is shown in the two possible orientations at the right.

The two structures fit almost exactly in this way without strain. In fact, the arrangement of chains at the composition plane is almost identical with that found in the montroseite structure, illustrated to the right of Fig. 10. It can be derived by means of a diagonal glide plane parallel to the *b* and *c* axes in the twin composition plane, such as is characteristic of the montroseite structure parallel to the *a* and *c* axes.

Origin of doloresite

Doloresite is commonly found intimately associated with paramontroseite, and single-crystal photographs show that the two crystals are always in parallel orientation. The *b* and *c* axes of doloresite are found to be parallel to the *c* and *a* axes of paramontroseite, respectively. If the slab of structure at the composition plane (see Fig. 10) is considered to constitute a montroseite structure, its orientation is just that found for paramontroeseite with respect to the two doloresite twin components. It follows, of course, that the doloresite structure will coalesce with the montroseite structure, as shown in Fig. 10.

On the basis of the information gained from the structure studies so far, a mode of origin of doloresite may be proposed, as described below.

1. Doloresite, as shown by Stern *et al.* (1957), is derived by secondary replacement of primary montroseite.

2. On exposure to ground waters containing oxygen, montroseite is altered to phase B.

3. The alteration mechanism, unlike that of montroseite to paramontroseite, is partially reconstructive, and involves a shifting of positions of vanadium, oxygen and hydrogen atoms and introduction of new atoms, according to the reaction:

$$\underset{\text{montroseite}}{3(V_2O_3 \cdot H_2O)} + 2H_2O + O_2 \rightarrow \underset{\text{phase B}}{V_2O_3 \cdot 2V_2O_4 \cdot 5H_2O}$$

4. In spite of the reconstructive nature of the alteration, structural control is maintained between montroseite and phase B, as shown in Fig. 10.

5. As in the case of paramontroseite (Evans and Mrose, 1955), the formation of phase B is nucleated on a very fine scale throughout the mass of the montroseite crystal.

6. With respect to the original montroseite crystal, the phase B nucleus may form with equal probability in either of two orientations.

7. When two adjacent nucleii in opposite orientations grow toward each other and finally consume the intervening montroseite, they may be joined at the contact in a manner shown in Fig. 10. It is also possible that there will be no coherent structural boundary, since the twin orientations were determined by the original montroseite structure and not by a direct structural relation between the twins themselves at the composition plane.

8. The size of the twin crystallites or lamellae of phase B, as suggested by the diffuseness of the single-crystal patterns, is of the order 10^{-5} cm.

9. When the alteration of montroseite to phase B is halted, perhaps by exposure to air, it is rapidly altered to doloresite according to the reaction:

$$\underset{\text{phase B}}{V_2O_3 \cdot 2V_2O_4 \cdot 5H_2O} + \tfrac{1}{2}O_2 \rightarrow \underset{\text{doloresite}}{3V_2O_4 \cdot 4H_2O} + H_2O$$

10. At this stage, the remaining unreacted montroseite is converted to paramontroseite, according to the mechanism proposed by Evans and Mrose (1955).

Evans and Garrels (1959) have determined the conditions of formation and stability of many vanadium minerals in aqueous environments in terms of acidity (pH) and oxidation potential (E_h). In Fig. 11 we have suggested how their diagram may be further modified to include the new oxide phases described in this paper. The sequence of events described above is shown by means of arrows. This diagram also shows the relation

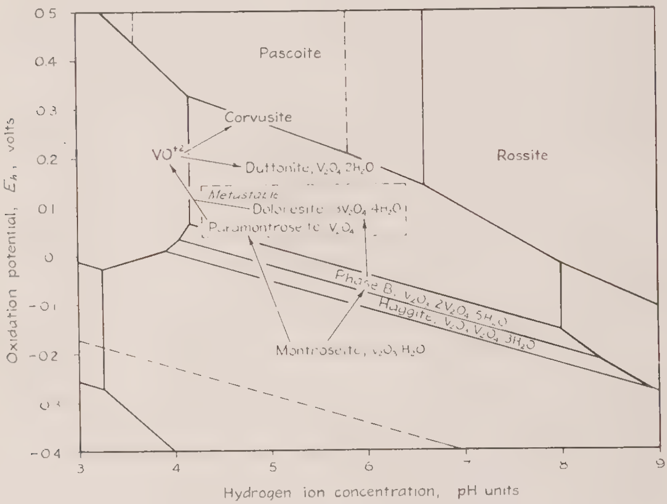

FIG. 11. Alteration sequences of montroseite to doloresite and higher oxides, shown on equilibrium diagram of Evans and Garrels (1959).

of these minerals to duttonite (Thompson, Roach and Meyrowitz, 1957) as it occurs at the Peanut mine, and to higher valence oxides ("corvusite") as it is found at most other localities.

It is important to remember in following the arguments set forth above that conclusive proof is not obtainable for every step. The weathering mechanism postulated and represented by the diagram presents what we feel is the most probable one in terms of all the accumulated evidence. The most uncertain aspect of the process is the change from phase B to doloresite. This question will be further discussed below.

ORIGIN OF HÄGGITE AND PHASE B

Intergrowth of häggite and phase B

As explained earlier, apparently single crystals from Carlile, Wyoming, were found to be an intimate intergrowth of two vanadium oxide phases, häggite and phase B. This situation is reminiscent of montroseite and

paramontroseite (Evans and Mrose, 1955), which were also found to be intergrown on a fine scale. In that case, the x-ray pattern for montroseite was found to be sharp, and for paramontroseite, diffuse. This was taken as evidence, together with other considerations, that the latter had been derived from the former by a solid state oxidation process. In the case of häggite and phase B, both superposed x-ray patterns are sharp. It is believed that a wholly different explanation must be sought for the existence of these two minerals.

Stability of häggite and phase B

An understanding of the mode of formation of the various oxides requires a knowledge of the stable phases under the various environments of oxidation potential and acidity. On the equilibrium diagram of Evans and Garrels (1959), only two lower-valence oxides appear as stable phases: montroseite ($V_2O_3 \cdot H_2O$) and duttonite ($V_2O_4 \cdot 2H_2O$). Paramontroseite was said by Evans and Mrose (1955) to be metastable, because of its unique mode of origin and the fact that it is unknown as a synthetic product. It is entirely possible, of course, that stable phases exist that have not previously been identified. Many such intermediate type phases have recently been discovered in the molybdenum-tungsten-oxygen system (Magnéli, 1956) and the titanium-oxygen system (Andersson, Collén, Kuylenstierna and Magnéli, 1957). Most of these phases have been proved by crystal structure study to be members of groups termed by Magnéli "homologous series," in which the average valence of the metal atom is slightly altered from one phase to the next. Thus, in the titanium-oxygen system, the homologous series denoted by the formula

$$Ti_nO_{2n-1}$$

is represented by known phases for which $n=4,5,6,7,8,9,10$ and ∞.

Häggite and phase B have structures which suggest the existence of a homologous series of the type:

$$H_{2n-2}V_nO_{3n-2}$$

In this series, häggite has $n=4$, phase B has $n=6$ and duttonite has $n=\infty$. For structural reasons, n must be even and cannot be less than 4, and montroseite is not a member of the series. The structural basis of this series is the combination in varying ratios of single and double octahedron chains (ratio $=n/2-2$) to form sheet structures as explained in the section on the structure of phase B. The relationship among these structures is shown in Fig. 12. In duttonite (Evans and Mrose, 1958) only single octahedron chains are present, and these are subject to distor-

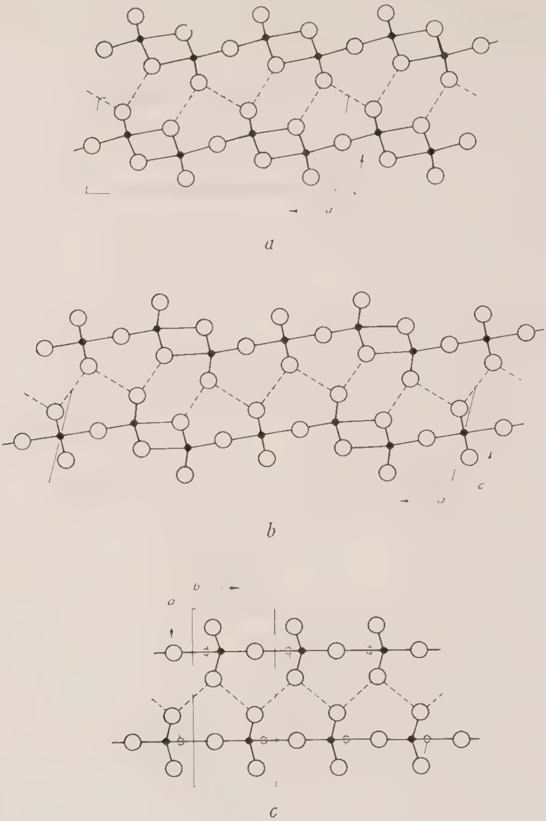

Fig. 12. Structures of the homologous series, (*a*) häggite, (*b*) phase B and (*c*) duttonite. Note hydrogen bond chains (dashed lines): 3 bonds (*a*), 5 bonds (*b*), and infinite (*c*) in length.

tions in the octahedral environment which have not been found in häggite and phase B.

Formation of häggite and phase B

It seems most probable that both häggite and phase B were formed as primary minerals in the sandstones at Carlile, Wyoming, from the mineralizing solutions. These oxides undoubtedly represent stable phases with narrow ranges in the oxidation potential variation between montroseite and duttonite. The minerals in this occurrence show no paramorphic relationship to other oxides such as montroseite. It may be imagined that the crystals grew in an environment in which the oxidation potential oscillated over a narrow interval bridging the stability ranges of häggite

and phase B. Under these conditions, the crystal may be expected to grow in an oscillatory manner, producing a crystal edifice consisting of fine lamellae of alternating häggite and phase B regions. These lamellae coalesce structurally at the interface in a natural way, as shown in Fig. 13, in a manner to produce a relative orientation just as found in the x-ray photographs.

Doloresite and Phase B ("protodoloresite")

Although doloresite and phase B have crystal structures so nearly identical that the difference between them cannot be detected, they have been treated in the previous sections as though they were distinct phases.

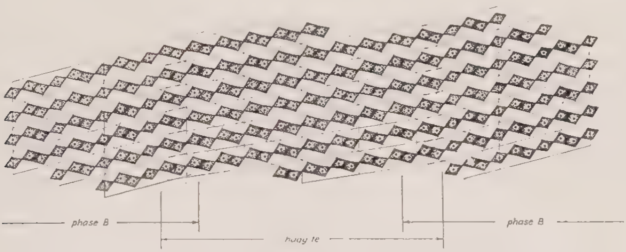

FIG. 13. Structural mechanism of intergrowth of häggite and phase B. Note parallelism of c axes of the two phases.

The reasons for this practice are partly structural, partly morphological and partly chemical in nature.

Definition of doloresite

As described in the section above on the structure of doloresite, the number of hydrogen atoms in the formula $H_nV_6O_{16}$ will have a maximum of 10, and a minimum of 8. In the description of doloresite by Stern *et al.* (1957), it was shown that chemical analyses of carefully prepared samples showed that V_2O_3 was present in insignificant amount. Mainly for this reason, the formula given for doloresite was $H_8V_6O_{16}$ or $3V_2O_4 \cdot 4H_2O$. On the other hand, other analyses made on doloresite have shown the presence of appreciable amounts of V_2O_3, but these samples were considered to contain admixed montroseite.

Hydrogen bonds and stable phases

There are sufficient hydrogen bond sites in the structure of doloresite to account for 10 hydrogen atoms in the formula. This formulation is that given to phase B, which, as explained in a previous section, is believed to be a member of a homologous series, and therefore, a stable

phase with a very narrow stability range. In doloresite, which is not a member of the postulated series, two of the ten possible hydrogen bonds are not occupied. No structural adjustments could be found tending to lengthen any of the oxygen-oxygen distances, but if the vacancies were distributed randomly over the ten hydrogen bonds, the corresponding structural changes would probably be so small as to escape detection by means of the limited diffraction data available.

We believe that doloresite is a metastable phase and bears the same relation to phase B as paramontroseite does to montroseite. It seems unreasonable that a stable tetravalent oxide hydrate phase could exist with such a complex structure, requiring as it does some special dispensation of the hydrogen atoms through disorder or other means. This reasoning is strengthened by evidence of the existence of this same structure with fully occupied hydrogen bonds as a stable phase. On the other hand, it is entirely reasonable to expect that phase B might undergo solid state oxidation by the loss of two hydrogen atoms per unit cell by a process of diffusion out of the structure, leaving the original structural framework intact. In the weathering diagram shown in Fig. 11, the transformation of phase B into doloresite would, therefore, be of the same type as that of montroseite into paramontroseite.

Phase B as a mineral species

Although we believe, as a result of the arguments given above, that phase B and doloresite are separate minerals, it is apparent that the evidence for their existence as distinct species is entirely circumstantial. Therefore, we are not in a position to define phase B as a valid species. If it should be possible at some later time to prove its existence, it would be proper to give it a name which indicates its relationship to doloresite, such as "protodoloresite."

Summary

A detailed crystal chemical study of the vanadium oxide hydrate minerals doloresite and häggite has been made. In this study, the following facts have been established:

1. In crystals from Carlile, Wyoming, two vanadium oxide minerals are intimately intergrown on a microscopic scale. These minerals have closely related monoclinic lattices which are oriented with respect to each other so that their *b* and *c* axes are parallel.

2. The crystal structure of both these intergrown phases has been determined. Application of crystal chemical principles has led to a formulation of their chemical constitution.

3. One of these phases is established as the mineral häggite. The

structure consists of double octahedron chains linked by octahedron corner-sharing into sheets parallel to the (001) plane, the sheets being tied together by hydrogen bonds.

4. The crystallography and crystal structure of the second phase (phase B) have been determined and found to be identical with that of doloresite within the limits of experimental error. The structure consists of double octahedron chains linked alternately with single octahedron chains in sheets parallel to (001), the sheets being tied together by hydrogen bonds.

From these facts and other associated information, the relationships among the various vanadium oxide hydrates (montroseite, paramontroseite, häggite, phase B, doloresite and duttonite) have been studied and interpreted. The following significant conclusions have been arrived at:

1. Häggite, phase B and duttonite form a homologous series of the type: $H_{2n-2}V_nO_{3n-2}$, with $n=4$, 6 and ∞ respectively. These phases are probably thermodynamically stable.

2. Doloresite is probably different from phase B, and has the formula $H_8V_6O_{16}$, corresponding to a pure quadrivalent oxide hydrate. It is believed to be metastable, like paramontroseite, and formed from phase B through the loss of two hydrogen atoms per unit cell.

3. Doloresite, was formed originally as phase B by secondary replacement of montroseite. This process is reconstructive but evidently occurs under the structural control of montroseite. Thus, any phase B nucleus formed is constrained to have one of two possible orientations with respect to the original montroseite crystal. The twinning of doloresite on a submicroscopic scale is thereby accounted for.

4. The lamellar intergrowth, with no evidence of twinning, of häggite and phase B in crystals from Carlile, Wyoming, is believed to be the result of oscillatory growth of the crystals from the original mineralizing solutions under conditions in which the oxidation potential varies over a narrow critical range.

Acknowledgments

Many persons have contributed to the accomplishment of the work described in this paper, which has extended over a period of several years. We wish especially to mention the assistance of A. D. Weeks, M. E. Thompson and T. W. Stern in acquiring and characterizing the materials on which the study was made. We are especially grateful to D. E. Appleman for assistance with the least squares analysis involving the use of the Burroughs 205 computer. All the work has been supported by the Division of Raw Materials and Division of Research of the U. S. Atomic Energy Commission.

References

Andersson, S., Collén, B., Kuylenstierna, U. and Magnéli, A. (1957), Phase analysis studies on the titanium-oxygen system: *Acta Chem. Scand.* **11**, 1641–1652.

Byström, A. and Wilhelmi, K.-A. (1951), The crystal structure of $(NH_4)_2Cr_2O_7$, with a discussion of the relation between bond number and interatomic distances: *Acta Chem. Scand.* **5**, 1003–1010.

Donnay, J. D. H. and Nowacki, W. (1957), Crystal Data: *Geol. Soc. Am. Memoir* No. **60**.

Evans, H. T., Jr., and Block, S. (1953), The crystal structure of montroseite, a vanadium member of the diaspore group: *Am. Mineral.* **38**, 1242–1250.

Evans, H. T., Jr. and Garrels, R. M. (1959), Thermodynamic equilibria of vanadium in aqueous systems as applied to the interpretation of the Colorado Plateau ore deposits: *Geochim. et Cosmochim. Acta*, **15**, 131–149.

Evans, H. T., Jr., and Mrose, M. E. (1955), A crystal chemical study of montroseite and paramontroseite: *Am. Mineral.* **40**, 861–875.

Evans, H. T., Jr., and Mrose, M. E. (1958), The crystal structures of three new vanadium oxide minerals: *Acta Cryst.* **11**, 56–57.

Magnéli, A. (1956), Some aspects of the crystal chemistry of oxygen compounds of molybdenum and tungsten containing structural elements of ReO_3 or perovskite type: *J. Inorg. and Nuclear Chem.* **2**, 330–339.

Pauling, L. (1957), Atomic radii and interatomic distances in metals: *J. Am. Chem. Soc* **69**, 542–553.

Stern, T. W., Stieff, L. R., Evans, H. T., Jr., and Sherwood, A. M. (1957), Doloresite, a new vanadium oxide mineral from the Colorado Plateau: *Am. Mineral.* **42**, 587–593.

Thompson, M. E., Roach, C. H., and Meyrowitz, R. (1957), Duttonite, a new quadrivalent vanadium oxide from the Peanut mine, Montrose County, Colorado: *Am. Mineral.* **42**, 455–460.

Manuscript received February 19, 1960.

THE AMERICAN MINERALOGIST, VOL. 45, NOVEMBER–DECEMBER, 1960

NEW OCCURRENCES OF TODOROKITE*

C. FRONDEL, U. B. MARVIN AND J. ITO, *Harvard University, Cambridge, Massachusetts.*

ABSTRACT

Chemical, x-ray and other data are given for todorokite, $(Mn, Mg, Ca, Ba, Na, K)_2Mn_5O_{12}\cdot 3H_2O$, from Charco Redondo, Cuba, Farragudo, Portugal, and Hüttenberg, Austria. Additional localities at Romanêche, France, Saipan Island, Bahia, Brazil, and Sterling Hill, New Jersey, are noted. Delatorreite of Simon and Straczek (1958) is identical with todorokite.

INTRODUCTION

We have identified todorokite, a manganese oxide mineral hitherto known only from Japan (Yoshimura, 1934), in manganese ore from the Charco Redondo district, Cuba, and in Museum specimens from six additional localities. Delatorreite, briefly mentioned as a new mineral in a publication by Simon and Straczek (1958) on the Charco Redondo deposit that appeared during the course of our work, is identical with todorokite. Our determination of this material as todorokite is based on a type specimen obtained by W. F. Foshag in 1946 in Japan and now deposited in the U. S. National Museum. Todorokite apparently is a widespread mineral and in the Charco Redondo deposit at least has been an important ore.

LOCALITIES

Charco Redondo, Cuba. The material from Charco Redondo is described in detail in an accompanying paper by Straczek, Horen, Ross and Warshaw (1960). Our specimens were obtained by T. C. Marvin in 1955 during a survey made for the Union Carbide Ore Company. In general they have a slightly divergent or exfoliate fine-columnar to fibrous structure (Fig. 1). The fibers range up to about 10 cm. in length. Fracture surfaces tend to be somewhat curved and show a weak silky sheen. The luster on surfaces broken across the fibrosity is dull. The color of the mineral is dark brownish black. The specific gravity as measured on small grains on the Berman balance varied between 3.1 and 3.4 and undoubtedly is low because of the fibrous structure. The hardness is low but could not be measured accurately. A chemical analysis of the mineral is cited in Table 1, and the x-ray powder data are given in Table 2 and Fig. 2.

Farragudo, Portugal. A stalactitic mass of todorokite (Fig. 1) was found in a small collection of secondary manganese minerals, chiefly crypto-

* Contribution from the Department of Mineralogy, Harvard University, No. 339.

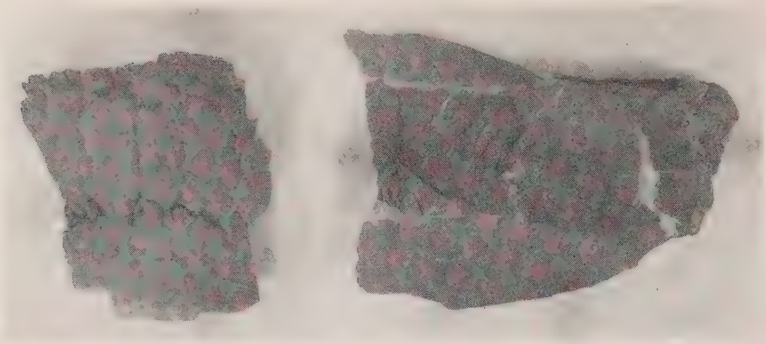

FIG. 1. Todorokite from Charco Redondo, Cuba (right) and from Farragudo, Portugal (left). About $\frac{1}{8}$ natural size.

melane, from this locality. The material is soft and porous, and shows the slightly divergent, long fibrous mode of aggregation and dark brown to brownish black color that appears to be typical of todorokite. A crude concentric layering is present and some of the inner layers have a dense

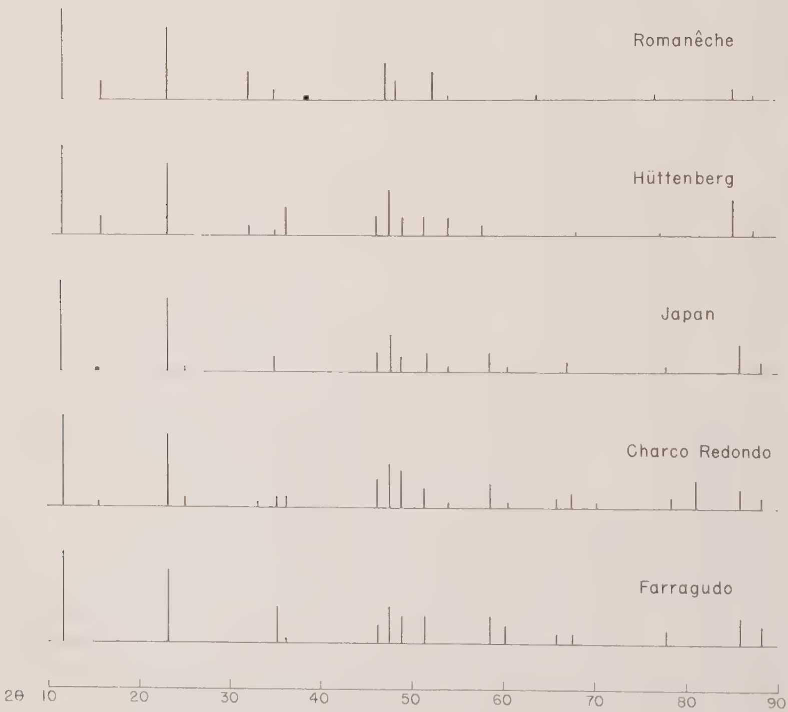

FIG. 2. Powder pattern diagrams.

TABLE 1. CHEMICAL ANALYSES OF TODOROKITE

	Farragudo	Charco Redondo	Hüttenberg	Japan (Yoshimura, 1934)
MnO_2	70.23	69.57	71.75	65.59
MnO	11.19	11.65	8.62	12.37
CaO	0.96	2.30	1.40	3.28
SrO*	~ 0.01	~ 0.05	~ 0.01	
BaO	0.00x	0.19	4.32	2.05
Li_2O*	~ 0.05	~ 0.001	~ 0.01	
Na_2O	1.16	1.14	0.17	0.21
K_2O	0.61	0.35	0.91	0.54
MgO	3.90	3.25	2.13	1.01
NiO*	~ 0.001	~ 0.05	~ 0.001	
CoO*	~ 0.01	~ 0.05	—	
CuO	0.001	0.01	0.001	
PbO*	~ 0.00x	~ 0.01	0.00x	
Al_2O_3	tr.	tr.	tr.	0.28
Fe_2O_3	0.01	tr.	0.02	0.20
SiO_2	0.68	0.27	0.23	0.45
SO_3	0.24	0.14	0.14	0.28
H_2O	10.50	10.83	9.95	11.28
Rem.	(Note 1)	(Note 2)	(Note 3)	(Note 4)
Total	99.73	100.16	99.89	99.24
		Molecular Quotients		
MnO_2	5.12	4.87	6.79	4.30
MnO	1	1	1	1
(Mg, Ca, Ba, Na, K)O	0.89	0.90	0.98	0.61
H_2O	3.69	3.66	4.55	3.10

Note 1. Rem. is P_2O_5 0.13, MoO_3 0.05, ZnO 0.00x, V_2O_5 0.00x, TiO_2 0.00x, Ag tr., As tr.
Note 2. Rem. is MoO_3 0.05, Sc_2O_3 tr., $(Y, Yb)_2O_3$ tr., Ag. tr., R_2O_3 0.26.
Note 3. Rem. is MoO_3 0.03, ZnO 0.00x, ZrO_2 tr., $(Y, Yb)_2O_3$ tr., R_2O_3 0.2.
Note 4. Rem. is P_2O_5 0.42, TiO_2 tr., insol. 1.28.
* Determinations by optical spectrograph.

structure and earthy luster. A chemical analysis is given in Table 1, and the x-ray powder data in Table 2 and Fig. 2.

Hüttenberg, Carinthia, Austria. This material comprised nodular masses about 5 cm. in diameter, without matrix, with an indistinct fibrous structure and coarse concentric layering. The material is very fragile and soft, falling to pieces when handled, and is so light and porous as to float on water. The color is brown, lighter in tone than that from Charco Redondo. The luster of fracture surfaces is dull, as in the other occurrences of todorokite, but the smooth outer surface of the nodules has a

TABLE 2. X-RAY POWDER DATA FOR TODOROKITE
Filtered iron radiation, in Angstroms

Farragudo, Portugal		Charco Redondo, Cuba		Todoroki Mine, Japan		Hüttenberg, Austria		Romanèche, France	
I	*d*	I	*d*	I	*d*	I	*d*	I	*d*
10	9.56	10	9.60	10	9.68	10	9.60	10	9.58
		¼ d	7.13	¼ d	7.15	3	7.02	2	6.98
8	4.80	8	4.80	8	4.80	8	4.79	8	4.79
——		1 d	4.45	½ d	4.45	——		——	
——		——		——		1	3.48	3	3.48
——		½ d	3.40	——		——		——	
4	3.19	1	3.20	1½	3.22	½	3.21	1	3.22
½	3.11	1	3.10	——		3	3.10	——	
——		——		——		——		½ d	2.98
——		——		——		——		½ d	2.88
2	2.46	3	2.46	2	2.46	2	2.46	——	
4	2.40	5	2.40	4	2.39	5	2.40	4	2.41
3	2.34	4	2.34	1½	2.34	2	2.33	2	2.36
3	2.23	2	2.23	2	2.22	2	2.23	3	2.19
		½ d	2.13	½ d	2.15	2	2.15	¼	2.15
3	1.98	2	1.98	2	1.98	1	2.00	——	
2	1.93	½	1.92	½	1.92	——		——	
——		——		——		——		½	1.83
1	1.78	1	1.78	——		——		——	
1	1.74	1	1.74	1	1.75	¼ d	1.73	——	
——		½	1.68	——		——		——	
1	1.54	1	1.53	½	1.54	1	1.55	½	1.56
——		3	1.49	——		——		——	
3	1.42	2	1.42	3	1.42	4	1.43	1	1.43
2	1.39	1	1.39	1	1.39	½	1.40	¼	1.40

d = diffuse line.

faint bronzy appearance. A few thin intercalated layers of a black dense mineral were identified by *x*-rays as pyrolusite. A chemical analysis of the mineral, cited in Table 1, shows it to be relatively high in Ba. The *x*-ray powder data are given in Table 2 and Fig. 2. Meixner (1957) notes that a soft "wad" occurs at Hüttenberg together with hard, black coatings of secondary manganese minerals that probably include cryptomelane and hollandite.

Saipan, Mariana Islands, Pacific Ocean. This material was identical in form of aggregation and color with that from Charco Redondo. It is relatively brittle and hard, however, because it is intimately admixed with finely divided silica. Although the mineral appears homogeneous to the eye, grains when leached with acid leave a skeleton of silica amounting

in some instances to 50 per cent of the sample or more. Efforts to remove the silica by treatment with heavy liquids were not successful and a chemical analysis was not undertaken. A semi-quantitative spectrographic analysis revealed that Mg was present in amounts greater than Ba and Ca. Small deposits of unidentified manganese oxides have been mined on Saipan and their geology has been described by Cloud, Schmidt and Burke (1956).

Romanêche, France. A Museum specimen from this locality showed a hard, black crust of "romanechite" (=psilomelane) that inwardly was porous and cavernous. Some of the openings were filled with soft brown aggregates of fibrous todorokite. *X*-ray data for this mineral are given in Table 2 and Fig. 2. The *x*-ray pattern resembles that of the barium-rich todorokite from Hüttenberg in that it has a definite line rather than a diffuse darkening at about *d* 7.1 Å. The summary description by Lacroix (1910) of romanechite from Romanêche mentioned soft to porous fibrous varieties that probably refer in part to todorokite.

Sterling Hill, New Jersey. Todorokite was identified in a small collection of secondary manganese oxides from the old surface workings at the south end of the orebody at this place (Palache, 1935). The todorokite forms soft, dark brownish black masses with a confused leafy-fibrous structure. It occurs associated with chalcophanite and secondary calcite crystals in altering franklinite-willemite ore. Efforts to separate the todorokite from admixed chalcophanite were unsuccessful and a chemical analysis was not made.

Bahia, Brazil. We have also identified todorokite by *x*-ray means as a rare constituent of the manganese oxide deposits at Saude and at Urandi, Bahia. The deposits of both areas are largely the result of supergene enrichment of metamorphic country rock containing spessartite and other manganese minerals.

Optical Properties

Under the microscope the mineral is dark brown in color and is not well suited for optical study; all but the thinnest grains are opaque. It appears as irregular, flattened shreds and as minute cleavage flakes, rarely also as irregular laths and then apparently with parallel extinction on both the flattening and perpendicular thereto. Cleavage flakes and laths are not pleochroic; on edge the laths are pleochroic in brown with the long direction dark brown to opaque. The intensity of the pleochroism varies from faint to strong in material from different localities. The indices of refraction were observed to be over 2.00. According to Yoshimura (1934) the mineral from Japan is lath-like, flattened on (010) and elongated [001] with terminal edges inclined ca. 60° and 70° to [001].

Cleavages on (100) and (010). He states that Y = *b* with Z near or parallel [001] and absorption Z > X. Our sample of the Japanese material conformed to the description first given above, although it was relatively dark colored and had a tendency to break into needles rather than into laths or plates.

Thermal Behavior

DTA graphs of analyzed material from Charco Redondo, Hüttenberg and Farragudo showed an endothermal peak at about 625° C.; the Hüttenberg material showed an additional endothermal peak at about 980°. *X*-ray study of samples that had been heated in air to temperatures above and below 625° showed that the mineral breaks down near that temperature to hausmannite, Mn_3O_4, together with small amounts of unidentified decomposition products that presumably contain the Ba, Mg, and Ca reported in the chemical analyses.

X-ray Powder Data

The *x*-ray powder spacing data for the original todorokite from Japan and for the three analyzed specimens from Charco Redondo, Farragudo, and Hüttenberg are given in Table 2 and Fig. 2. The patterns were recorded in iron radiation on both film in a 114 mm. diameter camera and by the diffractometer (chart) method. The film data, slightly superior to that obtained from charts, is here given. The *x*-ray patterns show little variation other than in the relative intensity of certain lines, notably at *d* 7.1 Å.

Chemical Composition

Chemical analyses of the todorokite from Charco Redondo, Hüttenberg, and Farragudo are cited in Table 1 together with the original analysis of the Japanese material. These analyses (and those reported in an accompanying paper by Straczek, Horen, Ross and Warshaw (1960)) do not permit a straightforward interpretation. This is often found to be the case with the complex manganese oxides. The crystal chemistry of these minerals generally involves both the coupled substitution of ions of unlike valence in one or more cation positions and valence-coupled omissions, and a satisfactory answer usually is not obtained until the crystal structure is worked out. The ratios of the Charco Redondo and Farragudo material suggest that the idealized formula contains a total of 7 cations and 12 oxygen ions, probably as

$$(Mn^{2}, Mg, Ca, Ba, K, Na)_2Mn^{4}{}_5O_{12}\cdot 3H_2O$$

The amount of water present does not appear to be less than $3H_2O$ and may be greater. The SiO_2, Fe_2O_3, Al_2O_3, SO_3, and P_2O_5 reported in the

analyses may be due to admixture. The Hüttenberg material is relatively high in Mn^4, perhaps due to a small admixture of pyrolusite. The ratios of the analysis of the original todorokite from Japan depart relatively widely from the formula suggested, and the formula (Mn, Ba, Ca, Mg) $Mn_3O_7 \cdot H_2O$ has been proposed, but the sample analyzed evidently was rather impure since it contained a total of 2.43 per cent insoluble, P_2O_5 SO_3, and SiO_2.

The formula suggested here for todorokite is analogous to that earlier obtained for woodruffite, $(Zn, Mn)_2Mn_5O_{12} \cdot 4H_2O$, by Frondel (1953). This mineral appears from x-ray study to be isostructural with todorokite.

References

P. E. Cloud, Jr., R. G. Schmidt, H. W. Burke (1956). Geology of Saipan, Mariana Islands. Part 1: General Geology. U. S. Geol. Surv. Prof. Pap. **280-A,** 119.

C. Frondel (1953). New manganese oxides: hydrohausmannite and woodruffite. *Am. Min.*, vol. **38,** 761.

A. Lacroix (1910). *Minéralogie de la France*, vol. 4, 6.

H. Meixner (1957). Die Minerale Kärntens, Klagenfurt. Part 1, 49.

C. Palache (1935). The minerals of Franklin and Sterling Hill, Sussex County, New Jersey. U. S. Geol. Surv. Prof. Paper **180**.

F. S. Simons and J. A. Straczek (1958). Geology of the manganese deposits of Cuba. *U. S. Geol. Surv. Bull.* **1057**.

J. A. Straczek, A. Horen, M. Ross and C. M. Warshaw (1960). Studies of the manganese oxides, IV. Todorokite, *Am. Min.*, **45,** 1174.

T. Yoshimura (1934). Todorokite, a new manganese mineral from the Todoroki mine, Hokkaido, Japan. J. Fac. Sci. Hokkaido Imp. Univ., Ser. 4, Vol. 2, 289.

Manuscript received March 3, 1960.

STUDIES OF THE MANGANESE OXIDES. IV. TODOROKITE*

J. A. Straczek,† Arthur Horen,‡ Malcolm Ross,§ and Charlotte M. Warshaw,|| *U. S. Geological Survey, Washington, D. C.*

Abstract

Todorokite is a very abundant manganese oxide mineral in many deposits in Cuba and has been noted from other localities. Six new analyses are given; they lead to the approximate formula

$$(Na, Ca, K, Mn^{+2})(Mn^{+4}, Mn^{+2}, Mg)_6O_{12}\cdot 3H_2O.$$

Electron diffraction data show the mineral to be orthorhombic, or monoclinic with β near 90°. The x-ray powder pattern is indexed on a cell with $a=0.75$A, $b=2.84_9$A, $c=9.59$A, $\beta=90°$. A differential thermal analysis curve is given.

Introduction

From 1940 to 1945, the U. S. Geological Survey made a study of the manganese deposits of Cuba and especially those in Oriente Province. Several preliminary reports were published and the results were summarized in papers by Lewis and Straczek (1955) on the geology of south-central Oriente and by Simons and Straczek (1958) on the geology of the manganese deposits of Cuba. The latter paper describes the deposits, but gives only a sketchy account of the mineralogy of the manganese oxides, which was known incompletely although a considerable amount of x-ray data had been accumulated.

The present paper deals with a manganese oxide mineral, whose x-ray pattern was recognized as being distinctive in 1941 and which was designated for some years as "Mineral T." X-ray studies by J. M. Axelrod from 1946 to 1948 showed that this mineral was an abundant constituent of the ores at many localities in Oriente Province, but that it was so intergrown with other minerals that the preparation of samples pure enough to warrant chemical analysis was extremely difficult. The best five samples were finally selected and their analysis was completed in 1952. At that time, it was learned that Arthur Horen, who had made a field study of the manganese ores of the Charco Redondo-Taratana district in 1951–1952, had also identified the same material by x-ray study at Harvard

* Publication authorized by the Director, U. S. Geological Survey.

† Present address—Union Carbide Ore Company, 30 East 42nd Street, New York 17, New York.

‡ Present address—Universal Atlas Cement, 100 Park Avenue, New York 17, New York.

§ U. S. Geol. Survey, Washington, D. C.

|| Present address—Pennsylvania State University, University Park, Pennsylvania.

University, and it was decided to publish the results jointly. At about this time, the mineral was named delatorreite in honor of Carlos de la Torre y de la Huerta (1858–1950), eminent Cuban paleontologist. The name has frequently been used since within the U. S. Geological Survey and unfortunately appeared in print (Simons and Straczek, 1958, p. 66) without a description of the mineral, before the identity with todorokite (Yoshimura, 1934) had been established by Frondel, Marvin, and Ito. See preceding article, p. 1167. The name delatorreite should now be dropped.

Changes in assignments for several of the authors plus frequent absences abroad for one of us have long delayed publication of our results. We had hoped to do more work on the mineral, but in view of its abundance and widespread distribution, it seemed best to present our data now.

Occurrence and Origin

Todorokite has been found at many mines in Oriente Province, Cuba, and is one of the dominant manganese oxide minerals at the Charco Redondo, Taratana, Ponupo, and Quinto mines; probably many thousands of tons of it have been mined. Commonly associated minerals are pyrolusite, cryptomelane, manganite, psilomelane (including a very poorly crystalline variety), quartz, feldspar, and calcite. A list of localities in Oriente Province is given in Table 1; the page numbers refer to the descriptions of the deposits in Simons and Straczek (1958).

Table 1. Occurrences of Todorokite in Oriente Province, Cuba

Mine	Name of workings, shafts, or pits	Reference Simons and Straczek, 1958 (pages)
Boston mine		158–161
Quinto mine		167–170
Charco Redondo	Socias, Marinez, Unitoria, K-1, K-6, Gutierrez Batey, No. 1, KX	185–191
Lucia mine		192–194
Taratana mine	Canada, Lego	195–198
Guanaba mine		202–204
Sorpresa mine		213
Manacas District		213–215
Fortuna mine		220
New York mine		226–227
Yeya mine		235–237
Abundancia mine		238–240
Ponupo mine	W., Center, and E. Sultana, No. 3, Juanita	243–256
Ponupo de Manacal		264–268

In addition, todorokite has been identified by x-ray study in the laboratories of the U. S. Geological Survey as a constituent of ores from the Embreeville mine, Embreeville, Tennessee; the Lucifer mine, Baja California, Mexico; the Nsuta mine, Ghana, Africa; and the Taxud area, Philippines, also as a constitutent of incrustations from Bikini Atoll and of a deep-sea nodule from the Pacific, from near Cadiz Dry Lake, California, and as a coating on colemanite from Furnace Creek, Death Valley, California.

The manganese ores at the Cuban localities are interbedded with volcanic tuff, now largely altered to montmorillonite clays, and with jasper (bayate), and limestone. At Charco Redondo the "delatorreite" is commonly the matrix for limestone and tuff and in part replaces them. It has commonly crystallized around kernels of tuff. The bayate occurs in lenses ranging in thickness from an inch or two to as much as a foot. It consists of rounded quartz spherulites in a ferruginous matrix; the spherulites range in size from a micron to several tenths of a millimeter and commonly show growth banding with silica alternating with layers of hydrous (?) iron oxides. The contact between the bayate and the massive todorokite is usually, but not always sharp, and there was no definite evidence of either replacing the other. Both were, however, cut by crystalline quartz, commonly amethystine, which lines vugs and contains shreds of bayate and inclusions of manganite or pyrolusite. The last mineral formed was rhombohedral calcite, which occurs in veins and perched on the vuggy quartz.

The todorokite has been altered near the surface and along faults or fissures to pyrolusite, and perhaps to manganite.

The origin of these deposits is discussed at some length by Simons and Straczek (1958, p. 103–110), who conclude that the source of the manganese was probably hot springs. Horen believes the deposits to be of marine sedimentary origin. In contrast, the type todorokite from the Todoroki mine in Hokkaido, Japan, was believed by Yoshimura (1934) to have been formed by late-stage hydrothermal solutions altering inesite.

Physical Properties

Todorokite from Cuba commonly occurs as columnar aggregates, but is also found as fine fibers and as irregular masses. The color and streak are brownish-black to dark brown; comparison by J. J. Fahey with Ridgway's Color Standards of the analyzed samples nos. 1–4 showed two matching dusky purplish gray and two matching sooty black. The apparent hardness is low, the material breaking into fibers; the true hardness is not known. Specific gravity measurements by Horen of six samples on the Berman balance gave an average of 3.49; four pycnometer de-

TABLE 2. ANALYSES OF "DELATORREITE" FROM CUBA AND TODOROKITE FROM JAPAN

	1	2	3	4	5	6	7
MnO_2	72.37	72.15	68.46	71.61	67.86	67.19	65.59
MnO	10.04	8.87	10.70	10.16	11.24	14.56	12.37
CaO	2.57	1.52	2.13	2.66	5.51	2.03	3.28
SrO	0.60	0.24	0.13	0.53	0.92	—	—
BaO	1.05	0.20	0.40	0.18	0.54	0.14	2.05
Na_2O	1.30	1.23	1.44	0.85	1.45	1.34	0.21
K_2O	0.24	0.48	0.75	1.48	0.06	0.43	0.54
MgO	1.04	3.51	3.22	1.58	0.88	3.13	1.01
CoO	—	0.02	0.18	—	—	0.23	—
CuO	tr	tr	0.44	tr	0.02	—	—
Al_2O_3	0.46	0.14	0.19	0.12	0.25	—	0.28
Fe_2O_3	0.06	0.06	0.07	0.06	0.18	—	0.20
SiO_2	0.95	0.24	0.41	0.64	0.64	0.14	1.73[a]
H_2O^-	8.80	10.61	10.99	9.03	9.47	10.69	1.56
H_2O^+							9.72
Others	—	—	—	—	—	—	0.70[b]
	99.48	99.27	99.51	98.90	99.02	99.88	99.24
Active O	13.31[c]	13.25[c]	12.60[c]	13.12[c]	12.49[c]	12.07	—
G	3.82	3.66	3.68	3.78	—	—	3.67

[a] Includes SiO_2 0.45, insol. 1.28%.
[b] Includes P_2O_5 0.42, SO_3 0.28, CO_2 tr., TiO_2 tr.
[c] Average of 2 determinations.

Analyses 1–5 by C. M. Warshaw; SrO in CaO by W. W. Brannock and E. A. Nygaard with flame photometer; SrO in BaO by K. J. Murata and R. S. Harner spectrographically; alkalies by W. W. Brannock with flame photometer; Fe_2O_3 colorimetrically by S. M. Berthold; cobalt by L. E. Reichen polarographically. Analysis 6 by F. A. Gonyer, Harvard University; analysis No. 7 from Yoshimura (1934).

Sample descriptions

Nos. 1–5. Collected by J. A. Straczek; No. 1 from Quinto, shown by x-ray study to contain a trace of pyrolusite; No. 2 from Tarantana; No. 3 from Charco Redondo, contains a trace of calcite; No. 4 from Guanaba, contains a small amount of cryptomelane; No. 5 from Ponupo; the x-ray pattern shows some weak unidentified lines; No. 6 collected by Arthur Horen from Charco Redondo, Batey No. 1 shaft.

terminations by Fahey and one by Yoshimura (Table 2) gave 3.66–3.82; the higher values by pycnometer are to be expected for such fibrous material.

CHEMISTRY

Analyses of six samples from Cuba are given in Table 2 along with the analysis of todorokite from Japan (no. 7). Spectrographic analysis of Nos. 1–5 by K. J. Murata showed the following:

Mo—.0X in samples 1, 2, and 4, 0.00X in 3 and 5
V and B—.0X in samples 1 and 5, .00X in 2 and 3
Ni—.0X in samples 2, 3, and 5, .00X in 4, .000X in 1
Cu—0.X in samples 3, .0X in 5, .00X in 4, .000X in 1 and 2
Co—0.X in samples 3, .0X in 2, .00X in 1, 4, and 5
Ti—.00X in samples 1, 2, and 5, .000X in 3 and 4

Not found—Ag, As, Au, Be, Bi, Cd, Cr, Ga, Ge, In, La, Li, Nb, P, Pb, Pt, Re, Sb, Sc, Sn, Tl, W, Y, Zn.

Analyses 1–7 (Table 2) were recalculated, neglecting SiO_2, Al_2O_3, Fe_2O_3, P_2O_5, and SO_3; it is possible that these are not actually impurities. For analysis 7, H_2O^+ was taken, for the others total H_2O. From the unit cell dimensions obtained by Ross, formulas with O=11 or O=12 (not including H_2O) seemed possible. The results are given in Tables 3 and 4.

TABLE 3. ANALYSES OF TODOROKITE RECALCULATED

No.	Ca[a]	Na	K	ΣX	Mn^{+4}	Mn^{+2}	Mg[b]	ΣY	ΣX +Y	H_2O	Mol. wt.
					For O=11.0						
1	0.33	0.24	0.03	0.60	4.78	0.81	0.15	5.34	5.94	2.81	563
2	0.17	0.23	0.05	0.45	4.74	0.71	0.50	5.95	6.40	3.36	564
3	0.25	0.27	0.09	0.61	4.59	0.88	0.51	5.98	6.59	3.56	576
4	0.31	0.16	0.18	0.65	4.74	0.82	0.23	5.79	6.44	2.88	564
5	0.64	0.27	0.07	0.98	4.56	0.93	0.13	5.62	6.60	3.00	576
6	0.22	0.25	0.05	0.52	4.49	1.19	0.47	6.15	6.67	3.44	579
7	0.44	0.04	0.08	0.55	4.64	1.07	0.15	5.86	6.41	3.32	583
					For O=12.0						
1	0.37	0.26	0.03	0.66	5.22	0.89	0.16	6.27	6.93	3.06	614
2	0.19	0.25	0.06	0.50	5.17	0.78	0.54	6.49	6.99	3.67	615
3	0.27	0.30	0.10	0.67	5.01	0.96	0.57	6.54	7.21	3.88	629
4	0.34	0.17	0.20	0.71	5.17	0.90	0.25	6.32	7.03	3.14	615
5	0.71	0.30	0.08	1.09	4.98	1.01	0.14	6.13	7.22	3.35	628
6	0.24	0.27	0.06	0.57	4.89	1.30	0.51	6.70	7.27	3.76	632
7	0.48	0.05	0.08	0.61	5.06	1.17	0.17	6.40	7.01	3.62	636

[a] Including Sr and Ba.
[b] Including Co and Cu.

The measured specific gravities, as shown in Table 4, do not agree well with those calculated on either assumption. They are lower than those calculated for O=12; because measured specific gravities tend to be low, the formulas in Table 3 calculated on the basis O=12 seem more probable. The formula of the mineral might then be written as

$$(Ca, Na, K)_{0.5-1.1}(Mn^{+4}, Mn^{+2}, Mg)_{6.1-6.7}O_{12}\cdot 3H_2O.$$

TABLE 4. CALCULATED AND MEASURED SPECIFIC GRAVITIES OF TODOROKITE

No.	G (calcd. for O=11)	G (calcd. for O=12)	G (measured)
1	3.49	3.81	3.82
2	3.49	3.81	3.66
3	3.57	3.90	3.68
4	3.49	3.81	3.78
5	3.57	3.89	—
6	3.59	3.91	—
7	3.61	3.94	3.67
Average	3.54	3.87	3.72

It will be noted that the sum of the cations is close to 7; if sufficient Mn^{+2} is taken to occupy Ca positions, the formula might alternatively be written as

$$(Ca, Na, Mn^{+2}, K)(Mn^{+4}, Mn^{+2}, Mg)_6O_{12}\cdot 3H_2O.$$

The Mg might also be placed with the first group. All the analyses, including No. 7 for which H_2O^- was determined, show more than $3H_2O$; presumably some of this in the first six analyses is H_2O^-.

Woodruffite (Frondel, 1953), which is probably isostructural with todorokite, was assigned the formula $(Zn, Mn^{+2})_2\ Mn_5{}^{+4}O_{12}\cdot 4H_2O$; here again the sum of the cations is 7.

ELECTRON MICROSCOPE AND ELECTRON DIFFRACTION DATA ON "DELATORREITE"

Electron micrographs of analyzed samples (Nos. 1–5, Table 2), show the crystals to be thin plates flattened on {001}. Many of the plates are broken into narrow laths or blades which are elongated parallel to the *b* axis (Figs. 1, 2). It appears as though the crystals have two perfect cleavages parallel to {001} and {100}.

All five samples give identical electron diffraction patterns. The electron diffraction single crystal pattern (superimposed on the todorokite powder pattern) shown in Fig. 3, gives the dimensions of the unit cell within the basal plane (within the plane of the plate). The single crystal pattern is indexed as shown in Fig. 4.

Measurement of the electron diffraction patterns of "delatorreite" yield: $a=9.75$ Å, $b=2.84_9$ Å and $S=90°$. The *x*-ray powder pattern of "delatorreite" shows lines at 9.6 Å, 4.77_1 Å, 3.19 Å, and 2.398 Å suggesting strongly that the spacings in the c-direction (basal reflections) are $0.59/n$ Å, where n is the order. The above data indicate that "delatorreite" is orthorhombic or monoclinic with $a=9.75$ Å, $b=2.84_9$ Å, and $c \sin \beta=9.59$ Å. The *x*-ray powder pattern can be indexed assuming an orthorhombic cell ($\beta=90°$), as shown in Table 5.

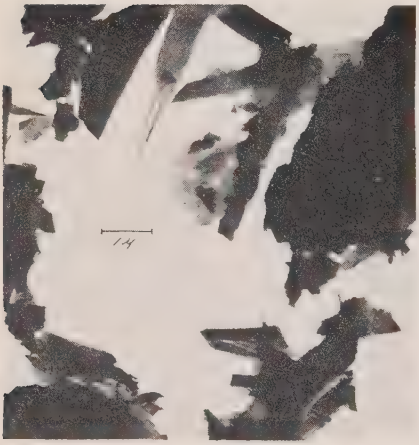

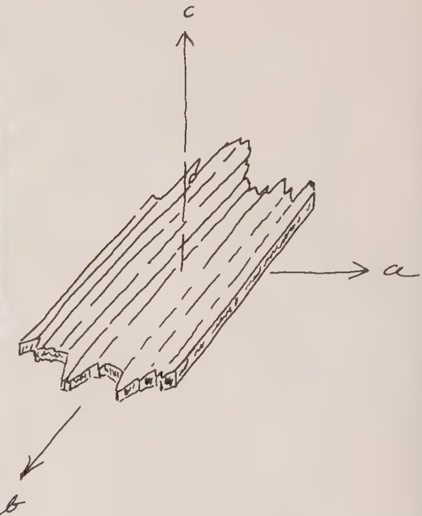

FIG. 1. (Left) Electron micrograph of todorokite.

FIG. 2. (Right) Sketch of a typical crystal of todorokite, showing plate flattened on (001) and broken into thin blades elongated along [010].

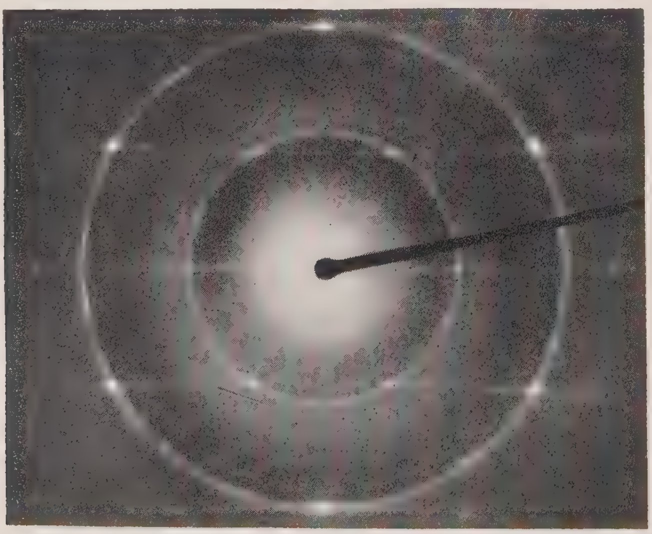

FIG. 3. Electron diffraction spot pattern superimposed on the todorokite powder pattern.

DIFFERENTIAL THERMAL ANALYSIS

A differential thermal analysis was kindly made by George T. Faust, U. S. Geological Survey, on the analyzed material from the Quinto Pit (Sample no. 1 of Table 2). The curve is given in Fig. 5. Interpretation of this complex curve is deferred; further investigations of this and other manganese oxides are under way at the U. S. Geological Survey.

ACKNOWLEDGMENTS

We are indebted to J. M. Axelrod, formerly of the U S. Geological Survey, who made x-ray studies of many samples from Oriente; to K. J.

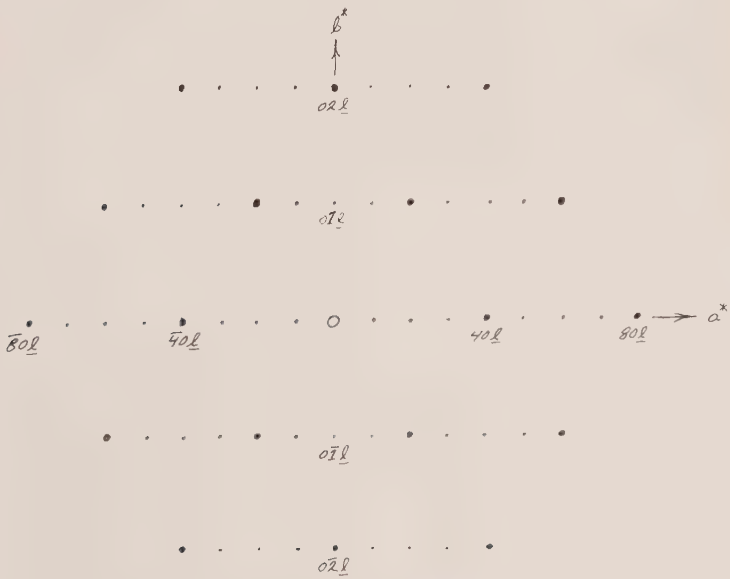

FIG. 4. Method of indexing the spot pattern shown in Fig. 3.

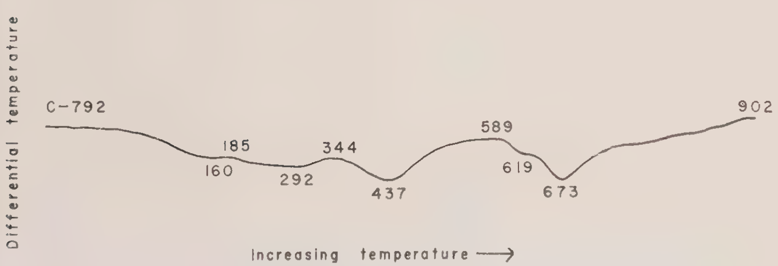

FIG. 5. D T A curve of todorokite, Quinto Pit, Cuba.

TABLE 5. *X*-RAY POWDER DATA FOR "DELATORREITE" AND TODOROKITE, Fe RADIATION, Mn FILTER, 114 MM. DIA. CAMERA

"Delatorreite"			Todorokite†		
I	*d* (meas)	*d* (calc)*	*hkl*	*d* (meas)	I
		9.747	100		
9.6	s	9.592	001	9.65	10
				7.2	½
		6.837	101		
		4.873	200		
4.77	s	4.796	002	4.81	8
				4.46	3
		4.345	201		
		4.303	102		
		3.418	202		
		3.256	300		
3.19	w	3.185	003	3.20	4
3.11–2.95	band	3.077	301		
		3.038	103		
		2.849	010		
		2.734	110		
2.7	band	2.731	011		
		2.690	302		
		2.673	203		
		2.630	111		
		2.460	210		
2.448	m	2.449	012	2.45	3
		2.437	400		
2.398	s	2.398	004	2.40	4
		2.382	211		
		2.376	112		
2.34	m	2.362	401		
		2.329	104		
		2.279	303		
2.21	m	2.189	212	2.216	4
		2.172	402		
2.16	f-b	2.152	204	2.15	1
		2.142	310		
		2.127	013		
2.11	f-b	2.091	311		
		2.078	113		
1.98	m	1.956	312	1.981	1
		1.950	500, 213		
		1.938	403		
		1.930	304		

* Assuming an orthorhombic unit cell with $a=9.75$Å, $b=2.849$Å and $c=9.59$Å.
† From Frondel, *Am. Mineral.*, **38**, p. 766 (1953).

TABLE 5 (*Continued*)

"Delatorreite"				Todorokite†	
I	*d* (meas)	*d* (calc)*	*hkl*	*d* (meas)	I
1.92	w	1.918	005		
		1.910	501		
		1.882	105		
		1.852	410		
		1.834	014		
		1.818	411		
		1.806	502		
		1.803	114		
		1.785	205		
		1.780	313		
1.74	wm	1.728	412		
		1.717	214		
1.69	f-b	1.709	404		
		1.664	503		
		1.652	305		
		1.623	600		
		1.612	510		
		1.605	601		
		1.602	413		
		1.599	006		
		1.597	314		
		1.591	015		
		1.587	511		
		1.578	106		
		1.570	115		
		1.543	512		
1.53	w	{1.539	602		
		{1.519	206		
		1.513	215, 504		
		1.507	405		
		1.466	414		
		1.448	603		
		1.437	513		
		1.434	306		
		1.429	315		
1.423	m	1.424	020	1.419	4
				1.392	1
				1.331	5

Murata for spectrographic analyses, to J. J. Fahey for determinations of specific gravity and color correlation, to George T. Faust for the differential thermal analysis, to W. T. Schaller for information on the occurrence in Death Valley, and to F. A. Gonyer, formerly of Harvard, who

made a chemical analysis. We also thank Clifford Frondel of Harvard for the use of this unpublished data and Michael Fleischer of the U. S. Geological Survey, who acted as liaison among the various groups and helped to assemble this paper.

References

FRONDEL, CLIFFORD (1953). New manganese oxides: Hydrohausmannite and woodruffite: *Am. Mineral.* **38,** 761–769.

LEWIS, G. E. AND STRACZEK, J. A. (1955). Geology of south-central Oriente, Cuba: *U. S. Geol. Survey Bull.* **975**-D, 1–336.

SIMONS, F. S. AND STRACZEK, J. A. (1958). Geology of the manganese deposits of Cuba: *U. S. Geol. Survey. Bull.* **1057**, 1–289.

YOSHIMURA, TOYOFUMI (1934). "Todorokite," a new manganese mineral from the Todoroki Mine, Hokkaido, Japan: *Jour. Faculty Sci. Hokkaido Imp. Univ., Ser IV*, **2,** 289–297.

Manuscript received March 3, 1960.

THE AMERICAN MINERALOGIST, VOL. 45, NOVEMBER-DECEMBER, 1960

A HEATING MICRO-COIL FOR THE STUDY OF MINERAL FRAGMENTS AND HEAT-ETCHING OF POLISHED SECTIONS

William C. Kelly and John M. DeNoyer,
Department of Geology, The University of Michigan, Ann Arbor, Michigan.

Abstract

A small heating coil is described that can be used to heat selected minerals grains in a microscopic field of view to partially controlled temperatures as high as 400° C. Preliminary tests have been made on mineral fragments and minerals in polished section. Samples can be watched as they are heated. A wide variety of effects such as color changes, release of sublimates, dehydration, melting, and the cracking and explosion of grains have been observed in testing mineral fragments. Many of the more heat sensitive ore minerals studied in polished section showed unusual reactions to the heat of the coil. The copper sulfides and some silver minerals proved to be most reactive. Heat-etching of chalcocite produced the distinctive patterns previously described by Stephens (1935).

Introduction

In the study of mineral fragments or polished ore sections, valuable data might often be gained by the application of known heats to mineral grains. For this reason, the writers have designed and constructed a small heating coil which can be brought into a microscopic field of view and there be used to heat selected grains to partially controlled temperatures as high as 400° C. A mineral may be continuously observed as its temperature is raised, and any reaction such as a loss or change of color, dehydration, release of a sublimate, or melting may be seen and recorded.

The coil is very effective in producing heat-etch patterns in chalcocite. A variety of effects, some diagnostic, may be obtained with other heat-sensitive minerals in polished section.

The apparatus has neither the range nor the accuracy of differential thermal analytical equipment and is certainly not proposed as any substitute for that method. It merely provides some types of information that cannot be won from a differential thermal curve.

This paper is presented to describe the instrument and to discuss the results of its preliminary trials with some minerals.

Equipment

The micro-coil control circuit was assembled into a single unit designed to stand beside a microscope as shown in Fig. 1. The coil, mounted in a phone plug, is inserted into the side of the control box and extends over the microscope stage. The coil was wound from a short length of chromel A 30 gauge wire. A convenient method of winding the filament is

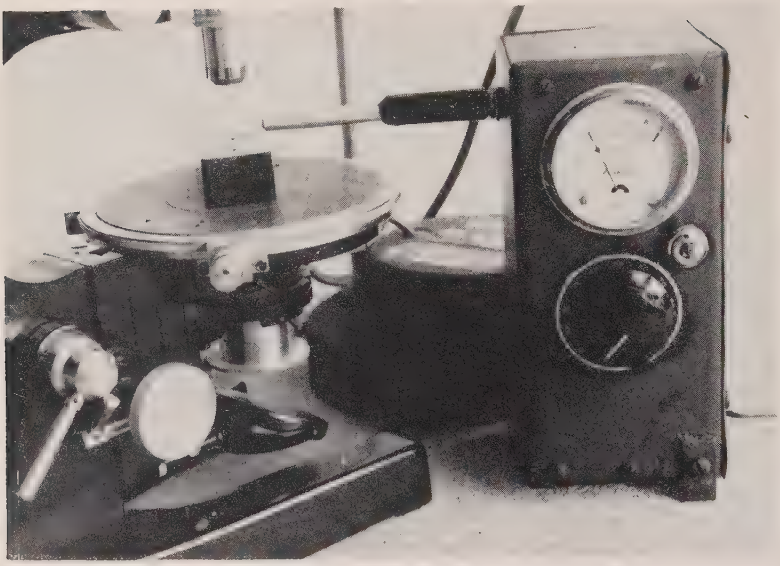

FIG. 1. The micro-coil in position for heat-etching of a polished section.

to wrap the chromel wire around a piece of bare 20 gauge wire. About $2\frac{1}{2}$ turns are sufficient to produce a satisfactory coil. The free ends of the chromel wire should be about 2 cm. long after the coil has been wound. A junction between these free ends and 20 gauge copper leads is formed by clamping the chromel wire into the ends of the copper leads. This junction must be smooth enough to permit it to be drawn into the tubular openings in the porcelain insulator and tight enough to prevent open circuits. It is important to have at least 1.5 cm. of chromel wire between the coil and the copper wire to prevent too rapid heat conduction along the leads. The lower chromel wire portion of the leads should be bent up sharply at the coil to prevent irregular heating below the coil.

The probe assembly consists of the micro-coil with its associated leads and insulator enclosed in an aluminum tube and attached to a Mallory, Type 75, Standard Phone Plug as shown in Fig. 2. This type of assembly has proved to be convenient to use and permits rapid replacement of the entire probe in case of burn out. Filament life varies with temperatures at which the coil is used and with the types of material studied. Sulfur fumes liberated by some minerals cause corrosion of the chromel wire and reduce the coil life. When used under varying conditions, a single coil can be expected to last about 20 hours.

A 0-1 ampere A.C. ammeter with a shunt resistor, Ri, was used to

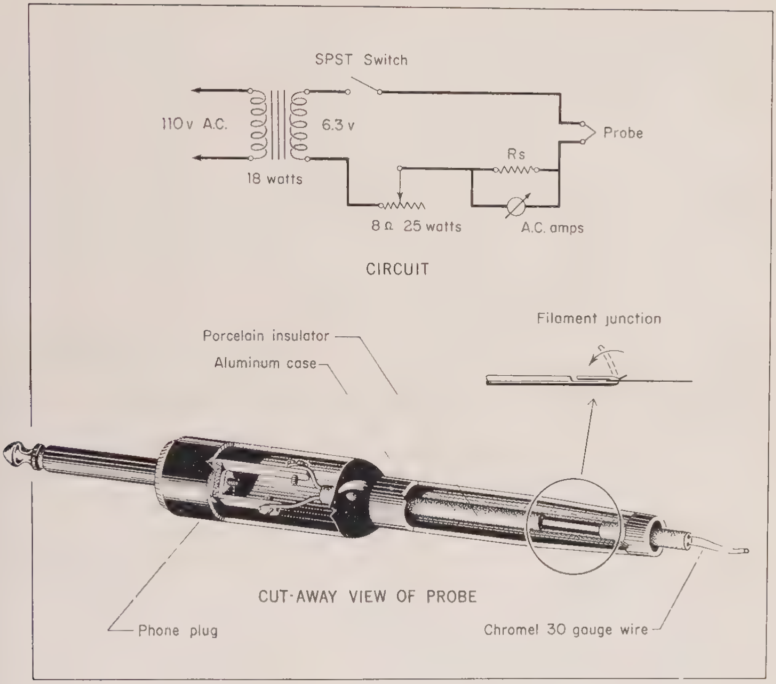

Fig. 2. Cut-away view of the heating probe and circuit diagram for the micro-coil apparatus.

measure the current flowing through the coil. The shunt resistor was made from the same resistance wire as the micro-coil and attached directly to the terminals in back of the meter. Ranges of current measurement from 0-1 to 0-4 amperes can be easily obtained by varying R_s. For most purposes a standard 0-3 ampere A.C. meter should prove satisfactory. If such a meter is used the resistor, R_s would not be necessary.

One difficulty encountered in operation of the equipment results from the heat liberated by the control circuitry. The rheostat and shunt resistor become quite hot when large currents are used. Rubber insulation in contact with these elements melts producing short circuits. This danger can be reduced by using stiff wire that will stay in place and attaching it so that it will not tend to come in contact with circuit elements that may become hot. As an added precaution, wire that is covered with heat resistant insulation can be used.

In operation, the coil must be used with an objective of low magnification that focuses at a safe distance from the hot wire. A 32 mm. lens with a working distance of 27 mm. was used throughout the present work without any evident damage.

Calibration

The micro-coil was calibrated by repeated measurements of the amounts of current required to melt fragments of "Tempil Pellets." These are commercially available temperature standards whose melting points are known within 1% limits.

The Tempil fragments were tested on glass slides placed on the stage of a mineralographic microscope which could be racked up toward the fixed height of the heating coil. A constant distance between the upper surface of the slide and the lower surface of the coil was maintained in all operations by use of a hard manila spacer.

The current required to melt any given Tempil material varied with the size of the fragment tested. This variation is illustrated in Fig. 3 (right). Higher currents are required for smaller grains because their upper surfaces lie at greater distances from the coil. Greater variance in current readings was also detected with smaller grains probably due to the facts that they respond more rapidly to small temperature fluctuations such as those caused by air currents and that any variation due to inhomogeneities of the Tempil Pellets is most apt to appear when these are finely subdivided. Fragments over 0.5 mm. gave consistent readings provided they were not so large as to touch the inside surface of the coil (inner diameter = 0.76 mm.).

The calibration curve for the heating coil is shown in Fig. 3 (left). Due to the changing slope of this curve, the temperature range indicated by

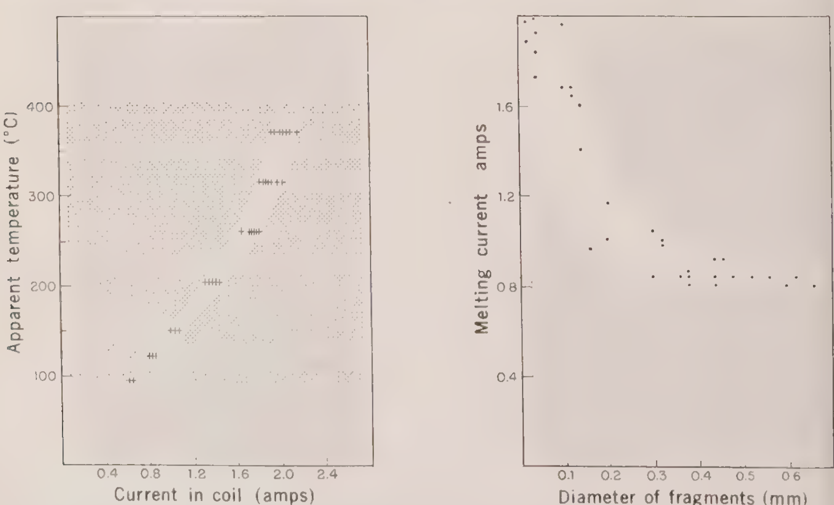

FIG. 3. (Left) Calibration curve of the micro-coil.
(Right) Effect of fragment size on the current required to melt a given standard material.

any setting on the instrument becomes larger as the temperature goes up. With elaborate equipment these temperature readings would undoubtedly be refined.

Testing Mineral Fragments

Table 1 presents a summary of the thermal tests made on different minerals by use of the heating coil. Published reaction temperatures are also listed for comparison, and, unless otherwise indicated, these data were taken from a recent review of geologic thermometry by Ingerson (1956).

Known mineral fragments were tested by selecting grains 0.5-0.6 mm. in diameter, bringing them to focus in the center of the field, and very gradually increasing the current flowing through the heating coil. Any change in the appearance of a fragment was noted and the corresponding ammeter reading was recorded. By simply watching a fragment heated in this manner different types of reactions can be distinguished and an approximate temperature range assigned by reference to the calibration curve (Fig. 3 left).

Minerals that melted within the range of the instrument usually showed marked color changes, development of droplets on the grain surfaces, or sudden conversions of a fragment to globular form. In some cases, melting was accompanied by the formation of condensates on that part of the glass slide surrounding the grain tested. Realgar, for example turned a deeper red and finally black on melting and a bright yellow condensate formed around the melted grain (Figure 5A).

Chalcanthite, gypsum, melanterite and goethite were analyzed as representative hydrated minerals. In the case of hydrates that decompose in several stages, the first and last dehydrations may usually be detected but the intervening reactions are masked by the opacity developed in the first stage. The final dehydrations of melanterite and chalcanthite were evidenced by contraction of the grains and changes in color.

The decomposition of goethite ($FeO \cdot OH \rightarrow \alpha Fe_2O_3$) proved sluggish and coil settings well above the equilibrium temperature were required before any visible signs of reaction appeared. A differential thermal analysis of the same material (heating rate, 12.5° C./min.) showed the first trace of an endothermic decomposition at 250° C. and the peak occurred at 320° C. When the heating coil was set at temperatures over 300° C. the goethite changed from yellow to red very rapidly, but there was no observable change in the mineral when the coil was left for five minutes at the equilibrium decomposition temperature. The heating rate of the micro-coil is manually controlled and so the instrument should prove of value in estimating reaction rates.

TABLE 1. THERMAL TESTS OF MINERAL FRAGMENTS

Mineral	Known Reaction		Observed Reactions		
	Reaction	Reported Temp. (° C.)	Observation	Current (Amps)	Appr. Temp. (° C.)
1) Sulfur, S	Melting	119°	Fragment melts, yellow condensate on glass slide	0.84	115°–130°
2) Realgar, AsS	Melting	320°	Fragment becomes a darker red, yellow condensate on slide	0.45	255°–320°
			Fragment turns black, melts	0.50	305°–400°
3) Orpiment, As_2S_3	Melting	310°	Fragment yellow→red, melts yellow condensate on slide	0.47	273°–350°
4) Bismuth, Bi	Melting	271°	Melting, silvery globules form white condensate on slide	0.45	255°–320°
5) Lead, Pb	Melting	327°	Fragment becomes iridescent	0.47	273°–350°
			Starts to melt, silvery globules form	0.50	305°–400°
			Entire fragment melts, white condensate on slide	0.54	345°+
6) Amber*	Softens	150°	Surface becomes soft, tacky	0.30	162°–187°
	Melting	250°–300°	Fragment→liquid globules	0.38	208°–245°
7) Copal	Melting	120° 166°	Rapid melting→globules	0.19	105°–120°
8) Niter, KNO_3	Melting	333°	Fuses rapidly to transparent droplets	0.51	315°–425°
9) Soda Niter, $NaNO_3$	Melting	310°	First signs of melting, some fragments move, edges melt	0.45	255°–310°
			Rapid melting, →globules	0.57	273°–350°
10) Chalcanthite, $CuSO_4 \cdot 5H_2O$	a) Dehydration b) Dehydration c) Dehydration	95° 114° 250°	Lowest coil temp. blue transparent grains slowly→white opaque cannot distinguish 1st & 2nd dehydration	0.17	95°–110°
			Fragments contract, surface appears sintered, tan color	0.43	240°–295°
11) Gypsum, $CaSO_4 \cdot 2H_2O$	a) Dehydration b) Dehydration	128° 163°	Transparent fragment→milky white, opaque sluggish at this setting (30 seconds)	0.23	122°-140°
			Same change very rapid, second dehydration not detected	0.25	133° 155°
12) Goethite, FeO·OH	Dehydration	135°	Yellow fragments→red (sluggish)	0.32	170°-200°
13) Melanterite $FeSO_4 \cdot 7H_2O$	a) Dehydration b) Dehydration c) Dehydration	57° 100° 300°	Lowest coil setting, fragments →opaque, white; coil left at this setting for five minutes —then turned up—No sign of 2nd dehydration	0.17	95°–110°

* Data from Dana, E. S., Textbook of Mineralogy (1932).

TABLE 1 (*Continued*)

Mineral	Known Reaction		Observed Reactions		
	Reaction	Reported Temp. (° C.)	Observation	Current (Amps)	Appr. Temp. (° C.)
			Rapid change, white→dark brown	0.49	295°–385°
14) Malachite, $CuCO_3 \cdot Cu(OH)_2$	Decomposes	200°	Tan spots appear on green translucent fragments, sluggish	0.40	220°–262°
			Fragments move, turn brown	0.52	325°+
15) Azurite $2CuCo_3 \cdot Cu(OH)_2$	Decomposes	200°	Grains→deeper blue to blackish blue	0.43	240°–295°
			Grains fuse, sinter, turn black	0.60	415°+
16) Smithsonite, $ZnCO_3$	Decomposes	296°	Grains→yellow, crack	0.57	380°+
17) Siderite, $FeCO_3$	Decomposes	282°	Gradual color change, white →tan	0.48	285°–365°
			Grains move, turn reddish brown	0.51	315°–425°
18) Magnesite, $MgCO_3$	Decomposes	373°	Grains move, turn lt. yellow, sintered appearance	0.53	335°+
19) Rhodochrosite, $MnCO_3$	Decomposes	400°	Gradual cracking of surface, grains become opaque: sluggish	0.50	305°–400°
			Grains→brown to black iridescent	0.55	360°+

Malachite, azurite, smithsonite, siderite, magnesite, and rhodochrosite were studied as examples of minerals losing CO_2 on decomposition. As a group, these reactions proved sluggish and were usually visible only at temperatures above published equilibrium values. The decompositions were evidenced by cracking, movement, and in some cases explosion of grains that disappeared from the field of view. Some of the decompositions were accompanied by a color change as indicated in Table 1.

Several specimens of fluorite were heated in a darkened room with the micro-coil to determine whether thermoluminescence could be observed with this equipment. The instrument proved unsatisfactory for this purpose, because the thermoluminescent glow, if any, is obscured by the red glow of the hot coil. Loss of radiation colors can, however, be detected and approximate temperatures assigned to the color loss. A specimen of violet fluorspar, for example, showed no change in color as its temperature was gradually raised to 400° C., but at coil settings above this the grains became less transparent in the center and fading began at the edges.

In Fig. 4, a graphical correlation is made between published and experimental thermal data. For the majority of reactions, the measured temperatures agreed with published data within the experimental errors. Exceptions are the more sluggish reactions such as the decomposition of goethite and some of the carbonate minerals as previously discussed.

Heat-Etching of Polished Sections

The photochemical properties of metallic minerals in polished section have been investigated by Guild (1917), Whitehead (1917), McKinstry (1927), Petrulian (1931), Schneiderhohn and Rahmdohr (1931), and Stephens (1931, 1935). In the majority of these studies, effects of intense light and heat were tested by bringing the beam of a carbon arc to focus on a mineral surface at high magnification. Among the many minerals studied by these researchers, the silver haloids and sulfo-salts, silver sulfide, some gold-silver tellurides, and some of the copper sulfides proved to be most reactive.

The most recent and extensive studies in this field are those of Stephens

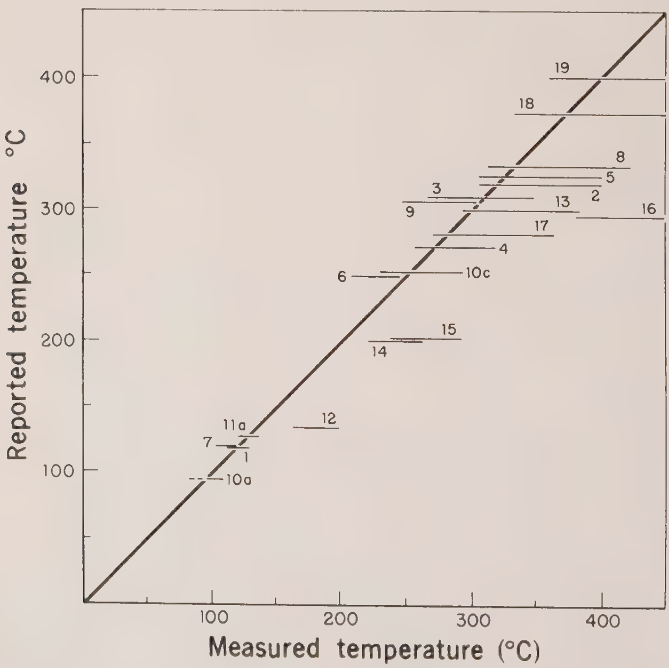

FIG. 4. Correlation of known reaction temperatures with temperatures determined with the heating coil. Numbers on the diagram refer to reactions listed in Table 1.

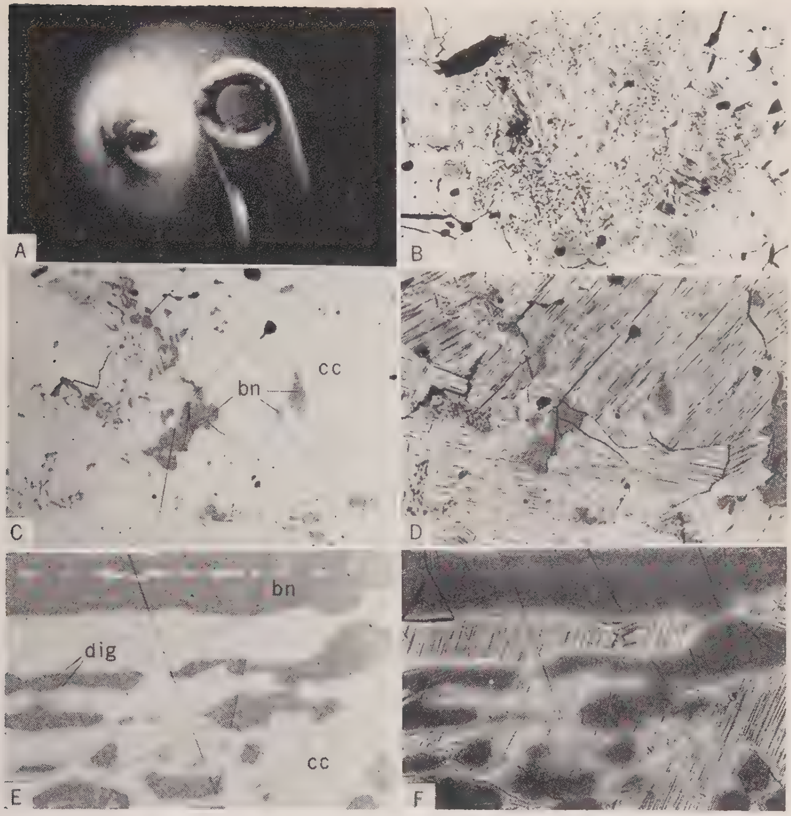

FIG. 5(A). The micro-coil moved aside for view of realgar fragment that has just been heated to 305°–400° C. The relict of realgar is red and is surrounded by a yellow condensate on the glass slide. (Magnification 8.9×.)

(B). Polished surface of chalcocite (white) and bornite (grey) heat etched for two minutes at 420° C.+. Etched chalcocite originally under the micro-coil is seen in the center of the photograph. (Magnification 20.8×.)

(C). Field of chalcocite with scattered remnants of unreplaced bornite before heat-etching. (Magnification 64.2×.)

(D). Same field as 5C after heat-etching at 135°–155° C. The bornite has become a light pinkish-violet and a distinct parallel etch cleavage has appeared in the chalcocite. Nitric acid etching produced a weaker two-directional cleavage in this same chalcocite. (Magnification 62.4×.)

(E). Field of chalcocite replacing bornite before heat-etching. A barely visible isotropic blue mineral (presumably digenite) rims the bornite remnants. (Magnification 64.2×.)

(F). Same field as 5D after prolonged heating at 250°–305° C. Bornite has become a deep purple and has begun to replace the chalcocite. The chalcocite remains grey but develops a deep etch pattern parallel over the field. The digenite fades and migrates as a diffuse band at the moving contacts of bornite and chalcocite. (Magnification 64.2×.)

who investigated the effects of light on polished surfaces of silver minerals (1931) and the use of a carbon arc in identification of different genetic types of chalcocite (1935). In etching the silver minerals, Stephens used Wratten filters to control the wave length of light impinging on the mineral surface and a cupric sulfate bath to eliminate the majority of heat from the arc light. Realizing that the reactions of the copper sulfides are due primarily to heat, Stephens used the full spectrum of the carbon arc in etching sections of chalcocite. He viewed the specimens being tested through a camera attachment to avoid the discomfort of an unusually bright image. When heated, chalcocite developed a variety of etch figures some of which are diagnostic of the origin of the mineral. Stephens concluded that these figures can be used to distinguish (1) hypogene from supergene chalcocite, (2) separate generations of chalcocite, and (3) chalcocite after bornite as opposed to chalcocite without any relation to a paragenetic predecessor.

As a strong and controllable source of heat, the micro-coil seemed a practical device for producing some of the reactions described by thes earlier workers. Any effects obtained could be ascribed primarily to heat since only a normal tungsten light source was used to observe the specimens during tests. No special equipment is required to view the polished sections as they are heated. At the maximum setting of the coil 420° C.+), the image of the specimen is still clear and there is no discomfort to the eyes.

A drawback to use of the coil is that its effects cannot be removed without re-surfacing the polished section. The area damaged depends on the temperature of the coil, the time of exposure, and the sensitivity of the mineral examined. A field of chalcocite heat etched at the maximum coil temperature for two minutes is shown in Fig. 5B. Grains of chalcocite near the edge of this field show no effects of heat but a large, roughly circular area in the center has developed one of the etch patterns characteristic of this mineral. The etched area has a maximum diameter of 2.1 mm. Another part of this same section was heat-etched at 135°–155° C. and details of this etch pattern may be seen at higher magnification in Fig. 5D.

A summary of observations made in applying the micro-coil to different minerals in polished section is presented in Table 2. A temperature range is given for each reaction based on the Tempil pellet calibration curve in Fig. 4. With polished sections, this range is only a relative indication of the temperature at which a reaction takes place. The principal source of error in applying the calibration curve to polished sections is the variable conduction of heat away from the tested area by adjacent mineral grains. In tests of mineral fragments on glass slides, the surrounding medium

TABLE 2. THERMAL TESTS OF POLISHED SECTIONS

Mineral	Composition	Observed Reactions
Argentite	Ag_2S	Rapid change from grey to dense black, finely pitted surface at 265°–325° C. Transparent film of sulfur released from argentite and spreads rapidly over the surface outward from the heated area. Numerous spheres with a silvery to iridescent luster appear on the surface and are most numerous near fracture, or scratches. These spheres can be remelted at 265°–325° C. They give an argentite x-ray pattern.
Bornite	$5Cu_2S \cdot Fe_2S_3$	Specimens originally orange turn reddish purple at 250°–305° C. With prolonged (2 minute) etching at this temperature, the color becomes a deep reddish purple. On prolonged etching over 400° C. bornite turns blue. Bornite that is originally violet purple becomes a lighter pinkish-violet at 140°–220° C. and then becomes progressively deeper purple on continued heating at this temperature. In presence of coarse chalcocite that has replaced bornite (Figure 5E–5F), the bornite dissolves chalcocite at 250°–305° C. Grains of bornite grow at expense of chalcocite.
Chalcocite	Cu_2S	*Chalcocite Replacing Covellite:* No change could be produced in chalcocite replacing covellite even at highest coil settings. However, veinlets of later chalcocite cutting across the non-reactive variety became visible on etching at 110°–125° C. This chalcocite develops an irregular etch pattern with very fine detail. *Chalcocite Replacing Pyrite:* Isolated blue patches of digenite (?) appear in the chalcocite at 110°–125° C. Fine-grained texture of chalcocite brought out at 115°–130° C. Parallel etch cleavage on fine scale appears at same temperature. No signs of reaction between chalcocite and pyrite after two minutes at 415° C.+. *Chalcocite Replacing Bornite:* Parallel etch cleavage (Figure 5E–5F) begins to develop at 110°–125° C. and forms rapidly at 135°–155° C. At 250°–305° C., chalcocite dissolves in bornite as contacts become diffused and migrate.
Covellite	CuS	Original material-laths and shreds of covellite surrounded and replaced by chalcocite. At 370° C.+, covellite reacts from borders inward. Contact with chalcocite remains sharp and stationary but covellite changes from blue to chalcocite grey losing vivid orange interference color. The grey alteration product is moderately anisotropic. Its surface appears rough in contrast to the adjacent chalcocite and unreplaced covellite. On prolonged heating at 370° C.+, the entire field is converted to a uniform grey color but original areas of covellite are still defined by relief at contacts and rough texture of material that has replaced the covellite.

TABLE 2 (*Continued*)

Mineral	Composition	Observed Reactions
Digenite	$Cu_{2-x}S$	Greyish-blue digenite turns grey at 150°–170° C. On prolonged heating, the color becomes a violet-grey. After cooling, areas originally hottest become blue again.
Freieslebenite	$Ag_5Pb_3Sb_5S_{12}$	Freieslebenite swells and cleavage fragments heave upward at 265°–335° C. Fluid emitted at this temperature spreads across the surface imparting a permanent dull gun-metal grey color to the mineral.
Goethite	FeO·OH	Decomposition of goethite, especially coarsely crystalline varieties, very sluggish in polished section. Some specimens showed no effects of heating even at maximum settings of the coil. One specimen heaved and cracked at 370° C.+ but no pronounced color changes were observed.
Hessite	Ag_2Te	Original specimen grey. Anomalous yellow-brown to bluish grey interference colors. A permanent change of color to light brown takes place at 350° C.+. No changes in anisotropism on cooling.
Petzite	Ag_3AuTe_2	At 370° C.+, petzite heaves and cracks as vermiform black markings appear on light grey mineral surface. In oblique light, a delicate network of crystalline gold is seen to have replaced the original petzite grain. Adjacent tellurides, in this case altaite, are unaffected by heat.
Proustite	$3Ag_2S \cdot As_2S_3$	At 405° C.+, surface of proustite suddenly melts. The liquid solidifies to a silvery metallic substance which can be remelted at 405° C.+. This material still gives an *x*-ray pattern for proustite.
Realgar	AsS	Color changes from grey to tannish-grey at 255°–320° C. At 308°–400° C., realgar melts and a bluish iridescent ring forms around the heated area. In oblique light, this ring is red to yellow.
Tellurium	Te	Metal begins to change at 305°–400° C. as a yellow coating of oxide collects on surface. Mineral melts at 415° C.+ forming a small liquid filled depression under the coil.

was air in every case, but this control does not apply to polished sections.

Of the results obtained and described in Table 2, it is most significant that the etch patterns of chalcocite described by Stephens (1935) can be produced with a device as simple as the coil. With the exception of some chalcocite replacing covellite, all specimens of this mineral formed a pronounced etch pattern on heating (Figs. 5C–5F). Additional specimens

and study would be required to determine whether patterns obtained with the heating coil differ in any way from those described by Stephens.

Reactions noted in the heat-etching of argentite and proustite are also worthy of some comment. McKinstry (1927) observed the formation of blebs, presumably of native silver, on surfaces of argentite and pyrargyrite etched with a carbon arc. When argentite was heated with the coil at 265°–325° C. numerous globules of an iridescent to silvery luster appeared on the blackened surface. It was at first assumed that these were native silver, but these spheres could be re-melted at 265°–325° C., well below the melting point of silver. Similar effects were noted with proustite which melted quickly at 405° C.+ forming a liquid with a bright metallic luster. After cooling, this material could be re-melted again at 405° C. Fragments of each of these minerals were extracted, transferred to glass slides, and there heated until they liquefied. On cooling, the samples were scraped from the slides, crushed, and x-rayed. The resulting powder patterns were those of the original minerals, not native silver. Flecks of what appeared to be silver were seen admixed with the crushed heated products of proustite but the metal comprised only a small proportion of the original liquid globule.

Along with the minerals listed in Table 2, a number of others were tested that proved negative to the heat of the coil. These include bismuthinite, chalcopyrite, cinnabar, copper, domeykite, dyscrasite, enargite, galena, pyrite, silver, sphalerite, stannite, stibnite, sylvanite, teallite, tetrahedrite, and violarite.

References

Dana, E. S. (1932), A Textbook of Mineralogy, Fourth Edition. W. E. Ford, Editor. John Wiley & Sons, 776.

Guild, F. N. (1917), Microscopic study of the silver ores: *Econ. Geol.*, **12**, 297–353.

Ingerson, Earl (1955), Methods and problems of geologic thermometry: *Econ. Geol.*, **50th Anniversary Volume,** Part 1, 341–410.

McKinstry, N. E. (1927), Magnetic, electro-chemical, and photochemical tests of opaque minerals: *Econ. Geol.*, **22**, 669–677.

Petrulian, N. (1931), Über Lichtätzung des Silberglanzes: *Schweiz. Min. u Petr. Mitt.*, **11**, 2.

Schneiderhohn, H., and Ramdohr, P. (1931), Lehrbuch der Erzmikroskopie II, 23.

Stephens, M. M. (1931), Effect of light on polished surfaces of silver minerals: *Am. Mineral.* **16,** 532–549.

———, (1935), The identification of types of chalcocite by use of the carbon arc: *Econ. Geol.*, **30,** 604–629.

Whitehead, W. L. (1917), Notes on the technique of mineralography: *Econ. Geol.*, **12,** 697–716.

Manuscript received February 19, 1960.

THE AMERICAN MINERALOGIST, VOL. 45, NOVEMBER-DECEMBER, 1960

PHASE EQUILIBRIUM DATA FOR THE SYSTEM $MgO\text{-}MgF_2\text{-}SiO_2$

WILHELM HINZ AND PETER-OLAF KUNTH, *German Academy of Sciences, Berlin, Germany.*

ABSTRACT

In completely anhydrous melts of the binary system $MgO\text{-}MgF_2$ a simple eutectic reaction at 1214° C. was established.

The binary system $Mg_2SiO_4\text{-}MgF_2$ is characterized by the formation of minerals of the humite-clinohumite group. All of them show incongruent high-temperature reactions, norbergite melting with a primary crystallization of chondrodite (stable) or forsterite (metastable) at 1345° C., chondrodite melting with primary crystallization of forsterite at 1450° C. On heating, clinohumite breaks down at 1380° C. to a mixture of forsterite and chondrodite. Humite is only sporadically observed in subsolidus reactions; the equilibrium temperature for the reaction clinohumite+chondrodite$\rightleftharpoons$humite could not be determined. Metastable crystallization of forsterite (in the place of chondrodite) occurs mostly on heating and fusion of norbergite.

In the ternary system $MgO\text{-}MgF_2\text{-}SiO_2$ some of the minerals of the humite-clinohumite series (on the join $Mg_2SiO_4\text{-}MgF_2$) could be outlined in their crystallization fields with boundary curves to the fields of primary periclase, sellaite, cristobalite and/or tridymite, forsterite, and clinoenstatite. No magnesium amphibole of the formula $Mg_7(Si_8O_{22})F_2$ was observed in the melt products.

INTRODUCTION

Phase equilibrium studies in ternary systems of the type oxide-fluoride-SiO_2 (oxide and fluoride with the same cation) have been investigated in only a few cases. In the main these investigations have been restricted to the system $CaO\text{-}CaF_2\text{-}SiO_2$. Special attention has been given to the influence of CaF_2 on the formation of tricalcium silicate, because of the special importance this substance plays in the hardening process of cements (Eitel (1), Bååk and Ölander (2)).

IMPORTANCE OF THE SYSTEM $MgO\text{-}MgF_2\text{-}SiO_2$

In the last two decades there have been many attempts to synthesize mica and amphibole asbestos. These took into account the necessity of substituting F for the OH-groups, if the process was to be undertaken from the melt at atmospheric pressure. While this method proved successful for mica synthesis, it is questionable whether the synthesis of asbestos is possible in the same manner. In any case, it seemed useful to go into more detail regarding the melting equilibria of this system.

REVIEW OF LITERATURE

The system $MgO\text{-}SiO_2$ was studied in 1914 by Bowen and Anderson (3) and supplemented by Greig (4) in 1927. According to these authors a

eutectic exists between periclase and forsterite at 1850° C. and a second between clinoenstatite and cristobalite at 1543° C. Forsterite melts congruently at 1890° C; clinoenstatite melts incongruently at 1557° C. with forsterite as solid phase. Melts rich in SiO_2 beyond the eutectic clinoenstatite-cristobalite unmix at 1695° C. and form two liquid phases.

The system MgO-MgF_2 was studied in 1953 by Eitel, Hatch and Denny (5), and *x*-ray investigation revealed no new compounds. The system MgF_2-SiO_2 could not be studied, because the samples partly showed strong hydrolysis and evaporation. For example, in a melt $MgF_2:SiO_2=2:1$, norbergite $Mg_2SiO_4 \cdot MgF_2$ and even forsterite Mg_2SiO_4 were found as reaction products.

Various partly successful attempts have been made to synthesize the minerals of the humite group: norbergite, chondrodite ($2Mg_2SiO_4 \cdot MgF_2$), humite ($3Mg_2SiO_4 \cdot MgF_2$) and clinohumite ($4Mg_2SiO_4 \cdot MgF_2$).*

In 1947 Rankama (6) succeeded in getting norbergite and chondrodite. On the other hand an attempt to synthesize clinohumite failed. (This paper includes a survey of literature since 1851).

In 1954 Karyakin and Gul'ko (7) succeeded in obtaining norbergite, chondrodite and humite, when they melted calcium fluoride and quartz in magnesite crucibles.

Finally, in 1955 van Valkenburg (8) succeeded in synthesizing all of the humite-minerals by using melting reactions or reactions in the solid state.

The system MgO-MgF_2-SiO_2 was studied by Fujii and Eitel (9) in 1957 by means of reactions in the solid state. A large number of mixtures was heated at 1200° C. and the reaction products were investigated for the most part by *x*-ray diffraction. The approximate limits of the individual compounds were represented in a triangular composition diagram. As such are mentioned: periclase, sellaite, norbergite, chondrodite, forsterite, clinoenstatite. and cristobalite. While humite and clinohumite could not be established with certainty in the mixtures heated for three hours, after 42 hours of heating at the same temperature they did appear. Clinohumite was more easily formed than humite.

Preparation of Samples

One of the main difficulties of these investigations was the extraordinarily high sensitivity of magnesium fluoride to moisture. Magnesium fluoride retains surface-adsorbed water up to high temperatures, and H_2F_2 is split off by hydrolysis. For this reason by "open" conditions it is impossible to melt MgF_2 once it has been exposed to the free air without the forming of MgO. The vapor pressure of MgF_2, even at 1400 to

* In the natural minerals F^- is substituted in part by OH^-.

1500° C., has very little disturbing effect (5). According to new investigations carried out by Günther (10), the vapor pressure is 0.1068 Torr at a temperature of 1282°C. and certainly does not have to be taken into account (at least, when the duration of the experiment is short).

The possibility of forming SiF_4 exists when the mixtures contain both MgF_2 and SiO_2 as shown in various references in literature, and clearly confirmed by our own experiments.

The escaping SiF_4 is hydrolysed instantaneously when moisture is present, and clouds of smoke escape. Therefore it was necessary to control the loss in weight, or better to determine the change in composition by analytical methods.

The greater part of the mixtures were prepared with purest MgO from the Schering Works. For some attempts "magnesium carbonate, p.a. Merck, Darmstadt" was used. Both substances were heated for about half an hour at 1150° C., and as is the case with the other raw materials, preserved above P_2O_5 until their application.

SiO_2 was obtained by hydrolysis of silicon tetrachloride (Institute of Silicon and Fluorcarbon Chemistry, Radebeul) in an ammoniac-water solution. The product was filtered off, slightly washed, dried, and heated at 1150° C. for one hour.

For the first orienting experiments "magnesium fluoride, precipitated, pure" produced by Riedel de Haën, Seelze near Hannover, was used. It is a fluffy white powder. Before its application it was melted as quickly as possible, poured from the crucible, and crushed. During the melting and pouring out, a distinct odor of hydrofluoric acid was noticeable (hydrolysis by adsorbed water and moisture of the air). A great number of experiments were made with a shortly fused "magnesium fluoride, pure, for optical use" of unknown origin. This substance was heavier than the first and it seems likely that it was produced at a higher temperature.

For the last experiments we had at our disposal a "magnesium fluoride, precipitated" (Werkstätten für Photochemie, Berlin-Charlottenburg). It had a slight resemblance to the first mentioned MgF_2; it was likewise quickly fused.

Concerning the degree of purity of the ingredients used, it should be said that MgO and SiO_2 were checked by spectral analysis. As contaminations, MgO contained only about 0.1% CaO; SiO_2 contained about 0.3% Al_2O_3 and below 0.05% of other oxides. MgF_2 was determined by chemical analysis.

The compositions of the samples after one melting are shown in Table 1. The three samples of MgF_2 contained only a small or very small quantity of MgO. The contaminations of the "magnesium fluoride, for optical use" may be far below the limit of analytical determination.

TABLE 1. COMPOSITION OF DIFFERENT SAMPLES OF COMMERCIAL MAGNESIUM FLUORIDE

A—from Riedel-de Haën;
B—pure, for optical use;
C—from Werkstätten für Photochemie

Weight %	A	B	C	Weight %	A	B	C
MgO	63, 79	64, 24	64, 31	MgF_2†	96, 97	99, 20	97, 02
CaO	1, 25	0, 12	0, 40	MgO†	1, 05	0, 06	1, 54
BaO	0, 41	0*	0*	SiO_2	0, 17	0, 10	0, 34
Fe_2O_3 Al_2O_3	0, 15	0, 20	0, 26	CaO	1, 25	0, 12	0, 40
				BaO	0, 41	—	—
SiO_2	0, 17	0, 10	0, 34	Fe_2O_3 Al_2O_3	0, 15	0, 20	0, 26
F_2	n.d.	60, 49	59, 16				
Sum	—	125, 15	124, 47	Sum	100, 00	99, 68	99, 56
$O=F_2$		25, 47	24, 91				
	—	99, 68	99, 56				

† Indirectly calculated.
* Not identified by spectral analysis.

Normally, before adding the weighed quantity of MgF_2, the corresponding mixture of MgO and SiO_2 was pulverized and heated for some time at 1350° C.–1400° C. to make the mixtures less voluminous. Likewise by sintering the MgO-SiO_2 mixtures the troublesome development of electrostatic charges in the MgO powder was avoided.

EXPERIMENTAL PROCEDURE

For most of the experiments a SiC resistor furnace with four vertically arranged heating elements was used. With this furnace, work was carried out at temperatures of up to 1450° C. For higher temperatures a molybdenum furnace, which consisted of a molybdenum resistor in sintered Al_2O_3, was at our disposal. The gas-tight construction of this furnace made it possible to work with unprotected platinum.

For the measurement of the temperature a Pt-Pt, 10 Rh thermocouple was used, the hot junction of which was dipped directly into the melt. The cold junction was kept at 20° C. in a Dewar vessel. The thermocouple was compared with a calibrated standard element of the German "Amt für Maasse und Gewichte."

THERMOANALYSIS

The first runs were carried out using the dynamic method. The mixtures of 12 gm. were placed in a platinum crucible with a volume of 20 ml.

As soon as the sample was fused, the melt was stirred with a platinum sheet. At temperatures above 1350° C., however, the stirring had to be abandoned, because the crucible was often welded with the platinum stirrer.

After fusing and stirring, the thermocouple was introduced into the melt, avoiding a contact of the thermocouple with the crucible. Then the power of the furnace was diminished and the cooling curve taken.

This method was applied for the investigation of mixtures rich in MgF_2, which are inclined to a disturbing undercooling in the field of the primary crystallization of MgF_2; an undercooling effect of about 10° could be rather regularly observed. In order to grow single primary crystals, the dynamic method was partly modified. Shortly after the beginning of the primary crystallization the cooling curve was interrupted by removing the thermocouple with the adhering crystals. Relatively large, clear crystal needles of this rapid growth were very suitable for microscopic examination and for *x*-ray diffraction.

Quenching Method

In mixtures in the neighborhood of the binary system MgO-SiO_2, equilibrium is mostly not arrived at with sufficient speed in spite of the presence of magnesium fluoride which is known to be a strong mineralizer. Mixtures with as much as 15 mol% MgF_2 can be kept as clear glasses, if they are quenched with sufficient speed.

It also seemed undesirable in many experiments to work in certain regions of the system with open crucibles. Small tubes of platinum foil (of 0.06 mm. thickness) with a diameter of about 3 mm., and a length of 10 to 15 mm., were welded together and filled with about 100 mg. of substance. The opening was folded together, the platinum tube connected with a ceramic tube by a platinum wire and the whole put into the furnace, which was already at the required temperature.

Then the temperature of the furnace was slowly reduced to the equilibrium temperature in question and held there for some time. After the heat treatment, the samples were removed from the furnace and air-quenched from the fusion temperature.

This method allowed a clear differentiation between larger primary crystals and crystals formed by reaction in the solid state, or crystals simply formed by quenching.

The furnace temperature was controlled by hand by means of a transformer and kept constant to about ±2 to 3° C.

Microscopic Investigation

To identify the different crystalline compounds, the petrographic thin section method has been of great service. Thus periclase (MgO) could be

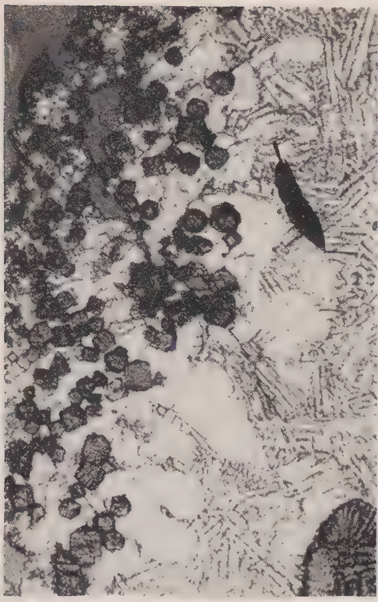

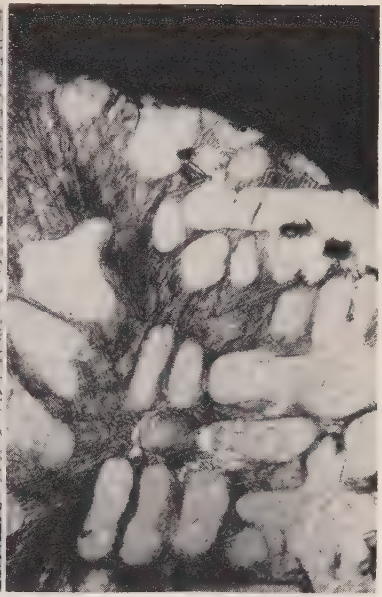

FIG. 1. (left) Periclase grains in periclase-sellaite-eutectic-Analyser 60° (Composition 10 mol. % MgO; 90% MgF_2). ×85

FIG. 2. (right) Sellaite skeletons, between them periclase-sellaite eutectic-Analyser 90°. ×85

clearly distinguished from the other minerals. It showed crystals with well-developed faces, mostly combinations of cubes and octahedra (Fig. 1). Sellaite (MgF_2) also often showed characteristic skeleton forms (Fig. 2) and peculiar cracks, by which, with suitable light incidence, it could nearly always be distinguished from the other minerals. These cracks may be caused by the polymorphic change of MgF_2, observed by Counts, Roy and Osborn (11) by high-temperature x-ray investigation at about 800° C.

SiO_2 could be identified just as easily. It showed irregular grains marked by a very slight birefringence. (Regarding the differentiation between cristobalite and tridymite, see later.)

In some cases it was possible to determine the angle of the optical axes; for norbergite it is $2V = 45° 15'$.

X-ray Investigation and Chemical Analysis

X-ray patterns were taken from samples of the fused products as well as from single crystals, after having determined for clearly identified specimens which crystal interferences lie on the equatorial line.

Sometimes only one needle or a few very small, thin needles which could not be investigated by the powder method were at our disposal.

Rotation patterns were made with a camera 57.3 mm. in diameter, the powder patterns in a Debye-Scherrer camera, 114.6 mm. in diameter, and a Guinier camera, 57.3 mm. in diameter. Both Cu Kα, and Co Kα radiation were used. For comparison, the x-ray data of the humite-minerals, as determined by Sahama (12) were used.

The Shell and Craig methods (13) were used for bulk analysis, but fluorine was precipitated as calcium fluoride. From a special sodium carbonate melt all the other ingredients were determined (cf. Thomas (14)).

Discussion of the Results

The system MgO-MgF_2

The experiments of this binary system were carried out using the dynamic method. The system proves to be simply eutectic, as shown in Fig. 3.

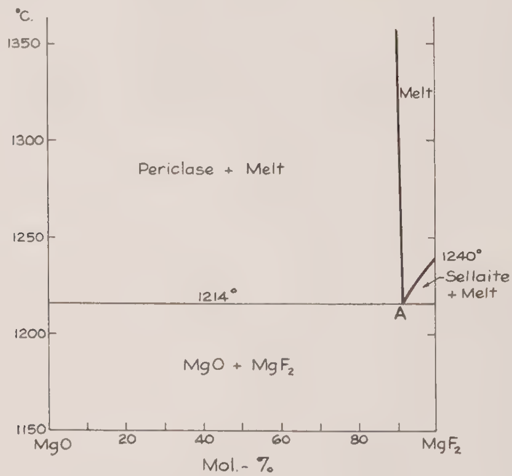

Fig. 3. Phase equilibrium diagram of the binary system MgO-MgF_2.

The fusion point of an especially pure substance "magnesium fluoride, for optical use" was found to be at 1238° C. In consequence of the slight contamination, by extrapolation a value of 1240° C. was obtained, in exact agreement with the value found by Venturello (15). In the literature the values vary between 1221° and 1270° C. To identify the substances, microscopic investigation was sufficient.

Refractive indices and x-ray pattern showed no indication of solid solution.

Under the microscope the eutectic showed sellaite crystals which were interspersed with straight parallel veins (Fig. 1). An addition of as little

as 10 mol% of MgO to MgF_2 brings about periclase as the primary crystallization.

The system MgF_2-SiO_2

The border system MgF_2-SiO_2 is not binary under normal experimental conditions as Eitel, Hatch and Denny (5) had previously observed. Mixtures of MgF_2 and SiO_2 showed, on heating, an intense smoke evolution; the solid reaction products belong to the ternary system MgO-MgF_2-SiO_2 (see below).

The white smoke evolved from a mixture of the composition $MgF_2:SiO_2 = 2:1$ on heating to 1300° C. in a platinum crucible was condensed in a water-cooled tube of copper fixed above the crucible. A voluminous white mass was deposited. The result of the analysis was 85.6% SiO_2 and 1.05% MgO. No determination was made for fluorine. The remainder may have consisted of adsorbed water. It is to be supposed that according to the equation

$$2\ MgF_2 + SiO_2 \rightarrow 2\ MgO + SiF_4,$$

SiF_4 forms first of all, which under the influence of air is hydrolysed to SiO_2 and H_2F_2.

The system Mg_2SiO_4-MgF_2

The join Mg_2SiO_4-MgF_2 of the ternary system can be considered as a binary system, and minerals of the humite group appear as pseudo-binary compounds. Of the humites, only norbergite and chondrodite could be found as primary crystallization products from melts which bears out the observations of previous authors (6, 9), while clinohumite and humite are only obtained by reaction in the solid state.

According to Fig. 4, there is an eutectic between norbergite and sellaite. Norbergite melts incongruently at 1345° C. with primary crystallization of chondrodite. Forsterite, however, is often formed as a metastable primary crystallization of a melt of norbergite, so norbergite shows a double incongruent melting type. The stable incongruent melting point of chondrodite may be about 1450° C.

Clinohumite appears only below about 1380° C. as shown by x-ray diffraction patterns; at higher temperatures forsterite and chondrodite are formed.

Starting materials with the composition of humite, after heating at 1252° for $8\frac{1}{2}$ hours, showed forsterite, clinohumite and chondrodite. The boundaries of the crystallization range of humite could not be established. The thermoanalysis showed, beside the arrest point at 1215° C., a second one at about 1192° C. The cause of this may be seen from the following:

According to chemical analysis all of the samples contain a little more MgO than corresponds to the proportion 2 $MgO:SiO_2$ for forsterite. Therefore the observed thermal data are not fully valid for the binary system Mg_2SiO_4-MgF_2 but rather for points lying in the ternary system on the MgO-side of the join Mg_2SiO_4-MgF_2. Thus it may be assumed that the mentioned second thermal effect has to be coordinated to the arrest point of the ternary eutectic periclase-norbergite-sellaite.

The system MgO-MgF_2-Mg_2SiO_4

Beside the eutectic periclase-norbergite-sellaite, E, two reaction points, F and G, exist. The corresponding compositions and temperatures are contained in Table 2. The position and temperature of the ternary eutectic and the reaction point F for periclase, chondrodite, norbergite and melt were relatively accurately determined, while the data for the reaction point G for periclase, chondrodite, forsterite, and melt are to be considered as approximate (see Fig. 5). As is to be expected, the fusion temperatures in the periclase field rise very sharply, so their determination was seldom possible.

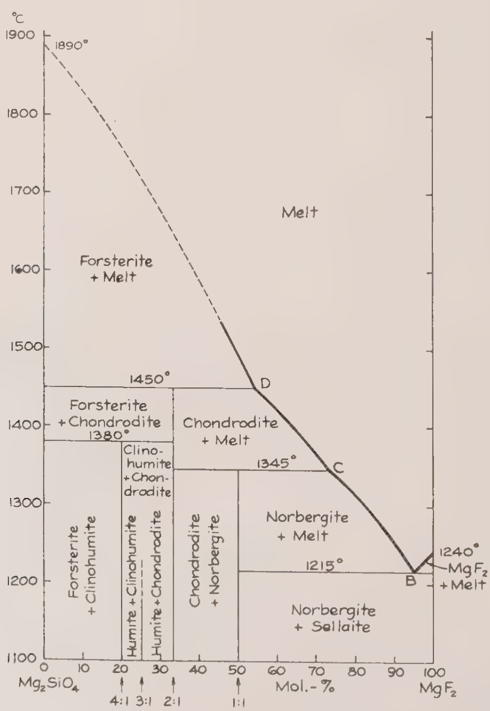

FIG. 4. Phase equilibrium diagram of the binary system Mg_2SiO_4-MgF_2.

TABLE 2. INVARIANT POINTS

Points in Figs. 3, 4, 5	Crystal Phases	Equilibrium	Temp. ° C.	Composition		
				MgO	MgF_2	SiO_2
	Binary Equilibria					
A	Periclase, Sellaite	Eutectic	1214	9	91	—
B	Norbergite, Sellaite	Eutectic	1215	10	85	5
C	Chondrodite, Norbergite	Reaction Point	1345	33	51	16
D	Forsterite, Chondrodite	Reaction Point	1450	48	28	24
	Ternary Equilibria					
E	Periclase, Sellaite, Norbergite	Eutectic	1192	14	82	4
F	Periclase, Chondrodite, Norbergite	Reaction Point	1330	34	53	13
G	Periclase, Forsterite, Chondrodite	Reaction Point	1440	49	29	22
H	Chondrodite, Norbergite, Tridymite	Reaction Point	1250	37	28	35
J	Forsterite, Clinoenstatite, Chondrodite	Reaction Point	1340	44	16	40
K	Clinoenstatite, Chondrodite, Tridymite	Reaction Point	1300	43	16	41
L	Clinoenstatite, Cristobalite, Tridymite	Inversion Point	1470	46	5	49

Note: The data of Bowen and Anderson (3) and Greig (4) are omitted.

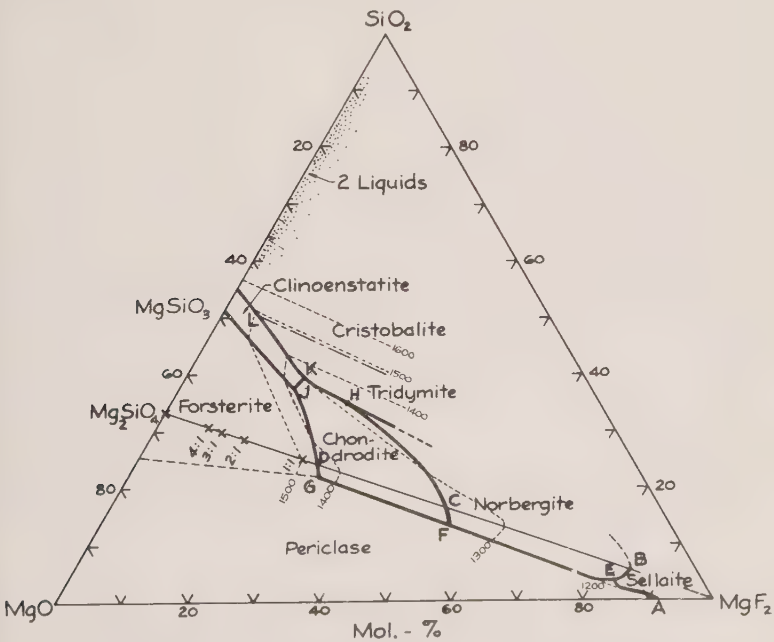

FIG. 5. Phase equilibrium diagram of the ternary system MgO-MgF_2-SiO_2.

The system Mg_2SiO_4-MgF_2-SiO_2

On the side beyond the join Mg_2SiO_4-MgF_2 (Fig. 5) the position of the ternary eutectic could not be determined. In this region such strong reactions take place, at the required temperatures, that methods applied here could not be used. A further difficulty must be noted here, obviously caused by the very great fluidity and low surface tension of the melts. Quite frequently, they crept over the margins of the platinum capsule. In the open atmosphere, the melt was hydrolysed, and MgO formed. This often happened also on nearly imperceptible pores and scratches formed in welding the platinum capsules. Nothing can be said on the entire extension of the sellaite field, but some statements can be made for the fields of chondrodite and norbergite extending toward the MgF_2 apex. The boundary against the SiO_2 field (see Table 2) could be established only approximately. The fields of crystallization of chondrodite and clinoenstatite with their boundaries against forsterite and SiO_2 could be established more precisely.

The question of a clear differentiation between cristobalite and tridymite in the products was rather difficult, especially in milky glasses

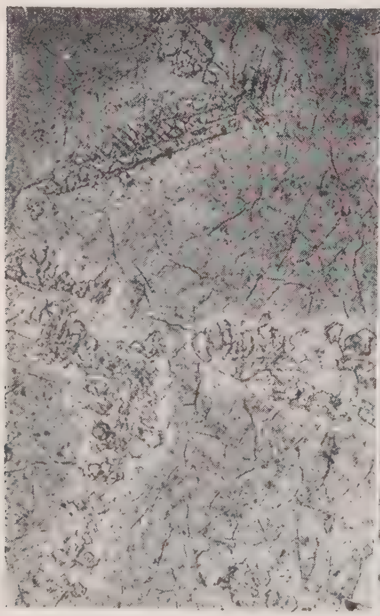

FIG. 6. (left) Cristobalite skeletons embedded in milky glass—Analyser 60° (Composition 35 mol. % MgO; 25% MgF_2; 40% SiO_2). ×85

FIG. 7. (right) Two large norbergite needles, between them quenched substance (sellaite in characteristic dendrites)—Analyser 60° (Composition 15 mol. % MgO; 75% MgF_2; 10% SiO_2). ×85

FIG. 8. (left) The chondrodite crystal in the middle shows many little periclase grains. Analyser 70° (Composition 40 mol. % MgO; 45% MgF_2; 15% SiO_2). ×85

FIG. 9. (right) Chondrodite crystals surrounded by a fringe of quenched substance embedded in glass.—Analyser 60° (Composition 40 mol. % MgO; 25% MgF_2; 35% SiO_2). ×85

quenched from the melts. Usually the silica is observed in granular aggregates, but sometimes in dendrites (Fig. 6) or octahedral shapes. The x-ray patterns of these crystallizations show the lines of cristobalite, which was also identified by its refractive index. Because of the smallness of the cristobalite crystals in the milky glasses, the index of refraction could not be determined, and the x-ray photographs showed no lines; evidently too little crystalline material was present. In Fig. 5 and Table 2 the inversion tridymite$\rightleftharpoons$cristobalite is considered to be 1470° C.

Particularly well developed lath-shaped primary crystals of norbergite (together with characteristic sellaite dendrites in the matrix) are seen in Fig. 7.

Chondrodite crystals with many inclusions of periclase grains are observed in Fig. 8, and euhedral chondrodites surrounded by a fringe of quenched material in a glass in Figure 9.

A mixture of the composition of a hypothetical magnesium-amphibole ($6MgO \cdot MgF_2 \cdot 8SiO_2$) was heated to 1315° and 1614° C., but no new phases could be found.

No compositions near, or in, the field of liquid immiscibility on the side MgO-SiO_2 was investigated.

Summary

In a part of the system MgO-MgF_2-SiO_2 the liquidus points were determined. For this purpose dynamic and static methods were applied. The identification of the crystalline phases was undertaken by the microscopic investigation of thin sections, by determination of the refractive indices, and by the x-ray diffraction method.

The position and temperature of the eutectics, incongruent melting points and reaction points were as far as possible determined.

The join Mg_2SiO_4-MgF_2 proved to be a binary system, where the humite-minerals norbergite and chondrodite appear as incongruently melting compounds. Neither here nor in the three-component system could humite and clinohumite be obtained as products of crystallization. No further compounds could be found.

Acknowledgment

The authors wish to express their gratitude to Dr. Wilhelm Eitel, of the Institute of Silicate Research at the University of Toledo, for his critical survey of this paper.

References

1. Eitel, W., (1937), Das System CaO-CaF_2-Ca_2SiO_4: *Z. angew. Mineral.* **1,** 269–284.
2. Bååk, T. and Ölander, A., (1955), The system $CaSiO_3$-CaF_2: *Acta Chem. Scand.* **9,** 1350–1354.
3. Bowen, N. L. and Andersen, O., (1914), The binary system MgO-SiO_2: *Amer. J. Sci.*, 4 Ser., **37,** 487–500.
4. Greig, J. W., (1927), Immiscibility in silicate melts: *Amer. J. Sci.* 5 Ser., **13,** 1–44.
5. Eitel, W., Hatch, R. A. and Denny, M. V., (1953), Synthetic mica investigations II. Role of fluorides in mica batch reactions: *J. Amer. Cer. Soc.* **36,** 341–348.
6. Rankama, K., (1947), Synthesis of norbergite and chondrodite by direct dry fusion: *Am. Mineral.* **32,** 146–157.
7. Karyakin, L. I. and Gul'ko, N. V., (1954), Formation of Cuspidine and of the Minerals of the Humite Group: *Dokl. Akad. Nauk SSSR,* **96,** 581–584.
8. Valkenburg, A. van, (1955), Synthesis of the humites: *Amer. Miner.* **40,** 339.
9. Fujii, T. und Eitel, W., (1957), Reaktionen im festen Zustand im System MgO-MgF_2-SiO_2: *Radex-Rdsch.* 1957, 445–469.
10. Günther, K.-G., (1958), Zur Messung von Dampfdrucken und Verdampfungsgeschwindigkeiten an glasbildenden Substanzen: *Glastechn. Ber.* **31,** 9–15.
11. Counts, W. E., Roy, R. and Osborn, E. F., (1953), *Fluoride model systems. II.* The binary systems CaF_2-BeF_2, MgF_2-BeF_2 and LiF-MgF_2: *J. Amer. Ceram. Soc.* **36,** 12–17.
12. Sahama, T. G., (1953), Mineralogy of the humite group: *Ann. Acad. Sci. Fenn.*, Ser. A, III, Nr. 31.
13. Shell, H. R. and Craig, R. L., (1954), Determination of silica and fluorides in fluorsilicates: *Anal. Chem.* **26,** 996–1001.
14. Thomas, F., (1959), Beiträge zur Bestimmung der Kieselsäure in Fluorsilikaten: *Silikattechnik* **10,** 129–130.
15. Venturello, G., (1940/41), Studio termico-roentgenografico del systema BeF_2-MgF_2: *Atti reale Accad. Sci.*, Torino, **76 I,** 556–565.

Manuscript received February 2, 1960.

THE AMERICAN MINERALOGIST, VOL. 45, NOVEMBER–DECEMBER, 1960

CRYSTAL SYNTHESIS BY REFRIGERATION

C. W. Wolfe, *Boston University, Boston, Massachusetts.*

Abstract

Maser operation requires crystals containing paramagnetic ions such as chromium or nickel in minute percentages which substitute generally for cobalt, aluminum, or magnesium. Crystals of K_3 $(Co_{0.995}Cr_{0.005})(CN)_6$ have been grown in freezer compartments at temperatures of 4° to 5° C. Seeds for crystals are inserted in solutions which are saturated at ~0° C. in the freezer. Controlled quantities of solutions which are saturated at room temperature are periodically introduced into the freezer solution. The desired effect is that the growing crystals will adsorb all precipitating ions above the saturation level to eliminate additional spontaneous seeding. Daily turning of the crystals is conducive to homogeneous growth. Growth rates have been measured. Small crystals have a faster growth rate per unit weight but a lesser mass accumulation per unit time than larger crystals. Space restrictions are the only limitations on the maximum size that can be developed. Single crystals as large as: $c=12$ cm., $b=4$ cm., $a=3$ cm. have been prepared during a three month growing period.

Introduction

In the development of a device that would produce *M*icrowave *A*mplification by *S*timulated *E*mission of *R*adiation, now known as a *MASER*, paramagnetic crystals of various types can be used. Dr. J. W. Meyer of the Lincoln Research Laboratories of the Massachusetts Institute of Technology made a thorough analysis of what atoms would be best suited in a MASER crystal, and chromium was indicated as being one of the most desirable. Upon searching through the literature for chromium bearing crystals he chanced on the isomorphous series of K_3 (Co, Fe, Cr) $(CN)_6$. These crystals had been grown from solution; their crystallography was known; and the amount of chromium that could be introduced could be rigorously controlled. Dr. Meyer asked Dr. Harry Gatos, also of Lincoln, to prepare crystals of the composition K_3 $(Co_{0.995}$ $Cr_{0.005})$ $(CN)_6$. Shortly thereafter the author was consulted concerning the preparation of such crystals, and three different methods were initiated, all of which were successful, but only one of which will be considered here, synthesis by refrigeration.

A normal household upright refrigerator was used in the first synthesis in the Boston University Laboratories and at Lincoln. Several disadvantages of the upright refrigerator became apparent; and when the author was contacted by Dr. Harold I. Ewen and Mr. William From of the Ewen Knight Corporation of Needham to prepare comparable crystals with various chromium contents, a switch over to the horizontal freezer type of refrigerator was made. Miss Irita Vilks was engaged by Ewen Knight to do the actual synthesis under the direction of the author, and the results of this program follow.

Basic Philosophy of the Refrigeration Technique

Although crystals can readily be grown by evaporation of a saturated solution, two major problems often arise when such a technique is used. The first of these, the excessive precipitation in the meniscus region between the solution and the beaker with subsequent capillary flow in the precipitate and further precipitation until, if permitted, the inside and outside walls of the container are covered with precipitate, can be controlled by lining the container with a non-wetting agent at the junction region between the surface of the solution and the container. This procedure is often unsatisfactory, and the operator is compelled to change containers periodically. Other difficulties with the non-wetting agent are often encountered. Obviously, then, crystallization without evaporation is desirable.

The second major difficulty with crystallization by evaporation is the customary over seeding, particularly in the surface tension film at the surface of the solution. Since this area, along with the meniscus region are the only places where supersaturation initially occurs, excessive seeding occurs. The density of the surface tension layer, for all practical purposes, is very high, witness the floating of a greased needle on water; and the newly formed seeds may grow to considerable size while floating at the surface, even though their density far exceeds that of the solution as a whole. Hopper shaped crystals comparable to those formed in saline water bodies gradually develop. Periodically these sink to the bottom in random orientation with the crystals already lying on the bottom, and the total result is a chaotic arrangement of many small crystals. This difficulty can also be controlled in part, but excessive seeding is one of the major problems of crystal synthesis by evaporation.

Since single, homogeneous crystals approaching maximum sizes of 40–50 mm. were desired for the maser experimentation, the use of the evaporation technique seemed undesirable. It is, of course, well known that solubilities of most substances differ at different temperatures, and it was decided to use the temperature differential method of synthesis. Solutions were kept in a bath at 40° C. in the Lincoln Laboratory, and periodically some of this stock solution was added to the crystal growing bath at 30° C. The bath was covered with a perforated plate reducing, but not completely eliminating, evaporation. Seeds, mounted on pedestals, which will be described later, picked up the excess ions developing from the temperature differential. Both stationary and moving seeds were employed in this phase of the synthesis program. Although most of the disadvantages of the evaporation technique were eliminated by this approach, the problems involved in maintaining bath temperatures, in

controlling weekend growth, and others made the use of this technique of crystallization somewhat unattractive.

Simultaneously with the above approaches to synthesis the same basic approach of crystallization by *thermal differentiation* was begun under refrigeration conditions. A common upright type of household refrigerator was employed; in this refrigerator the beakers were placed which were to hold the host solution in which the crystals were to grow. Feed solutions at room temperature were kept available, and periodically small amounts of these solutions were added to the host solution. The general philosophy of approach suggested that the thermal differentiation would produce an excess of ions over saturation. If the feeding process were adequately controlled, all excess ions would precipitate on the seeds; no new nucleii would form; and the rate of growth would depend on the rate that ions could be added which could be concomitantly absorbed.

Technique of Crystallization by Refrigeration Equipment

The first refrigerator employed was the normal upright type; and although excellent crystals were grown in it, certain disadvantages such as wide temperature variations during open and shut phases of operation suggested that the horizontal freezer type of unit could be better employed. The opening of such a chest at the top inhibited the flow of cold air from the chest, and manual operation of crystal turning in the chest and of crystal feeding could be done without a marked temperature variation. The temperature of operation of the chests was in the region $-4°$ to $+5°$ C. at the bottom of th chest. The temperatures in the higher part of the chest were as much as 10 degrees warmer than at the bottom.

The stock solutions were composed of 150 grams of potassium cobaltichromi cyanide in 450 grams of distilled water. This yielded a solution which was not saturated at room temperature but which was significantly supersaturated at refrigerator temperatures. The solubility curves will not be reproduced here. A magnetic stirrer was used to facilitate solution. The preparation of the *host solution* in which the crystals would grow involved two steps. Thirty cubic centimeters of stock solution were placed in a beaker and introduced into the refrigerator. Seeding very quickly took place. After the solution had stood an adequate time to permit complete equilibrium to be established, the solution remaining in the beaker was decanted into another previously cooled beaker and was set back into the refrigerator for observation to make sure seeding was completed. If it were not, the process was continued until the host solution was free and remained free of all seeds.

The procurement of seeds to be placed in the stock solution was made in several ways. The crystalline mass that precipitated when the stock solution was placed in the refrigerator was inspected, and the better crystals were separated from the remainder of the mass. Care was required that no foreignly oriented material was present on the selected seeds. Crystals of two or three habits could sometimes be found in the crystalline mass, but the general tendency was for all crystals to have essentially the same habit. Since it was discovered that the final habit of the crystals could be largely controlled by the habit of the seed crystal, considerable effort was employed to find seeds with the desired initial habit. Seeds were also produced by evaporation of the stock solutions under vacuum and in the open air. The best seeds were obtained early in the evaporation process before many nucleii had developed. Seeds less than 1 mm. in maximum dimension were often employed. One of the most successful seed production methods was that of crystallization from a residue film from an emptied beaker in which the solution had been standing. After pouring the solution from the beaker, the beaker was left to stand without washing, and a few isolated crystals formed on the beaker bottom or walls. These were usually of the habit desired in the final crystals.

Once the seeds were selected they were handled with plastic forceps to eliminate fracturing because of differential thermal expansion when held in the hands. The fractures were never sufficiently large to cause a breakup of the crystals, but they did cause the development of cloudy zones in the growing crystals. Whenever it was necessary to handle the crystals with the hands, rubber gloves cut down heat conductivity to the crystals. It was important that the crystals not undergo any strong temperature variation, and to this end the crystal seeds were inserted on filter paper into the chest and were cooled until they were the same temperature as the host solution. Cooling by this method was less shocking than by direct insertion from the outer warm air into the cold host solution.

In order to eliminate the possibility of subsequent seeding on the seeds, the crystals were mounted on pedestals to keep them off the bottom; the sizes of the pedestals varied with the size of the growing crystals. The greatest difficulty in controlling seeding was always in the very early phases of growth. At this stage, although the individual seeds grew proportionately very fast, it was impossible to add such a small quantity of stock solution that the seeds in the host solution could adsorb all of the precipitating ions as they were available, and some random seeding was the common result. This could be eliminated in part by placing many seedlets in the same host solution and, aside from the mechanical prob-

lems of keeping the seedlets on the pedestals, this technique kept foreign seeding at a minimum. Once the crystals reached maximum dimensions of three or more millimeters, they were easily handled, and non-desirable seeding could be completely controlled. As the crystals grew to larger dimensions, they were placed on larger pedestals. When all danger of seeding was past, the crystals which were 1 cm. in at least one direction could be placed directly on the base of the container. The larger the crystals became, the fewer seed units were kept in any one container, for there could be a complete pick-up of all precipitating ions on the larger surfaces of the fewer crystals.

The feeding of the crystals was practically as simple as the feeding of animals. By simple experimentation it was possible to determine how much stock solution could be added daily and be utilized by the growing crystal. Since evaporation was practically negligible from the host solution, the general practice was to remove practically as much solution daily before feeding as was to be added. This kept the degree of saturation upon the addition of stock solution practically constant. The quality of crystallization depended largely on the rate of feeding and on the practices employed in handling the crystals. The general practice we adopted was to feed the crystals three times a day with particular care not to overfeed before the long night period when no attention could be given the crystals. Pipettes and droppers were used for feeding upon occasion. Hollow glass tubes with the finger capping one end to keep the solution within until brought to the host solution were also used. Micro-graduated flasks were used in special control cases where the rate of addition and crystal growth were being carefully checked.

At the peak of crystal synthesis by the above technique at the Ewen Knight facility as many as 400 crystals were being grown simultaneously in beakers and other containers in two freezer units. The beakers were held in trays, with one tray superimposed over another to depths as great as four or five trays. The beakers were labeled as to the percentage of chromium which was present in the solution, and as the crystals reached sizes adequate for maser experimentation, they were removed from the solutions and properly stored.

Turning of the crystals at least once a day proved both desirable and necessary when good quality crystals were desired. This was true both when the crystals were mounted on pedestals and when they were on the beaker bottoms. Crystals set on pedestals grew around the pedestals and enclosed them unless turned. If turning were not frequent enough, the impression of the shape of the pedestal was left on the supporting crystal face, and this impression was often difficult to eliminate. Crystals which

lay on the beaker floor developed a large, non-smooth concavity on the floor side unless turned periodically. Generally, a turning of once a day was adequate.

One point of interest arose during checking of the effects of turning. It was stated earlier that the habit of the adult crystal was to a large degree determined by the habit of the embryo. Nevertheless, we discovered that habit could be controlled in part by the orientation of the crystal in the host bath. If a large *a* face were desired, that face was kept horizontal in the solution; and if a large *b* faced crystal were sought, that face or position was made horizontal. No attempt was made to develop a large *c* face, but it is doubtful that any degree of positional maneuvering would be adequate to induce the development of that face.

The ultimate shape of crystalline unit desired was a cylinder for the early masers. Since the hardness of the crystals is about 3.5, they could easily be cut to the desired shape if the proper *a* or *b* face were adequately developed at the onset. The use of a simple power jigsaw or hand jigsaw proved adequate for cutting the crystals. As a matter of interest, however, relative to the shape of the finished crystal, it was decided to grow the crystals to the size and shape desired directly. An *a* faced or *b* faced crystal of about 2 cm. maximum dimension was placed in a cylindrical form and into a host solution. The crystal grew until its maximum dimensions reached 3.5, the inner diameter of the hollow cylinder. The crystal could grow no further in that direction, and further ion accretion took place on the other surfaces until a cylinder 3.5 cm. in diameter and 1 cm. high of the crystalline substance was formed. Some stresses developed in the crystal during this procedure, and flaws appeared, but the crystals thus produced were of fairly good quality.

Due to lack of proper control upon occasion, foreign seeds would grow in random orientation on the desired crystal. These were scraped off while holding the crystals in rubber gloved hands. If the embedding had gone quite far, scraping was difficult, stresses were induced in the crystal, and the quality of the subsequently growing crystal was diminished.

Results of Crystal Growing by Refrigeration

Crystals as large as $3.1 \times 4.3 \times 12.5$ centimeters were grown in the refrigerator bath. This size is certainly not a maximum; the cutoff at this size was purely a matter of convenience. From the data at hand it appears that the only limitations to size imposed by the method are those mechanical controls such as size of container, size of freezer, and amount of ingredients available. The internal and external quality of the crystals was apparently independent of the size. This may be only apparent, for none of the large crystals was mounted under reflecting goniometric con-

ditions. The quality of the faces of the smaller crystals was not a function of size but, primarily, of the method used in removing the crystal from the bath.

The *rate of growth* of the crystals was dependent upon three primary variables. Obviously, the rate of feeding is important. No attempt was made to attain maximum growth rate, since the quality of the crystals suffers with too rapid growth, and crystals of best quality were desired. The second factor affecting growth rate was the size of the crystal which was growing. All other factors being equal, the larger the crystal receiving ions, the more ions it could pick up. In other words, the absolute growth rate was roughly proportional to size of the crystal. The ratio of growth increment to weight of the host crystal, the percentage growth rate, was inversely proportional to crystal weight. Small crystals grew much faster, percentage-wise than did the large ones. Miss Irita Vilks made a detailed analysis of growth rates relative to crystal size, and this study will appear later. The third factor affecting rate of growth was the habit of the growing crystal. There was a marked slowdown in growth rate for prismatic crystals and *b* faced crystals as compared with *a* faced crystals. No precision measurements were made on this factor, however.

Crystal Habit

The habit which developed was usually one of three simple types, with {100}, {010}, or {110} predominant, respectively. Figure 1 (left) shows two {100} crystals grown by the refrigeration methods. Figure 1 (right)

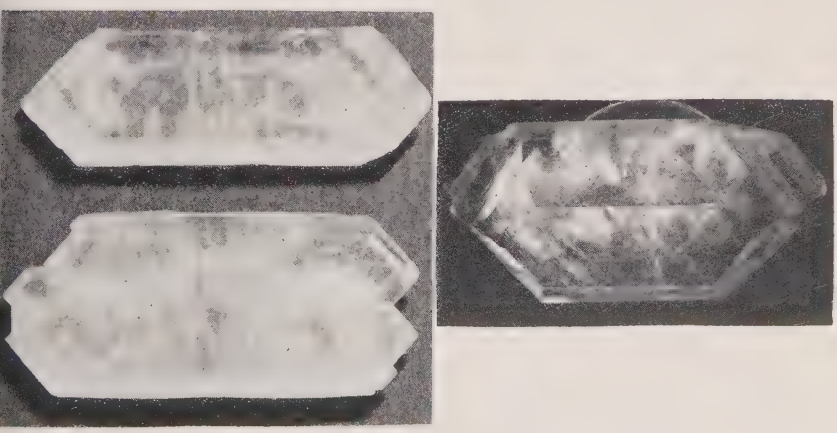

Fig. 1. Crystals of $K_3(Co_{0.995}Cr_{0.005})(CN)_6$.

Left: Elongated parallel to [001] and flattened on {100}. {110} and {111} are modifying forms. (About 8 cm. long.)

Right: Crystal with {110} habit, sitting on pedestal. (About 4 cm. long.)

shows a {110} crystal grown in a 35° C. bath. Three factors were most important in controlling crystal habit. The first of these was the habit of the initial seed chosen as the nucleus for growth and the habit or habits of adjacent growing crystals. The second factor was the orientation of the seed in the bath. No absolute measurements have yet been made concerning the effectiveness of orientation on crystal habit, but qualitative results indicate a significant influence for this factor. The third factor which influenced crystal habit was the composition of the feeding solution. Two variables in this composition occurred. The first was intentional and involved variation in the percentage of potassium chromi-cyanide introduced into the stock solution. Other factors being equal, a higher chrome content in the solutions was generally more favorable to either *m* faced or *b* faced crystals. By proper choice of the initial seed habit, this effect could be minimized. Another compositional variable was accidentally introduced. In the process of adding fresh stock solution to the host bath, some of the old simply saturated solution of the host bath was removed. This was allowed to stand in containers and to evaporate to saturation at room temperature. If this solution were then used as stock solution for later feeding, the growth habit usually became *m* faced. The explanation for this shift lies in the fact that the potassium chromi-cyanide is far less stable than the potassium cobalti-cyanide and hydrolyzes with time. This was in part circumvented by the introduction of potassium cyanide into the solution, but hydrolysis did take place, and the chromium product deriving therefrom was not in an accruable form in the crystal growth. Another serious effect of this process was that the composition of the growing crystal was not the same as that of the original solution, and the saving of the extracted solution from the host containers was discontinued.

The Unit Cell

The unit cell has been measured and reconciled with the morphology. Two polymorphic forms may exist, and the entire subject of unit cell and morphology will be treated in a later paper. It can be stated here, however, that notable deviation from the pseudo-orthorhombic symmetry usually ascribed to the substance is characteristic of the low temperature form.

Quality of Crystals

The effect of rate of growth on the crystals has been mentioned above. The two other primary factors affecting the quality of the crystals were the degree of temperature variation and the amount of mechanical handling required when undesired seeding took place. The temperature vari-

able induced by lifting the trays of beakers from the chest occasionally to permit turning and examination of the crystals for non-oriented seeds was apparently of little influence on the crystal quality. If, however, the crystals were handled, particularly without gloves, differential thermal expansion did induce fractures and other imperfections. The use of gloves partially obviated this difficulty. The mechanical scraping of unwanted seeds from the growing crystals also induced fractures and imperfections, both as a result of the mechanical forces involved in the scraping and because of the temperature variable induced in the handling. The general quality, however, was a transparent slightly greenish yellow excellent crystal. The crystals which contained higher percentages of chromium were deeper yellow in color, less transparent, and generally of poorer quality than the lower percentage crystals.

Successful Use in a Maser

Masers which used the above crystals as amplifying devices were successfully constructed at Lincoln and at Ewen Knight. A microwave signal was successfully beamed at Venus and reflected and picked up at Lincoln Laboratories, using one of the potassium cobalti-cyanide crystals with the slight doping percentage of the chromi-bearing salt. It might be pointed out that early predictions by N. Bloembergen (1956) that such a device would operate with a very low noise factor were completely born out by this experiment.

Limitations of the Technique of Crystal Growth by Refrigeration

One of the outstanding limitations of the technique lies in the difficulty of automatic feeding or automation in general. Any feed line from outside the refrigerator to the container carrying the growing crystal automatically must pass through a cooling zone in which precipitation takes place in the feed tube, finally clogging it and bringing the automatic feeding to a standstill. The fact that the crystals should be periodically turned to make them as perfect as possible also is a limitation to automation. The occasional cleaning of crystals where unwanted seeds have lodged upon them requires a periodic examination. When hundreds of crystals are being grown simultaneously, as in the Ewen Knight Facility, the full-time attention of an operator is required to produce satisfactory results.

The method is, of course, not universal in its application. There must be a significant but not too great a solubility variation with temperature. It is, therefore, necessary to have a fairly rigorous picture of the solubility curve for the substance being grown in order to get the proper

differential between the number of ions in solution outside the refrigerator as compared with the saturation conditions in the refrigerator.

The attainment of this goal is particularly difficult if the solubility curve is very steep. Substances with particularly high solubilities do not respond very readily to crystallization by refrigeration. Crystals in which the unit cell has one notably shorter direction, that is, crystals which normally develop an extremely elongated habit, cannot be grown very satisfactorily by the method, although continued study is being made of this variable.

Reference

Bloembergen, N. (1956), *Phys. Rev.* **104**, 324.

Manuscript received February 15, 1960.

VEATCHITE AND *p*-VEATCHITE*

JOAN R. CLARK AND MARY E. MROSE, *U. S. Geological Survey, Washington 25, D. C.*

ABSTRACT

Comprehensive single-crystal x-ray precession studies on type material of two strontium borate hydrates, veatchite (Switzer, 1938; Switzer and Brannock, 1950; Clark *et al.*, 1959) and *p*-veatchite (Braitsch, 1959), show that despite striking similarities the two minerals can be distinguished by single-crystal x-ray diffraction patterns. Both minerals are monoclinic: veatchite $A2/a$ (or Aa), $a=20.81$, $b=11.74$, $c=6.62_6$ Å (all $\pm 0.3\%$), $\beta=92°07' \pm 05'$ perfect cleavage parallel to dominant plate form {100}, optical orientation $Z=b$, $X=c$, $Y \wedge a=2°$; *p*-veatchite $P2_1/m$ (or $P2_1$), $a=6.72_9$, $b=20.70$, $c=6.58_1$ Å (all $\pm 0.3\%$), $\beta=119°40' \pm 05'$, perfect cleavage parallel to dominant plate form {010}, optical orientation $Y=b$, $X=c$, $Z \wedge a=29°40'$. Indexed x-ray powder data, presented for both minerals, are inadequate for positive identification. Assumption of the chemical formula, $SrO \cdot 3B_2O_3 \cdot 2H_2O$, for each mineral yields the following comparison of calculated and observed densities (g. cm.$^{-3}$): veatchite 2.85_7 calc. (8 formula units per cell), 2.78 ± 0.03 obs. (Clark *et al.*, 1959); *p*-veatchite 2.90_7 calc. (4 formula units per cell), 2.60–2.65 obs. (Braitsch, 1959). Dimorphism is possible but not established by present evidence.

A new mineral *p*-veatchite, $(Sr, Ca)O \cdot 3B_2O_3 \cdot 2H_2O$, has been described by Braitsch (1959) from an occurrence in Reyershausen, near Göttingen, Germany. Noted by Braitsch were numerous striking similarities of *p*-veatchite to veatchite, $SrO \cdot 3B_2O_3 \cdot 2H_2O$ (Switzer, 1938; Switzer and Brannock, 1950; Clark *et al.*, 1958, 1959). Chemical, spectrographic, and x-ray fluorescence analyses, as well as indices of refraction, measured density values, crystal habit and crystal class, and x-ray powder patterns, all are the same within limits of observational errors for the two minerals. The only distinction between them was found in the single-crystal x-ray study, which revealed a change in direction of the unique monoclinic symmetry axis in *p*-veatchite compared with veatchite, together with variations outside the limits of error for values of the observed cell constants. Such a close relationship between two different substances is sufficiently unusual to raise doubts concerning the validity of the descriptions. However, the relationship has been fully confirmed by the present authors, who give briefly here the results of concurrent single-crystal and powder x-ray examinations.

Crystals from the following localities were studied: veatchite from drill core no. 5, Four Corners area, Kramer district, San Bernardino County, California, supplied by R. C. Erd, U. S. Geological Survey, and described previously by Clark *et al.* (1958, 1959); veatchite taken from the type specimen, USNM 105697, Lang, Los Angeles County, California

* Publication authorized by the Director, U. S. Geological Survey.

(Switzer, 1938; Switzer and Brannock, 1950); *p*-veatchite from type material, USNM 113264, Reyershausen, Germany (Braitsch, 1959). The latter two specimens were made available to us through the courtesy of Dr. George Switzer, U. S. National Museum. Because the *p*-veatchite specimen consists of only two large crystals, preparation of a powder spindle was not feasible; however, Dr. Otto Braitsch, Mineralogical Institute, University of Göttingen, Germany, kindly permitted our use of the *p*-veatchite powder spindle prepared at the University of Göttingen from Reyershausen material. We are most grateful to each of these individuals, as well as to several colleagues at the U. S. Geological Survey: D. E. Appleman who suggested that the type veatchite be reexamined and carried out calculations for *d*-spacings of *p*-veatchite on a digital computer, E. C. T. Chao who gave valuable suggestions on presentation of the optical data, and C. L. Christ who provided critical guidance and helpful discussion during the course of the study. We are also indebted to Dr. C. A. Beevers, University of Edinburgh, Scotland, for permission to present his unpublished data on Eskdale material, originally described by Stewart, Chalmers, and Phillips (1954).

Single-crystal *x*-ray studies were carried out on quartz-calibrated precession cameras using Zr-filtered Mo radiation ($\lambda = 0.7107$ Å) and Ni-filtered Cu radiation ($\lambda = 1.5418$ Å). Film measurements were corrected for both horizontal and vertical film shrinkage. The crystallographic data found during the present study for veatchite and *p*-veatchite are given in Table 1. Several crystals were examined from the specimen of type veatchite from Lang, and all give single-crystal *x*-ray data identical within limits of observational errors with the data found for the Four Corners veatchite by Clark *et al.* (1959). No *p*-veatchite crystals were discovered on the Lang specimen, although the possibility of their presence in association with veatchite cannot be definitely ruled out. Comparison of available data for *p*-veatchite is made in Table 2. The findings of Braitsch (1959) are confirmed not only by the present study but also by Beevers (written communication, October 14, 1959) for Eskdale material, which his study identifies as *p*-veatchite.

The unit cell of *p*-veatchite can be chosen so as to be analogous in dimensions to the cell taken for veatchite (Clark *et al.*, 1959), and comparison of these two similar cells is made in Table 1 and throughout the following discussion. Both minerals have a dominant plate form, to which the perfect cleavage is parallel and to which the short reciprocal axis (associated with the ~21 Å direct axis) is normal. In *p*-veatchite this axis is the monoclinic symmetry axis, its character being demonstrated by the intensity relationships among appropriate *hkl* reflections and the exactly 90° angles the axis makes with a^* and c^*, respectively.

TABLE 1. CRYSTALLOGRAPHIC DATA FOR VEATCHITE AND *p*-VEATCHITE*

	Veatchite		*p*-Veatchite[a]	
	Four Corners[b]	Lang[c]	Reyershausen	
			(1)[d]	(2)
a	20.81Å	20.81Å	11.69Å	6.72_9
b	11.74	11.74	20.70	20.70
c	6.63_7	6.62_6	6.58_1	6.58_1
β	92°02′	92°07′	90°24′	119°40′
	(All cell lengths ±0.3%; angles ±05′)			
$a:b:c$	1.773:1:0.565	1.773:1:0.564	0.565:1:0.318	0.325:1:0.318
Space Group	$A2/a$ (or Aa)	$A2/a$ (or Aa)	—[e]	$P2_1/m$ (or $P2_1$)
Volume	1620 Å³	1618 Å³	1592 Å³	796 Å³
Number of $[SrO \cdot 3B_2O_3 \cdot 2H_2O]$ per unit cell	8	8	8	4
Density, calc.	2.85_7 g.cm.$^{-3}$	2.86_1 g.cm.$^{-3}$	2.90_7 g.cm.$^{-3}$	
obs.	2.78±0.03	2.69[f]	2.60–2.65[g]	

* Data of present study unless otherwise noted.
[a] Values for *p*-veatchite crystals from type material (USNM 113264).
[b] Values taken from Clark *et al.* (1959).
[c] Values for veatchite crystals from type specimen (USNM 105697).
[d] Values obtained from (2) using transformation matrix 201/010/001.
[e] $B2_1/m$, not a standard setting of Int. Tables (1952).
[f] Switzer (1938).
[g] Braitsch (1959).

In veatchite the short reciprocal axis is at a distinct 88° angle to c^* and the intensity relationships among hkl reflections are not compatible with assignment of twofold symmetry to the short reciprocal axis. Accordingly, the axis normal to the plate must be b^* in *p*-veatchite, and, following the convention $c<a$, it becomes a^* in veatchite. Direct comparison of precession photographs of the similar reciprocal nets, veatchite $h0l$ with *p*-veatchite $0kl$, and veatchite $0kl$ with *p*-veatchite $h0l$, immediately reveals these distinctive differences. The *p*-veatchite x-ray cell chosen by Braitsch (1959) can be transformed to the cell that is analogous to veatchite with the matrix 201/010/001 (as noted by Braitsch).

The optic plane in each mineral is parallel to the plate form, and correlation of the optical directions and the x-ray crystallography is shown in Fig. 1a for veatchite and in Fig. 1b for *p*-veatchite. It is not clear whether the optical orientation given for *p*-veatchite by Braitsch (1959) is for the

TABLE 2. COMPARISON OF CRYSTALLOGRAPHIC DATA FOR *p*-VEATCHITE

	Present Study[a]	Braitsch (1959)[b]	Beevers[c]
a	$6.72_9 \pm 0.02$ Å	$6.72_1 \pm 0.02$ Å	6.74 Å
b	20.70 ± 0.04	20.81 ± 0.02	20.62
c	$6.58_1 \pm 0.02$	$6.64_7 \pm 0.02$	6.60
β	$119°40' \pm 05'$	$119°04' \pm 10'$	119°38′
$a:b:c$	0.325:1:0.318	0.323:1:0.319[d]	0.327:1:0.320[d]
Space Group	$P2_1/m$ (or $P2_1$)	$P2_1/m$ or $P2_1$	$P2_1/m$ (or $P2_1$)
Volume	796 Å^3	813 ± 5 Å^3	797 Å^3[d]
Cell Contents	$4[SrO \cdot 3B_2O_3 \cdot 2H_2O]$?	$4[(Sr, Ca)O \cdot 3B_2O_3 \cdot 2H_2O]$?	—
Density (calc.)	2.90_7 g.cm.$^{-3}$	—	—
(obs.)	—	2.60–2.65	—

[a] Cell constants from precession film measurements; Reyershausen *p*-veatchite (USNM 113264).

[b] Cell constants from Weissenberg film measurements; Reyershausen *p*-veatchite.

[c] Values found for crystals from Eskdale no. 2 borehole near Aislaby, north Yorkshire, England (Stewart, Chalmers and Phillips, 1954); written communication from Beevers, October 14, 1959.

[d] Values calculated by authors from data of original investigator.

cell defined by his *x*-ray study. The observation $Z \wedge c = -30°$ (Stewart, Chalmers, and Phillips, 1954) is evidently not correct for the present description of the cell (Table 2, Fig. 1*b*).

Lang veatchite was described by Switzer (1938) as occurring in vein fibres; an angle of $-38°$ was observed between the Z optical direction and the fibre axis (taken as *c*), an observation confirmed by Murdoch (1939). In the present study two crystals of fibrous habit from the original Lang specimen of veatchite were examined. On one crystal an angle of approximately 39° was observed between the elongation direction and the Z optical direction. *X*-ray examination shows that in the present veatchite cell, the elongation direction of this crystal is [042]; the crystal is flattened on {100}. Rotation about [042] would produce a bewildering array of closely spaced reflections, undoubtedly explaining the two approximately 41 Å cell lengths originally reported by Switzer (1938). The second crystal examined from the original specimen in the present study was observed to extinguish parallel and perpendicular to the fibre direction, and *x*-ray study of this crystal shows that in the present veatchite cell the elongation axis is [001], and the crystal is flattened on {100}.

Neither optical nor *x*-ray evidence for twinning was found during the present study for either mineral. Evidence for some stacking disorder in veatchite occurs in the streaking of reflections along the a^* direction;

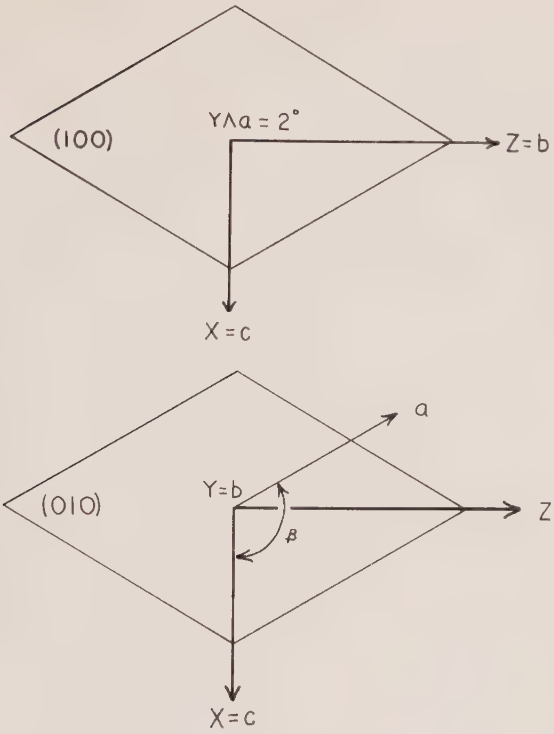

FIG. 1*a* (above). Optic plane (100) of veatchite. Orientation referred to crystal cell with $a=20.81$, $b=11.74$, $c=6.63_7$ Å, $\beta=92°02'$.

b (below). Optic plane (010) of *p*-veatchite. Orientation referred to crystal cell with $a=6.72_9$, $b=20.70$, $c=6.58_1$ Å, $\beta=119°40'$. $Z\wedge a=29°40'$.

such streaking is not observed in any direction for the *p*-veatchite reflections.

X-ray powder patterns for both veatchite and *p*-veatchite were taken with a 114.59 mm. diameter powder camera using Ni-filtered Cu radiation ($\lambda=1.5418$ Å), and the measurements were corrected for film shrinkage. Single-crystal intensities for each *hkl* reflection were estimated visually from precession films of varying exposure times. These intensities, together with the observed and calculated d_{hkl} and the intensities of the observed powder lines, are listed in Table 3 for both minerals. As might be expected from the similarity of the minerals, their powder patterns are much alike. Specifically, the observed *d*-spacings for the first three lines in order of strongest intensities are the same for each. The remainder of the lines have *d*-spacings so nearly alike that unless powder patterns are prepared and measured with extreme care the minor differ-

TABLE 3. *X*-RAY POWDER DATA FOR VEATCHITE AND *p*-VEATCHITE, $SrO \cdot 3B_2O_3 \cdot 2H_2O$(?)

Veatchite					*p*-Veatchite				
Calculated[a]		Measured			Measured			Calculated[a]	
		Single Crystal[b]	Powder[c]		Powder[c]		Single Crystal[b]		
hkl	d_{hkl}	I	d_{hkl}	I	I	d_{hkl}	I	d_{hkl}	*hkl*
200	10.40	vs	10.5 ±0.1	100	100	10.4 ±0.1	vs	10.35	020
			8.29[d]	1	2	8.17[d]			
020	5.870	abs.					abs.	5.847	100
011	5.775	w					vw	5.752	$\bar{1}01$
							abs.	5.718	001
120	5.649	s	5.64 ±0.05	6	20	5.64 ±0.05	s	5.627	110
111	5.609	m							
111	5.521	m					m	5.542	$\bar{1}11$
							w	5.512	011
400	5.199	m					m	5.175	040
$\bar{2}11$	5.115	m }	5.12 ±0.05	6	10	5.10 ±0.05	s	5.091	120
220	5.112	s }					w	5.028	$\bar{1}21$
211	4.985	w					vw	5.005	021
$\bar{3}11$	4.505	m }	4.51 ±0.03	2					
320	4.480	w }					{ vw	4.461	130
					5	4.43 ±0.03	{ w	4.418	$\bar{1}31$
							{ m	4.403	031
311	4.372	w	4.37 ±0.03	2					
$\bar{4}11$	3.924	s }	3.92 ±0.03	4					
420	3.892	m }					{ m	3.875	140
					10	3.85 ±0.03	{ m	3.847	$\bar{1}41$
							{ s	3.837	041
411	3.807	s	3.81 ±0.03	3					
600	3.466	vs	3.47 ±0.02	20	20	3.46 ±0.02	vs	3.450	060
$\bar{5}11$	3.425	ms							
520	3.394	w							
							{ w	3.379	150
031	3.370	s	3.37 ±0.02	3	15	3.38 ±0.02	{ vs	3.364	$\bar{2}01$
							{ ms	3.360	$\bar{1}51$
							ms	3.353	051
131	3.336	ms }					vs	3.344	101
511	3.328	m }	3.32 ±0.02	35			{ ms	3.320	$\bar{2}11$
131	3.318	m }			60	3.31 ±0.02	{ s	3.301	111
002	3.316	vs }					{ vs	3.290	$\bar{1}02$

[a] d_{hkl} calculated from the following data: veatchite $a=20.81\pm0.04$, $b=11.74\pm0.03$, $c=6.63_7\pm0.02$ Å, $\beta=92°02'\pm05'$, space group $A2/a$ or Aa; *p*-veatchite $a=6.72_9\pm0.02$, $b=20.70\pm0.04$, $c=6.58_1\pm0.02$ Å, $\beta=119°40'\pm05'$, space group $P2_1/m$ or $P2_1$. All calculated spacings listed for $d\geq2.800$ Å.

[b] Single crystal intensities estimated visually from various precession films taken with different exposure times; vs = very strong, s = strong, ms = medium strong, m = medium, w = weak, vw = very weak, abs. = absent.

[c] 114.59 mm. diameter camera, Ni-filtered Cu radiation ($\lambda=1.5418$ Å). Film measurements corrected for shrinkage; b = broad. Lower limit of 2θ measurable: approximately 7° (13 Å). Veatchite from Four Corners area, Kramer district, San Bernardino County, California, film no. 13418, spindle no. 10104; type *p*-veatchite from Reyershausen, near Göttingen, Germany, film no. 14856 (spindle courtesy of Dr. O. Braitsch, University of Göttingen).

[d] Fe Kα radiation: (200) of veatchite, (020) of *p*-veatchite.

TABLE 3 (*Continued*)

Veatchite					*p*-Veatchite				
Calculated[a]		Measured			Measured			Calculated[a]	
		Single Crystal[b]	Powder[c]		Powder[c]		Single Crystal[b]		
hkl	d_{hkl}	I	d_{hkl}	I	I	d_{hkl}	I	d_{hkl}	hkl
$\bar{2}31$	3.223	s	3.22 ±0.02	3			m	3.250	$\bar{1}12$
$\bar{2}02$	3.192	w			5	3.19 ±0.02	s	3.199	$\bar{2}21$
231	3.190	m					s	3.182	121
202	3.128	vw					w	3.136	$\bar{1}22$
$\bar{3}31$	3.053	w							
$\bar{6}11$	3.013	ms					w	3.024	$\bar{2}31$
331	3.010	m	3.00 ±0.02	3b	5	3.02 ±0.02	s	3.009	131
620	2.985	ms			5	2.97_1 ±0.01	ms	2.971	160
							vw	2.970	$\bar{1}32$
							ms	2.959	$\bar{1}61$
							m	2.954	061
040	2.935	s	2.93_6±0.01	2					
611	2.933	m							
							s	2.923	200
140	2.906	m							
022	2.887	vw					m	2.895	210
$\bar{1}22$	2.872	s	2.865±0.01	9			w	2.876	$\bar{2}02$
$\bar{4}31$	2.851	w					w	2.859	002
122	2.848	s			15	2.854±0.01	s	2.849	$\bar{2}12$
$\bar{4}02$	2.841	vw					vs	2.832	012
240	2.825	s					w	2.820	$\bar{2}41$
							s	2.813	220
431	2.806	vw	2.798±0.01	1			w	2.809	141
$\bar{2}22$	2.804	m							
					2	2.782			
			2.763	1					
					2	2.746			
			2.704	1	2	2.696			
			2.600	25	30	2.592			
			2.564	1					
			2.495	1	2	2.517			
			2.398	6	10	2.394			
			2.245	2					
			2.204	3	10	2.200			
			2.171	2	5	2.161			
			2.155	2	2	2.140			
			2.115	2					
			2.079	6	10	2.078			
			2.045	4					
			2.029	4	10	2.033			
			plus many additional lines, all with I≤4		5	2.002			
					10b	1.938			
					plus many additional lines, all with I≤5				

ences in line positions will not be significant. There are variations in the line intensities between the veatchite and *p*-veatchite patterns, but variations in line intensities among known veatchite patterns have been observed and are attributed to preferred orientation, a hazard that is common with these minerals because of their micaceous cleavage parallel to the common plate form. Therefore, line intensity variation is not considered a reliable means of differentiation.

The powder data for veatchite that are given in Table 3 are taken from Clark *et al.* (1959) and are from measurements of a film made using a spindle of the Four Corners veatchite. Powder patterns of type veatchite from Lang were also prepared. All the lines found on the Four Corners veatchite patterns are present and identifiable on the Lang patterns, but an additional compound which has eluded all efforts at identification is also present on the Lang patterns, giving rise to additional lines and possible superpositions. Therefore, an indexed pattern of type veatchite has not been presented; the pattern of Four Corners veatchite (Table 3) is considered to represent the best available *x*-ray powder data for veatchite.

Assignment of the chemical formula $SrO \cdot 3B_2O_3 \cdot 2H_2O$ to veatchite was made by Clark *et al.* (1959) on the basis of previously reported chemical analyses (Switzer and Brannock, 1950; Stewart, Chalmers and Phillips, 1954), taken together with a confirming spectrographic analysis, observed density determinations, and the *x*-ray crystallography. Braitsch (1959) gives for *p*-veatchite the chemical formula $(Sr, Ca)O \cdot 3B_2O_3 \cdot 2H_2O$. The calculated density based on $4[SrO \cdot 3B_2O_3 \cdot 2H_2O]$ per cell is not as close in value to the observed range of densities (Table 1) as might be expected, and a similar situation exists for veatchite (Clark *et al.*, 1959). Substitution of Ca for Sr in amounts sufficient to lower the calculated density to a value more in accord with the observed densities would require the presence of a much higher percentage of Ca than the relatively small percentages reported to date from the chemical analyses of Switzer and Brannock (1950) and of Stewart, Chalmers and Phillips (1954).

From consideration of the structural principles governing hydrated borate crystals (Christ, 1959, 1960) and the chemical composition of veatchite and *p*-veatchite, it is possible to make some prediction of the composition and structure of the boron-oxygen polyanions contained in these crystals. The polyanion will probably contain boron-oxygen tetrahedra and triangles, sharing corners, in the ratio 1:2. One such possible arrangement, corresponding to the proposed composition $SrO \cdot 3B_2O_3 \cdot 2H_2O$, would consist of infinite chains of composition $[B_6O_8(OH)_4]_n^{-2n}$. Another possibility suggested by Christ (1960) is a linkage of the same boron-oxygen elements to form isolated dimers of

composition $[B_6O_7(OH)_6]^{-2}$. The presence of such dimers in the crystal structure would require that the chemical formula of veatchite be $SrO \cdot 3B_2O_3 \cdot 3H_2O$.

Veatchite and *p*-veatchite might be polymorphs if the same anion element is present in each but arranged differently about the cation, or if the boron-oxygen triangles and tetrahedra link together differently in each compound. However, the two minerals need not be polymorphs, for even if they contain identical anion elements, the one might have a different water content from the other. Another complication that might occur is the substitution of silicon for some of the tetrahedrally-coordinated boron in one or the other compound. Final determination of the chemical formula or formulas of the two minerals and elucidation of the interesting relationship between them probably will be revealed only after crystal structure analyses have been completed.

References

Braitsch, Otto (1959), Über *p*-Veatchit, eine neue Veatchit-Varietät aus dem Zechsteinsalz: *Beitr. zur Mineralogie und Petrographie* **6,** 352–356.

Christ, C. L. (1959), Nature of the polyions contained in hydrated borate crystals [abs.]: *Program and Abstracts, American Crystallographic Association Annual Meeting, Ithaca, N. Y.*, p. 28.

Christ, C. L. (1960), Crystal chemistry and systematic classification of hydrated borate minerals: *Am. Mineral.* **45,** 334-340.

Clark, Joan R., Mrose, Mary E., Christ, C. L., Block, S., Perloff, A. and Burley, G. (1958), Investigation of veatchite [abs.]: *Geol. Soc. America Bull.* **69,** 1547.

Clark, Joan R., Mrose, Mary E., Perloff, A. and Burley, G. (1959), Studies of borate minerals (VI): Investigation of veatchite: *Am. Mineral.* **44,** 1141–1149.

Murdoch, Joseph (1939), Crystallography of veatchite: *Am. Mineral.* **24,** 130–135.

Stewart, F. H., Chalmers, R. A., and Phillips, R. (1954), Veatchite from the Permian evaporites of Yorkshire: *Mineral. Mag.* **30,** 389–392.

Switzer, George (1938), Veatchite, a new calcium borate from Lang, California: *Am. Mineral.* **23,** 409–411.

Switzer, George and Brannock, W. W. (1950), Composition of veatchite: *Am. Mineral.* **35,** 90–92.

Manuscript received February 15, 1960.

THE AMERICAN MINERALOGIST, VOL. 45, NOVEMBER-DECEMBER, 1960

CLEAVAGE AND THE IDENTIFICATION OF MINERALS

G. A. WOLFF* AND J. D. BRODER,* *U. S. Army Signal Research and Development Laboratory, Fort Monmouth, New Jersey.*

ABSTRACT

"Mechanical etching" of substances gives a characteristic pattern that can serve as a means of identifying unknown minerals and other crystalline materials. The surfaces of single crystals can be ground with coarse abrasives in several ways; the microcleavage pits obtained can then be investigated by the light figure method. Sharp and diffuse spots and zonal reflections make up the pattern observed. The spots correspond to plane cleavages (macrocleavage) and the zones correspond to cylindrically curved microcleavages. There is always a center of symmetry introduced into the pattern, because in cleavage and micro-cleavage, the two newly created surfaces match.

Minerals and synthesized materials of various kinds have been investigated, and their patterns recorded. These patterns are arranged according to their structural relationship; similar patterns have been found for members of identical structure groups. Charts of these patterns, when arranged according to crystal systems and structures, will aid in the iden- fication of unknown crystalline materials. Among the groups investigated were pyrit- marcasite, sphalerite, wurtzite, barite, halite, chrysolite and other structure groups.

Cleavage has been used since the beginning of the study of mineralog to characterize minerals. Many minerals have been identified by the cleavage habit, i.e., "rhombohedral" for calcite; "cubic" for halite, an so on. Yet, the majority of mineral specimens are identified mainly from their natural habit, or from the results of chemical etching and/or from chemical and other analyses. In these cases, cleavage serves only as an auxiliary method of identification, or merely confirms the results. The reason for this is that reported cleavage data are often ambiguous. Differ-ences among cleavage data have been reported by several authors. There are instances where different cleavages are shown for the same materia obtained from different geographical locations. Dana (1) reports tha stannite crystals from Cornwall show (110) and (001) cleavage, whil stannite crystals from Bolivia show no cleavage. For this mineral, as for others, it has been suspected that the "cleavage" is caused by "parting" and finally there are instances where, under the heading "cleavage" only fracture is reported and described in general terms as "conchoidal," "sub-conchoidal" or "hackly." This lack of reliability of the cleavag data has relegated it to a minor means of identifying minerals. An at-tempt has been made by Seaman (2) and Tertsch (3) to utilize cleavage as a means of classifying minerals. Though this work is an extensive collec-tion of cleavage and habit data, there is little or sometimes no correlation apparent among the observed cleavages of one mineral and other min-

* Present address: The Harshaw Chemical Company, Solid State Research. Clevelan 6, Ohio.

erals structurally related to it. Initially there was rapid progress toward an understanding of the principles of cleavage but a comprehensive interpretation of the data is still lacking.

Generally speaking, the study of habit and etch patterns is a successful method of identifying minerals because many planes are to be observed in growth and in etching. This method has a disadvantage, however, since each growth matrix and etch solution results in different growth or etch-pit habit. For successful identification, the different habit types and/or growth and etch solutions must be known. It may be, therefore, that microcleavage will provide a rapid and efficient means of identification.

"Microcleavage" and Mineral Identification

Whereas cleavage, or "macrocleavage" refers to a separation of a crystal parallel to a crystal plane, "microcleavage" refers to the separation of a crystal parallel to crystallographic directions or zones which represent important atomic arrays (4) (PBC vector (5) Fig. 1). Where two or more microcleavage zones meet, macrocleavage occurs. A method utilizing both types of cleavage has the following advantages in identifying minerals: (1) Any particular material, of a specific structure, shows only one specific microcleavage pattern which, for all practical purposes, is independent of small amounts of impurities, temperature and cleaving technique; (2) In chemical etching, a suitable etchant must be found. This is a matter of trial and error in most instances. The natural habit may help to identify the substance, but for substances having many known habits it is a tedious process. Obviously, if the habit is not visible, the problem becomes a difficult one; (3) Within a group of similar structure, the cleavage should be similar, with possible minor variations. It will be shown in the text, and in the tables that this holds true for microcleavage of substances with identical structure but dissimilar chemical properties, for example $KMnO_4$ and $BaSO_4$, and $CaCO_3$ and $NaNO_3$; (4) Since a center of symmetry is introduced in the patterns, the number of symmetry classes that can be identified is reduced to eleven.

The statement given under (4) is the ideal case. Deviations from this rule are observed and an elaboration should be given. For a substance with a known crystal class, the corresponding class to be observed in microcleavage is predetermined. Yet, there are cases to be expected where the observed symmetry is higher. Let us consider, for example, $NaClO_3$ (class 23), hauerite (MnS_2), $Pb(NO_3)_2$, $Ba(NO_3)_2$ (class $2/m\bar{3}$). The supposed cations and anionic groups are centered in positions which correspond to the Na^+ and Cl^- positions in NaCl. When the interionic distance is large as compared to the intraionic distance, then the interaction between the cations and "anions" is such that no complexity is introduced

between them. The situation is then similar to that in NaCl. In other words, the interaction of the cation and anionic group is non-directional and non-specific; therefore, instead of the expected $2/m\ \bar{3}$ symmetry, the $4/m\ \bar{3}$ symmetry of the NaCl structure is observed. Correspondingly, cubic symmetry may be observed rather than tetragonal symmetry (as in $BaTiO_3$) etc. Multiple twinning may also lead to a higher order of symmetry and thus deceive the observer. Arsenopyrite (FeAsS) for instance, which is actually monoclinic with $\beta = 90°$, shows orthorhombic symmetry (6). In addition, there are cases, as in tellurium and cinnabar (32), where no decision can be made between the symmetry classes $\bar{3}\ 2/m$ and $6/m\ 2/m\ 2/m$ because the macrocleavage and microcleavage planes are in special positions (*i.e.* symmetry positions).

The Interpretation of Microcleavage; Microcleavage and PBC Vectors

In the investigation of microcleavage, it is important to determine the crystallographic zones of microcleavage. These zones represent atomic or ionic arrays of strong bonding at the surface ("PBC Vectors"). The interpretation of the results yields useful information of surface structure and bonding. Since it applies only indirectly in the identification of crystalline materials by their microcleavage patterns, only a short discussion follows. Each plane of a crystal of any given structure has a specific value of surface free energy, E. The specific surface free energy plots of a crystal, in spherical coordinates, show maxima, cusp valleys, and cusps arranged according to the symmetry of the crystal structure. The cusp valleys and the cusps are of importance; the valleys correspond to bond arrays and the cusps correspond to the intersection of two or more such arrays. In a Wulff's Plot (7), they correspond to edges and planes, respectively. The total area, S, of any particular crystallographic plane of a crystal decreases rapidly with increasing surface free energy E for growth and etch habits; as a first approximation, S, for microcleavage is proportional to e^{-BE} where B is a constant. Since for parallel light of uniform light flux, as is employed in the light figure method described below, the sum of the reflected light is proportional to S, the growth, etch and cleavage habit can be determined. As a matter of fact, this is the only general method of determining the cleavage habit when more than one cleavage plane is observed. The following can occur: (1) when the valleys are "complete," that is, cover an angle of 360°, the atoms lie either in one straight line, as in the simple cubic structure, in [001] (Fig. 2a), or they are composed of zig-zag arrays of atoms which are at least triple ([0001] in wurtzite). (2) Any zig-zag array is composed of at least two vectors, and as such results in an "incomplete" valley, that is, a surface free energy minimum valley covering a fraction of 360° (Fig. 2b). (3) The

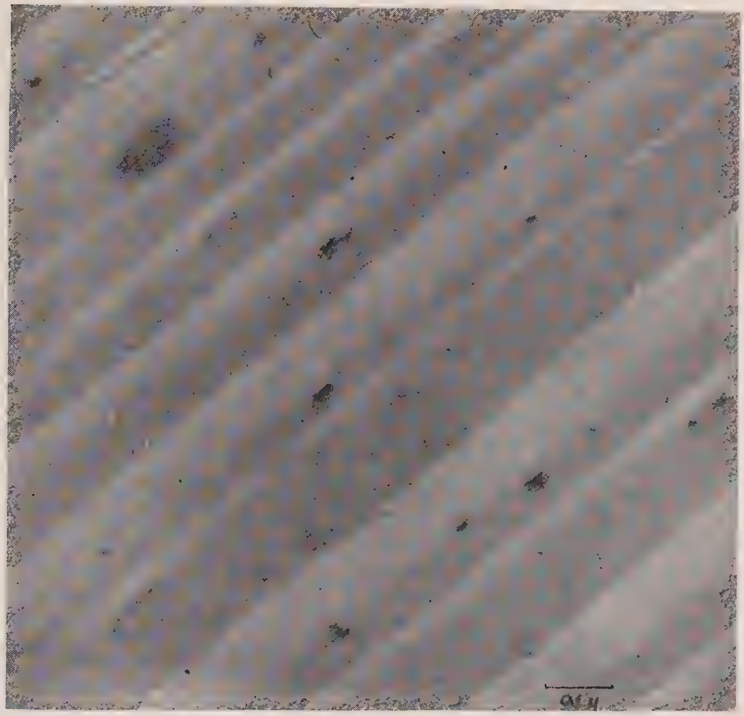

FIG. 1. Electron micrograph of the surface of a "(110) cleavage" in diamond showing a system of troughs parallel to [110]. The cylindrically curved portions of the troughs represent *hhl* planes with $h>l$; the lighter and darker portions correspond to (111) and ($\bar{1}11$) cleavage planes, respectively.

same is sometimes true for PBC vectors composed of two different bond vectors (V_1, V_2; *e.g.* Sb and Te). It is characteristic of this type that when the ratio of the two bond strengths exceeds a critical value, one of the valleys disappears, giving way to another. (4) The valley does not coincide with a zone parallel to a PBC vector derived from the crystalline structure. In this case, the PBC vectors are present only at the surface, where, during the separation of the two planes during the cleavage process, the atoms move into positions energetically superior to the positions of the ideal unchanged surface. Thus, a new PBC vector appears which is not present in the bulk structure and therefore, the surface energy is lowered. The vector is mostly of the zig-zag type. (5) New PBC vectors can also appear when adsorption takes place. They determine the growth, solution and equilibrium forms, but since adsorption takes place only after the cleavage planes have formed, for cleavage this effect can be disregarded.

It can be shown that the microcleavage pattern is closely related to

the surface energy plot (Wulff's Plot) and the PBC vector diagram of the corresponding structure. The following examples where this relationship was studied and found to hold are: diamond, arsenolite, senarmontite, cuprite, fluorite, magnesite and marcasite. The ideal pattern, as predicted on this basis, is also shown by GaSb and other materials of the B3 structure type, with their ionic character reflected in the appearance of (011)

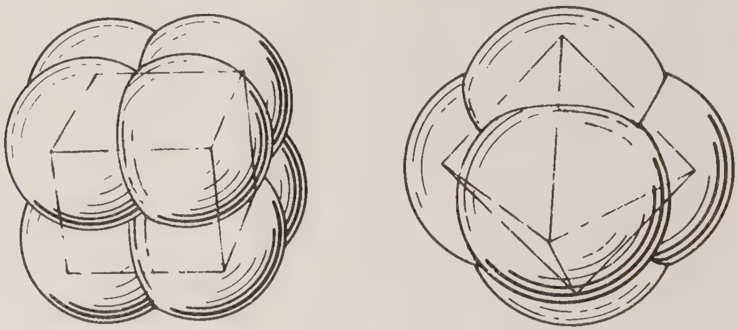

a *b*

FIG. 2a. Surface free energy plot of a crystal of simple cubic structure in spherical coordinates. Only nearest neighbor interaction is taken into account. Each cusp corresponds to an equilibrium plane (001); each valley connecting the cusps correspondingly represents an edge. This edge is [100] and is the common boundary to two adjacent (001) planes. The valleys are "complete," i.e. they can be traced 360° from cusp to cusp around the plot along one zone. A complete valley corresponds to a straight array of atoms. The equilibrium form (001) is inscribed.

FIG. 2b. Surface free energy plot for a crystal of diamond structure in spherical coordinates. Only nearest neighbor interaction is taken into account. The cusps correspond to (111) planes and the valleys connecting them correspond to [011] edges which are common to two neighboring (111) planes. The valleys are "incomplete" *i.e.*, they cannot be traced 360° around the plot. An incomplete valley corresponds to a zig-zag array. The equilibrium form (111) is inscribed.

cleavage planes (4). The (011) cleavage of NaCl which appears in addition to the expected pattern is apparently caused by the combined action of microcleavage in [010] and glide in $[0\bar{1}1]$.

Prismatic microcleavage patterns reveals the chain structure of both tellurium and the related compound cinnabar.

MECHANICAL ETCHING AND EXPERIMENTAL DETERMINATION OF MICROCLEAVAGE

Microcleavage may be observed when the crystals are "mechanically etched" (4). Mechanical etching can be described as follows: first, the material under investigation is cut roughly, or ground into spherical

FIG. 3. Photomicrograph of fractured silicon surface showing two sets of stress wave patterns. No structural features are revealed in the light figure investigation.

shape. Next, it is subjected to a rough grinding process that can be carried out in any of the following ways: either the sphere is rolled under moderate pressure between two sheets of very coarse SiC paper, or it is rotated in a coarse SiC slurry, carried in a hollow pipe mounted on the shaft of a counter rotating motor, or it can be spun with SiC particles in a modified Bond Wheel (8). For materials which are as hard or harder than SiC, coarse diamond powder is used. For soft materials, or materials having predominantly metallic character, slipping is observed rather than cleavage. At low temperatures, metals or soft materials are more brittle and then are subject to the same laws of cleavage as brittle material at room temperature. When this type of etching is employed, a cleavage pattern is observed when the surface of the sphere is studied by the light figure method (9). The light figure apparatus consists of a point source of light, a collimating lens system mounted on an optical bench, and a modified goniometer. A screen is mounted so that the light which comes through a hole in the center of the screen impinges on the crystal mounted on the goniometer. The crystal is spherical in shape, of about the same size as the hole and this permits observation of the major portion of the

surface at one time. The advantage of this method over conventional goniometry is that zones can be observed with greater ease, and the differences in intensities can be seen with greater accuracy. This apparatus also permits the observer to make a photographic record of the cleavage pattern. By reducing the size of the hole to small diameters, ($\sim$0.25 mm.), the illuminated and reflecting area of the crystal can be reduced. Thus a polycrystalline sample can be scanned and evaluated, crystal for crystal, with respect to their orientation and to crystallographic differences for different areas of each single crystal. Multiple reflections can be discerned and eliminated by the difference in their rate and direction of motion on the screen, when compared with the rate and direction of motion of the primary reflections. The angular motion of the latter is 2α when the crystal in the goniometer is rotated by an angle of α.

Various substances, both minerals and laboratory synthesized materials, have been investigated. Their patterns have been observed and recorded and arranged in charts according to structural relationships, so that they can serve as a method of identification.

Discussion of the Patterns

Table 1 compares the cleavage data as reported in Dana (1) with the stereographic projections of the observed cleavages. The reported cleavage is tabulated above the stereogram. It should be understood that the stereograms represent an idealized picture and do not show all the nuances that are actually observed. The spots represent reflections from individual planes, and the zones (unbroken lines) represent reflections from a whole series of planes lying along a particular direction. An attempt has been made to indicate the relative intensities of the reflections by the heaviness of the spots or zones. The open circles represent broad, diffuse reflections. It should be noted that cleavage zones are not mentioned directly in Dana. Their existence is recorded in the mention of the terms conchoidal, hackly, etc. In the majority of cases, there are indications that conchoidal fractures represent microcleavages of a complex nature. They are a combination of a number of micro- or macrocleavages parallel to one, or more, directions (a unifold infinite number, parallel to each direction). Visually, this is noticeable only in rare cases.

Generally, the more hackly the pattern, the more the fracture is determined by the action of shock waves and stress propagation rather than by structural aspects. The microscopic inspection of hackly fracture patterns in silicon, for instance, strikingly reveals the stress wave pattern Fig. 3.

The variation in appearance of the zones and the relative intensities of the reflections can also aid in the identification of crystalline materials.

Table 1. The Microcleavage Patterns of Minerals and Artificial Single Crystal Materials Recorded as Stereographic Projections. The Chemical Formula and the Cleavage as Reported in Dana Are Also Given

	DIAMOND	ARSENOLITE	SILICON	GREY TIN	GaSb
	C	As_4O_6	Si	α-Sn	
	111 PERFECT	111			
		 SIMILAR PATTERN FOR SENARMONTITE	 SIMILAR PATTERN FOR Ge		 SIMILAR PATTERN FOR InAs, InSb
	Al Sb	SPHALERITE	TIEMANNITE	COLORADOITE	CUPRITE
		ZnS	HgSe	HgTe	Cu_2O
		011 PERFECT	NONE	NONE	111 INTERRUPTED 001 RARE
	 SIMILAR PATTERN FOR GaAs, InP, ZnTe	 SIMILIAR PATTERN FOR GaP, AlP, AlAs, ZnSe, CuI.	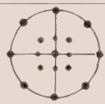		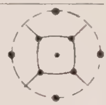
	FLUORITE	Au Ga_2	HALITE	PERICLASE	GALENA
	Ca F_2		NaCl	MgO	PbS
	111 PERFECT 001 SOMETIMES		001 PERFECT	001 PERFECT 111 IMPERFECT 011 PARTING	001 EASY & PERFECT 111 PARTING
CUBIC	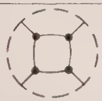	 SIMILAR PATT. FOR $AuIn_2$	 SIMILAR PATT FOR LiF, KBr,		 SIMILAR PATT FOR PbTe, SnSe
	Na ClO_3	HAUERITE	PYRITE	COBALTITE	ULLMANNITE
		MnS_2	FeS_2	CoAsS	NiSbS
		001 PERFECT	001, 011, 111 INDISTINCT	001 PERFECT	001 PERFECT
	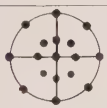	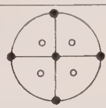	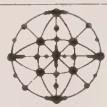	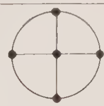	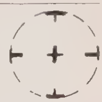
	$Pb(NO_3)_2$	$Ba(NO_3)_2$	MAGNETITE	SPINEL	FRANKLINITE
			Fe_3O_4	$MgAl_2O_4$	$ZnFe_2O_4$
			111, 001, 011, 138 PARTING	111 INDISTINCT "SEPARATION" PLANE	111 PARTING
	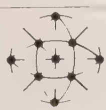	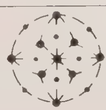	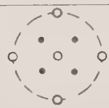	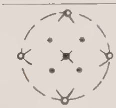	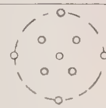

TABLE 1 (*Continued*)

	ZIRCON	KDP	ADP	SCHEELITE	WULFENITE
	$ZrSiO_4$	KH_2PO_4	$NH_4H_2PO_4$	$CaWO_4$	$PbMoO_4$
	110 IMPERFECT 111 INDISTINCT			101 DISTINCT 112 INTERRUPTED 001 INDISTINCT	011 DISTINCT 001 } INDISTINCT 013 }
		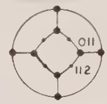	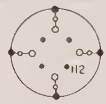		
TETRAGONAL	RUTILE	CASSITERITE	ANATASE	HAUSMANNITE	CHALCOPYRITE
	TiO_2	SnO_2	TiO_2	Mn_3O_4	$CuFeS_2$
	110 DISTINCT 100 LESS SO 111 IN TRACES	100 IMPERFECT 110 INDISTINCT 111 OR 011 PARTING	001 } PERFECT 011 }	001 NEAR PERF. 112 } INDISTINCT 011 }	011 SOMETIMES DISTINCT
	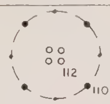	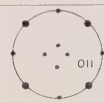	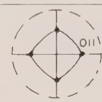	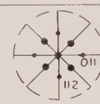	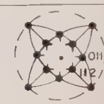
	BARITE	CELESTITE	ANGLESITE	$KMnO_4$	ANHYDRITE
	$BaSO_4$	$SrSO_4$	$PbSO_4$		$CaSO_4$
	001 PERFECT 210 LESS PERF. 010 IMPERFECT	001 PERFECT 210 GOOD 010 POOR	001 GOOD 210 DISTINCT 010 TRACES		010 PERFECT 100 NEAR PERF. 001 GOOD
	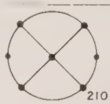	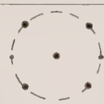		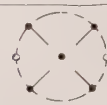	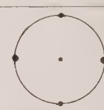
	CHRYSOLITE	FAYALITE	TEPHROITE	CHRYSOBERYL	TRIPHYLITE
	$(Mg,Fe)_2SiO_4$	Fe_2SiO_4	Mn_2SiO_4	$BeAl_2O_4$	$LiFe(PO_4)$
	010 DISTINCT 100 LESS SO	010 DISTINCT 100 LESS SO	DISTINCT IN TWO DIRECTIONS AT RIGHT ANGLES	110 DISTINCT 010 IMPERFECT 001 POOR	100 NEAR PERF. 010 IMPERFECT 011 INTERRUPTED
RHOMBIC	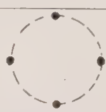 SIMILAR PATTERN FOR OLIVINE	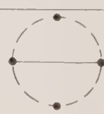	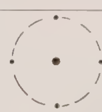		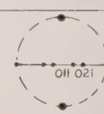
	CERUSSITE	STIBNITE	BISMUTHINITE	MARCASITE	ENARGITE
	$PbCO_3$	Sb_2S_3	Bi_2S_3	FeS_2	Cu_3AsS_4
	110 & 021 DIST 010 & 012 IN TRACES	010 PERFECT & EASY 100,110 IMPERF.	010 PERFECT & EASY 100,110 IMPERF.	101 DISTINCT 110 TRACES	110 PERFECT 100,010 DIST. 001 INDISTINCT
	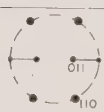	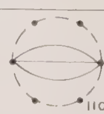		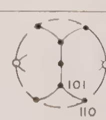	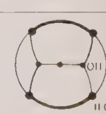

TABLE 1 (*Continued*)

	QUARTZ	BERLINITE	CORUNDUM	HEMATITE	Cr_2O_3
	SiO_2	$AlPO_4$	Al_2O_3	Fe_2O_3	
	$10\bar{1}1, 10\bar{1}0, 01\bar{1}1$ 0001 DIFFICULT	NONE	NONE 0001, $01\bar{1}2$ PARTING	NONE 0001, $01\bar{1}2$ PARTING	
				 SIMILAR PATTERN FOR RUBY (98% Al_2O_3 2% Cr_2O_3)	
	WURTZITE	GREENOCKITE	ZINCITE	CARBORUNDUM	TELLURIUM
	ZnS	CdS	ZnO	SiC	Te
	$11\bar{2}0$ EASY 0001 DIFFICULT	$11\bar{2}2$ DISTINCT 0001 IMPERFECT	$10\bar{1}0$ PERFECT 0001 PARTING	CONCHOIDAL FRACTURE	$10\bar{1}0$ PERFECT 0001 IMPERFECT
HEXAGONAL	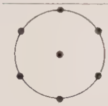	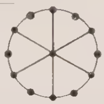 SIMILAR PATTERN FOR CdSe		 SIMILAR PATTERN FOR AgI	
	CALCITE	MAGNESITE	SIDERITE	RHODOCHROSITE	DOLOMITE
	$CaCO_3$	$MgCO_3$	$FeCO_3$	$MnCO_3$	$CaMg(CO_3)_2$
	$10\bar{1}1$ PERFECT 0001, $01\bar{1}2$ PARTING	$10\bar{1}1$ PERFECT	$10\bar{1}1$ PERFECT	$10\bar{1}1$ PERFECT $01\bar{1}2$ PARTING	$10\bar{1}1$ PERFECT $02\bar{2}1$ PARTING SOMETIMES
		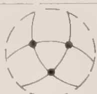			
	WILLEMITE	PHENACITE	PROUSTITE		
	Zn_2SiO_4	Be_2SiO_4	Ag_3AsS_3		
	0001 MORSENET $11\bar{2}0$ N.J. 0001 DIFF. N.J	$11\bar{2}0$ DISTINCT $10\bar{1}1$ IMPERFECT	$10\bar{1}1$ DISTINCT		
					
	CROCOITE	SPODUMENE	WOLLASTONITE	ARSENOPYRITE	MANGANITE
	$PbCrO_4$	$LiAl(SiO_3)_2$	$CaSiO_3$	FeAsS	MnO(OH)
	110 DISTINCT 001,100 INDIST.	110 PERFECT	100,001 PERF. $\bar{1}01$ LESS SO	101 DISTINCT 010 TRACES	010 VERY PERF. 110,001 LESS PERFECT
MONOCLINIC		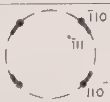	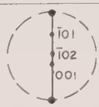	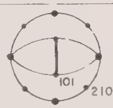	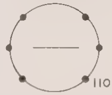

Cubic System

In Dana, (111) macrocleavage is reported for diamond, arsenolite and senarmontite, but no mention is made of the zones as shown in the stereogram. Also, note that Si, Ge and α-Sn, which crystallize with the diamond structure have a zonal pattern different from that of diamond. This has been explained in previous papers by the authors and by others (4, 10) and is the result of surface deformation.

Halite and periclase are both structurally and chemically similar and both are strongly ionic crystals. The same cleavage would be expected to be observed for both, yet in Dana, NaCl is reported as having (001) macrocleavage and periclase (001), (111) and "(011) parting." It is our belief that the cleavages of the two materials should be consistent and no (111) macrocleavage should be found because of the strongly ionic character of the substances. The same reasoning would account for the fact that no (111) macrocleavage is to be observed in PbS. Furthermore, the reported (011) parting as sometimes occurring in periclase is also dubious since it is consistently revealed in our samples. It should also be noted that (011) appears in NaCl; though not reported in Dana, it has been reported by others (3).

$AuGa_2$ and $AuIn_2$, having the same structure as CaF_2, show additional zonal structure.

Artificial HgSe and HgTe have patterns consistent with their structural group but differ from those of the III–V compounds (4).

Hauerite, cobaltite, $Pb(NO_3)_2$ and $Ba(NO_3)_2$ show a higher order of symmetry than pyrite, as explained in the text. Gersdorffite, which has the same cleavage pattern as cobaltite, has not been included in the charts.

Tetragonal System

Note the complex structure revealed by chalcopyrite in contrast to the reported (011) in Dana. Higher index planes were observed in ADP ($NH_4H_2PO_4$) that could not be indexed; the "(112)" in rutile is an approximation.

Pyrolusite and stannite have been investigated, though not recorded on the chart; pyrolusite showing a continuous prismatic microcleavage reflection and stannite shows microcleavage between (001) and (012), between (012) and (112) and between (112) and (110). Distinct cleavage found for (012), (112) and (001) in order of increasing intensity.

Orthorhombic System

Barite and $KMnO_4$, both chemically different, yet structurally related, give very similar patterns. Barite also has a microcleavage pattern that differs from the other sulfates studied.

Glaucodot and loellingite, not shown on the charts, reveal (010) and (101) cleavage and a strong zone between (101) and ($\bar{1}$01). In addition, glaucodot shows (100) cleavage and a weak microcleavage zone between (100) and (101), while loellingite shows weak cleavage in (011) and weak microcleavage between (011) and (001). Laboratory grown specimens of sulfur crystals show (111) cleavage.

Hexagonal System

ZnS, CdS and ZnO are structurally and chemically closely related, yet three different cleavages are reported in Dana. The stereograms reveal that all have basically the same cleavage. One group of CdS samples also consistently reveals a pyramidal macrocleavage which could not be explained.

Cinnabar has a cleavage pattern similar to that of Te except that the basal cleavage (0001) is not present.

Parting is mentioned for ZnO, $CaCO_3$, Fe_2O_3 and Al_2O_3. This implies a random observation of the particular plane, yet the plane (or planes) consistently appear as many tiny cleavage pits over the different, but equivalent, directions affected and should be considered as true cleavage planes.

Note the zones that appear in magnesite and siderite in addition to the planes, and the difference between these minerals and the other carbonates.

The following minerals are not listed on the charts: ilmenite ($FeTiO_3$) exhibits (10$\bar{1}$1) cleavage planes; millerite (NiS) shows a pattern very similar to that of calcite, however no zones run through the (10$\bar{1}$1) spot; $NaNO_3$ shows a pattern identical to that of calcite.

Monoclinic System

In addition to the reported cleavage planes for spodumene and wollastonite, other planes and zones have been found and are shown on the stereograms.

Conclusion

In conclusion, this method of producing and observing cleavage offers a new tool for the mineralogist, not only for the identification of unknown minerals by their cleavage habit, as first attempted by Seaman (2) and Tertsch (3) but also as a means of a systematic and scientific investigation of the cleavage phenomena. An analysis of the cleavage patterns, together with a knowledge of the crystal structure can yield information concerning the type of bonding in the crystal. The ratio of ionic to covalent bonding in crystals with the sphalerite structure has been determined this way.

Acknowledgments

The authors would like to acknowledge the invaluable aid given them by Mr. D. Seaman of the Mineralogy Department of the American Museum of Natural History and Mr. R. Hesse of the Academy of Natural Sciences in Philadelphia, Dr. G. Switzer and Mr. P. E. Desautels of the U. S. National Museum in Washington, D. C., as well as others for supplying mineral and crystal specimens used in this work. Special thanks are due Mr. P. Bramhall of this Laboratory for growing $Ba(NO_3)_2$, $Pb(NO_3)_2$, $NaClO_3$, crystals and Mr. C. F. Cook of this Laboratory for the electron micrography. Thanks are also due to Drs. R. M. Denning of the University of Michigan and F. W. Leonhard of this Laboratory for stimulating discussions, and to Dr. S. B. Levin of this Laboratory for his interest in this work.

References

1. J. D. Dana, "The System of Mineralogy," 1944–1951, John Wiley & Sons, N. Y.
2. W. A. Seaman, "Mineral Classification," Michigan College of Mining and Technology, 4th Edition, 1935; K. Spiroff, "Seaman's Mineral Tables," The Michigan College of Mining and Technology Press, 1959.
3. H. Tertsch, "Die Festigkeits erscheinungen der Kristalle," 1959, Springer, Vienna.
4. G. A. Wolff and J. D. Broder, *Acta Cryst.* **12,** 313 (1959).
5. P. Hartman and W. G. Perdok, *Acta Cryst.* **8,** 49 (1955).
6. M. J. Buerger, *Z. Krist,* **94,** 83 (1936).
7. G. Wulff, *Z. Krist.* **34,** 449 (1901).
8. W. L. Bond, *Rev. Sci. Instrum.* **22,** 344 (1951).
9. G. A. Wolff, J. M. Wilbur, Jr., and J. C. Clark, *Z. Elekrochem.* **61,** 101 (1957).
10. W. B. Pearson and G. A. Wolff, *Faraday Soc. Discussions,* **28,** 142 (1959).

Manuscript received March 2, 1960.

THE AMERICAN MINERALOGIST, VOL. 45, NOVEMBER–DECEMBER, 1960

SPECTROCHEMICAL DETERMINATION OF LEAD IN ZIRCON FOR LEAD-ALPHA AGE MEASUREMENTS*

HARRY ROSE, JR. AND THOMAS STERN, *U. S. Geological Survey, Washington 25, D. C.*

ABSTRACT

A spectrochemical method is described for determining lead in zircon. A synthetic "zircon" standard is used to cover a range of concentration between 1 and 560 ppm. The method is designed for use in lead-alpha age measurements. Results of the analysis of 22 zircons indicate an overall 5% average deviation from isotope dilution and chemical values. This method differs from a spectrochemical method described previously in the composition of the standards and in the use of a full set of standards in preference to bracketing the samples.

INTRODUCTION

The lead-alpha method for the determination of the geologic age of igneous rocks was described by Larsen, Keevil, and Harrison (1952). The age calculation is based on the determination of the lead content and alpha activity of certain accessory minerals, particularly zircon, separated from the rocks. A spectrochemical method was described by Waring and Worthing (1953) for determining lead in zircon and other minerals. These authors have since 1953 used opal glass (National Bureau of Standards, standard sample 91) diluted in silica as a lead standard (Gottfried, Jaffe, and Senftle, 1959). Until recently an evaluation of the accuracy of the method could not be made owing to the few available comparison analyses by independent techniques. Webber, Hurley, and Fairbairn (1956) reported lead values higher than results determined by C. L. Waring on four samples of zircon, but discarded the higher lead values. Some serious discrepancies between the spectrochemical lead values and the lead values determined by isotope dilution were noted by Gottfried, Jaffe, and Senftle (1959). A comparison of the spectrochemical results by the method of Waring and Worthing with the lead values determined by isotope dilution is given in Table 1. The variation in values ranges between 0.92 and 2.36 when expressed as the ratio of the isotope dilution values to the spectrochemical values. For reconnaissance age determinations, the agreement between five of the samples can be considered reasonably good, but the remaining samples indicate a bias greater than the precision of the spectrochemical method.

The magnitude of the differences between the lead values obtained by the two techniques prompted an interlaboratory study to determine the nature of the variation. This study includes an investigation of the behavior of zircon in the d-c arc, the preparation of a standard having arc-

* Publication authorized by the Director, U. S. Geological Survey.

ing properties similar to the natural mineral, and a comparison of the determination of lead in 20 zircon samples by the method of Waring and Worthing (1953) and by the method described in this report.

Spectrographic Equipment

A grating spectrograph with Wadsworth mounting is used with a 15,000 lines-per-inch grating having a dispersion of 5.0 Å per mm. in the first order. A 250 volt direct current motor generator is used to provide a

Table 1. Comparison of Spectrochemical Values (Opal Glass Standard) with Isotope Dilution Results

Sample	Spectrochemical[a] lead (ppm.)	Isotope dilution lead (ppm.)	Isotope dilution: Spectrochemical ratios
N-7 Oslo	19	17.5[b]	0.92
S-2 Wemback	31	46[b]	1.48
M-51 Cranberry gneiss	39	59.5[c]	1.53
S-10 Halbmeil	28	47[b]	1.68
B-4 Baltimore gneiss	93.5	104[c]	1.11
6-37 Natural Bridge[d]	66.5	127[c]	1.91
S-7 Martinskapelle	69	163[b]	2.36
Storm King	346	337[c]	.97
Wichita Mountains[d]	351	376[c]	1.07
Z-22 Essonville[d]	433	461[c]	1.06
SQ-81 Mountain Pass[e]	1140	1760[c]	1.54

[a] Analyses by Helen Worthing using method of Waring and Worthing (1953). National Bureau of Standards, standard sample 91, opal glass, diluted in silica as standard. The values reported are averages of all determinations.

[b] Isotope dilution by Henry Faul, U. S. Geological Survey, Washington, D. C.

[c] Isotope dilution by G. R. Tilton, Geophysical Laboratory of the Carnegie Institute of Washington.

[d] Gottfried, Jaffe, and Senftle (1959, p. 35).

[e] Gottfried, Jaffe, and Senftle (1959, p. 25).

current of 15 amperes during arcing of the sample. The current is controlled by a series resistance capable of providing current adjustments of 0.5 ampere. The resistance circuit is wired through a shorting switch that changes the amount of resistance and instantaneously increases the current from 5 to 15 amperes.

A series of neutral filters is used in the optical path to control the amount of light entering the slit. Spectra are recorded on a 10-inch Eastman type III-O plate (10–560 ppm. lead) or Eastman type II-O plate (1–40 ppm. lead).

Open trays are used for developing and fixing solutions with continu-

ous agitation. The temperature is maintained at 20° C. The emulsion is washed in running water and dried by a stream of warm air.

The transmittances of iron calibration lines and the lead line in standards and samples are measured with a projection comparator-microphotometer using a scanning slit at the plate.

Standard Samples

A synthetic "zircon" was prepared by thoroughly grinding together a high-lead glass, zirconia, and silica glass in proportions that were equivalent to the composition of zircon containing 5% lead. The mixture was sealed in a platinum crucible that was welded shut and heated to a temperature of 1450° C. for 12 hours in a platinum-wound electric furnace. After the material was cooled and mixed thoroughly by grinding in a boron carbide mortar a portion was analyzed chemically; gravimetric and colorimetric analyses by Frank Cuttitta of the U. S. Geological Survey of the material used in this study was found to contain 4.60% lead. Mineralogical and *x*-ray diffraction examination by D. B. Stewart and B. J. Skinner of the U. S. Geological Survey of a material prepared as described above revealed a mixture containing zircon, the high-temperature form of zirconia (baddeleyite), and a silicate glass. Although differential solution studies by Frank Cuttitta of the U. S. Geological Survey suggest that more than 90% of the lead was in the silicate glass, moving plate studies indicate that the volatilization pattern of lead from the synthetic "zircon" mixture was identical with the pattern established for the natural mineral.

A series of standards is prepared by diluting the synthetic "zircon" mixture with lead-free zircon base (68% zirconia and 32% silica) to cover a range of lead concentration from 1 to 560 ppm. A step-wise dilution of the lead by a factor of 0.562 is recommended to provide points sufficiently close to characterize the analytical curve. At each level the standard and zircon base are thoroughly mixed by hand grinding in a boron carbide mortar for half an hour.

Most sources of zirconia contain a few parts per million lead which requires a correction in the assigned lead content of the standard. We were fortunate in obtaining zirconia from the U. S. Bureau of Mines that contained less than one part per million lead. The source of silica is a ground silica glass (Corning glass no. 7940 lump cullet) that has no detectable lead.

Preparation of Sample

The concentration of zircon from the rock prior to spectrochemical analysis is a specialized operation. The final yield of zircon is extremely

small when compared to the initial rock sample. The general procedure, simply outlined, requires breaking up the rock in a jaw crusher and feeding the resultant chips into a roller-type grinder and passing the ground material through a 50-mesh sieve. The sample that passes through the sieve is concentrated over a Wilfley shaking table (Gottfried et al., 1959) for bulk removal of light-weight minerals (principally quartz and the feldspars). The heavy mineral fraction is passed through the Frantz isodynamic magnetic separator to remove the ferromagnetic minerals. The sample is then further fractionated by treatment with bromoform and methylene iodide, and the heavier mineral fraction is passed through the magnetic separator repeatedly raising the current in small increments before each pass. The current at which the zircon will concentrate varies considerably for the metamict varieties. Fresh zircon concentrates as a nonmagnetic fraction.

The zircon-rich fraction is normally leached with hot concentrated nitric acid for 20 minutes to remove pyrite and apatite which may have been concentrated with the zircon.

The last and most important operation is a petrographic examination, accompanied by hand-picking to remove the last traces of impurities. The pure sample is ground in a boron carbide mortar to a very fine powder.

Fifteen milligrams of the sample is then mixed with 35 mg. of sodium carbonate and transferred to the electrode in the same manner as are the standards. Occasionally a sample will be submitted that has a lead content higher than the range of the standards. Such a sample is diluted with zircon base to bring it within the range.

Electrode System

The lower sample-carrying electrode (anode) is a $\frac{1}{4}$ inch diameter pure graphite rod $1\frac{5}{8}$ inches in length with a cup at one end. The crater has a 0.144 inch inner diameter and a 0.020 inch wall thickness and has a depth of 0.238 inches with a 60° truncated cone ending in a 0.031 inch diameter base.

The upper electrode (cathode) is a pure $\frac{1}{8}$ inch graphite rod.

Excitation

The samples and standards are arced so that single exposures of each are recorded consecutively in the upper part of the plate. An iron calibration spectrum is then recorded in the center of the plate. The same order of exposure of samples and standards initially recorded is repeated.

The samples and standards are arced in the above exposure pattern at an initial current of 5 amperes for 10 seconds. The current is then instantaneously raised to 15 amperes by a shorting switch that changes the

amount of series resistance. The arc is continued for 80 seconds at 15 amperes. During this time the lead evolves, and the relatively low temperature of the sodium vapor prevents the zirconia from entering the arc.

An iron bead is arced at 5 amperes for 120 seconds through a 50 per cent two-step quartz filter at the slit. The resultant two-step spectra is used to calibrate the emulsion. To obtain more reproducible spectra from plate to plate, the iron bead should be subjected to a 2-minute preburn period.

Exposure conditions

The exposure conditions are given below:

Spectral region, Angstroms	2230–3480
Slit width, microns	25
Slit height	2 mm. for samples and standards, 4 mm. for iron bead exposures.
Image	Focus on grating
Arc preburn	None
Arc exposure	10 seconds at 5 amp. 80 seconds at 15 amp.

The exposure is adjusted to maintain the transmittance of Pb 2833.07 Å at 30 ppm. at approximately 60 per cent. An Eastman type III-O plate is used to give an effective lead concentration range between 10 and 560 ppm. The exposure may be adjusted by use of neutral filters in the optical path.

For low concentrations of lead the exposure conditions are adjusted to maintain a transmittance of approximately 50 per cent for Pb 2833.07 Å at a concentration of 5 ppm. lead. An Eastman type II-O plate is used for low concentration lead determinations between 1 and 40 ppm. lead. The exposure conditions for the two-step iron bead calibration are adjusted for each type plate to maintain a transmittance of approximately 20 per cent for Fe 3175.45 in the filtered step.

Emulsion Calibration

Calibration is accomplished by the two-step method (Harvey, 1950). The method is a modification of the procedure proposed by Churchill (1944). The series of homologous iron lines selected for calibration (Hodge, 1951) given below are convenient for this purpose.

Iron calibration lines, Å

Fe	Fe
3157.04	3205.40
3157.88	3207.09
3165.01	3215.94
3165.86	3217.34
3168.86	3230.97
3175.45	3248.20

The preliminary curve is established by plotting on log-log paper the per cent transmission of the lighter step of a given line as ordinate against the corresponding per cent transmission of the darker step as abscissa. The two steps of each spectral line obtained from a two-step filter give a single point. In like manner, points are plotted for each of the iron lines listed above.

The best curve is drawn through the points. The highest reliable point of the ordinate is selected from the preliminary curve, its value and its corresponding abscissa value are recorded. Using the abscissa value as the ordinate, its corresponding abscissa value is recorded, thus working down the curve recording all values to the end of the preliminary curve.

The emulsion calibration curve is established by plotting directly on log-log paper the above recorded values as ordinates against intensities as abscissa in intervals equal to the step ratio of the two-step filter. A two-step filter with a step ratio of approximately 1.50 is recommended; its exact ratio can be determined photometrically. For a 1.50 step ratio the interval points are 1.00, 1.50, $(1.50)^2$, $(1.50)^3$, $(1.50)^4$ . . . $(1.50)^n$. A line drawn through these points constitutes the calibration curve.

Photographic Processing

The photographic processing procedure is altered slightly with a change in the emulsion.

Emulsion	Eastman Type III-O Eastman Type II-O
Development	Eastman D-19 with continuous agitation at 20° C. Type III-O for 5 minutes, Type II-O for 3 minutes
Fixing	Eastman acid fixer, 6 minutes at 20° C.
Washing	Running water at 20° C. for 10 minutes
Drying	Blower-heater

Photometry

Transmittance measurements for the Pb 2833.07 Å line and the iron lines for calibrating the emulsion are made on a projection comparator-microphotometer. No background correction is made for the high range emulsion (Type III-O). The low-range emulsion (Type II-O) requires a full background correction. The transmittances of the lead line are converted to relative intensities by means of the plate calibration curve. Where applicable, background transmittances are converted to relative intensities and subtracted from the line intensities. The standard samples

serve to establish an analytical curve relating log intensity to log concentration. The intensities of the analytical lines of the unknown samples are converted to concentrations by reference to the analytical curve.

Precision

The precision of this method is illustrated by the following data:

Sample	Average conc. %	Coefficient of variation	Number of determinations
ZS-9	0.0306	4.9	10
ZS-10	0.0048	3.5	8
SR-1	0.00020	11.0	6

The coefficient of variation is calculated by the following formula:

$$\nu = \frac{100}{C}\sqrt{\frac{\Sigma d^2}{n-1}}$$

where

C = average concentration, in per cent
d = difference of the determination from the mean, and
n = number of determinations.

Accuracy

A measure of the accuracy is obtained by comparing the spectrochemical results with those obtained by other techniques, most commonly by isotope dilution. The spectrochemical values gave an overall average deviation of less than 5 per cent. Table 2 gives data on 22 samples which were submitted as unknowns. The data given in the table are shown graphically in Fig. 1 by relating the spectrochemical lead values with the lead values obtained by isotope dilution and chemical analysis. Also shown in Fig. 1 is a comparison between the spectrochemical lead values obtained by the method of Waring and Worthing (Tables 1 and 3) with the lead values obtained by independent techniques.

Discussion

To determine the variation between the lead analyses by the method described here and the method of Waring and Worthing (1953), 20 zircons were analyzed by both methods. The results are given in Table 3. The 20 test samples were later revealed to be duplicate splits of each of 10 zircons. Six of the 10 samples were composites of 2 zircons prepared in the proportions given in the table. In addition to an analysis value, each composite sample has a value calculated by totaling the lead contribution of each component.

Table 2. Comparison of Spectrochemical (Synthetic "Zircon" Standards) Lead Analyses with Isotope Dilution and Chemical Results

Sample No.	Description	Spectrochemical[a]	Isotope dilution[b]	Chemical[c]	Chemical	Isotope dilution
		Lead ppm.	Lead ppm.	Lead ppm.	Spectrochemical	Spectrochemical
ZS-10	Zircon from syenite at Old Whitestone Farm, 1 mile east of Natural Bridge, N. Y. Collected by Arthur Montgomery.	48		47	.98	
ZS-6	Zircon from a pegmatite, Pacoima Canyon, San Gabriel Mts., Calif. Collected by G. J. Neuerburg.	33	35			1.06
ZS-9	Zircon from pegmatite, Quanah Mt., Okla. Collected by F. L. Hess and R. L. Dott.	303	313	275	.91	1.03
NBS-197	Zircon from beach sand, Jacksonville, Fla. National Bureau of Standards zircon ore sample.	34		34	1.00	
ZS-4	Zircon. A mixture containing 68% ZS-6 and 32% ZS-10.	38		38	1.00	
ZS-12	Zircon. A mixture containing 32% ZS-9 and 68% ZS-6.	117		109	.93	
S-10	Zircon from granite, Halbmeil, Schwarzwald. Collected by Henry Faul.	43	47			1.09
N-7	Zircon from Oslo nordmarkite, Oslo region, Norway. Collected by Henry Faul.	18	18			1.00
S-7	Zircon from granite, Martinskapelle, Schwarzwald. Collected by Henry Faul.	152	163			1.07
G-5	Zircon from Wilson Creek gneiss, Mortimer, N. C. Collected by G. R. Tilton.	168	160			.95
SK	Zircon from Storm King granite, Bear Mt., N. Y. Collected by G. R. Tilton.	335	337			1.01
P-16	Zircon from Baltimore gneiss, Spring Mill, Pa. Collected by G. R. Tilton.	187	168			.90
Hybla	Zircon. Cyrtolite McDonald mine, Hybla, Ontario. Collected by G. R. Tilton.	970[d]	1045			1.08

[a] Lead values represent an average of all determinations.

[b] Isotope dilution analyses as follows: ZS-6 and R-200 by L. T. Silver, Calif. Inst. of Tech.; ZS-9, L. R. Stieff, U. S. Geological Survey; S-10, and S-7, by Henry Faul, U. S. Geological Survey. All other samples b G. R. Tilton of the Geophysical Laboratory, Carnegie Inst. of Wash., D. C.

[c] Chemical analysis of samples SQ-81 and 52Mt8 by R. A. Powell, U. S. Geological Survey. Other chemica analyses by Frank Cuttitta, U. S. Geological Survey.

[d] Samples diluted with 8 parts zircon base (68% ZrO_2 and 32% SiO_2)

TABLE 2 (*Continued*)

Sample No.	Description	Spectro-chemical[a]	Isotope dilution[b]	Chemical[c]	Chemical	Isotope dilution
		Lead ppm.	Lead ppm.	Lead ppm.	Spectro-chemical	Spectro-chemical
52Mt8	Monazite from placer, Warren Creek, tributary of Salmon River near Warren, Idaho County, Idaho. Collected by J. B. Mertie, Jr.	1070[d]		1080	1.01	
SQ-81	Monazite from rare earth carbonate body, Mountain Pass. Calif. Collected by H. W. Jaffe.	1760[d]	1760	1770	1.01	1.00
M-51	Zircon from Cranberry gneiss, Deyton Bend, N. C. Collected by G. R. Tilton.	57	59.5			1.04
G-70	Zircon from rare earth vein, Laurel Gap, Tenn. Collected by G. R. Tilton	165	163			.99
G-15	Zircon from granite, Crossnore, N. C. Collected by G. R. Tilton.	33	32			.97
R-200	Zircon from pegmatite, Pacoima Canyon, San Gabriel Mts., Calif. Collected by L. T. Silver.	37	41.6			1.12
G-64	Zircon from Beech granite, West Roan Mts., Tenn. Collected by G. R. Tilton.	54	58			1.07
6-37	Zircon from Scarn, Old Whitestone Farm, 1 mile east of Natural Bridge, N. Y. Collected by A. F. Buddington.	110[e]	127			1.15
B-15	Zircon from gneiss, Mary's Rock Tunnel, Shenandoah National Park, Va. Collected by G. R. Tilton.	78	83			1.06

[e] Analysis obtained on 4 mg. sample (diluted in zircon base) and the value reported is from a single exposure.

The precision of each method is indicated by comparing the lead analysis value of duplicate samples, and by comparing the values of the composite samples with the calculated values.

The variation in lead determinations between methods is reported in the table as a ratio of this method to the method of Waring and Worthing (1953). For the range of concentration of the analyses, the ratios range from 1.11 to 1.48, making an interpretation of the variation difficult and application of a single empirical correction factor impossible.

To determine the factors causing the variations in the lead values reported by the two spectrochemical methods, a study was made to investigate the chemical breakdown of natural zircon during its excitation in the d-c arc, and to compare the rate of volatilization of lead from the min-

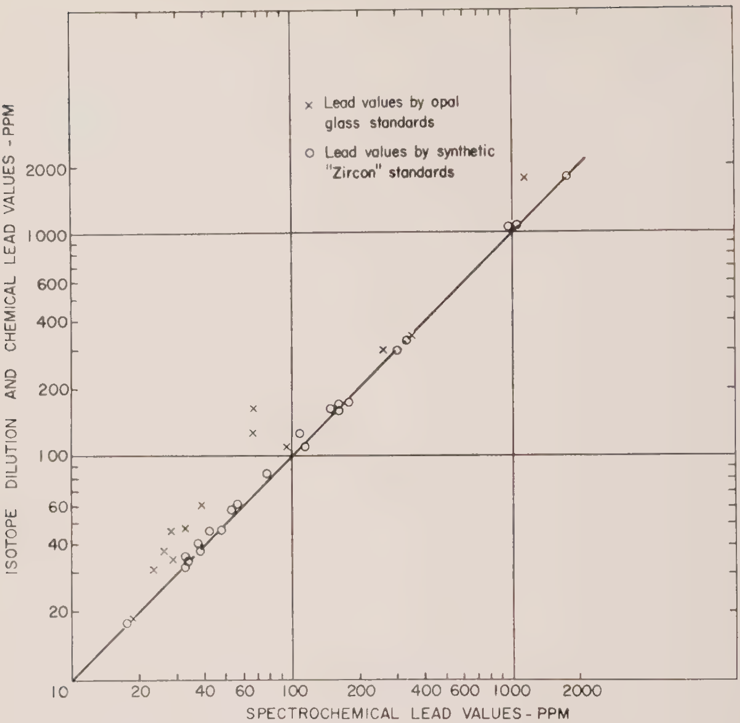

FIG. 1. Comparison of spectrochemical with isotope dilution and chemical analyses.

eral with the rate of volatilization of lead from the spectrochemical standards used by each method.

X-ray and mineralogical examinations of the material remaining in the crater of the electrode after excitation periods of 10, 20, 40, and 60 seconds disclosed that the decomposition products of zircon are baddeleyite and tridymite, high temperature forms of zirconia and silica, respectively. These oxides appear as a thin layer at the surface of the crater after 10 seconds of excitation. As excitation continues, the decomposition layer extends deeper into the electrode and after 40 seconds zircon is no longer identified in the remaining material. Examination of the crater material after 60 seconds of excitation indicated that only baddeleyite remained, the silica having volatilized from the crater. The above studies also reveal that the lead is released into the arc column during the decomposition of zircon. Lead can no longer be detected after the mineral has completely decomposed in the crater.

The rate at which lead volatilizes from the natural mineral, from synthetic "zircon," and from opal glass was observed by moving plate stud-

... METHOD (WARING AND WORTHING, 1953) AND PRESENT METHOD ON 20 ZIRCON SAMPLES

Sample No.	Source	Previous method: Number of detns.	Previous method: Range (ppm.)	Previous method: Lead (ppm.)	Previous method: Average of 2 samples[a]	Present method: Number of detns.	Present method: Range (ppm.)	Present method: Lead (ppm.)	Present method: Average of 2 samples[a]	Ratio Present/Previous
ZS-2	NBS-197 Zircon ore	4	27– 30	28.5	28.9	3	32– 34	33	32.9	1.16
ZS-18		4	28– 30	29.2		3	33– 36	34.7		1.19
ZS-6	Pacoima Canyon, San Gabriel Mountains, Calif.	4	23– 25	24.3	23.5	6	31– 34	33	33	1.36
ZS-17		4	21– 24	22.7		3	32– 34	33		1.45
ZS- 1	10% ZS-10, 90% ZS-6	4	22– 25	23.7	23.5 (24.5)	2	34– 36	35	34.8 (34.5)	1.48
ZS-8		4	22– 24	23.3		2	33– 36	34.5		1.48
ZS-4	32% ZS-10, 68% ZS-6	4	26– 28	26.7	26.3 (26.6)	3	37– 39	38	37.5 (37.8)	1.42
ZS-20		4	25– 27	26.0		3	36– 38	37		1.42
ZS-15	50% ZS-10, 50% ZS-6	4	27– 29	28.5	28.4 (28.5)	2	39– 41	40	40.2 (40.5)	1.40
ZS-11		4	27– 30	28.3		2	40– 41	40.5		1.43
ZS-10	Old Whitestone farm, Natural Bridge, N. Y.	4	32– 33	32.5	33.5	5	46– 50	46.8	48	1.44
ZS-16		4	34– 35	34.5		3	48– 51	49.3		1.43
ZS-7	10% ZS 9, 90% ZS-6	4	44– 46	45.0	46.1 (47.4)	3	58– 62	60.3	60.3 (60.7)	1.34
ZS-19		4	46– 48	47.3		3	59– 63	60.3		1.27
ZS-3	15% ZS-9, 85% ZS-6	4	58– 62	60.0	60.7 (59.1)	2	75 79	77	76 (74.5)	1.28
ZS-5		4	59– 63	61.3		2	74– 76	75		1.22
ZS-12	32% ZS-9, 68% ZS-6	4	94–100	97.5	97.3 (99.9)	3	114–125	119	117.5 (121.6)	1.22
ZS-14		4	94–100	97.0		3	113–117	116		1.20
ZS-9	Quanah Mountains, Wichita Mountains, Okla.	4	255–265	260	262	7	280–325	310	303	1.19
ZS-13		4	260–270	265		3	285–305	295		1.11

[a] The values reported in parentheses were calculated by totaling the amount of lead contributed by each component of the mixture using the analysis value reported in the determination.

ies. The results indicate that while the lead volatilizes from the synthetic "zircon" in the same pattern rate as the natural mineral, opal glass releases lead into the arc column much more rapidly.

A series of each of the standard materials was exposed on the same plate, the emulsion calibrated, and the analytical curves constructed as illustrated in Fig. 2. The synthetic "zircon" standards form a straight line working curve. The opal glass curve, although shifted in the direction of lower lead analysis values, does not parallel the synthetic "zircon" curve. No single correction factor can be applied to align the curves.

It is apparent from the preceding studies that the most significant factor causing variations in the lead analyses is the difference in the chemical and physical properties of the spectrochemical standards. Because the relative intensities of analytical lines are influenced markedly by the reactions occurring in the electrode crater and in the arc column, the composition of the standards should be as nearly identical to the sample as possible. The tendency of the upper portion of the opal glass curve to flatten indicates that self-absorption is causing a decrease in the line intensities of the standards above 100 ppm. lead. The fact that the two

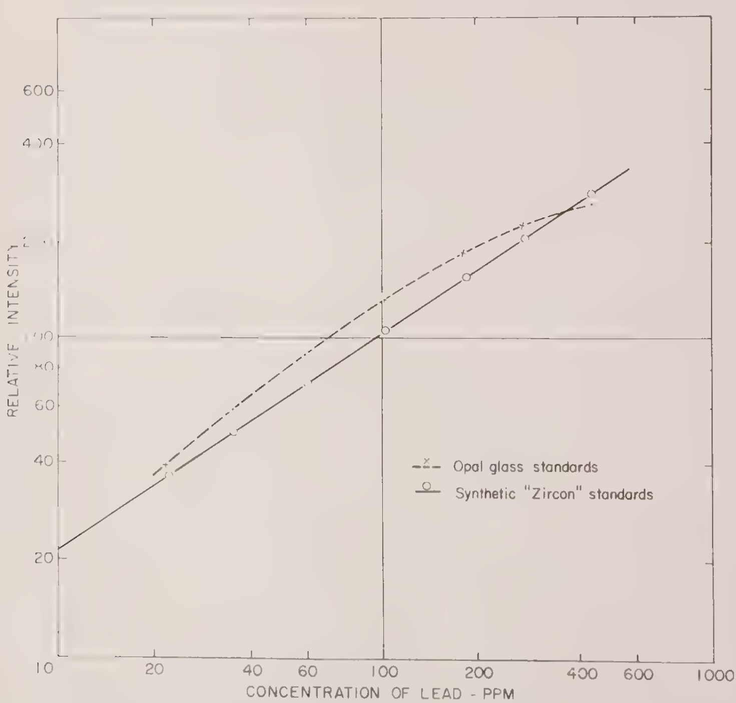

FIG. 2. Comparison of working curves of opal glass and synthetic "zircon" standards.

rorking curves cross at approximately 350 ppm. explains the favorable omparison of lead values by the Waring and Worthing method (1953) rith the analyses of isotope dilution in this range of concentration, alhough only a limited number of samples are involved (Table 1).

The higher intensities displayed by the opal glass standards cause a hift in the analytical curve resulting in lower analytical values. Whether he increase in intensity is due to the more rapid rate of lead volatilizaion from opal glass affecting the vapor density of the arc gas at these oncentrations is not known. It can only be concluded that in this range f concentration low analytical values result when opal glass is used as a tandard. It should be mentioned that chemical analyses by several hemists and isotope dilution analyses by L. R. Stieff of the U. S. Geoogical Survey, indicate that the certificate value of 900 ppm. lead for opal lass (National Bureau of Standards, standard sample 91) is low.

This method is applicable to the determination of lead in monazite. Monazite is more radioactive and contains higher lead concentrations han zircon. Dilution of the sample in zircon base (68% zirconia and 32% ilica) reduces the lead to a more suitable analytical range and at the ame time creates a matrix similar to the standards. When sufficient uantities of monazite and zircon are concentrated from the host rock, ead-alpha ages can be determined by analysis of each of these minerals. The results of the analysis of two monazites by isotope dilution and hemical techniques and by this method are given in Table 2.

The spectrochemical method described for the determination of lead is contribution to the lead-alpha method which is valuable for obtaining econnaissance age estimates of zircon from igneous rocks. The present tudy emphasizes the importance of the composition of the standard and ecommends the use of a full set of standards in quantitative spectrohemical analysis.

Acknowledgments

The authors express appreciation to G. R. Tilton, Carnegie Institute of Washington, L. T. Silver, California Institute of Technology, and Henry Faul, U. S. Geological Survey, who furnished samples on which they had nade isotope dilution analyses. W. S. Connor and S. M. Young of the Statistical Engineering Laboratory, National Bureau of Standards, deised the controlled experiment given in the discussion.

We acknowledge the help of the following colleagues, all of the U. S. Geological Survey; D. B. Stewart and B. J. Skinner synthesized the maerial used as our standard and made numerous mineralogical and x-ray lentifications. Frank Cuttitta, R. A. Powell, and L. R. Stieff analyzed ome of the samples chemically or by isotope dilution. Helen Worthing

aided in the dilution of the standards and in the spectrochemical analysis of many samples.

References

Churchill, J. R., 1944, Techniques of quantitative spectrographic analysis: *Indus. Eng. Chemistry, Anal. Ed.*, **16,** 653–670.

Gottfried, David, Jaffe, H. W., and Senftle, F. E., 1959, Evaluation of the lead-alpha (Larsen) method for determining ages of igneous rocks: *U. S. Geol. Survey Bull.* **1097-A,** 63.

Harvey, C. E., 1950, Spectrochemical procedures, Glendale, Calif., *Applied Research Laboratories*, **402**.

Hodge, E. S., 1951, Selected iron lines on commercial spectrographs for emulsion calibration: *Anal. Chemistry and Applied Spectroscopy Symposium, Pittsburgh, Pa.*, March 7 1951.

Larsen, E. S., Jr., Keevil, N. B., and Harrison, H. C., 1952, Method for determining the age of igneous rocks using the accessory minerals: *Geol. Soc. America Bull.*, **63** 1045–1052.

Waring, C. L., and Worthing, Helen, 1953, A spectrographic method for determining trace amounts of lead in zircon and other minerals: *Am. Mineral.*, **38,** 827–833.

Webber, G. R., Hurley, P. M., and Fairbairn, H. W., 1956, Relative ages of eastern Massachusetts granites by total lead ratios in zircon: *Am. Jour. Sci.*, **254,** 574–583.

Manuscript received March 4, 1960.

THE AMERICAN MINERALOGIST, VOL. 45, NOVEMBER-DECEMBER, 1960

WHEWELLITE AND CELESTITE FROM A FAULT OPENING IN SAN JUAN COUNTY, UTAH*

A. J. Gude, 3rd., E. J. Young, V. C. Kennedy and L. B. Riley, *U. S. Geological Survey, Denver, Colorado.*

Abstract

Whewellite ($CaC_2O_4 \cdot H_2O$) in two large crystals, yellow celestite, and several other minerals were found in vuggy openings along a fault in the Radon mine near Moab, San Juan County, Utah. This is the second reported occurrence of whewellite from North America, the first being from limestone concretions in Montana. Paragenetically whewellite is later than the celestite and its origin is believed related to associated carbonaceous material.

Introduction

In April 1958 one of the writers, Vance C. Kennedy, found two large crystals of whewellite in a uranium mine in eastern Utah. This is the second occurrence of whewellite reported from North America, the first having been described by Pecora and Kerr (1954) from a septarian limestone concretion in marine shale near Havre, Montana. The two crystals here described are much larger and are from a considerably different geological environment. They were collected from the Radon mine located on the southwest flank of the Lisbon Valley anticline, about 35 miles southeast of Moab in sec. 28, T. 29 S., R. 24 E., Salt Lake Meridian, San Juan County, Utah. The crystals were found in celestite-lined vuggy openings along the "Radon" fault where it cuts high grade uranium ore on the 280 level. Near the sampling site the Radon fault is normal, strikes about N55 W, dips 67° SW, and has a vertical displacement of about 3.5 feet (C. L. Dodson and T. Botinelly, written communication). Wall rock of the vugs consisted of the lower few feet of the Triassic Chinle formation, just above its contact with the Permian Cutler formation. Here the Chinle is composed of interbedded lenses of medium-grained sandstone, fine-grained sandstone, mudstone, and claystone.

Descriptive Mineralogy

The larger of the two whewellite crystals weighs 8.6 gms. and measures roughly $2\frac{1}{2}$ by 2 by $1\frac{1}{2}$ cm. A small part of the crystal is intergrown with yellow celestite and very minor amounts of pyrite, marcasite, calcite, and black asphaltic material. When found, parts of the crystal were covered by very thin gray coatings of loosely-adhering micro-crystalline calcite, most of which were gradually rubbed off by handling. The crystal is milky white in color, but where broken on an edge, the interior appears blue-gray and more translucent. One good cleavage, parallel to the form

* Publication authorized by the Director, U. S. Geological Survey.

$(\bar{1}01)$, is evident. A stereographic photograph and the morphology of this crystal are shown in Fig. 1. Crystallographic data were obtained by A. J. Gude, 3rd., and are described below, under Crystallography and x-ray data.

The smaller of the two crystals of whewellite, 2 by 1 by 0.7 cm., is attached to the matrix of a large piece of buff-colored medium to coarse-grained sandstone which is coated with small crystals of celestite and calcite. A third, or satellitic, whewellite crystal 3 mm. in diameter and about 5 mm. from the one in place was removed with an ultrasonic needle and all physical, spectrographic and x-ray work was performed on it. Table 1 records the physical properties of whewellite from Utah and compares them with those of the whewellite specimen from Montana as given by Pecora and Kerr (1954).

Table 1. Physical Properties of Whewellite

	San Juan County, Utah	Havre, Montana
α	1.491 ±0.002	1.491 ±0.002
β	1.556 ±0.002	1.555 ±0.002
γ	1.650 ±0.002	1.654 ±0.002
2V (+)	84°±2°	82°
Specific gravity	2.21±0.05 Berman balance 2.19±0.01 Suspension method	2.21±0.01
Hardness	~2.5	3

Measurement of the indices of refraction was greatly facilitated by the use of a rotating needle stage devised by Wilcox (1959). Measurement of the optic angle was made on a universal stage and represents the average of two readings taken from the acute bisectrix to an optic axis. The specific gravity as determined by a Berman balance represents an average of four determinations on two grains. The specific gravity was also determined on two grains by the suspension method, but the lighter of the two grains was strongly suspected of having air voids due to skeletal structure in the whewellite fragment. Hence the average value by this method, 2.19, is probably low.

Spectrographic Data

Semiquantitative spectrographic analyses (Table 2) were made on both the whewellite from Utah and from Montana. The latter sample was kindly furnished by W. T. Pecora.

Although both samples are extremely pure calcium oxalate monohydrates, it is noted that the whewellite from Utah, which is intimately

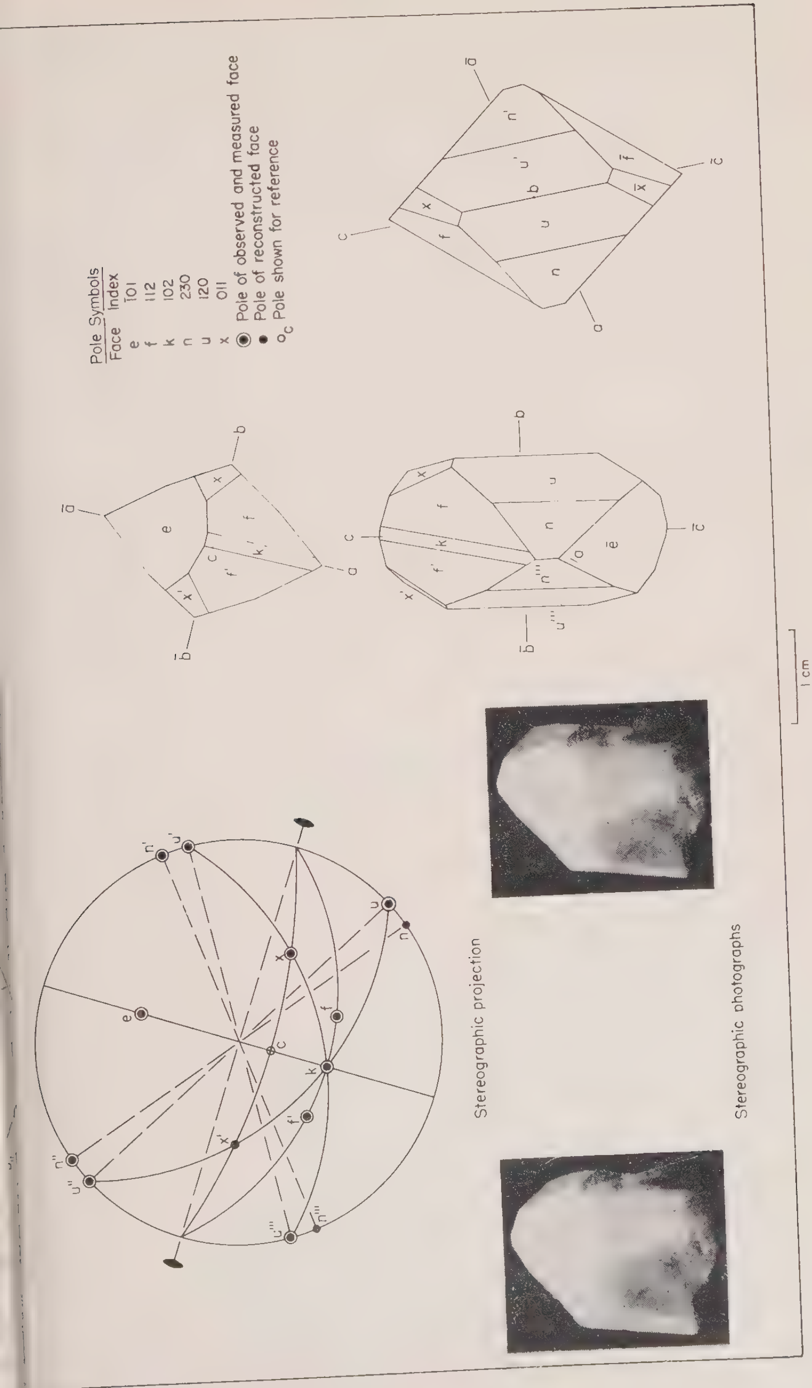

FIG. 1. Crystal morphology of whewellite from Lisbon Valley, Utah.

associated with celestite, contains considerably more strontium than the whewellite from Montana.

Table 2. Semiquantitative Spectrographic Analyses of Whewellite
(J. C. Hamilton, Analyst)

	San Juan County, Utah	Havre, Montana
Si	0.015%	0.03%
Al	0.0015	0.007
Fe	~0.0008*	~0.0008*
Mg	<0.0005	<0.0005
Ca	M	M
Mn	<0.0002*	0.0003
Na	0.07	0.07
Ba	0.0007	0.0003
Sr	0.007	0.0007
Cr	0.00015	0.00015
Cu	<0.0001*	0.0007

Notes: Figures are reported to the nearest group in the series 7, 3, 1.5, 0.7, 0.3, 0.15, etc., in per cent. The numbers represent midpoints of group data on a geometric scale. Comparisons of this type of semiquantitative results with data obtained by quantitative methods, either chemical or spectrographic, show that the assigned group includes the quantitative value about 60 per cent of the time.

M = major constituent—greater than 10 per cent.

* Limit of detection.

The following elements were looked for and not found: K, Ti, P, Ag, As, Au, B, Be, Bi, Cd, Ce, Co, Dy, Er, Eu, Ga, Gd, Ge, Hf, Hg, Ho, In, Ir, La, Li, Lu, Mo, Nb, Nd, Ni, Os, Pb, Pd, Pr, Pt, Rb, Re, Rh, Ru, Sb, Sc, Sn, Sm, Ta, Tb, Te, Th, Tl, Tm, U, V, W, Y, Yb, Zn, Zr.

Crystallography and *X*-Ray Data

The largest crystal of whewellite was used to determine its morphology (Fig. 1). *X*-ray data are shown and compared in Table 3 with similar data by Pecora and Kerr (1954).

Both large crystals show the same morphology. Neither is twinned although casual preliminary inspection and comparison with the figures given by Palache, Berman and Frondel (1951) caused some delay in interpreting the goniometric data before the correct orientation shown in Fig. 1 was determined. The upper domatic faces and the two prisms are partially developed. None of the lower terminations are present.

The crystal has poorly reflecting faces and is somewhat oversize for ordinary optical goniometry. Attached fragments of the matrix minerals, facial overgrowths that formed step-like apparent curvatures, shallow and flat obtuse angles, and combinations of these and similar imperfec-

tions, made contact goniometer measurements generally unreliable. Accordingly, the crystallographic data were obtained by using a spectrometer adapted as a one-circle goniometer. Four sets of each of the interfacial angle measurements were made from independent resettings of the crystal and goniometer.

A well-developed prism zone was proved to be present. From the stereographic plot of face poles e $(\bar{1}01)$ was found to be the prominent face on the crystal. Careful examinations of the lower fractured areas then revealed a parallel cleavage surface which agrees well with the published descriptive data of Palache, Berman and Frondel (1951). A face pole for c (001) is shown in Fig. 1 for convenience of reference although no development of this face was found. The flat obtuse angle between n(230) and u(120) can be seen on the crystal only in oblique illumination and then only with difficulty. However, these two faces were easily and distinctly resolved when measured on the goniometer. Face k(102) was found and verified by measurement after plotting a preliminary stereogram and reexamining the crystal. Axial angle β is not easily determined from the sets of faces found on this particular specimen.

Celestite and Other Associated Minerals

The celestite that is intimately associated with the whewellite occurs in clear yellow blade-shaped crystals which attain several millimeters in length and several tenths of a millimeter in thickness. Practically all the celestite contains abundant inclusions of pyrite and marcasite which occur as cubes and bladed crystals up to about 0.3 mm. in size. The iron sulfide inclusions were segregated into cube-like and lath-like fractions and x-rayed separately. The cube-like fraction proved to be only pyrite; the lath-like forms consisted of both pyrite and marcasite, with pyrite predominant. The celestite has the following optical properties and specific gravity:

$\alpha = 1.622$ (by calculation)
$\beta = 1.624 \pm 0.002$
$\gamma = 1.632 \pm 0.002$
$2V(+) = 55° \pm 2°$
Pleochroism $\alpha = \gamma =$ almost colorless
$\beta =$ pale yellow
Absorption $\beta > \alpha = \gamma$
Sp. gr. $= 4.03 \pm 0.05$

A noteworthy feature of some of the celestite crystals is that the yellow coloration is not equal through all the parts of a single crystal when β is being viewed. Contact between the yellow tints is generally curved, but

Table 3. X-Ray Powder Diffraction Data for Whewellite from Utah and Montana

Diffractometer[1]		Film	
Utah		Montana (Pecora and Kerr, 1954, p. 210)	
d(Å, meas.)	I	d(Å, meas.)	I
14.3	13		
10.0	5		
8.42	5		
5.95	75	5.95	100
5.79	27	5.81	5
4.52	8	4.53	5
4.33	5		
4.15	5		
4.09	8		
3.860	8		
3.770	11	3.773	5
3.633	100	3.652	90
3.480	7		
3.401	7	3.414	1
		3.321	1
3.278	7		
3.110	14	3.105	5
2.998	14	3.002	1
2.969	100	2.971	50
2.903	18	2.906	10
2.840	14	2.842	10
2.754	7		
2.706	6		
2.637	8	2.639	1
2.607	7		
2.578	7		
2.529	8		
2.494	35	2.497	20
2.448	9	2.455	1
2.411	10	2.422	1
2.380	9	2.388	1
2.356	68	2.357	80
2.293	7		
2.253	25	2.262	20
2.212	10	2.213	5
2.127	8	2.135	1
2.103	6		
2.094	10		
2.070	21	2.076	10
2.045	5		
1.977	20	1.978	5
1.949	16	1.955	5

[1] CuKα (Ni filter), $\lambda = 1.5418$ Å.

TABLE 3 (*Continued*)

Diffractometer[1]		Film	
Utah		Montana (Pecora and Kerr, 1954, p. 210)	
d(Å, meas.)	I	*d*(Å, meas.)	I
1.933	22	1.930	5
1.892	16	1.891	5
1.859	7	1.859	1
		1.848	1
1.841	10		
		1.826	1
1.814	13	1.818	1
1.791	15	1.794	1
1.774	4		
1.759	5		
1.734	15	1.737	1
1.707	4		
1.689	6	1.693	1
1.639	3	1.644	1
1.583	8	1.588	1
		1.522	1
1.547	10		
1.526	8	1.528	1
1.499	6	1.505	1
1.484	9	1.480	1
		1.458	1
1.406	6		
1.397	5		
1.379	6		
1.375	7		
1.331	10		
1.304	4		
1.282	5		
1.248	4		
1.214	4		
1.185	9		
1.152	7		
1.130	4		
1.108	3		
1.097	6		

sharp. The optic angle was measured by using a universal stage and represents the average of four direct measurements. Specific gravity was measured on a Berman balance and represents an average on nine determinations on several grains. Extreme measurements were 3.95 and 4.09.

A semiquantitative spectroscopic analysis of the celestite, was made by John C. Hamilton of the U. S. Geological Survey and showed the following impurities in per cent: Al 0.07, Fe 0.03, Ca 0.15 and Ba 3.0. The

sample submitted for this analysis still contained some iron sulfide inclusions even after careful handpicking; these inclusions although estimated at less than 0.1 per cent by volume, based on a micrometer ocular measurement, probably account for most or all of the iron found. Part or all of the aluminum may be due to clay impurity, although none could be seen with a microscope. The specific gravity and indices of refraction of this celestite are slightly higher than those of pure celestite ($SrSO_4$), no doubt due to the 3.0 per cent Ba.

It is the optic angle of 55°, however, which poses a problem since the barytocelestite series is reported to vary in 2V from 50° to 37° 30′ according to Winchell (1951). This is not an isolated instance of 2V anomaly for celestite, for earlier unpublished work by one of us has shown that celestite from the Cripple Creek District, Colorado, had a 2V of $51° \pm 3°$ (by universal stage) and thus the 2V reported for pure celestite. Yet this had a composition of 64 per cent $SrSO_4$ and 36 per cent $BaSO_4$ estimated from the indices of refraction and confirmed by spectrographic analysis.

Black lustrous conchoidally-fracturing asphaltic material occurs intergrown with the celestite and very thin coatings of iridescent iron sulfides cover some of the celestite crystals. Colorless calcite caps some of the celestite and also is found free as small dogtooth spar crystals. It was checked optically and found to be uniaxial negative with ω about 1.657. Finally strontianite occurs sparsely as tiny tufts of acicular crystals capping both calcite and celestite. These needles show parallel extinction and are length fast; their optic sign is negative and their 2V is very small. α is approximately equal to 1.516 and β and γ are both close to 1.666.

Paragenesis

Paragenesis is rather clear in this whewellite occurrence, and the minerals are listed from first-formed to last-formed:

celestite
pyrite and marcasite
asphaltic material
whewellite
calcite
strontianite

None of the crystals in this sequence show corrosion. The iron sulfides and celestite are mainly contemporaneous, but thin iridescent coats of sulfides on celestite indicate the sulfides to be later also. The occurrence of both pyrite, marcasite and marcasite altered to pyrite suggests changing conditions during the iron sulphide deposition. Asphaltic material, partially intergrown with celestite, and also covering it, indicates its

early formation. Whewellite clearly shows evidence of enclosing and crystallizing around the celestite. Calcite was found capping celestite, asphaltic matter, and whewellite. Finally, strontianite caps both calcite and celestite.

The association of whewellite with asphaltic material strongly suggests that the oxalate part of the whewellite is of organic origin and is either derived from the asphaltic material or from the same source as the asphaltic material. This source is most probably the carbonaceous detritus ("carbonaceous trash") known to be present in the lower part of the Chinle formation.

References

Palache, C., Berman, H., and Frondel, C., 1951, Dana's System of Mineralogy, Vol. II, Seventh edition, John Wiley and Sons, New York.

Pecora, W. T., and Kerr, J. H., 1954, Whewellite from a septarian limestone concretion in marine shale near Havre, Montana, *Am. Mineral.*, **39,** 208–214.

Wilcox, R. E., 1959, Use of spindle stage for determining refractive indices of crystal fragments, *Am. Mineral.*, **44,** 1272–1293.

Winchell, A. N., 1951, Elements of optical mineralogy, Part II—Descriptions of minerals, Fourth edition, John Wiley and Sons, New York.

Manuscript received March 3, 1960.

THE AMERICAN MINERALOGIST, VOL. 45, NOVEMBER–DECEMBER, 1960

A STRUCTURAL PROPOSAL FOR BOULANGERITE

L. BORN AND E. HELLNER, *Mineralogical Institute of the University, Kiel, Germany.*

ABSTRACT

A structure for the sub-cell of boulangerite is proposed which explains the morphology (as needles) and shows the boundary between the "galena-like" and the "stibnite-like" structures of complex sulfides.

The last reported research on boulangerite was by Berry (1940), who made Weissenberg photographs. If the weak first layer is neglected, the unit cell can be taken as

$$a_0 = 21.14, \quad b_0 = 23.46, \quad c_0 = 4.035 \text{ Å}; \quad \text{space group } Pbnm.$$

Including the weak first layer, Berry proposed a monoclinic cell, or an orthorhombic *B* cell, the latter with doubled *a* and *c* axes.

This paper gives the result of a structure determination for the sub-cell of boulangerite. The specimen used was labelled "Heteromorphit" or "Federerz" = "plumosite," from Pribram, Bohemia.* Weissenberg photographs of the 0 and 2nd level were similar to those published by Berry, and with respect to the sub-cell there is full agreement with his results. However the weak first level on our film shows orthorhombic symmetry, and not the monoclinic symmetry shown by Berry's photograph.† Nevertheless, the differences in the intensities of related reflections are slight in Berry's photograph, and therefore we prefer the orthorhombic symmetry for the large unit cell with

$$a_0 = 42.28, \quad b_0 = 23.46, \quad c_0 = 8.07 \text{ Å}; \quad \text{space group } Bb2_1m$$

The chemical analysis by Berry leads to the formula $Pb_{20}Sb_{16}S_{44}$ for the sub-cell, which is also the basis for our structure determination. The calculations were made on an IBM 650 machine, using the INCOR program (by Zalkin/Jones, 1957); the least-squares program (by Templeton/Senko, 1957); and the Patterson-Fourier-Program (Darmstadt-Sindelfingen-Program). A proposed structure for the metal atoms was derived from two Patterson sections $P(u, v, o)$ and $P(u, v, \frac{1}{2})$. With the aid of these metal positions a Fourier synthesis was calculated; this Fourier synthesis also gave the positions of most of the sulfur atoms. During the least-squares refinement the remaining sulfur atoms were located.

Both the first layer and the very weak reflections of the 0 and 2nd layer were neglected in the first estimation of the structure, because the

* For this and other material, we are greatly indebted to Prof. Ramdohr, Heidelberg, Germany.

† Professor L. G. Berry kindly sent us his film.

Weissenberg photographs showed a large anisotropic influence of the absorption factor, and in addition these weak reflections are influenced by the superstructure. Table 1 shows the estimated parameters of boulangerite which gave an R-factor of 17.6%. This seems unexpectedly favorable in view of the neglect of the weak reflections.

Boulangerite has 3 positions occupied by Pb and 3 by Sb. Positions 4–6 are occupied in the sub-cell by a statistical distribution of Pb and Sb

TABLE 1. ATOMIC PARAMETERS OF BOULANGERITE

Number of Atom	Symbol	Parameter		
		x	y	z
1	Pb	0.307	0.160	0.250
2	Pb	117	498	250
3	Pb	206	323	250
4	Pb, Sb	458	433	750
5	Pb, Sb	132	098	750
6	Pb, Sb	486	129	750
7	Sb	287	462	750
8	Sb	046	232	250
9*a*	Sb/2	388	283	750
9*b*	Sb/2	372	307	750
10	S	069	017	250
11	S	247	028	250
12	S	156	175	250
13	S	420	219	250
14	S	330	375	250
15	S	372	088	750
16	S	014	138	750
17	S	278	251	750
18	S	096	295	750
19	S	186	415	750
20	S	013	441	750

with the atomic form factor $(f_{Pb}+f_{Sb})/2$. This is reasonable for the superstructure and indicates in this case that Pb and Sb alternate in the c direction. Position 9 was split up in two antimony atoms, which were shown by the Fourier synthesis. Therefore the atomic form factor for 9*a* and 9*b* has the value of $f_{Sb}/2$. We recognize this splitting by the strong deviation of the temperature factors from the average of all the other atoms.

In contrast to Berry's formula $Pb_{20}Sb_{16}S_{44}$, our rough structure estimation for the sub-cell indicates a formula $Pb_{18}Sb_{18}S_{44}$. The later refinement for the superstructure and the calculation of the anisotropic absorption

factor may change our formula in the direction of Berry's formula. Figure 1 shows the result of the structure determination; the hatched parts indicate the chains in the *c* direction, which are responsible for the plumose morphology.

A first proposal to derive the structure of complex sulfides from the galena (NaCl) type was made by Hofmann (1935) and extended by Hellner (1958). A number of sulfides, like miargyrite, meneghinite, cosalite,

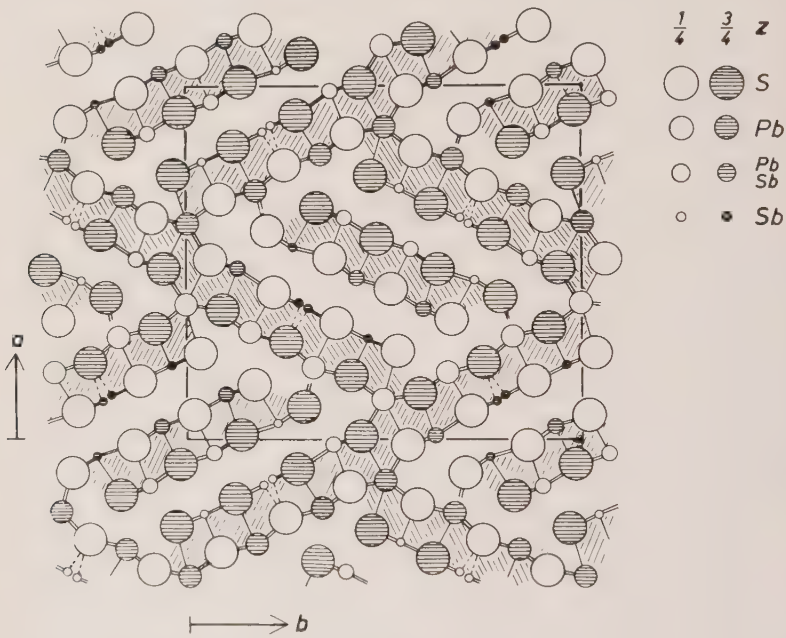

FIG. 1. Structure of boulangerite for the sub-cell, projected on (001); the hatched parts indicate the chains in the *c*-direction.

and the andorite group follow this pattern and it was shown that it is possible to extend it also to stibnite, but it was mentioned that the coordination number of the metal atoms increases from 6 to 7 in stibnite.

Figure 2 shows an ideal galena type, projected on (110). In Fig. 3 the atoms have the same x and y parameter, but the z parameters of half of the atoms are interchanged in such a way that the coordination number of the metal atoms becomes $5+2$ $(=7)$, the latter with a larger distance. The 3-dimensional network of the galena structure (Fig. 2) has been divided into 2-dimensional nets. This change from a galena-like structure to a net structure can be considered to be produced by a large replace-

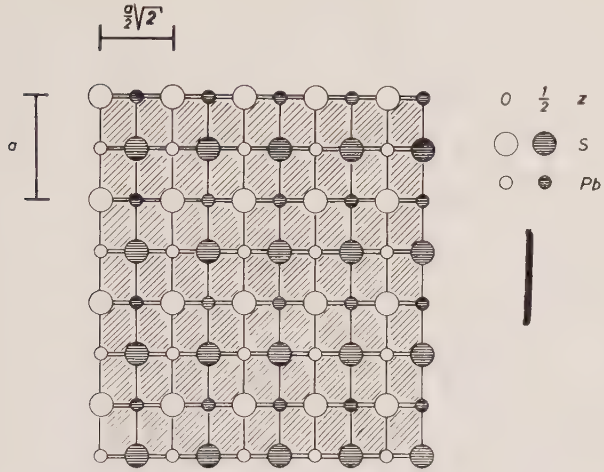

FIG. 2. Structure of the galena (NaCl) type, projected on (110).

ment of Pb and Sb. But hand in hand with this replacement the ratio between metal and sulfide atoms decreases and the nets are cut off into chains of variable width in respect to the two factors mentioned above. Typical representatives of this group are jamesonite (Niizeki and Buerger, 1957*b*) and boulangerite.

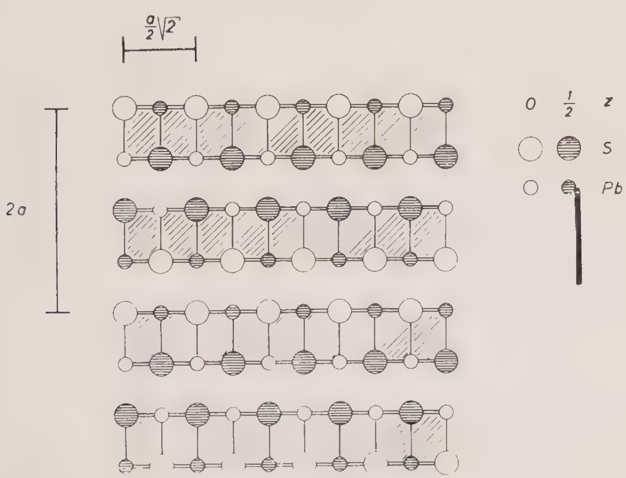

FIG. 3. Projection of the galena type on (110), but half of the *z* parameters of the sulphur and metal atoms are interchanged in such a way that the 3-dimensional network of the galena type changes into 2-dimensional infinite nets. The coordination number changes from 6 in the galena type to 5+2(=7) in the "net" structure. These nets are cut off in chains in respect to the *c*-direction, as we can find in boulangerite and jamesonite.

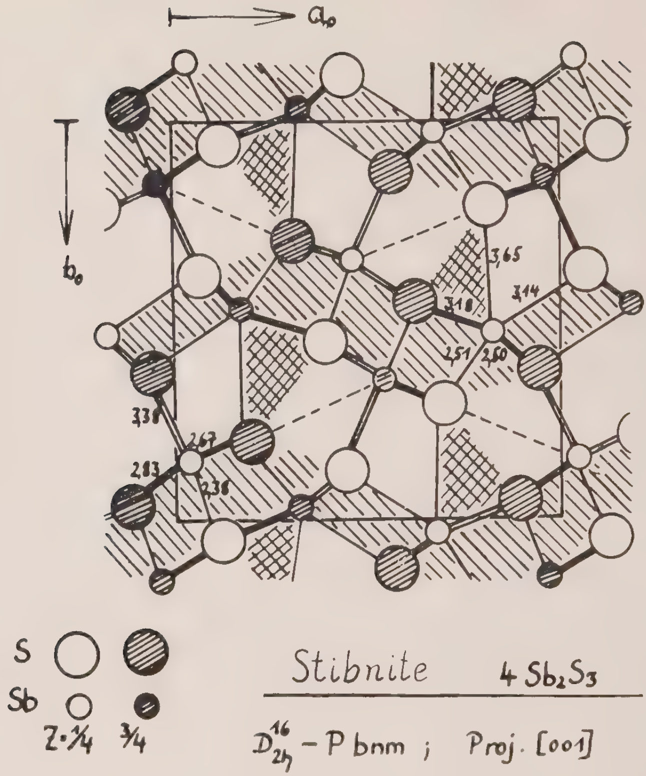

FIG. 4. Structure of stibnite projected on (001) indicating chains which are arranged in such a distorted way that the relations to the "net" structures are difficult to recognize.

If Sb constitutes the major part of the metal atoms, the ratio between metal and sulfide atoms becomes smaller and smaller until the limit, $f = n_{me}/n_s = 0.67$, is reached in stibnite. One third of the metal positions become unoccupied and the deformation of the octahedral holes reaches a maximum because the Sb atoms are strongly connected with only three sulfur atoms. Therefore the chains are small and irregularly arranged in respect to a changed galena type. Livingstonite (Niizeki and Buerger 1957*a*) also belongs in this group.

Summary

The structures of the complex sulfides can be divided in two groups:

1) "Galena-like" structures have large portions with a distorted galena type (Fig. 2), with the coordination number 6 for most of the metal atoms; only the metal atoms on the edge of the galena parts

have another coordination number. Miargyrite, schapbachite, cosalite, meneghinite, the andorite group, galenobismutite, the krennerite, sylvanite and calaverite belong to this type.

2) The chain structure or "stibnite-like" structures are characterized by a high Sb (or Bi) content and by a change in their relation to the galena type indicated by the transformation from Fig. 2 to 3. The coordination number changes from 6 to 5+2 (=7); the chains have variable compositions and orientations to each other. The relation to Fig. 3 is shown by the structures of jamesonite and boulangerite; other sulfides with a chain structure but less closely related to Fig. 3 are livingstonite, stibnite, aikinite and wolfsbergite.

It seems reasonable to derive the "galena-like" complex sulfide structures from distorted three-dimensional lattice complexes, *i.e.* F-lattices, and the "stibnite-like" types from two-dimensional lattice complexes which indicate the chain character.

Acknowledgment

We are indebted to the "Deutsche Forschungsgemeinschaft," which contributed to this work by a personal grant and financial support.

References

Berry, L. G., 1940, Studies of mineral sulpho-salts: III.—Boulangerite and "Epiboulangerite": *Univ. Toronto Studies, Geol. Ser.*, **44**, 5–19.

Hellner, E. 1958, A structural scheme for sulphide minerals: *Journal of Geology*, **66**, 503–525.

Hofmann, W. 1935*a*. Ergebnisse der Strukturbestimmung komplexer Sulphide, I. Die Struktur von Zinnsulfur, SnS, und Teallit, $PbSnS_2$: *Zeits. Krist.*, **92**, 161–173.

Niizeki, N. and Buerger, M. J., 1957a, The crystal structure of livingstonite, $HgSb_4S_8$: *Zeits. Krist.* **109**, 129–157.

———, 1957b, The crystal structure of jamesonite, $FePb_4Sb_6S_{14}$: *Zeits. Krist*, **109**, 161–183.

Templeton, D. H. and Senko, M. E., 1957. The use of the IBM 650 for crystal structure analysis computations: *Acta Cryst.*, **10**, 385.

Zalkin, A., and Jones, R. E. 1957, The use of the IBM 650 for crystal structure analysis computation: *Acta Cryst.*, **10**, 385.

Manuscript received March 6, 1960.

THE AMERICAN MINERALOGIST, VOL. 45, NOVEMBER-DECEMBER, 1960

NOTES AND NEWS

PARATELLURITE, A NEW MINERAL FROM MEXICO[1]

GEORGE SWITZER, *United States National Museum, Washington, D. C.*
AND HOWARD E. SWANSON, *National Bureau of Standards, Washington, D. C.*

INTRODUCTION

Tellurium dioxide, TeO_2, occurs in tetragonal and orthorhombic dimorphous forms. Orthorhombic TeO_2 is found in nature as tellurite. The tetragonal form, well known as a chemical compound, has been found associated with tellurite and native tellurium at Cananea, Sonora, Mexico. The name paratellurite is proposed for the new mineral.

TETRAGONAL TELLURIUM DIOXIDE

The structure of tetragonal TeO_2 has been determined by Stehlik and Balak (1949), who found that it has either the space group $P_{4_12_12}$ or $P_{4_32_12}$ with $4(TeO_2)$ per unit cell.

X-ray powder data for tetragonal tellurium dioxide are given in Table 1. Column 1 gives data obtained on "Specpure" TeO_2 manufactured by Johnson, Matthey and Co., Ltd., London. Data in column 2 were obtained on the naturally occurring material. The two materials give essentially identical patterns.

PARATELLURITE

Paratellurite occurs very sparingly with tellurite in thin seams in native tellurium as an alteration product of tellurium and tellurite.

The mineral is very fine grained, grayish white in color, with a resinous to waxy luster and hardness of 1. A specific gravity of 5.60 was determined on a 13.7 mg. sample with the Berman balance. This value is apparently low due to the fine-grained nature of the material. The calculated density is 6.017 gms./cm.^{3}. Indices of refraction are greater than 2.05.

Scarcity of material and difficulty in its purification made analytical work difficult. A chemical analysis was made by George B. Magin, Jr., of the United States Atomic Energy Commission, on a solution prepared from a 50 mg. sample. Two 20 ml. aliquots were taken and Te was precipitated and weighed. The results of the two determinations were 78.5% and 78.0% Te. Theoretical Te in TeO_2 is 79.94%.

A quantitative spectrographic analysis of paratellurite was made by

[1] Publication authorized by the Secretary, Smithsonian Institution and the Director, National Bureau of Standards.

TABLE 1. TELLURIUM (IV) OXIDE, PARATELLURITE, TeO_2 (TETRAGONAL)
(Cu, 1.5405 at 25° C.)

Synthetic (Johnson Matthey Co. Ltd., London)*			Paratellurite, Sonora, Mexico U.S.N.M. R8861	
hkl	d(Å)	I	d(Å)	I
101	4.07	9	4.068	12
110	3.40	88	3.404	86
111	3.10	13	3.107	13
102	2.98	100	2.988	100
112	2.536	1	2.536	1
200	2.407	20	2.407	20
201	2.293	2	2.296	3
210	2.151	2	2.151	3
211	2.071	6	2.071	5
113, 202	2.034	1	2.033	1
004	1.903	8	1.904	10
212	1.872	65	1.873	55
203	1.745	< 1	1.746	2
220	1.700	12	1.701	12
114, 221	1.660	22	1.661	22
213	1.6401	4	1.641	4
301	1.5684	3	1.569	2
310	1.5210	12	1.5212	9
204	1.4923	15	1.4925	12
302	1.4775	9	1.4777	8
223, 312	1.4127	2	1.4129	2
303	1.3554	1	1.3554	< 1
321	1.3139	2	1.3142	2
313	1.3048	< 1	1.3048	2
224	1.2681	4	1.2682	5
322	1.2590	4	1.2590	7
215	1.2433	1	1.2431	2
106, 304	1.2270	5	1.2269	5
400	1.2020	< 1	1.2026	2
116, 314	1.1881	6	1.1882	6
323	1.1806	< 1	1.1812	4
411	1.1531	< 1	1.1530	3
225	1.1341	< 1	1.1339	< 1
331	1.1212	< 1	1.1214	1
412	1.1158	2	1.1159	2
216, 324	1.0928	4	1.0929	3
403, 332	1.0866	< 1	1.0867	1
315, 240	1.0753	< 1	1.0760	< 1
421	1.0647	< 1	1.0646	< 1
107, 413	1.0601	< 1	1.0599	< 1
226, 404	1.0164	1	1.0167	2

Lattice Constants

Synthetic	Paratellurite
$a_0=4.809$ Å $c_0=7.614$ Cal. density $=6.019$ g/cm.^{3}	$a_0=4.810$ Å $c_0=7.613$ $=6.017$ g/cm.^{3}

* N.B.S. Circular 539, Vol. 7, page 56 (1957).

Harry J. Rose, of the United States Geological Survey. Only Te was found in amounts greater than a few tenths of a per cent. The analysis follows: Te major, Sn .04%, Pb .004, Mn .02, Fe .06, Zr .01, Mg .04, Ca .05, Ba .01. (Al .2 and Si .5% were found but are due to impurity.) Selenium was looked for but not detected. The sensitivity of Se is poor by this method and quantities as high as 10 per cent may not be detected. However, the fact that the unit cell dimensions of paratellurite and "specpure" TeO_2 are practically identical would indicate that if any Se is present it is minor.

Paratellurite occurs as a fine-grained crystalline aggregate, either massive or pseudomorphous after tellurite. Some well-defined tellurite crystals are transparent and unaltered; others, while retaining the tellurite crystal form, are in part or entirely altered to paratellurite. That these latter paratellurite "crystals" are fine-grained aggregates rather than single crystals was demonstrated by placing the tip of one in an *x*-ray powder camera. A powder-type diffraction pattern was obtained without grinding the sample.

The relationships described above clearly indicate that the orthorhombic form of TeO_2 was the first to form, but that the tetragonal form is the more stable.

Attempts to synthesize orthorhombic TeO_2 were unsuccessful, whereas tetragonal TeO_2 can be readily prepared by heating Te in air at 400° C. An attempt was made to convert tetragonal TeO_2 to the orthorhombic form by heating it in a hydrothermal bomb at 300° C. and 30,000 psi for four days. The tetragonal form persisted.

A sample of tellurite (orthorhombic TeO_2) from Mexico was run with a high temperature *x*-ray specimen mount on a diffractometer to determine the inversion point to the tetragonal form. The inversion took place at between 600° and 650° C. The change in the natural material apparently took place at a much lower temperature since tellurite and paratellurite occur in native tellurium, and tellurium has a melting point of 452° C.

The specimens of native tellurium with tellurite and paratellurite upon which this work was done were purchased from mineral dealers and are in the United States National Museum collections under numbers R8861 and C5995. The locality was given as Cananea, Sonora, Mexico. Richard V. Gaines (personal communication) reports that the material probably came either from La Moctezuma, or the Santa Rosa mine, near Cananea.

Reference

Stehlik, B. and Balak, L. The Crystal Structure of Tellurium Dioxide. *Coll. Czech Chem. Commun.*, **14**, 595–607 (1949).

THE AMERICAN MINERALOGIST, VOL. 45, NOVEMBER DECEMBER, 1960

ETTRINGITE ("WOODFORDITE") FROM CRESTMORE, CALIFORNIA

JOSEPH MURDOCH AND ROBERT A. CHALMERS, *University of California, Los Angeles*, and *University of Aberdeen, Scotland.*

INTRODUCTION AND OCCURRENCE

In the process of studying minerals from Crestmore, California, A. O. Woodford and his associates, Woodford *et al.* (1941), Woodford (1943), observed veins of a hexagonal mineral which they could not identify, and provisionally called Mineral "K." This was later, in part at least, determined to be thaumasite, Switzer and Bailey (1953). Very similar material from their specimen, and from other specimens collected by Col. Clarence Jenni from the same general locality, was not thaumasite. This was submitted to the authors for identification. Its properties were found to be very close to those of ettringite (from published descriptions), but x-ray study showed the unit cell to have twice the dimension of ettringite in the a_0 direction. A chemical analysis also showed the presence of 3.15 SiO_2 and 3.35 CO_2, and a perceptibly smaller amount of H_2O than called for in ettringite.* Further, the indices of refraction were somewhat lower, and accordingly the mineral was considered to be new, and given the name "woodfordite." After presentation of a report on this mineral, Murdoch and Chalmers (1958), it became possible to obtain crystals of type material, from Ettringen, and x-ray measurements were made on them for comparison. This study showed that the determination of the unit cell is in error, and that the a axis is really twice the published value, Bannister (1936). This finding has been confirmed by Hurlbut (see page 1141 in this issue) on crystals from Scawt Hill, and the authors are forced to the conclusion that "woodfordite" is ettringite. The difference in composition, although important, and the slight variation in indices of refraction, cannot be considered enough to warrant giving this material a new species name. The name "woodfordite" thus must be considered withdrawn.

Ettringite occurs as a vein filling in the massive contact rock of the 910′ level of the Commercial quarry at Crestmore, and is locally rather abundant in some of the veins. The matrix rock is rather variable, and is made up of varying proportions of a merwinite, spurrite, gehlenite mixture, with associated diopside, idocrase, wollastonite and rarer small bright yellow grains of garnet. In the veins ettringite occurs as an open

* This determination was made on material which appeared to be fresh, but which apparently was somewhat de-hydrated, perhaps during the rather considerable time lapse between collecting and analyzing.

space filling of small (maximum length 1 mm.) hexagonal crystals associated with calcite and afwillite, and as somewhat larger grains showing few crystal faces, usually penetrated by afwillite prisms. The well-formed crystals are stout prismatic in habit, terminated, sometimes doubly, by the base and a series of pyramid forms which are not usually well-developed. The prism faces are sometimes perfectly smooth, but not uncommonly striated parallel to *c*. This is in part due to incipient alteration, and serves as an easy criterion for distinction of the mineral from thaumasite, which is invariably very smooth-faced and much more glassy in luster than ettringite. The accompanying calcite is usually in small very steep rhombohedral crystals, and the afwillite is normally in slender bladed prisms.

Physical Properties

The Crestmore ettringite is colorless when fresh, but often coated, or completely replaced by a white, powdery alteration product. Its hardness is 2.5; specific gravity 1.78 (measured in bromoform-acetone mixture); cleavage $\{10\bar{1}0\}$ perfect; soluble with moderate to slight effervescence in cold dilute acid, leaving a visible residue of silica. The crystals show

Table I. *X*-Ray Powder Data for Ettringite
Cu radiation, Ni filter, $\lambda = 1.5418$

Crestmore		Synthetic		Crestmore		Synthetic	
d	I	*d*	I	*d*	I	*d*	I
10.53	½	—		2.81	½	2.806	½
9.72	10	9.73	10	2.773	5	2.773	4
8.88	½	8.86	1	—		2.714	½
5.60	7	5.61	8	2.69	½	2.697	1
4.97	2	4.98	2	2.68	½	2.680	½
—		4.86	½	2.618	1	2.616	2
4.68	3	4.69	4	2.568	5	2.564	4
4.55	½	—		2.525	½	2.524	½
—		4.41	½	2.490	½	2.487	½
4.025	½	4.02	1	—		2.434	½
3.88	4	3.88	5	2.427	½	2.422	½
3.67	½	3.67	½	2.410	½	—	
3.59	½	3.60	1	2.403	½	2.401	1
3.476	2	3.48	3	2.356	½	2.347	½
—		3.27	½	—		2.230	2
3.24	1	3.24	2	2.208	5	2.209	4
3.03	½	3.016	½	2.180	½	2.185	1
2.93	½	—		2.154	2	2.154	2
				plus additional lines			

$\{10\bar{1}0\}$ with occasionally only $\{0001\}$, but more commonly one or more pyramids rather poorly developed. The commoner of these approach $\{10\bar{1}2\}$ and $\{10\bar{1}1\}$ (or $\{70\bar{7}8\}$), but are in such poor position that an axial ratio derived from them would be quite unreliable. The indices of refraction appear to be somewhat variable from specimen to specimen, common observed values being from 1.450 to 1.455 for ϵ, and from 1.465 to 1.470 for ω. One specimen, showing good crystals terminated by $\{0001\}$ only, gave values of $\epsilon = 1.470$, $\omega = 1.485$.

The white alteration product is found to be largely a mixture of calcite and gypsum. Residual needles of ettringite in this mixture usually give a higher index than normal.

X-Ray Study

X-ray powder photographs of the Crestmore ettringite match almost exactly that of synthetic ettringite, Bur. Standards (1959), (Table I). Single crystal x-ray photographs were taken about [0001], $[10\bar{1}0]$ and $[11\bar{2}0]$. From these the cell-dimensions were derived (Table II). In this table are given published values for ettringite from other localities, and also of thaumasite, for comparison as a similar mineral. The space group, $P6_3/mmc$ was determined from the observed systematic extinctions, and agrees with the findings of Bannister (1936) and Hurlbut (1960).

Table II. Unit Cell Dimensions

	a_0	c_0
Ettringite 1	22.48 Å	21.31 Å
Ettringite 2	22.33 Å	21.35 Å
Ettringite 3	22.28 Å	21.29 Å
Ettringite 4	11.26 Å x2=22.52	21.48 Å
Ettringite 5	22.47 Å	21.46 Å
Thaumasite 1	10.95 Å x2=21.90	10.30 Å
Thaumasite 2	22.12 Å	10.54 Å

Ettringite 1. Ettringen, Germany (Murdoch, this study)
2. Crestmore, California (Murdoch, this study)
3. Franklin, N. J. (Hurlbut, 1960)
4. Scawt Hill, Co. Antrim (Bannister, 1936)
5. Scawt Hill, Co. Antrim (Hurlbut, 1960)

Thaumasite 1. Långban, Sweden (Welin, 1957)
2. Paterson, N. J. (Murdoch, this study)

The revised value for *a* for thaumasite was derived from a rotation photograph about $[10\bar{1}0]$, on a good single crystal.

References

Bannister, F. A. (1936) Ettringite from Scawt Hill, Co. Antrim, *Miner. Mag.*, **24**, 324.

Woodford, A. O., Crippen, R. A. and Garner, K. B. (1941) Section across Commercial quarry, Crestmore, California, *Am. Mineral.*, **26**, 351–381.

Woodford, A. O. (1943) Crestmore Minerals, *Calif. Divis. Mines Report*, **39**, 333–365.

Switzer, G. and Bailey, E. H. (1953) Afwillite from Crestmore, California, *Am. Mineral.*, **38**, 629–633.

Welin, E. (1957) Crystal structure of thaumasite, *Arkiv. för Mineralogi och geologi, K. Svenska Vetenskaps—Academien*, **2** H 1–2, 137–147.

Murdoch, J. and Chalmers, R. A. (1958) Woodfordite, a new mineral from Crestmore, California, abstr. *Geol. Soc. Am. Bull.*, **69**, 1620–21.

National Bureau of Standards (1959) Aluminum Calcium Sulphate Hydrate (ettringite) *Circular* 539, **8**, 3, 4.

Hurlbut, C. S. (1960) Ettringite from Franklin, N. J. This issue, 1137–1143.

THE AMERICAN MINERALOGIST, VOL. 45, NOVEMBER–DECEMBER, 1960

N,N-DIMETHYLFORMAMIDE, A NEW DILUENT FOR METHYLENE IODIDE HEAVY LIQUID*

Robert Meyrowitz, Frank Cuttitta, and Betsy Levin,
U. S. Geological Survey, Washington 25, D. C.

Dimethyl sulfoxide (DMSO), $(CH_3)_2SO$, has been recommended as a diluent for methylene iodide (diiodomethane) in heavy liquid separations (Cuttitta, Meyrowitz, and Levin, 1960). Dimethyl sulfoxide-methylene iodide liquids of low density (approximately 2.92) become blood red on long standing. Storing the liquids in contact with copper wire or shavings reduces markedly the rate at which the red color deepens.

N,N-Dimethylformamide (DMF), $HCON(CH_3)_2$, is recommended as a diluent for methylene iodide. Its physical properties are similar to dimethyl sulfoxide. Its vapor pressure is low; its boiling point is high and it is completely miscible with water and acetone. The advantage of the dimethylformamide liquids over the dimethyl sulfoxide liquids is that they remain transparent for a longer time. Mixtures of dimethylformamide and methylene iodide stored in contact with copper wire or shavings do not become red on long standing (seven months). They remain light yellow. They do become red when not stored in contact with copper wire or shavings. Table 1 compares the salient properties of dimethylformamide, dimethyl sulfoxide, acetone, ethyl alcohol, and methylene iodide.

In order to test the constancy of the dimethylformamide-methylene iodide solutions during use, a series of solutions, each having a 90 ml. volume, was prepared. The specific gravities of the liquids were 2.85,

* Publication authorized by the Director, U. S. Geological Survey.

TABLE 1. SOME PHYSICAL PROPERTIES OF N,N-DIMETHYLFORMAMIDE, DIMETHYL SULFOXIDE, ACETONE, ETHYL ALCOHOL, AND METHYLENE IODIDE

	Melting point ° C.	Boiling point ° C.	Vapor pressure mm.Hg at 20° C.	Vapor pressure mm.Hg at 30° C.	Specific gravity	Flash point ° F.	Viscosity 25° C. cp
N,N-Dimethylformamide[1]	−61	153	2.7	5.0	0.95	153	0.80
Dimethyl sulfoxide[2]	18.4	189	0.37	0.79	1.10	203	1.98
Acetone	−95[3]	56.5[3]	185[4]	283[4]	0.79[3]	15[3]	0.32[3]
Ethyl alcohol	−114[3]	78.4[3]	43.9[4]	78.8[4]	0.79[3]	70[3]	1.1[3]
Methylene iodide	5–6[3]	180[3]	1.01 (20.6° C.)[5]	1.90 (29.5° C.)[5]	3.33[3]	None	0.02[6]

[1] Grasselli Chemicals Department, E. I. Dupont de Nemours and Co., Inc. DMF Product Information Bull., April 1, 1954.

[2] Stepan Chemical Co., Technical Bulletin, Dimethyl sulfoxide, Dec. 29, 1954.

[3] Hodgman, 1957.

[4] National Research Council, 1928.

[5] Gregory and Style, 1936.

[6] Timmermans and Hennaut-Roland, 1932.

2.91, 2.94, 3.06, 3.07, and 3.15. For each solution in the series, 12 to 16 heavy liquid separations, which included a filtration step, were made on approximately 10 gram portions of mineral mixtures over a period of 4 weeks. The remaining liquid (in contact with copper wire) was stored for an additional 6 months. The specific gravities of these liquids were determined again. The specific gravities of all of the liquids increased slightly.

Specific gravity before use	Specific gravity after use	Δ Specific gravity	Number of Separations
2.85	2.87	+0.02	16
2.91	2.94	+0.03	12
2.94	2.97	+0.03	14
3.06	3.09	+0.03	12
3.07	3.08	+0.01	15
3.15	3.17	+0.02	15

The combining volumes of dimethylformamide-methylene iodide solutions are additive and a straight-line mixing curve (volume+volume) can be used to prepare a liquid of desired specific gravity. Acetone, dimethylformamide, and water are miscible in all proportions. The separated minerals can be washed free of a dimethylformamide-methylene iodide liquid using acetone. The methylene iodide can be recovered from the washings by mixing the washings with large volumes of water in the manner conventionally used when alcohol or acetone is the diluent. When a dimethylformamide-methylene iodide solution, prepared for a specific job, is no longer needed, the methylene iodide can be recovered in the same way.

Information supplied by the manufacturers of dimethylformamide

states that toxicity does not seem to be a problem. Although the maximum allowable concentration in the atmosphere of dimethylformamide is relatively small, its "low volatility appears to make its use less hazardous from a vapor standpoint than that of many of the commonly-used organic solvents." It is suggested that contact of the dimethylformamide with the skin should be avoided and if it is spilled on the skin, it should be immediately flushed with a generous quantity of water. Breathing of the vapors should be avoided and adequate ventilation should be provided during use.

References

Cuttitta, Frank, Meyrowitz, Robert, and Levin, Betsy (1960), Dimethyl sulfoxide, a new diluent for methylene iodide heavy liquid: *Am. Mineral.*, **45**, 726–728.

Gregory, R. A., and Style, D. W. G. (1936), The photo-oxidation of methylene iodide: *Faraday Soc. Trans.*, **32**, 730.

Hodgman, C. D. (1957), Handbook of chemistry and physics, 39th ed.: Cleveland, Chemical Rubber Publishing Co.

National Research Council (1928), International critical tables of numerical data, physics, chemistry and technology, 1st ed., v. 3: New York, McGraw-Hill Book Co., Inc.

Timmermans, M. J. and Hennaut-Roland, Mme. (1932), Travaux du bureau international d'étalons physico-chimiques. V. Étude des constantes physiques de vingt composés organiques: *Jour. Chimie Physique*, **29**, 536.

THE AMERICAN MINERALOGIST, VOL. 45, NOVEMBER DECEMBER, 1960

PLANCHET PRESS AND ACCESSORIES FOR MOUNTING X-RAY POWDER DIFFRACTION SAMPLES

R. W. Rex and R. G. Chown, *California Research Corporation, La Habra, California*

Quantitative x-ray powder diffraction by the technique described by Klug and Alexander (1954) requires uniform packing of finely ground powder samples with minimal preferred orientation. Ideally the technique should be simple, fast, and reliable. Widely used mounts for powders are a smear on a glass slide and powder packed into depressions in glass slides (Klug and Alexander, 1954). Another approach to the problem of mounting samples is to sediment or press the powder into a mold, mount, or planchet (Adams and Rowe, 1954; Holland, *et al.*, 1955; and McAfee, 1956). All of the described devices had some shortcomings for our requirements. We therefore modified a pellet press* to pack samples to meet our needs. A monel planchet is used to avoid iron fluorescence in Cu Kα x-ray radiation.

* Parr Instrument Co., Moline, Illinois.

We feel that this press is an improvement over other methods because: (1) preferred orientation is minimized by compressing the sample from the side not exposed to x-rays (also recognized by McAfee, 1956); (2) the density is easily controlled by manual pressure; (3) the planchet is rigid, rugged, and permits manipulation of the sample in any orientation; (4) the planchet is interchangeable among the G. E. XRD-3 and -5 x-ray diffractometer head, the Norelco glass slide holder, and the Norelco flat sample spinner; and (5) the process of mounting the sample is very simple, fast, and reliable.

Birks (1945) has pointed out that fine grinding of powders is the best way to minimize preferred orientation errors. We find that samples must

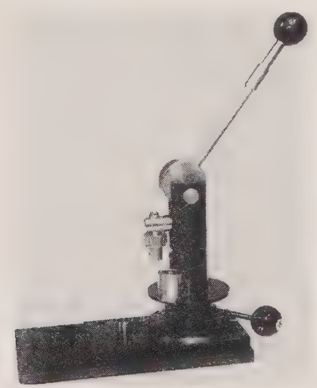

FIG. 1. Planchet press ready to be loaded with powder sample. An extra planchet sits on the press base.

be ground finer than 15 microns for best results. Grinding must be done under a solvent such as a ketone, alcohol, or hydrocarbon to avoid the mineral decomposition which occurs if one grinds dry samples. A per cent of gum arabic gives cohesion to those powders that otherwise fail to pack properly.

Using the techniques described by Klug and Alexander (1954) we obtain calibration curves of NaCl-KCl mixtures, mounted with this press, with a standard deviation of 1.1 per cent. Quartz determinations in multiphase matrices (aluminum internal standard) show a standard deviation of 2.4 per cent. These calibrations were obtained by rate meter techniques and still better results can be obtained with scalar techniques.

Photographs of the press, planchet, a clip to hold the planchet to the Norelco slide holder, and a minor modification of the Norelco flat sample spinner are shown in Figs. 1 through 3. These modifications are readily made by a good machinist.

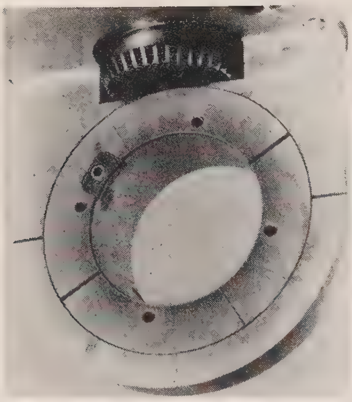

FIG. 2. Modification of the Norelco rotating flat sample holder to properly position the planchet. We have discarded the original indexing ring which obstructed the beam at low angles. This present arrangement permits studies at very low values of 2θ.

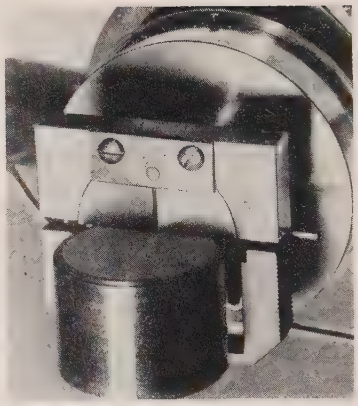

FIG. 3. Packet planchet held by a special clip on the Norelco glass slide holder. The clip slides off readily and even when left on does not interfere with the use of glass slides.

REFERENCES

ADAMS, L. H. AND ROWE, F. A., Preparation of specimens for the focusing-type X-ray spectrometer: *Am. Mineral.*, **39,** 215–221 (1954).

BIRKS, L. S., Naval Research Laboratory, Washington, D. C., Report No. H-2517, April 20, 1945.

HOLLAND, H. D., HEAD, W. B., III, WITTER, G. G., JR., AND HESS, G. B., New Method for mounting samples for powder X-ray spectrometry: *Am. Mineral.*, **40,** 761–767 (1955).

KLUG, H. P. AND ALEXANDER, L. E., X-ray diffraction procedures for polycrystalline and amorphous materials: J. Wiley, New York, 716 p. (1954).

MCAFEE, J. L., JR., Modified sample holder for the Norelco rotating specimen device: *Am. Mineral.*, **41,** 942–944 (1956).

THE AMERICAN MINERALOGIST, VOL. 45, NOVEMBER-DECEMBER, 1960

ORIENTED OVERGROWTHS OF TENNANTITE AND COLUSITE ON ENARGITE

RICHARD A. BIDEAUX, *College of Mines, University of Arizona, Tucson, Arizona.*

A specimen from the Cerro de Pasco mine, Cerro de Pasco, Peru, now in the writer's collection, consists of a radiating aggregate of prismatic enargite crystals up to 20 mm. long. The enargite crystals are covered

with a druse of minute tetrahedra which seemed to have a preferred orientation on the enargite. These tetrahedra were found to be a member of the tetrahedrite-tennantite series with $a_0 = 10.22$ Å. Several of the enargite crystals were selected for measurement on the two-circle reflecting goniometer: the orientation was determined as {111} [111] tennantite // {001} [001] enargite.

As shown in Fig. 1, the tennantite tetrahedra on (001) of enargite are further oriented with an apex pointing towards (00$\bar{1}$) of enargite and with their opposite edges parallel to [010], [210] or [2$\bar{1}$0] of the enargite. The larger tetrahedra growing on {101} of enargite maintain this same orientation. The structural control of the tetrahedra incrusting the enargite

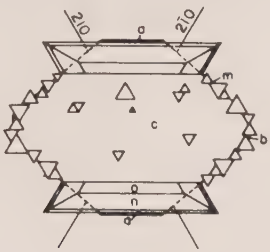

FIG. 1. Basal projection of enargite showing c{001}, b{010}, a{100}, m{110} and k{101} with oriented tennantite tetrahedra showing o{111}, n{112} and a{001}. Cerro de Pasco mine, Cerro de Pasco, Peru.

prism zone appears not to be so rigid, as a number are in random orientation; however, reflections from tetrahedra with an apex pointed towards (001) of enargite were searched for but not observed. This is taken as indirect confirmation of the polar character of both the c axis of enargite and the [111] directions of tetrahedrite-tennantite. While {010} and {110} of enargite are thickly incrusted, {100} is not; the few tetrahedra observed on this form are developed along striations parallel to [001] of enargite.

In the structural study of enargite by Pauling and Weinbaum (1934) it is pointed out that this structure can be derived from that of wurtzite by the appropriate substitution of copper, arsenic and sulfur atoms for the zinc and sulfur atoms of the wurtzite. Similarly, Pauling and Neuman (1934) consider that the structure of tetrahedrite-tennantite can be arrived at through the replacement of the zinc and sulfur atoms in eight unit cells of sphalerite by copper, arsenic and/or antimony, and sulfur atoms, with some sites vacant. Further, the structure of sphalerite in the [111] direction and wurtzite in the [0001] direction differ only in the sequence of stacking of similar layers of sulfur-zinc tetrahedra.

Mitchell and Corey (1954) describe artificial oriented overgrowths of sphalerite tetrahedra on wurtzite prisms. The orientation of the sphalerite on wurtzite is identical to that described above for tennantite on enargite. As the [0001] direction of wurtzite is analogous to the [001] direction of enargite, the observed orientation of tennantite on enargite is not unexpected.

A fine group of enargite crystals from the Leonard mine, Butte, Montana in the collection of Edward McDole of Butte, contains a number of enargite prisms which are capped by complex silver-white crystals which were thought to be colusite. Other specimens of these overgrowths were supplied to the writer by Richard W. Thomssen and Sidney A. Williams of Tucson, and Albert L. McGuinness of Eugene, Oregon. All of these specimens were collected in the past few years.

Several of these groups were measured on the optical goniometer, and the identity of the enargite and the isometric, hextetrahedral character of the colusite established. The largest colusite crystals seen reached a maximum dimension of about 6 mm. An x-ray powder pattern of these capping crystals gives spacings essentially in agreement with the published pattern of colusite in Murdoch (1953). The unit cell edge of this recent material is 10.64 Å, with values around 10.61 Å previously reported. Additionally, the carbon-arc spectrogram of this material shows strong lines of copper and arsenic, and weaker lines of antimony, tin, iron and vanadium. This particular set of elements seems to characterize the reported analyses of colusite, and helps to distinguish it from the similar minerals germanite, reniérite and gallite.

All of the colusite crystals examined, with one exception, show large {111}, and smaller {012}, {112} and {011}. As noted by Wolfe in Berman and Gonyer (1939), colusite is the only mineral in the hextetrahedral class which shows the combination of {111} and {012}. All colusite crystals seen were twinned by rotation about [111], but with the two or more colusite individual's [111] axes parallel rather than coincident, allowing the alternate morphological explanation of reflection across {112} with {112} as the composition plane. Characteristically, the twinned individuals are also displaced slightly along [111] from one another, so that their (111) faces are not continuous. The enargite prisms, deeply striated parallel to [001], show development of {010}, {100}, {110}, {120}, {130} and {150} in the prism zone, and are terminated by smooth (001). (Figs. 2 and 3). One of the colusite twins lacked {111}. (Fig. 4). These colusite twins are oriented on enargite in the same manner as the above described tennantite crystals from Cerro de Pasco, Peru. This can be construed as additional evidence of a structural similarity between colusite and tetrahedrite-tennantite.

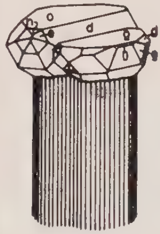

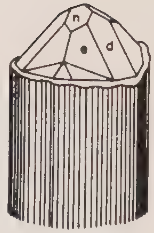

Fig. 2 (left). Group of three twinned colusite crystals oriented on an enargite prism. Leonard mine, Butte, Montana. Photograph by John W. Anthony.

Fig. 3 (center). Colusite twin oriented on enargite. Forms on the colusite twin are $o\{111\}$, $e\{012\}$, $n\{112\}$ and $d\{011\}$.

Fig. 4 (right). Colusite crystal oriented on enargite. This crystal lacks $o\{111\}$; other forms as in Fig. 3.

Thanks are due to Professor John W. Anthony, Department of Geology, University of Arizona, and Professor A. Pabst, Department of Geology, University of California, Berkeley, who read the manuscript and made a number of helpful suggestions.

References

Berman, H. and Gonyer, F. A. (1939), Re-examination of colusite: *Am. Mineral.*, **24,** 377–379.

Mitchell, R. S. and Corey, A. S. (1954), The coalescence of hexagonal and cubic polymorphs in tetrahedral structures as illustrated by some wurtzite-sphalerite crystal groups: *Am. Mineral.*, **39,** 773–782.

Murdoch, J. (1953), *X*-ray investigation of colusite, germanite and reniérite: *Am. Mineral.*, **38,** 794–801.

Pauling, L. and Neuman, E. W. (1934), The crystal structure of binnite: *Zs. Krist*, **88,** 54–62.

Pauling, L. and Weinbaum, S. (1934), The crystal structure of enargite: *Zs. Krist*, **88,** 48–53.

THE AMERICAN MINERALOGIST, VOL. 45, NOVEMBER–DECEMBER, 1960

A METHOD FOR THE DIRECT DETERMINATION OF LATTICE PARAMETERS

Lorin Hawes, *Department of Chemistry, Canberra University College, Canberra, Australia.*

Although the calculation of lattice parameters by Cohen's method of least squares (1) has proved a highly successful means of attaining accuracy and precision from *x*-ray powder data, it incorporates an analyti-

cal extrapolation of $\cos^2\theta$ to $\theta=90°$, as suggested by Bradley and Jay (2) to eliminate errors inherent in Debye-Scherrer type cameras. This dependence upon the error characteristics of a specific recording geometry may limit the universal applicability of the method to data obtained from other types of recording devices in which the systematic errors are either negligibly small (3), (4) or at any rate are not proportional to $\cos^2\theta$.

In the absence of systematic errors, it is still advantageous to minimize residual random errors, and this may be done conveniently and directly by finding values of Q_{hkl} (where $Q=1/d^2$) for each of the reflections concerned, and combining these by the method of least squares to yield the lattice parameters of the crystal in question.

The derivations of the method for the cubic, tetragonal and orthorhombic systems are as follows:

1. Cubic system (where $\alpha=h^2+k^2+l^2$, $A=1/a_0^2$, and Δ is the error) $Q=\alpha A+\Delta$, Rearranging and squaring, $\Delta^2=Q^2+\alpha^2A^2-2\alpha AQ$. Differentiating with respect to A, $2\alpha^2A=2\alpha Q$. Hence, for a series of observations,

$$A=\frac{\Sigma\alpha Q}{\Sigma\alpha^2} \tag{1}$$

2. Tetragonal system (where $\alpha=h^2+k^2$, $\gamma=l^2$, $C=1/c_0^2$ and the other terms have the same meanings as in the cubic case). $Q=\alpha A+\gamma C+\Delta$, Rearranging and squaring,

$$\Delta^2=Q^2+\gamma^2C^2+\alpha^2A^2-2\alpha AQ-2\gamma CQ+2\alpha A\gamma C$$

Differentiating with respect to A and C, respectively,

$$\begin{cases}2\alpha^2A-2\alpha Q+2\alpha\gamma C=0\\ 2\gamma^2C-2\gamma Q+2\alpha\gamma A=0\end{cases}$$

Hence, for a series of observations,

$$\begin{cases}A\Sigma\alpha^2+C\Sigma\alpha\gamma=\Sigma\alpha Q\\ C\Sigma\gamma^2+A\Sigma\alpha\gamma=\Sigma\gamma Q\end{cases}$$

Solving by determinants,

$$A=\frac{\Sigma\gamma Q\cdot\Sigma\alpha\gamma-\Sigma\alpha Q\cdot\Sigma\gamma^2}{D^*} \tag{2}$$

and

$$C=\frac{\Sigma\alpha Q\cdot\Sigma\alpha\gamma-\Sigma\gamma Q\cdot\Sigma\alpha^2}{D^*} \tag{3}$$

where D* is the determinant of the system, *i.e.* $(\Sigma\alpha\gamma)^2-\Sigma\alpha^2\,\Sigma\gamma^2$

3. Orthorhombic system (where $\alpha=h^2$, $\beta=k^2$, $B=1/b_0^2$ and the other terms are as previously defined)

$$Q = \alpha A + \beta B + \gamma C + \Delta$$

Rearranging and squaring,

$$\begin{aligned}\Delta^2 = Q^2 &+ \alpha^2 A^2 + \beta^2 B^2 + \gamma^2 C^2 - 2Q\alpha A - 2Q\beta B - 2Q\gamma C \\ &+ 2\alpha A\beta B + 2\alpha A\gamma C + 2\beta B\gamma C\end{aligned}$$

Differentiating with respect to A,B, and C, respectively,

$$\begin{cases} 2\alpha^2 A - 2\alpha Q + 2\alpha\gamma C + 2\alpha\beta B = 0 \\ 2\beta^2 B - 2\beta Q + 2\alpha\beta A + 2\beta\gamma C = 0 \\ 2\gamma^2 C - 2\gamma Q + 2\alpha\gamma A + 2\beta\gamma B = 0 \end{cases}$$

Hence, for a series of observations,

$$\begin{cases} A\Sigma\alpha^2 + B\Sigma\alpha\beta + C\Sigma\alpha\gamma = \Sigma\alpha Q \\ B\Sigma\beta^2 + A\Sigma\alpha\beta + C\Sigma\beta\gamma = \Sigma\beta Q \\ C\Sigma\gamma^2 + A\Sigma\alpha\gamma + B\Sigma\beta\gamma = \Sigma\gamma Q \end{cases}$$

Solving by determinants,

$$\begin{aligned} AD^* &= [\Sigma\gamma Q\ \Sigma\alpha\beta\ \Sigma\beta\gamma + \Sigma\beta Q\ \Sigma\beta\gamma\ \Sigma\alpha\gamma + \Sigma\alpha Q\ \Sigma\beta^2\ \Sigma\gamma^2] \\ &\quad - [\Sigma\alpha Q\ (\Sigma\beta\gamma)^2 + \Sigma\alpha\beta\ \Sigma\beta Q\ \Sigma\gamma^2 + \Sigma\alpha\gamma\ \Sigma\beta^2\ \Sigma\gamma Q] && (4) \\ BD^* &= [\Sigma\alpha\gamma\ \Sigma\beta\gamma\ \Sigma\alpha Q + \Sigma\alpha\beta\ \Sigma\gamma Q\ \Sigma\alpha\gamma + \Sigma\alpha^2\ \Sigma\beta Q\ \Sigma\gamma^2] \\ &\quad - [\Sigma\alpha^2\ \Sigma\gamma Q\ \Sigma\beta\gamma + \Sigma\alpha Q\ \Sigma\alpha\beta\ \Sigma\gamma^2 + \Sigma\beta Q\ (\Sigma\alpha\gamma^2] && (5) \\ CD^* &= [\Sigma\alpha\gamma\ \Sigma\alpha\beta\ \Sigma\beta Q + \Sigma\alpha\beta\ \Sigma\beta\gamma\ \Sigma\alpha Q + \Sigma\alpha^2\ \Sigma\beta^2\ \Sigma\gamma Q] \\ &\quad - [\Sigma\alpha^2\ \Sigma\beta\gamma\ \Sigma\beta Q + (\Sigma\alpha\beta)^2\ \Sigma\gamma Q + \Sigma\alpha\gamma\ \Sigma\beta^2\ \Sigma\alpha Q] && (6) \\ D^* &= [2(\Sigma\alpha\gamma\ \Sigma\alpha\beta\ \Sigma\beta\gamma) + \Sigma\alpha^2\ \Sigma\beta^2\ \Sigma\gamma^2] \\ &\quad - [\Sigma\alpha^2\ (\Sigma\beta\gamma) + \Sigma\beta^2\ (\Sigma\alpha\gamma)^2 + \Sigma\gamma^2\ (\Sigma\alpha\beta)^2] \end{aligned}$$

In order to illustrate the ease and directness of application of this least squares treatment of the reciprocal lattice, equation (I) will be used to calculate the lattice parameter of sodium chloride. The data in this example were derived from a 2.4 cm. radius precision low angle device (4); the preliminary treatment of the data involved correction for film shrinkage, and the graphical conversion of RZ values (4) to Q values.

hkl	α	α^2	Q_{obs}	αQ_{obs}
111	3	9	.0936	.281
200	4	16	.1255	.502
220	8	64	.2510	2.008
311	11	121	.3475	3.823
222	12	144	.3765	4.518

$\sum\alpha Q = 11.132$, $\sum\alpha^2 = 354$, $A = 0.03145$, $a_0 = 5.639$ Å.

ACKNOWLEDGEMENTS

It is a pleasure to acknowledge the generous help provided by F. H. Kelly, M.O.B. in making available his computers. I also wish to thank Professor J. B. Polya and M. H. Ra-Stas for their valued discussions and advice.

REFERENCES

1. COHEN, M. U., *Rev. Sci. Inst.* **6,** 68 (1935).
2. BRADLEY AND JAY, *Proc. Phys. Soc.* **44,** 563 (1932).
3. GUINIER, A., *Ann. Phys.* **12,** 161 (1944) et seq.
4. HAWES, L., *Acta Cryst.* **12,** 443 (1959).

THE AMERICAN MINERALOGIST, VOL. 45, NOVEMBER-DECEMBER, 1960

THE DEVELOPMENT OF AN ACCURATE LOW ANGLE X-RAY POWDER DIFFRACTION CAMERA

LORIN HAWES, *Department of Chemistry, Canberra University College, Canberra, Australia.*

INTRODUCTION

Most attempts at increasing the degree of accuracy attainable from low powder angle powder diffraction data have hitherto been directed toward the recognition and mathematical correction of general systematic errors, toward the manual correction of collimation and recording geometry distortions and towards the construction of larger and more intricate cameras and diffractometers. There are limits to the practicability of attempting to eliminate errors entirely by these means; usually it is found that the random errors of observation become more serious at low angles than any or all of the systematic errors attributable to the nature of the recording instrument or to the specimen.

Random errors

Quantitative assessments of the effect of random errors may be obtained upon consideration of the instantaneous magnification, M_i, defined as the rate of change of measured film distance, S, with respect to the interplanar spacing, D, in the crystal. In the case of the familiar Debye-Scherrer type of camera, the measured film distance is proportional to θ, and, in the terms of Bragg's equation,

$$M_i = \frac{dS}{dD} = \frac{-4R}{n\lambda \cot\theta \csc\theta}$$

The magnitude of a random error of observation may be regarded as independent of ϕ, and its effect upon a derived lattice spacing is inversely proportional to M_i, that is,

$$\Delta \propto \frac{n\lambda \cot\theta \csc\theta}{4R}$$

Since $\cot\theta$ and $\csc\theta$ are functions which increase in value rapidly with

decreasing θ, any recording device which measures in units proportional to θ must, as a corollary, produce increasingly inaccurate "D" data at low angles.

To a large extent therefore the problem of equalizing and minimizing the effects of random errors at different angles is the problem of recording the diffracted rays so that a linear relationship exists between D and the measured distance on the film; *i.e.* so that the magnification is constant and independent of θ. The geometrical surface conforming to this requirement is depicted in Fig. 1, in which the specimen is at the origin and the

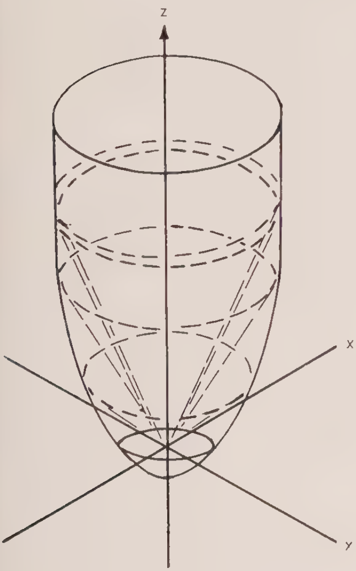

FIG. 1. The ideal surface of constant magnification.

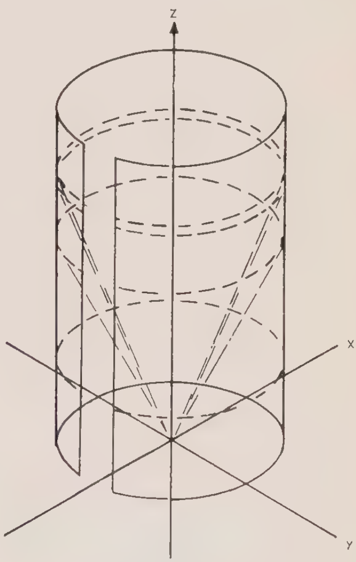

FIG. 2. The limiting cylinder.

x-ray beam is coincident with the Z axis. Such a surface unfortunately would be difficult to fabricate accurately and would be limited to a particular wavelength of x-rays.

By using the limiting circular cylinder (1) which becomes asymptotic to such a surface at low angles however, very nearly the same effect may be obtained. This arrangement is depicted in Fig. 2. The film is held in the form of a circular cylinder coaxial with the x-ray beam, the specimen is in a plane perpendicular to the beam, the diffracted rays strike the film at a distance Z above the specimen plane intercept, and the relationship between Z and D is nearly linear, the relationship being

$$D = \frac{n\lambda}{2 \sin \frac{(\text{arc cot } Z)}{2}}$$

The magnification factor for this geometry is given by the relationship

$$M_i = R\frac{dZ}{dD} = R(n\lambda \cos^3 \theta)$$

Since $\cos \phi$ approaches unity at low angles, M_i approaches a constant value.

The relative effectiveness of the arrangement of the film in a circular cylinder coaxial with the x-ray beam may be judged from Table I in which the instantaneous magnifications are compared at various angles

TABLE I. M_i AS A FUNCTION OF θ FOR DEBYE-SCHERRER AND COAXIAL FILM ARRANGEMENTS (CuKα RADIATION)

θ	M_i coaxial	M_i Debye	Ratio
45	1.835×10^8	1.835×10^8	1.00
40	1.441×10^8	1.40×10^8	1.03
35	1.180×10^8	1.04×10^8	1.13
30	0.998×10^8	0.75×10^8	1.33
25	0.874×10^8	0.51×10^8	1.71
20	0.782×10^8	0.32×10^8	2.42
15	0.720×10^8	0.18×10^8	4.00
10	0.679×10^8	0.08×10^8	8.54
5	0.656×10^8	0.02×10^8	33.1
Very small	0.648×10^8	0	—

for the circular Debye-Scherrer type of camera and for the coaxial cylinder arrangement, both of unit radius. It will be noted that the value of M_i for the coaxial arrangement is large and reasonably constant over the entire low angle range.

Systematic Errors

The major systematic errors which could affect data from a coaxial camera are essentially analogous to those encountered with other types, namely

1) absorption of diffracted x-rays by the specimen.
2) non coaxial placement of the film cylinder in relation to the x-ray beam.

In addition to these, an error which in the Debye-Scherrer type of camera is a random error of small magnitude now becomes a systematic error of some importance, *i.e.*

3) definition of the base line on the film from which all measurements are made. (In the case of the Debye camera it is the position $\theta=0°$ and/or $\theta=90°$, in the case of the coaxial it is the position of the specimen plane, $Z=0, \theta=45°$)

The elimination of each of these systematic errors will be discussed in later sections.

Construction of the Camera

In addition to minimizing, as far as practicable, the sources of systematic error of an instrumental nature, it is desirable that a camera constructed along the lines discussed should possess the following features:

1) A means for specimen rotation about the beam axis.
2) A means for printing fiducial reference marks on the film during exposure for later use in film shrinkage correction.
3) A means for accurately locating the $Z=0$ line on the film.
4) The camera should be lightproof, easy to load, easy to align in the x-ray beam, and, once so aligned, should be removable at will without requiring further adjustment.

A camera incorporating these features is illustrated in Fig. 3.

The camera body is constructed from a length of two inch copper tubing, accurately machined on the interior to form a true circular cylinder. Film is held in place by being expanded against this surface by two elliptical cams, these being spring tensioned so that a steady tangential compression is applied to the film during exposure. A series of small holes (0.009″) in the side of the camera body permits the direct printing of fiducial marks. The specimen holder provides a means for

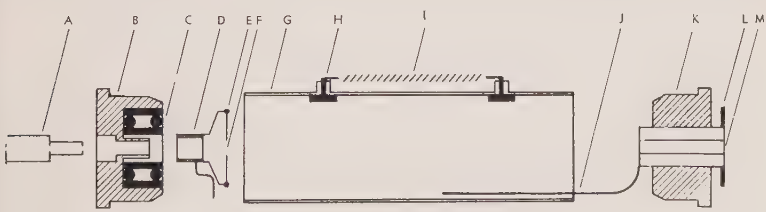

FIG. 3. A coaxial camera.

A Collimator
B Front end piece
C Double row ball race
D Specimen holder
E Rim of disc
F Specimen position
G Camera body
H Tensioning cam
I Tensioning spring
J Longitudinal rod
K Rear end piece
L Sprocket
M Black paper

positioning the powder wafer in the x-ray beam and a means* for printing the $Z=0$ line on the film. It consists of a levitated thin (0.003″) brass disc with a central hole; it is the shadow of the rim of this brass disk which defines the position of the specimen plane during exposure.

The specimen itself may be conveniently prepared and mounted by sprinkling the powdered sample onto a piece of scotch tape which is then stretched tightly across the central hole of the brass disc. The thickness of the powdered specimen need not exceed 0.001″; thus errors due to absorption are usually negligible.

The rear end piece, when in place completes the closure of the camera body and contains part of the mechanism for specimen rotation, a longitudinal rod attached to a large hollow bushing. The bushing is drilled with four small holes, 90° apart, through which a thin wire may be strung to form a crosshair for later use in alignment. The longitudinal rod rotates eccentrically about the common camera axis and engages a protruding arm on the specimen holder. The motive power for specimen rotation is transmitted from an external synchronous motor to a sprocket on the bushing by a chain drive. A lightproof exit port for the x-ray beam is provided by gluing a piece of black paper over the end of the bushing.

Alignment and Calibration of Camera

The camera is mounted opposite a point focus x-ray source and adjusted until a collimated circular beam is centered in the crosshairs in the bushing of the rear end piece. A sample of standard grating crystal, such as rocksalt or calcite, is then placed on the specimen holder and an exposure made.

Accurate values of θ can be calculated for all lines from these substances (2) and used to determine the camera radius by means of the relationship

$$R = L \tan 2\theta$$

(Only the lowest angle lines should be used in this determination; those lines for which $\tan 2\theta$ is greater than 2 are generally unsuitable because corresponding L values can be read to only two or three significant figures. Lines near $\theta=45°$ may be used to advantage in locating the $Z=0$ plane in the calibration since changes in R do not appreciably affect their position.) The calibration of the camera in this manner provides a good check on the presence of measurable systematic errors, which if present, would cause a drift in the calculated values of R at different values of θ.

* See Fisher, D. J., A modified coaxial powder x-ray camera: *Rev. Sci. Instr.* (Accepted for publication, probably Dec. 1960).

Line Breadth and Exposure Technique

The accuracy and precision of data obtained from the coaxial camera is to a certain extent limited by the breadth of the lines on the film, and this in turn can be shown to be governed by the relationship

$$B \propto t + A\,\frac{m}{l}\cot 2\theta + \frac{R(\sin\phi + \sin\gamma)}{\sin^2 2\theta}$$

where B is the line breadth, t the specimen thickness, A the size of the limiting collimator aperture, l the distance from the X ray source to the specimen, θ the Bragg angle, m the distance from the limiting collimator aperture to the specimen, R the camera radius, ϕ the angle of divergence

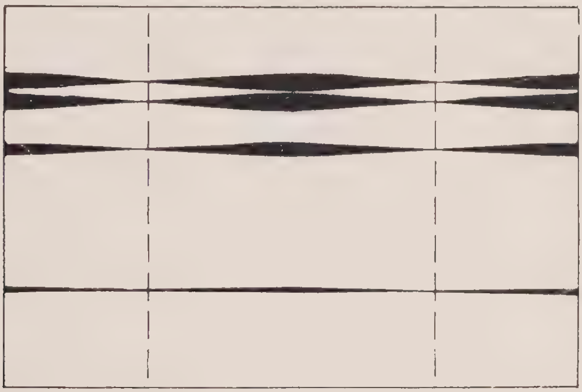

FIG. 4. High resolution trace pattern.

of the x-ray beam and γ the angular range of reflection of the crystal. A point source of x-rays is assumed.

Two essentially different exposure techniques are possible depending upon the degree of accuracy sought from the data; for photographs of the highest resolution and finest line breadth, such as for calibration or for the resolution of closely spaced doublets, a slit collimator (0.1 mm. by 0.6 mm.) is desirable. The slit should be in the same plane as the x-ray tube target, or as nearly so as possible; when this condition is fulfilled the x-ray beam has virtually no divergence normal to the plane of the tube target but great divergence in that plane, and the diffraction traces are focused sharply on two narrow areas of the film and spread out widely on all others, as shown in Fig. 4. In the terms of Fig. 2, if the plane of the x-ray tube target and the collimator slit is the XZ plane, lines will be highly resolved on the film cylinder where it is intercepted by the YZ plane.

Under these conditions of exposure the line breadth is extremely small, even at the lowest angles; the actual breadth of lines is usually smaller, in relation to resolution, than that attainable with any other type of camera in existence. Exposure times for such photographs are of the order of four hours, when the camera is sixteen centimeters from the x-ray tube.

For photographs of lesser accuracy but requiring vastly shorter exposure times, a rather large circular pinhole collimator is used and the specimen is held stationary during exposure. In this circumstance it is desirable to use a somewhat coarser specimen and to vary the camera angle so that the camera axis is no longer coplanar with the tube target,

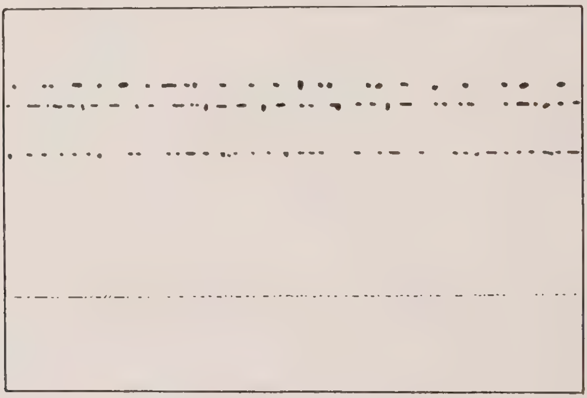

FIG. 5. Stationary spot pattern.

but so that the beam appears perfectly circular at the exit port. Photographs taken using this technique contain the diffraction spots in random array on parallel lines as shown in Fig. 5, and any flattening of the beam due to incorrect camera angle with respect to the target will be evident in that the spots may tend to form sinusoidal curves, as in the previous case.

The continuous reflection from a stationary crystal is far more effective in exposing the film than in the previous case since all of the diffracted energy is concentrated upon a small spot instead of being swept around the film, and exposure times for such photographs may be as brief as a few minutes, depending upon the size of the collimator and the nature of the specimen.

Such photographs of isolated spots can provide useful data during the study of an unknown lattice since the number of spots along a given line is proportional to the multiplicity of equivalent planes in the crystal, all other factors being the same. This makes it possible, at an early stage

in the study of an unknown lattice, to differentiate between basal reflections, octahedral reflections and so forth by simply counting the number of spots having a common value of Z.

Table II. Relation of Z to Other Functions

θ	Z	$\sin^2\theta$	D	Q
5	5.671	0.0076	8.846	0.01278
6	4.705	0.0109	7.375	0.01838
7	4.011	0.0149	6.325	0.02500
8	3.487	0.0194	5.540	0.03258
9	3.078	0.0244	4.928	0.04118
10	2.748	0.0302	4.438	0.05077
11	2.475	0.0364	4.036	0.06139
12	3.246	0.0432	3.705	0.0728
13	2.050	0.0506	3.421	0.0854
14	1.881	0.0585	3.182	0.0988
15	1.732	0.0670	2.975	0.1130
16	1.600	0.0760	2.795	0.1280
17	1.483	0.0855	2.633	0.1442
18	1.376	0.0955	2.492	0.1610
19	1.280	0.1060	2.366	0.1786
20	1.192	0.1170	2.252	0.1972
21	1.110	0.1285	2.149	0.2165
22	1.036	0.1403	2.058	0.2361
23	0.966	0.1526	1.972	0.2571
24	0.900	0.1654	1.895	0.2785
25	0.839	0.1786	1.824	0.3006
26	0.781	0.1922	1.756	0.3243
27	0.726	0.2061	1.696	0.3477
28	0.674	0.2204	1.640	0.3718
29	0.625	0.2350	1.590	0.3956
30	0.577	0.2500	1.542	0.4206
31	0.532	0.2652	1.495	0.4474
32	0.488	0.2809	1.454	0.4730
33	0.445	0.2970	1.413	0.5009
34	0.404	0.3125	1.378	0.5198
35	0.364	0.3295	1.342	0.5553
36	0.324	0.3457	1.310	0.5827
37	0.287	0.3624	1.280	0.6104
38	0.249	0.3795	1.250	0.6400
39	0.213	0.3960	1.225	0.664
40	0.176	0.4132	1.198	0.6968
41	0.141	0.4305	1.174	0.7255
42	0.105	0.4477	1.152	0.7535
43	0.070	0.4651	1.130	0.7831
44	0.035	0.4826	1.109	0.8131
45	0	0.5000	1.090	0.8417

Elimination of Systematic Errors

In a properly constructed camera defining the $Z=0$ position by fiducial spots as suggested by Fisher, and using a thin specimen and slit collimator as discussed previously, the only remaining source of error of a systematic nature is that of misalignment of the film cylinder with respect to the x-ray beam.

The effect of a coaxial misplacement of the camera axis so that it lies in the YZ plane is to tend to reduce the Z value of a given trace in one of the two areas of high resolution and to increase it in the other by the same amount. Correction therefore simply involves reading the Z values independently for each of the two areas and averaging them together, a desirable course of action in any case since it reduces random errors of observation. Misalignment of the film cylinder so that its axis lies in the XZ plane is of no consequence since it affects the film only at those positions where the lines have a maximum breadth and where precise Z values would not be expected.

Application to Lattice Parameter Determination

The use of data from the coaxial camera is an indirect process since it involves conversion to $\sin^2\theta$ or Q terms which may be used in the least squares treatment. In an earlier article (1), the application of data from the coaxial camera was used to calculate the lattice parameters of iodine by the Cohen least squares method (3). Although the Cohen method may be used with data from the coaxial camera it involves an unnecessary analytical extrapolation based upon the error characteristics of the Debye-Scherrer camera. A different least squares treatment, rigidly applicable to data from the coaxial camera, will be presented elsewhere.

Useful values relating Z to other functions are given in Table II.

ACKNOWLEDGEMENTS

Part of the work reported in this article was carried out at the University of Tasmania under the Titan research fellowship. The author is indebted to G. H. Chessman and J. Lemm for many valuable discussions and for their active interest and help in assembling the initial apparatus.

REFERENCES

1. HAWES, L., *Acta Cryst.* **12**, 443, 1959.
2. SWANSON AND FUYAT, *NBS Circ.* **539**, 1953.
3. COHEN, M. U., *Rev. Sci. Inst.* **6**, 68, 1935.

THE AMERICAN MINERALOGIST, VOL. 45, NOVEMBER-DECEMBER, 1960

A NOTE ON THE STRAIN-DEPENDENCE OF REFRACTIVE INDEX IN CRYSTALS

EDWARD H. POINDEXTER, *California Research Corporation, La Habra, California.*

The refractive index of a substance is closely related to the atomic property of polarizability. In any study of the strain-dependence of refractive index, one must ultimately consider the strain-dependence of the polarizability. In a previous paper (1) this author presented a mathematical expression governing polarizability. Subsequently, it was discovered that the expression could be simplified, and that it then became nearly identical to the result obtained by earlier authors. Here, the mathematical simplification is presented, and a few comments on the physical significance of the result are offered.

Polarizability is fundamentally a measure of the distortion produced in the electron distribution within the refracting substance by the incident light wave. Formally, polarizability may be defined by the relation

$$E' = -\tfrac{1}{2}\alpha F^2.$$

Here, E' is the increment to the steady-state energy of the system. This increment is due to the interaction of the electrons and the electric field associated with the light wave. The field strength is F, the polarizability is α. The relation is valid for static fields and for alternating fields (light), so long as the frequency is below the value necessary to excite the electrons to a more nearly permanent higher energy state; i.e., below an absorption band.

Polarizability may be approximately calculated from a knowledge of the electron distribution. The formula given below relates the polarizability of a single bonding electron to its wave function; this is the mathematical expression mentioned in the first paragraph. The formula was derived in a dissertation (2).

$$\alpha = -\frac{8\pi^2 me^2}{h^2}\cdot\frac{\left[\iiint_{-\infty}^{+\infty}\psi^2 z^2 dxdydz\right]^2}{\int \psi z\frac{\partial\psi}{\partial z}dxdydz}. \qquad (1)$$

As written here, a minus sign appears before the right side; an error was made in the original derivation. Also, the more conventional ψ has been used for the electron distribution function, instead of ϕ. The proton mass is m; the electron charge is e; Planck's constant is h.

The denominator may be integrated by parts. We have the formula

$$\int u\,dv = uv - \int v\,du.$$

We substitute as follows:

$$u = z \qquad dv = \psi \frac{\partial \psi}{\partial z} dz$$

$$du = dz \qquad = \psi d\psi - \psi \frac{\partial \psi}{\partial x} dx - \psi \frac{\partial \psi}{\partial y} dy.$$

We at first integrate with respect to z, while we hold x and y constant.

$$dv = \psi d\psi \quad \text{or} \quad v = \frac{\psi^2}{2} + C$$

We then obtain the relation:

$$\iiint_{-\infty}^{+\infty} \psi z \frac{\partial \psi}{\partial z} dxdydz = \iint \left[\frac{\psi^2}{2} z \right]_{-\infty}^{+\infty} dxdy - \frac{1}{2} \iiint_{-\infty}^{+\infty} \psi^2 dxdydz.$$

The first term on the right vanishes, since ψ^2 varies essentially as $\exp(-\sqrt{x^2+y^2+z^2})$ and thus goes to zero much faster than z tends to infinity. The second term is simply $-[(\frac{1}{2})\cdot 1]$ or $-\frac{1}{2}$, because ψ was assumed normalized in the original derivation.

Returning to equation (1), we obtain a new result:

$$\alpha = \frac{16\pi^2 me^2}{h^2} \left[\iiint_{-\infty}^{+\infty} \psi^2 z^2 dxdydz \right]^2.$$

This integral represents the second moment of the electronic charge distribution, again of a single electron. Since we have assumed a normalized ψ, the integral also represents the mean square deviation of the electron from its average position, i.e., $\overline{(z-\bar{z})^2}$.

The quantity $16\pi^2 me^2/h^2$ is equal to $4/a_0$, where a_0 is the Bohr radius for a hydrogen atom in the ground state. We may then substitute and obtain the new relation:

$$\alpha = \frac{4}{a_0} [\overline{(z - \bar{z})^2}]^2 \tag{2}$$

This is now similar to the expression given by Hirschfelder (3), based on work by Hylleraas (4), Hasse (5), and Kirkwood (6), which is:

$$\alpha = \frac{4N}{a_0} [\overline{(z - \bar{z})^2} - (N-1)\overline{(z_1 - \bar{z})(z_2 - \bar{z})}]^2. \tag{3}$$

The total number of electrons considered is N. The term in z_1 and z_2 represents the mean correlation between two electrons. If we consider only one electron, equation (3) reduces to equation (2).

Abbott and Bolton (7) have observed that polarizability may be proportional to the fourth power of a linear dimension. This may be seen

from equation (2) if it is assumed that it is possible to expand or contract a bound electron's wave function uniformly. It might be expected that bonding electrons in a covalent crystal would approximate such behavior. A covalent electron circulates around at least two nuclei, so its wave function is more directly affected by any change in internuclear spacing. We would not expect any simple first-order effect in ionic crystals. In the idealized, simplified covalent crystal, a reduction in internuclear spacing, perhaps caused by externally applied stress, would lead to a rapid reduction in polarizability.

Polarizability is commonly related to refractive index by the somewhat empirical Lorentz-Lorenz formula

$$\frac{n^2 - 1}{n^2 + 2} = \frac{4\pi L}{3M} \alpha\rho.$$

Here, L is Avogadro's number, ρ is density, and M is the molecular weight associated with the unit for which α is defined. This formula, as well as that of Drude and of Kurz and Ward, contains a term in $\alpha\rho$. A third power dependence of α upon a linear dimension, i.e., an inverse first power dependence upon density, would lead to no change in refractive index upon compression of the substance. A fourth power dependence would lead to a reduction in the index upon compression.

In equation (3), the correlation terms in z_1, z_2 are of significance because of the mutual repulsion of electrons. These terms would become more significant as the interatomic distance is reduced. As a qualitative estimate, one might expect that repulsion between electrons would tend to prevent proportional collapse of the wave function with reduction in internuclear spacing. This would mean that polarizability would not decline in accord with the fourth power of the internuclear spacing. It is inadvisable, however, to draw any conclusions from this crude reasoning. The actual disposition of electronic wave functions and dependent properties is often entirely nonintuitive.

No rigorous calculations of the strain-dependence of polarizability have been made for any system more complex than the hydrogen molecule. Furthermore, experimental determinations of $\partial n/\partial \rho$ for such simple covalent crystals as diamond are too inaccurate to establish with certainty even the sign of the change.

I wish to thank Dr. Lee Stephenson and Dr. William Holser for their helpful discussions of this subject.

References

1. E. Poindexter, *Am. Mineral.*, **40**, 1032 (1955).
2. E. H. Poindexter, Thesis, Univ. of Mich. (1955).

3. Hirschfelder, Curtiss, and Bird, *Molecular Theory of Gases and Liquids*, John Wiley and Sons, New York, p. 946 (1954).
4. E. Hylleraas, *Z. Physik*, **65**, 209 (1930).
5. H. R. Hasse, *Proc. Cambridge Phil. Soc.*, **26**, 542 (1930); 27, 66 (1931).
6. J. G. Kirkwood, *Physik Z.*, **33**, 57 (1932).
7. J. A. Abbott and H. C. Bolton, *Proc. Roy. Soc.* **A 216,** 477 (1953).

THE AMERICAN MINERALOGIST, VOL. 45, NOVEMBER–DECEMBER, 1960

BERTRANDITE FROM MICA CREEK, QUEENSLAND

R. H. Vernon and K. L. Williams, *Mineragraphic Investigations, Commonwealth Scientific and Industrial Research Organization, University of Melbourne, Parkville, Victoria.*

Bertrandite, $Be_4(OH)_2Si_2O_7$, a mineral whose occurrence in Australia has not previously been recorded, has been observed in a beryl-bearing pegmatite from the Mica Creek area, near Mt. Isa, Queensland. Specimens of this pegmatite were submitted to the Mineragraphic Investigations section of the Commonwealth Scientific and Industrial Research Organization by Mr. A. K. Denmead, Chief Geologist of the Queensland Geological Survey. An analysis of one of the specimens was reported as follows:

SiO_2	54.9
Al_2O_3	17.7
Fe_2O_3	2.6
BeO	13.1
MgO	0.9
CaO	—
K_2O	3.9
H_2O^+	5.2
H_2O^-	0.2
Total	98.5 wt. per cent

The analyzed specimen is a micaceous pseudomorph after beryl, but, despite the extensive alteration, the analysis shows 13.1 per cent BeO, compared with 13.4 per cent BeO previously found for unaltered beryl from the same locality. The other specimens are mostly composed of massive mica, without apparent beryl, and such material has been reported to assay up to 14.1 per cent BeO.

Examination of thin sections has shown that the specimens consist of bertrandite, residual beryl, abundant fine-grained mica, quartz, albite, and limonitic material. Bertrandite contains 42.0 per cent BeO, which explains the high BeO contents reported in the analyses.

The bertrandite is colorless when viewed under the binocular microscope and in thin section. It is biaxial negative, and its refractive indices (measured in sodium light by the immersion method) are $\alpha=1.589 \pm 0.003$, $\beta=1.603 \pm 0.002$ and $\gamma=1.613 \pm 0.002$ ($\gamma-\alpha=0.024$). Its birefringence, as measured with the Berek compensator, is 0.025. Its 2V, calculated from the refractive indices, is approximately 80°. It shows weak dispersion, $r<v$. The bertrandite has two good cleavages parallel to (001) and (010), assuming X=a, Y=b (Winchell and Winchell, 1951, p. 479). Some sections also show a weak cleavage parallel to (100) and a weak oblique ?(110) cleavage. Some grains show simple twinning, but the trisector twinning described and figured by Phemister (1940) and others was not observed.

The bertrandite grains always show negative elongation, indicating that they are tabular, flattened parallel to (001).

An x-ray powder diffraction pattern of the Mica Creek bertrandite, prepared from material drilled from a thin section, matches exactly a pattern of bertrandite from Mt. Antero, Colorado (Table 1). The Mt. Antero specimen was kindly provided by Dr. Brian Mason, of the American Museum of Natural History.

Bertrandite is present in all of the specimens examined. It comprises up to 30 and locally even 50 volume per cent of some specimens, and it is

TABLE 1. BERTRANDITE $Be_4(OH)_2Si_2O_7$—X-RAY POWDER PATTERN

Bertrandite, Mica Creek, Queensland†

CuK_{α_1} radiation; $\lambda=1.5405$ Å Camera diameter 114.6 mm.

d(Å)*	$I_{(est.)}$	d(Å)*	$I_{(est.)}$	d(Å)*	$I_{(est.)}$	d(Å)*	$I_{(est.)}$
7.56	1	2.02	0.5	1.305	4	0.940	0.5
4.85	<0.2	1.983	2	1.251	1	0.899	0.5b
4.38	10	1.923	0.5	1.233	0.5	0.860	1
3.94	4	1.787	0.5	1.220	2b	0.843	0.2
3.80	0.7	1.698	1.5	1.167	1b	0.838	0.3
3.19	9	1.650	1	1.117	1.5	0.828	0.5
{2.93	1	1.628	<0.2	1.105	0.3	0.813	2
{2.88	1	1.579	0.3	1.090	<0.2	0.800	0.2
2.54	8	1.555	3	1.076	1	0.790	1
2.42	0.5	1.491	<0.2	1.057	<0.2	0.783	1
2.28	6	1.465	3	1.015	<0.2	0.778	1
2.22	6	1.440	1	0.986	0.2b		
2.18	0.2	1.363	0.2	0.970	0.2b		
2.10	0.3	1.338	0.3	0.953	<0.2		

* Interplanar spacings corrected for film shrinkage.

† An identical pattern was obtained for bertrandite from Mt. Antero, Colorado.

b Denotes broad line.

most abundant where beryl is absent. It occurs as scattered, generally subhedral, prismatic grains up to 2.3 mm. long and 0.5 mm. wide, and also as aggregates of prismatic to granular grains. It is generally enclosed in areas of fine-grained, yellowish green, sericitic mica (Fig. 1). Such areas may be veinlets in large crystals of beryl; more commonly they are more extensive, and the most completely altered specimens consist of sericitic mica containing scattered residual grains of beryl, beryl plus bertrandite, or bertrandite alone. Most of the bertrandite shows marginal replacement by the mica. A pure bertrandite concentrate for analysis was

FIG. 1. Bertrandite (largely at extinction) intergrown with and partly replaced by fine-grained sericitic mica. Transmitted light, crossed nicols. ×60.

not prepared, because of the intimate nature of the bertrandite-mica intergrowths (Fig. 1).

The beryl has commonly been extensively altered along fractures to sericitic mica. The optical continuity of the beryl residuals and the hexagonal form of the pseudomorphs indicate that some of the original beryl crystals were up to ten or more centimeters long and several centimeters wide. The beryl is uniaxial negative and has $\omega=1.570\pm0.002$ and $\epsilon=0.565\pm0.002$ (sodium light).

Less abundant constituents of these specimens include muscovite, quartz and albite. The muscovite occurs in small patches containing flakes averaging 0.3 mm. long and, more rarely, as "books" up to 2 cm. wide and several mm. thick. X-ray powder diffraction photographs of both the muscovite and fine-grained "sericite" were prepared, and dis-

tinctly different patterns were obtained. The differences are due to polymorphism, and comparison with the x-ray data of Yoder and Eugster (1955) suggests that the coarse-grained "books" of mica consist of muscovite with a two-layer monoclinic (2M) structure, whereas the fine-grained "sericite" has a one-layer monoclinic (1M) structure. Yoder and Eugster indicated that 1M muscovite polymorphs are not uncommon in nature, and suggested by analogy with experimental results, that they would form most commonly in relatively low temperature geological environments, namely "the sediments, low grade metamorphic rocks, secondary alteration zones, and some pegmatite deposits" (p. 249). The present occurrence is in accord with this concept.

Quartz occurs as scattered grains, up to 0.5 mm. wide, intergrown with beryl or enclosed in the sericite. Albite is slightly more common, occurring as small inclusions in the sericite and also as larger aggregates, up to 3.5 cm. across.

One specimen consists mainly of felspar and quartz, with a few hexagonal micaceous pseudomorphs after beryl, up to 5 cm. long. These suggest that the alteration has affected the beryl, but not the adjacent felspar. The sericite-rich specimens, therefore, presumably represent large, altered crystals of beryl or local phases of the pegmatite in which felspar has also been converted to mica.

Since bertrandite is most abundant where beryl is absent, it appears most probable that the bertrandite was formed during the alteration of the beryl, with the beryllium from the beryl entering the hydrous bertrandite. The fact that most of the bertrandite also shows marginal replacement by the sericitic mica suggests that it was formed by hydrothermal processes and not by the later action of meteoric waters.

Apart from accounting for the apparently anomalous analyses, this discovery of bertrandite also shows that material rich in beryllium may easily be overlooked in the field. In the Mica Creek specimens, the bertrandite could only be detected by microscopic examination and, moreover, the specimens containing the most bertrandite are those which are least impressive in hand specimen massive aggregates of fine-grained greenish mica which display no obvious evidence of their high beryllium content.

References

Phemister, J. (1940), Note on an occurrence of bertrandite and beryl at the South Crofty mine, Cornwall: *Miner. Mag.*, **25**, 573–578.

Winchell, A. N., and Winchell, H. (1951), Elements of Optical Mineralogy: ed. 4, Part II, New York: John Wiley and Sons.

Yoder, H. S., and Eugster, H. P. (1955), Synthetic and natural muscovites: *Geochim. et Cosmochim. Acta*, **8**, 225–280.

THE AMERICAN MINERALOGIST, VOL. 45, NOVEMBER–DECEMBER, 1960

CHALCEDONY AND QUARTZ CRYSTALS IN SILICIFIED CORAL

ERNEST H. LUND, *University of Oregon, Eugene, Oregon.*

Silicified corals and mollusks from the Tampa formation at Ballast Point, Florida are well-known for their intrinsic beauty and exceptionally good preservation. Ballast Point has been a popular collecting ground for professional scientists and amateurs alike, and by as early as 1842 fine specimens were reported by Conrad (1846) to be rare. Occasionally good specimen material is still found by collectors who are willing to grabble through the mud adjacent to the Point at low tide.

The silicified coral masses from Ballast Point are of varying sizes and shapes. Some are globose and range up to a foot or more in diameter, some are tubular, and others are irregular in shape. Many of the masses are hollow, and the preserved "shell" is commonly only 2 or 3 cm thick or less. The "shell" is characteristically comprised of two distinct layers. The outer layer consists of replaced coral in which the features are preserved in remarkable detail, and the inner part consists of either banded chalcedony or banded chalcedony over which quartz crystals have grown. Most of the hollow forms are lined with colloform chalcedony, a few are lined with small quartz crystals, and less commonly specimens are partitioned and lined with both kinds of material, each in a separate chamber.

Two of the partitioned variety were collected and lent to the writer by Meade Norman, who was at the time a student of his at Florida State University. The two specimens are essentially alike and differ only in such minor details as size, shape, thickness of chalcedony bands, and size of quartz crystals.

In the specimen shown in Fig. 1, the wall ranges in thickness from about 1 to 2 cm. The outer layer in which the coral structures are preserved ranges from less than 1 mm. to about 2 cm. thick. The next is a series of very thin layers of white and gray chalcedony. Part of these layers appears to have been removed by corrosion, and they are therefore not continuous. They are common to the walls of both chambers, however, so were deposited before the partition which separates the interior into two distinct chambers was completed.

Covering the first series of chalcedony layers is a second series which is not so finely laminated as the first. The earlier part of the second series is a thin yellowish layer that is discontinuous because of corrosion, but is common to the walls of both chambers. It grades into a thicker layer of brown chalcedony. During the deposition of the second series the partition, consisting partly of replaced coral, was completed. On one side of

the partition the brown chalcedony continued to be deposited for a time, but on the other side its deposition apparently stopped much sooner, for on the one side the thickness is about 2 to 3 times that on the other side. In the one chamber where chalcedony continued being deposited, the interior is lined with a thin white layer with a botryoidal surface. In the other chamber quartz crystals were developed and they line the interior of that chamber. The total thickness of deposited silica in both chambers is about equal. Details in the layering and similar total thickness of de-

FIG. 1. Exterior and interior views of silicified coral.

posited silica in both chambers suggest that both the chalcedony and the coarsely crystalline quartz were deposited at the same time and at about the same rate. This poses a problem in the genesis of the silica.

The silicification of the corals and other fossils at Ballast Point is part of the general silicification that has taken place in the Tampa formation there. The silicified part of the formation has been referred to as the "silex bed," although it has no stratigraphic significance. Cooke and Mossom (1929) believe the silicification is a surface or near-surface process and that it is still going on. They state that the famous "silex bed" of Ballast Point is merely a superficial accumulation and that it is not confined to any particular stratigraphic level. In places the near-surface part of the formation consists almost wholly of chert in which fossil molds and silicified forms are abundant.

A basic premise to solving the problem of the silicification of the Ballast Point fossils is that silica is transported in true molecular solution rather than in colloidal solution or suspension. Until recently geologists generally believed that silica in natural water is in a colloidal state rather than in true molecular or ionic solution. Observations by Alexander, Heston, and Iler (1954) indicate that silica in low concentrations is in true solution. They found the solubility of amorphous silica to be between 120 and 140 p.p.m. at 25° C. and in the pH range between 5 and 8. Later observations by Krauskopf (1956) and White, Brannoch, and Murata (1956) are in accordance with those of Alexander and co-workers. Krauskopf states:

"In natural waters silica may be in either colloidal or in true solutions, but the colloidal particles are unstable and will disappear spontaneously in the course of a few days or weeks (provided total silica is less than about 100 p.p.m.). Hence the great majority of natural waters should have silica in true solution only."

The solubility of amorphous silica is about 10 times that of alpha quartz. Two values calculated by Siever (1957) are 7.25 p.p.m. and 14 p.p.m.

Most ground waters are low in dissolved silica. The Data of Geochemistry (1924) gives values ranging from 5 to 30 p.p.m. The subsurface water at Ballast Point is probably no exception.

Closely related to the concept that silica in natural waters is transported as a colloid is the belief that chalcedony is formed first as a gel from the colloidal silica and is later reconstituted into crystalline chalcedony. This origin for chalcedony is plausible in certain cases, as with the waters of many hot springs in which the amount of dissolved silica is unusually high, but it seems not to be applicable to a situation in which ordinary groundwater is the solvent. I therefore believe that both the quartz crystals and the banded chalcedony in the coral specimens were deposited as quartz from true solutions. The specimens indicate that chalcedony and quartz crystals can form under similar conditions of temperature, pressure, and concentration of silica in solution.

A feature that may give a clue to why two varieties of quartz have formed under essentially the same environmental conditions is a small opening a few millimeters in diameter in the wall of the chalcedony-lined chamber. The wall of the chamber lined with quartz contains no visible openings. The opening in the wall of one chamber gave the solutions free access, and perhaps at times permitted the cavity to be drained. In this chamber chalcedony was precipitated. In the other chamber, the relative imperviousness of the wall probably allowed the chamber to remain continuously filled with silica-bearing solutions, and quartz crystals were able to grow in this aqueous medium.

REFERENCES

ALEXANDER, G. B., HESTON, W. M., AND ILER, H. K. (1954) The solubility of amorphous silica in water: *J. Phys. Chem.* **58**, 453–455.

CLARKE, C. W. (1924) The data of geochemistry: *U. S. Geol. Survey Bull.* **770**, 841 p.

CONRAD, T. A. (1846) Observations on the geology of East Florida: *Am. Jour. Sci., ser. 2*, **2**, 36–48.

COOKE, C. WYTHE, AND MOSSOM, STUART (1929) Geology of Florida: Florida State Geol. Survey 20th annual rpt., 227 p.

KRAUSKOPF, KONRAD B. (1956) Dissolution and precipitation of silica at low temperatures: *Geochim. et Cosmochim. Acta* **10**, 1–26.

SIEVER, RAYMOND (1957) The silica budget in the sedimentary cycle: *Am. Mineral.* **42**, 821–841.

WHITE, DONALD E., BRANNOCH, W. W., AND MURATA, K. J. (1956) Silica in hot spring waters: *Geochim. et Cosmochim. Acta* **10**, 27–59.

THE AMERICAN MINERALOGIST, VOL. 45, NOVEMBER-DECEMBER, 1960

VOLBORTHITE FROM BRITISH COLUMBIA

J. L. JAMBOR, *Ottawa, Canada.*

Volborthite, $Cu_3(VO_4)_2 \cdot 3H_2O$, is present as a weathering product of a thin, interlava sedimentary rock of Upper Triassic age which crops out west of Menzies Bay on Vancouver Island, and north of Gowland Harbour on Quadra Island, British Columbia.

The vanadium-bearing rock is a black, extremely finely laminated, fossiliferous, non-clastic sediment which consists chiefly of carbonaceous matter and microcrystalline to cryptocrystalline quartz. Spectrographic analyses indicate that the carbonaceous material contains vanadium. Hypogene chalcocite is generally an additional major constituent of the sediment, in some cases making up over 50% of the rock. The associated volcanic flows are predominantly pillowform and massive porphyritic basalts, andesites, and spilites which are commonly amygdaloidal. The amygdule material is largely quartz, calcite, chlorite, zeolites, epidote, and pumpellyite. Prehnite, chalcocite, chalcopyrite, bornite, and native copper, as amygdule fillings, are widespread in small amounts; analcite, heulandite, and greenockite are of rare occurrence.

Minor quantities of volborthite coat exposed surfaces of the laminated sediment, but the mineral is more abundant along planes exposed by splitting the rock along the laminae.

PHYSICAL PROPERTIES

The vanadate assumes many colors and habits, most of which are briefly summarized below:

Dark green to yellowish green, habit massive, compact, with good cleavage. Scaly crusts and rosette-like, honey-combed, or boxwork-like aggregates. Scales with a triangular or hexagonal outline, occasionally with impurities some distance from the center arranged in a hexagonal outline. Scaly bright yellow to brownish yellow incrustations on massive or cleavable emerald green to dark green hexagonal cores of up to 0.6 mm. diameter. Yellow, brownish yellow, light brown, and blackish brown, with habit flocculent or reticulated; also radiating fibrous and circular in outline, occurring singly or in groups, usually with a succession of colored zones and a minute, massive, central teat. Less commonly bright yellow and spherulitic.

Most of the British Columbia volborthite is yellow or brownish yellow. The mineral is translucent in immersion oil, and not pleochroic. Lamellar twinning is common; the units are length fast and are twinned in a plane almost perpendicular to perfect (001) cleavage. Rare plaid twinning was also observed. The measured indices, determined on yellowish green scales and cleavage fragments, depart greatly from those reported in the literature:

α 1.793 ± .005	Biaxial negative
β 1.801 ± .005	(−) 2V large
γ 1.816 ± .005	$r < v$

Dilute acids readily attack the mineral, turning it reddish-brown and leaving a clear silica residue. The results of several spectrographic analyses are given in Table I. Abundant water is yielded in the closed tube.

Table 1. Spectrographic Analyses of B.C. Volborthite

Habit	Major	Minor	Strong trace
Flocculent	Cu, V	Si, Al	Ca
Flocculent	Cu, V	Al	Si, Ca
Hexagonal cores[1]	Cu, V	Si	Fe, Al
Rosette scales	Cu, V	Si	Al, Mg, Ca

[1] Identical results were obtained from three separate analyses. Ca is present in trace amounts.

X-ray powder photographs of volborthite were taken with 57.3 and 114.59 mm. diameter Philips cameras, using nickel-filtered copper radiation. The observed intensities and measured spacings (corrected for shrinkage) are listed in Table II.

The British Columbia volborthite is associated with abundant malachite and brochantite, and small amounts of cuprite, tenorite, azurite, calcite, cyanotrichite, connellite, and an unidentified light blue hydrous copper sulphate. Although carnotite was reported from the locality by

TABLE II. VOLBORTHITE; X-RAY POWDER PATTERN

I	d(meas) Å	I	d(meas) Å	I	d(meas) Å
1	7.9	3	2.64	4	1.79
10	7.18	6	2.57	4	1.71
½	5.15	<½	2.46	3	1.68
½	4.43	6	2.39	½	1.57
½	4.26	½	2.28	½	1.55
2	4.10	2	2.23	5	1.51
½	3.59	½	2.13	3	1.50
2	3.10	3	2.04	1	1.49
4	3.00	<½	1.96	1	1.47
6	2.88	½	1.92	1	1.46
2	2.72	3	1.80	2	1.44
				1	1.43

Ellsworth (1932), no additional carnotite or uranium minerals have been found in the area. The maximum reported value of V_2O_5 in the sediment is over 3 per cent, but the lack of sufficient quantities of the copper and vanadium-bearing rock has resulted in the deposits generally being classified as uneconomical.

ACKNOWLEDGMENT

The writer is grateful for the supervision and assistance of Dr. R. M. Thompson, Professor of Mineralogy, the University of British Columbia.

REFERENCE

ELLSWORTH, H. V. (1932): Rare-element Minerals of Canada; *Geol. Surv., Canada, Economic Geol. Ser.* **11**, 139.

THE AMERICAN MINERALOGIST, VOL. 45, NOVEMBER–DECEMBER, 1960

THE BULK COMPOSITION OF A ZONED CRYSTAL*

ANDREW GRISCOM, *U. S. Geological Survey, Washington, D. C.*

Quantitative petrographic studies often require an estimate of the bulk composition of zoned crystals, such as plagioclase feldspars. Bowen (1928, p. 143) pointed out in this connection that "the outer shell of a crystal requires to have only about one-tenth the thickness of the whole crystal in order to constitute half the volume." X-ray or oil immersion methods of bulk composition determination suffer from similar diffi-

* Publication authorized by the Director, U. S. Geological Survey.

culties and, furthermore, require extracting the entire grain from the rock. Chemical analysis, homogenization, refractive index of glass, or specific gravity determination also require removal of the entire grain. A simple and direct method is based upon measurements of zoned crystals in thin section. It is assumed that the compositional variation can be expressed by two components and that the section cuts the nucleus of the grain being studied.

Let r be the distance from the nucleus of a crystal to any point on the rim and let x be some lesser distance from the nucleus along this line. Let V be the volume of the crystal and V_x be the volume at the earlier moment of growth when x was on the rim, with the assumption that there has been no change in crystal shape throughout growth. Then:

$$V = kr^3 \tag{1}$$

$$V_x = kx^3 \tag{2}$$

$$dV_x = 3kx^2dx. \tag{3}$$

Further, let D be the composition difference between the nucleus and the rim, and let D_x be the composition difference between the nucleus and x. As a first approximation many crystals are zoned so that D_x can be expressed as some power function of x, or, specifically x/r, in order to normalize the measuring unit:

$$D_x = ax^p = D\left(\frac{x}{r}\right)^p. \tag{4}$$

Even in the case of discontinuously zoned crystals or limited zone reversals, a plot of composition against radius can often be arbitrarily smoothed to approximate a power function. It is assumed that this power function holds for any direction of r, *i.e.* that p and a are constant.

In order to compute the bulk composition we need to know the average composition difference (D_{av}) between the nucleus and the rim. This difference is added to the composition of the nucleus to obtain the bulk composition of the crystal. As is the case for any average property of a variable sample, D_{av} is computed by summing the products of the individual increments of volume (dV_x) by their composition difference (D_x) and dividing this sum by the total volume of the crystal. This is expressed in integral form as:

$$D_{av} = \frac{\int_0^r D_x dV_x}{V}. \tag{5}$$

Substituting (1), (3), and (4) into (5) gives:

$$D_{av} = \frac{3D}{r^{p+3}} \int_0^r x^{p+2}dx = \frac{3D}{p+3}. \tag{6}$$

This result may then be added to the nucleus composition to give the bulk composition.

Fig. 1 provides a graphical solution for bulk composition and a way to approximate p. A plot of normalized composition difference against normalized radius is made for the crystal concerned and scaled to match Fig. 1. Then the two diagrams are superimposed and the approximating power function ascertained, interpolating when necessary. The intersection of this power function with the bulk composition curve (indicated by the heavy line on the right side of the diagram) determines the bulk composition. This may be read off the vertical scale. As a simplified example let us imagine a zoned plagioclase crystal ranging from An_{60} at the nucleus to An_{30} on the edge. Suppose the crystal has a composition against radius plot which approximates a power function where p equals 7. This power function will intersect the bulk composition curve at a

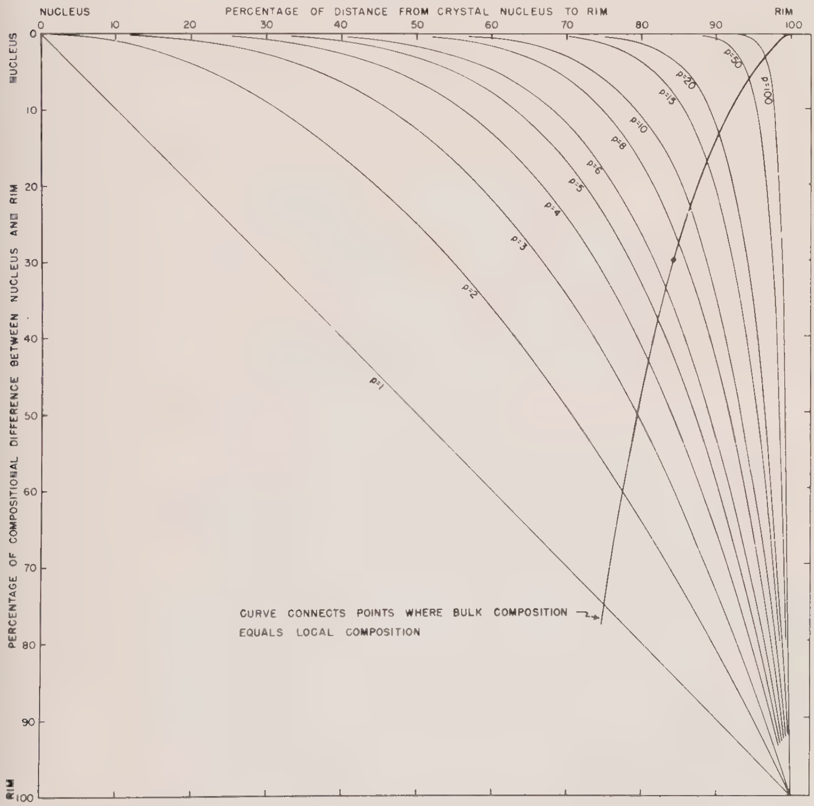

FIG. 1. Graph used to approximate the bulk composition of certain zoned crystals. Explanation in text.

point (shown as a dot on the figure) which is compositionally thirty percent of the way from An_{60} to An_{30}. Hence the bulk composition is An_{51}. The horizontal intercept of this point is about 84, indicating that the An_{51} position is .84 of the way from the center out to the rim. The result may also be computed from relation (6).

Some crystals have a composition distribution so complex that a piecemeal integration is necessary if one wishes to know the bulk composition. However experience indicates that many rocks do contain crystals having a composition distribution which can be approximated by a power function. For these rocks the method finds useful application. The method is equally applicable for determining the bulk composition of one zone of a complexly zoned crystal should the composition distribution between the inner and outer edges of the zone approximate a power function.

Reference

Bowen, N. L. (1928), The evolution of the igneous rocks: Princeton Univ. Press, Princeton, New Jersey.

We regret to announce the deaths of two Fellows of the Mineralogical Society of America:

Dr. A. B. Edwards, The University of Melbourne, Melbourne, Australia.

Dr. John T. Lonsdale, University of Texas, Austin, Texas.

Dr. Paul F. Kerr, Newberry Professor of Mineralogy at Columbia University, has been spending eight weeks at the University of Oslo, as NATO guest professor in the Department of Geology.

A forty page booklet on the minerals of Boron, California, has been published by the Mineral Research Society of California, at Montebello, California, with Earl Pemberton as editor. A short account of the history and geology is followed by brief descriptions and some photographs of 21 of the most significant minerals of this locality.

NEW MINERAL NAMES

Fleischerite, Itoite

C. Frondel and H. Strunz. Fleischerit und Itoit, zwei neue Germanium-Mineralien von Tsumeb. *Neues Jahrb. Mineral., Montash.* **1960,** 132–142 (English summary).

The minerals were found in the upper oxidation zone of the Tsumeb Mine, associated with cerussite, mimetite, and altered tennantite, also as a crust on plumbojarosite and mimetite on dolomite. A preliminary description of fleischerite (unnamed) was given by Frondel and Ito in *Am. Mineral.* **42,** 747 (1957).

Fleischerite occurs as white to pale rose fibrous aggregates, with silky luster. Analysis by Jun Ito gave PbO 63.34, GeO 8.18, Ga_2O_3 0.86, Fe_2O_3 0.05, SO_3 15.06, H_2O^+ 11.35, H_2O^- 0.21, insol. 0.56, sum 99.61%, corresponding to $Pb_3Ge^{+2}(OH)_4(SO_4)_2 \cdot 4H_2O$.

Oscillation, rotation, and Laue photographs show fleischerite to be hexagonal, space group probably $P6_3/mmc$, a_0 8.89, $c_0$10.86 Å. $Z=2$. Indexed x-ray powder data are given; the strongest lines are 3.619 (10), 2.635 (8), 3.437 (6), 2.214 (6), 1.889 (6). No cleavage was observed.

G. 4.2–4.4 (measured), 4.59 (calcd.) Hardness low.

Optically uniaxial, pos., *ns* ϵ 1.776, ω 1.747. Not fluorescent under UV light, becomes rose-violet when irradiated with x-rays.

DTA study showed a distinct endothermal effect at 263°, a weak endothermal effect at 314°, and a small exothermal effect at 463°. When heated and observed under the microscope becomes turbid at 175–200°, inverts to an isotropic phase at 465°. When ground for a long time in an agate mortar, inverts to itoite by loss of water and oxidation of Ge^{+2} to Ge^{+4}.

The name is for Michael Fleischer of the U. S. Geological Survey; the name has also been used for wurtzite-6H (*Am. Mineral.* **36,** p. 639–640 (1951).

Itoite was found as fine-grained pseudomorphs after fleischerite. It has mean n 1.84–1.85. White, luster silky. Qualitative analysis and spectrographic study showed only Pb, Ge, and sulfate. The x-ray powder diagram is identical with that of fleischerite heated at 300° and nearly identical with that of anglesite; the strongest lines are 2.065 (10), 3.326 (9), 3.003 (9), 4.240 (8), 2.027 (8), 3.209 (7). The composition is formulated as $Pb_3[GeO_2(OH)_2](SO_4)_2$, i.e. anglesite with one-third of the (SO_4) replaced by $[GeO_2(OH)_2]$. From the powder data, the unit cell is a 8.47, b 5.38, c 6.94 Å, $Z=4$, G. calcd. 6.67.

The name is for Prof. Tei-ichi Ito, Univ. of Tokyo.

Michael Fleischer

Coesite

E. C. T. Chao, E. M. Shoemaker, and B. M. Madsen. First natural occurrence of coesite. *Science,* **132,** No. 3421, 220–222 (1960).

Coesite, the high-pressure polymorph of SiO_2, was first made by Coes in 1953. The mineral was found as an abundant constituent of the sheared Coconino sandstone at Meteor Crater, Arizona, in the debris under the crater floor and in drill cuttings of breccia from a depth of 600–650 feet, beneath the crater floor. It has also been found in sandstone outside the crater rim, and as a subordinate constituent of glass (lechatelierite) in lake beds in the crater. Coesite occurs in irregular grains 5 to more than 50 microns in size. It has mean index of refraction 1.595 and very low birefringence. Spectrographic analysis of a concentrate containing a little quartz gave more than 99% SiO_2. The x-ray pattern was identical with that of synthetic coesite.

Coesite has since been identified by Chao in samples collected by Shoemaker from the Rieskessel caldera, Bavaria (Pecora, 1960).

The properties of synthetic coesite are as follows: G. 3.01 (Coes), 3.01 (Ramsdell),

2.93±0.02 (Dachille and Roy), calcd. 2.90. Biaxial, positive, 2V 54° (Coes); biaxial, positive, 2V 64° (Boyd and England); biaxial, negative, 2V 61° (Khitarov *et al.*); *ns* α 1.599, γ 1.604 (Coes), α 1.593±0.002, γ 1.597±0.002 (Boyd and England), α 1.594, γ 1.597 (Khitarov et. al.). Hardness (Knoop) 1200 (near Mohs 8) (Coes).

Monoclinic, *a* 7.23, *b* 12.52, *c* 7.23, β 120° (Ramsdell); *a* 7.17, *b* 7.17, *c* 12.38, γ 120.0° (Zoltai and Buerger); *a* 7.16, *b* 12.39, *c* 7.16, β 120° (Dachille and Roy). Powder data are given by Coes, Boyd and England, Khitarov et al., and Dachille and Roy. The strongest lines (average of closely agreeing results by Boyd and England and Dachille and Roy) are 3.10 (100), 3.43 (50), 2.69 (15), 1.698–1.716 (10–15).

Coesite is nearly insoluble in 5% HF at room temperature, but is rapidly dissolved by fused NH_4HF_2. The stability relations and the quartz-coesite transition have been studied by Boyd and England, Dachille and Roy, and MacDonald. An analogous form of BeF_2 has been made by Dachille and Roy.

The name, proposed by Sosman in 1954, is for Loring Coes, Jr., of the Norton Company, who first synthesized it.

References

Boyd, F. R. and England, J. L. (1960) The quartz-coesite transition: *J. Geophys. Research*, **65**, 749–956.

Coes, Loring, Jr. (1953) A new dense crystalline silica: *Science*, **118**, 131–132.

Dachille, Frank and Roy, Rustum (1959) High-pressure region of the silica isotypes: *Zeitschr. Krist.*, **111**, 451–461.

MacDonald, G. J. F. (1956) Quartz-coesite stability relations at high temperatures and pressures: *Am. J. Sci.*, **254**, 713–721.

Pecora, W. T. (1960) Coesite craters and space geology: *Geotimes*, **5**, No. 2, 16–17, 32.

Ramsdell, L. S. (1955) The crystallography of coesite: *Am. Mineral.* **40**, 975–982.

Sosman, R. B. (1954) New high-pressure phases of silica: *Science*, **119**, 738–739.

Zoltai, Tibor and Buerger, M. J. (1959) The crystal structure of coesite, the dense, high pressure form of silica: *Zeitschr. Krist.*, **111**, 129–141.

M. F.

Nakaséite

Tei-Ichi and Hisashi Muraoka. Nakaséite, an andorite-like new mineral. *Zeits. Krist*, **113**, 93–98 (1960).

Analysis by H. M. gave Ag 9.3, Cu 4.6, Pb 19.8, Fe 0.5, Zn 1.1, Sb 39.4, S 23.4, SiO_2 0.2, (Cr_2O_3) 1.2, sum 99.5%. Spectrographic analysis showed Ag, Pb, Sb, and Cu, with small amounts of Fe, Bi, Sn, and Cd. (Note—the (Cr_2O_3) is not explained and Cr is not mentioned as being found spectrographically. M.F.) After deducting 10% of argentian tetrahedrite (freibergite) and 2% sphalerite, this gives nearly $Pb_4Ag_3CuSb_{12}S_{24}$ (andorite is $Pb(Ag, Cu)Sb_3S_6$).

X-ray study shows the mineral to be monoclinic, *a* 13.02±.04, *b* 19.18±.05, *c* 102.24 (=24×4.26±0.02) Å, β=90°, Z=24($Pb_4Ag_3CuSb_{12}S_{24}$), G. calcd. 5.37₉, G. observed 5.30. The *a* and *b* are essentially identical with those for andorite, but $c=24\times4.26$, whereas for andorite IV and andorite VI, it is 4×4.26 and 6×4.26 (Donnay and Donnay, *Am. Mineral.* **39**, 161–171 (1954)). Space group $P11a$. Slightly piezoelectric. *X*-ray powder data are given; they are essentially identical with those for andorite.

The mineral is light gray, luster metallic, opaque. Etch tests are given. It occurs in gold bearing stibnite quartz veins at the Nakasé Mine, Japan, intimately intergrown with argentian tetrahedrite and sphalerite.

The name is for the mine.

Discussion.—The authors state that the structural data suggest "that nakaséite is no other than a structural variety of andorite. That we propose nevertheless a new mineral name is because, apart from the difference in the chemical compositions, it has a very complicated twinned lattice essentially different from that of andorite."

These reasons for a new name seem unconvincing to me. The alleged chemical differences, based on a difficult analysis of impure material, do not seem significant. At least until these complex structures have been more thoroughly worked out, the material should be called andorite XXIV.

M. F.

Stranskiite

H. Strunz. Stranskiit, ein neues Mineral. *Naturwissenschaften*, **47**, No. 16, 376 (1960).

The mineral occurs as radiating aggregates on chalcocite in the 1000 m. level of the Tsumeb Mine, S.W. Africa. Color cyan-blue. It is triclinic, a 5.07, b 6.77, c 5.28 Å, α 111°, β 113.5°, γ 86°. The unit cell contains $(Zn_{1.73}Fe_{0.05}Mg_{0.09}Ca_{0.10})_{1.97}Cu_{1.07}As_{1.90}Si_{0.10}O_8$, or $Zn_2Cu(AsO_4)_2$. Analysis not given. Cleavage (010) perfect, (100) good, also (001) and $(\bar{1}01)$. Optically biaxial, negative, *ns* α 1.795, β 1.842, γ 1.874, 2V 80°. H. 4, G. 5.23. A blue powder, obtained by heating a mixture of $Zn_2As_2O_7+CuO$ for 14 hours at 850°, gave an x-ray powder pattern identical to that of the mineral. The x-ray powder data are not given.

The name is for Professor I. N. Stranski of Berlin.

M. F.

Talmessite

P. Bariand and P. Herpin. Un arséniate de calcium et de magnesium, isomorphe de la β-roselite. *Bull. soc. franc. mineral. et crist.*, **83**, 118–121 (1960).

The mineral occurs in pale green crystals, less than 0.1 mm., in the zone of oxidation of the Talmessi Mine, 35 km. west of Anarak, central Iran, associated with aragonite and dolomite. The ore contains abundant niccolite, algodonite, and domeykite. Analysis on 300 mg. gave As_2O_5 47.7, CaO 29.5, BaO 3.2, MgO 7.5, NiO 0.8, H_2O 6.7, sum 95.4%, corresponding to $(Ca_{2.29}Ba_{0.09})(Mg_{0.85}Ni_{0.05})H_{1.61}(AsO_4)_{1.80}$. The deviations from the formula $Ca_2Mg(AsO_4)_2\cdot 2H_2O$ may have been due to the presence of aragonite; CO_2 was not determined.

The indexed x-ray powder pattern is nearly identical with that of beta-roselite (Frondel, *Am. Mineral.* **40**, 828–833 (1955)). The strongest lines are 3.10 (10), 3.07 (10), 2.77 (9), 5.06 and 5.03 (8), 3.57 (8), 3.44 (7), 3.19 (7), 2.82 (7), 1.71 (7). By comparison with beta-roselite, this gives a triclinic unit cell with a 5.89, b 7.69, c 5.56 Å, α 112°38′, β 70°49′, γ 119°25′.

G. 3.421 (measured), 3.491 (calcd.). Biaxial negative, colorless in section, *ns* α 1.680, γ 1.69. A thermogravimetric curve shows loss of H_2O at 450°.

An analysis is also given of material called beta-roselite from Bou Azzer, Morocco, which contained As_2O_5 55.9, CaO 27.3, CoO 8.6, MgO 8.6, sum 100.4, corresponding to $Mg_{0.84}Co_{0.45}$, therefore actually a cobaltoan talmessite. It had G. 3.574 (measured), 3.597 (calcd.) optically biaxial negative, *ns* α 1.695, γ 1.73, pleochroic colorless to pale rose.

The name is for the mine.

Discussion.—The name was accepted by the Committee on Nomenclature of the French Society, which recommended that a new analysis be made. Evidently there is a triclinic series from beta-roselite (Co) to talmessite (Mg).

M. F.

Rusakovite

E. A. Ankinovich. A new vanadium mineral, rusakovite. *Zapiski Vses. Mineralog. Obshch.*, **89,** 440–447 (1960) (in Russian).

The mineral occurs in a surface, partially oxidized layer of carbonaceous shale, which contains apatite, collophane, vanadium-bearing mica, and sulfides of Cu, Zn, Pb, and V, in northwestern Kara-Tau. Steigerite, fervanite, satpaevite, and al'vanite have previously been described from these shales (*Am. Mineral.*, **44,** 1325–1326 (1959)).

Analyses of the mineral from Balasauskandyk by S. I. Potok and T. L. Vileshina gave MgO 1.40, 1.30, tr.; CaO 0.30, 0.20, 0.40; Al_2O_3 5.00, 4.80, 5.50; Fe_2O_3 45.00, 45.30, 43.70; SiO_2 1.80, 1.60, 2.50; V_2O_4 5.00, 4.80, 5.10; V_2O_5 16.60, 16.40, 16.13; P_2O_5 6.50, 6.40, 5.80; SO_2 (should be SO_3 ? M.F.) 1.00, not detd., 1.70; H_2O^+ 13.30, 14.50, 14.60; H_2O^- 5.00, 4.30, 4.80, total 100.90, 99.60, 100.23%. Neglecting MgO, CaO, SiO_2, SO_2, and V_2O_4, these give $(Fe,Al)_5\,[(V,P)O_4]_2(OH)_9\cdot 3H_2O$, with Fe:Al=4:1 and V:P=2:1. A D.T.A. curve by K. A. Sosenko showed a very strong endothermal effect at 50–190° and a weak one at 280–366° and exothermal effects at 450–535° and 575–610°. The mineral is easily soluble in cold dilute acids. When treated in the closed tube it gives off acid water and turns brick-red.

The mineral occurs as crusts, veinlets, and reniform concretions on a colloidal hydrated Fe-Al phosphate of composition $6(Fe,Al)_2O_3\cdot P_2O_5\cdot aq.$, and is replaced by ferri-allophane and iron hydroxides. Electron microscope photographs by E. I. Soboleva show the mineral to be in a form resembling rough splinter-like lamellae. Color yellow-orange to reddish-yellow, streak ocher-yellow, luster dull. Hardness 1.5–2, G. (by suspension) 2.73–2.80. Under the microscope gold-yellow grains up to a few microns in size, weakly polarizing, n 1.833±0.004 (by G. A. Pashkova).

X-ray powder data by G. I. Luk'yantsev and E. M. Baigulov are given. The strongest lines are 3.21 (10), 2.945 (9), 2.441 (8), 2.140 (7), 1.569 (6), 4.20 (5). Heating at 600° gave a different phase; strongest lines 1.691 (10), 1.450 (9), 1.482 (8), 2.689 (7). The pattern is distinctly different from those of the Fe-V minerals fervanite and nolanite.

The name is for Mikhail Petrovich Rusakov, geologist of Kazakhstan.

Discussion.—If the V_2O_4 is considered part of the mineral, the formula obtained is somewhat different.

M. F.

Vaterite

J. D. C. McConnell. Vaterite from Ballycraigy, Larne, Northern Ireland. *Mineralog. Mag.*, **32,** 535–544 (1960).

Vaterite was identified by *x*-ray study of a very finely fibrous or platy mineral with high birefringence in hydrogel pseudomorphs after larnite. This is the first reported natural occurrence, although paramorphs of calcite after vaterite were recently described by Ilyinskii, *Doklady Akad. Nauk SSSR*, v. **121,** p. 541 (1958). The artificial compound has long been known, see *Dana's System, 7th Ed.*, **2,** 181–182 (1951).

M. F.

Mozambikite

J. M. Cotelo Neiva and J. M. Correia Neves. Pegmatites of Alto-Ligonha, Mozambique, Poruguese East Africa. *Internatl. Geol. Congress, Rept. 21st Session, Copenhagen*, **1960,** Pt. 17, p. 53–62 (in English).

A preliminary report. The mineral occurs in the granite pegmatite at Muiane. The analysis "under reservations" gave SiO_2 11.00, ThO_2 58.80, U_3O_8 6.04, CaO 0.59,

$(R.E.)_2O_3$ 8.60, Fe_2O_3 0.22, Al_2O_3 4.40, H_2O 5.33%. *X*-ray spectrographic analysis also showed Zr, Y important; Pb, Er, Gd, "Sa" (Sm?) and Mn traces. The mineral loses H_2O at 115°. Its structure is the same before and after heating at 1000°; $a_0 = 5.704$ Å.

The mineral occurs in yellow-brown octahedra. G. 5.24. Index of refraction before heating variable, always below 1.735 and frequently 1.690–1.703; after heating at 1000°, isotropic with *n* (Na) 1.811.

"Mozambikite contains lamellar inclusions of lepidolite. Its faces are somewhat corroded by albite."

The name is presumably for Mozambique. The variant in spelling is not explained.

DISCUSSION.—Insufficient data. The mineral agrees with thorite or thorogummite in all respects except (1) in being cubic before being heated; (2) a_0 is larger than that of pure thorianite (5.596 A).

M. F.

Unnamed

HORST SAALFELD. Strukturen des Hydrargillits und der Zwischenstufen beim Entwässern. *Neues Jahrb. Mineral., Abhandl.*, **95**, 1–87 (1960).

Single crystals of gibbsite from Arö, Norway, were monoclinic, *a* 8.676 ± 0.002, *b* 5.070 ± 0.002, *c* 9.721 ± 0.003 Å, β $94°34' \pm 5'$, in agreement with Megaw, *Zeitschr. Krist.* **87**, 185 (1934). Crystals from Schischimsk, Urals, were in part monoclinic, in part triclinic, in part intergrowths of the two forms. The triclinic polymorph has *a* 17.33_8, *b* 10.08_6, *c* 7.73_0 Å, α 94°10′, β 92°08′, γ 90°00′. The monoclinic dimorph has 2V 0–5°, the triclinic dimorph has 2V 25–40°.

M. F.

NEW DATA

Bafertisite

E. I. SEMENOV AND P'EI-SHAN CHANG. New mineral bafertisite. *Sci. Record (Peking)*, **3**, 652–655 (1959) (in Russian), through *Chem. Abs.*, **54**, 13996 (1960).

Data given are as in the abstract in *Am. Mineral.* **45**, 754 (1960) with the following additions: Analysis SiO_2 23.68, TiO_2 15.39, Nb_2O_5 0.84, Al_2O_3 0.29, Fe_2O_3 1.08, FeO 22.56, MgO 0.50, MnO 1.62, CaO 0.37, BaO 29.98, K_2O 0.12, Na_2O 0.49, H_2O^+ 1.65, H_2O^- 1.14, Cl 0.63, sum 100.34 $(0 = Cl_2)$ $0.14 = 100.20\%$. The mineral occurs in the Baiyun-Obo deposit, Inner Mongolia.

M. F.

Batisite

S. M. KRAVCHENKO, E. V. VLASOVA, AND N. G. PINEVICH. Batisite, a new mineral. *Doklady Akad. Nauk SSSR*, **133**, 657–660 (1960) (in Russian).

New data added to that given in *Am. Mineral.* **45**, 908–909 (1960) are: Orthorhombic, *a* 10.41 ± 0.05, *b* 13.85 ± 0.05, *c* 8.06 ± 0.02 kX. Optically biaxial, pos., *ns* α 1.730, β 1.735, γ 1.791, all ± 0.001, 2V 7°, $r < v$, strong. Insol. in HCl, HNO_3, H_2SO_4. Easily melts B.B. to a brown transparent bead. Spectrographic analysis shows $0.0n\%$ V, $0.00n\%$ Pb, Cu; $0.000n\%$ Be. The formula is $Na_2BaTi_2(Si_2O_7)_2$. *X*-ray study shows it to be isostructural with shcherbakovite, $(K, Na, Ba)_3(Ti, Nb)_2(Si_2O_7)_2$, which is orthorhombic, not monoclinic as originally reported (*Am. Mineral.* **40**, 788 (1955)), and which differs in having K > Na and in containing appreciable Nb_2O_5. Indexed *x*-ray powder data are given for batisite; the strongest lines (appreciably different from the previous report) are 2.91 (10), 3.39 (5), 2.16 (5), 1.68 (5), and 2.09 (4).

M. F.

INDEX TO VOLUME 45

Leading articles are in **bold face** type; notes, abstracts and reviews are in ordinary type. Only minerals for which definite data are given are indexed.

GEORGE BANTA COMPANY, INC., MENASHA, WISCONSIN, U.S.A.